

THE GAS PHASE STRUCTURES OF SOME SILICON,
GERMANIUM AND PHOSPHORUS COMPOUNDS

by

C.M. Huntley

A thesis presented for the degree of Doctor
of Philosophy

Faculty of Science
University of Edinburgh
May, 1983



DECLARATION

This thesis is the original composition of the author's work, unless stated otherwise, and has not been submitted previously for any other degree. At the time of submission only the work discussed in Chapter 4 has been published, and these papers are contained in the Appendix of this thesis.

In memory of my fiancée, Katrina
Robertson, who was killed whilst
descending Sgurr Mhic Coinnich,
Isle of Skye, 15th May, 1982

CONTENTS

DECLARATION	i
DEDICATION	ii
CONTENTS	iii
ACKNOWLEDGEMENTS	vi
ABSTRACT	vii

CHAPTER 1: INTRODUCTION TO ELECTRON DIFFRACTION

1.1	Historical Background	1
1.2	Theory	2
1.3	Structure Determination	8
1.4	Apparatus for Electron Experiment	15
1.5	The Electron Beam	16
1.6	The Gas Sample	18
1.7	Detection of the Scattered Beam	19
1.8	Sample Purity	23
1.9	The Diffraction Experiment	24
1.10	Voltage and Wavelength Calculation	24
1.11	Data Reduction and Refinement	25
1.12	Characteristics of Silicon, Germanium and Phosphorus that effect the Structures of their Compounds	28

CHAPTER 2: EXPERIMENTAL TECHNIQUES

2.1	Introduction	34
2.2	Vacuum Techniques	34
2.3	Preparation of Samples	37
2.4	Physical Properties of New Compounds Prepared	49

CHAPTER 3: DIFLUOROPHOSPHINO, SILYL AND GERMYL ESTERS

3.1	Introduction	50
3.2	Difluorophosphino monothioacetate	52
3.2.1	Infra-red and Raman spectroscopy	52
3.2.2	Nuclear magnetic resonance spectra of $\text{CH}_3\text{C}(\text{OS})\text{PF}_2$: ^{31}P	61
3.2.3	Mechanism of exchange of bonding site	69
3.2.4	Thermodynamics of the exchange process	71

3.2.5	Nuclear magnetic resonance spectra of $\text{CH}_3\text{C}(\text{OS})\text{PF}_2$: ^1H , ^{13}C , ^{19}F	72
3.2.6	Summary of nmr data	76
3.2.7	Mass spectra of $\text{CH}_3\text{C}(\text{OS})\text{PF}_2$	80
3.3	Germyl monothioacetate	80
3.3.1	Nuclear magnetic resonance spectra: ^1H	82
3.3.2	Infra-red spectroscopy	84
3.3.3	Mass spectra of $\text{CH}_3\text{COSGeH}_3$	85
3.4	Silyl monothioacetate	85
3.5	Difluorophosphino monoselenoacetate	87
3.5.1	Nuclear magnetic resonance spectra: ^{33}P	89
3.5.2	Infra-red spectroscopy	90
3.6	Discussion	91
3.6.1	Bonding in the esters at equilibrium	91
3.6.2	Mechanism of exchange	93
<u>CHAPTER 4: THE GAS PHASE STRUCTURES OF $\text{CH}_3\text{CSOSiH}_3$ AND $\text{CH}_3\text{COSGeH}_3$ BY ELECTRON DIFFRACTION</u>		
4.1	Introduction	96
4.2	Structure Refinement	97
4.2.1	The molecular models	97
4.2.2	Refinement of $\text{CH}_3\text{CSOSiH}_3$	98
4.2.3	Refinement of $\text{CH}_3\text{COSGeH}_3$	99
4.3	Results and Discussion	109
<u>CHAPTER 5: THE GAS PHASE STRUCTURES OF $\text{CH}_3\text{SiH}_2\text{NCO}$ AND $(\text{CH}_3)_2\text{SiHNCO}$ BY ELECTRON DIFFRACTION</u>		
5.1	Introduction	119
5.2	Refinements and Models	122
5.2.1	Model of $\text{CH}_3\text{SiH}_2\text{NCO}$	122
5.2.2	Model of $(\text{CH}_3)_2\text{SiHNCS}$	122
5.2.3	Refinements of the $\text{CH}_3\text{SiH}_2\text{NCO}$ structure	123
5.2.4	Refinement of the $(\text{CH}_3)_2\text{SiHNCO}$ structure	131
5.3	Results and Discussion	137

<u>CHAPTER 6: THE GAS PHASE STRUCTURES OF CH₃SiH₂NCS AND (CH₃)₂SiHNCS BY ELECTRON DIFFRACTION</u>		
6.1	Introduction	148
6.2	Refinements and Models	152
6.2.1	Model of CH ₃ SiH ₂ NCS	152
6.2.2	Model of (CH ₃) ₂ SiHNCS	152
6.2.3	Refinement of the CH ₃ SiH ₂ NCS structure	154
6.2.4	Refinement of the (CH ₃) ₂ SiHNCS structure	161
6.3	Results and Discussion	168
<u>CHAPTER 7: THE GAS PHASE STRUCTURE OF CH₃SiH₂CN by ELECTRON DIFFRACTION</u>		
7.1	Introduction	179
7.2	Refinement and Model	180
7.2.1	Model of CH ₃ SiH ₂ CN	180
7.2.2	Refinement of the CH ₃ SiH ₂ CN structure	181
7.3	Results and Discussion	186
<u>CHAPTER 8: VIBRATIONAL, NMR, AND MASS SPECTRA OF METHYLSILYL PSEUDOHALIDES</u>		
8.1	Introduction	195
8.2	Vibrational Spectra of monomethyl cyanide	201
8.3	Vibrational spectra of monomethylsilyl isocyanate	212
8.4	Vibrational spectra of dimethylsilyl isocyanate	221
8.5	Vibrational spectra of monomethylsilyl isothiocyanate	230
8.6	Vibrational spectra of dimethylsilyl isothiocyanate	238
8.7	Assignments of Infra-red and Raman Spectra	246
8.8	Mass Spectra of methylsilyl pseudohalides	252
8.9	NMR Studies of methylsilyl pseudohalides	255
8.10	Discussion of NMR Results	256
<u>CHAPTER 9: FURTHER WORK</u>		265
<u>APPENDIX 1: PUBLISHED PAPERS</u>		269
<u>REFERENCES</u>		279

ACKNOWLEDGEMENTS

First and foremost I would like to thank my supervisors, Professor E.A.V. Ebsworth and Dr D.W.H. Rankin, who have suggested the present research topic and given me so much advice and encouragement. Also I would like to thank Dr S. Cradock who has given me much assistance with the analysis of the vibrational spectroscopy.

I am grateful to Dr I. Sadler, Dr D. Reed, Mr J. Miller and Mr L. Bell for running many of the nmr spectra, and to my colleagues, in particular Mr S.G.D. Henderson, for help and suggestions relating to the experimental work.

I thank the University of Edinburgh for providing me with a Departmental Demonstratorship and the James Watt Bursary (1981-82), and for providing the laboratory facilities; Dr H. Robertson for proof-reading and Mrs J. Kerr for typing the script.

Finally I would like to express my gratitude to my family and my friends who have given me unstinting support over the last year.

ABSTRACT

Difluorophosphino, germyl and silyl monothioacetate and difluorophosphino monoselenoacetate have been studied by nmr, infra-red and mass spectra to investigate the preferred bonding site of the $-PF_2$, $-SiH_3$ and $-GeH_3$ groups.

Also the gas phase structures of $CH_3COSGeH_3$ and $CH_3CSOSiH_3$ have been determined by electron diffraction, in particular noting the short non-bonded Ge/Si...M (M = O or S) distances, which are less than the sum of the Van der Waals' radii for Si and S or Ge and O. The final refined structures confirmed the vibrational and nmr data, indicating the $CH_3COSGeH_3$ to be entirely S-bonded, and $CH_3CSOSiH_3$ entirely O-bonded.

Finally a full study of the gas phase structures of CH_3SiH_2Ps (Ps = CN, NCO, NCS) and $(CH_3)_2SiHPs$ (Ps = NCO, NCS) has been carried out to find the influence of the methyl groups on the molecular structures, when compared to those of SiH_3NCO , SiH_3NCS and SiH_3CN . Additionally vibrational spectra of these compounds in the gas, liquid and solid phases have been recorded and are discussed.

CHAPTER 1: INTRODUCTION TO ELECTRON DIFFRACTION

1.1 Historical Background

Gaseous electron diffraction was first introduced as a structural technique by Mark & Wied¹ in 1930 following preliminary work by Rutherford², Debye^{3,4}, Davisson and Germer⁵, and Thomson^{6,7}, involving verification of De Broglie's hypothesis that a moving electron should have wavelike properties and that the wavelength should be related to the momentum by the expression

$$\lambda = h/p \quad [1]$$

λ = wavelength

p = momentum of particle

h = Planck's constant

A major improvement in the technique, suggested by Finbak⁹ and introduced by Debye¹⁰, involved modifying the image produced on the photographic plate by attenuating the wider scattered electrons using a heart shaped metal disc known now as the sector.

However, electron diffraction has vastly increased its power and usefulness with the development and spread of high speed electronic computing facilities. Now that electron diffraction has become less laborious, the chemist is able to test bonding and steric theories on a larger group of compounds and spend less time on menial tasks. Also, advances in the calculation of amplitudes of vibration and shrinkage corrections have contributed to

greater accuracy being possible in subsequent electron diffraction studies.

Hence the purpose of the work described in this thesis was to carry out a number of structural studies, using electron diffraction, on silicon and germanium compounds and also to collect appropriate infra-red, Raman, and nuclear magnetic resonance spectroscopic data which in all cases confirm the atomic arrangements but do not provide any geometric parameters.

1.2 Theory

When a beam of electromagnetic radiation encounters a material object a substantial portion of the beam may be reflected and a further part will be scattered through a wide range of angles from the incident direction. The scattering pattern arising from a gas is based on Young's classic double slit experiment in which he showed that when two parallel slits are placed in the path of a beam of electromagnetic radiation, regions of high and low intensity are produced, corresponding with constructive and destructive interference. The separation of the slits (d), the wavelength of the radiation (λ) and the scattering angle at an intensity maximum (θ) can be related by the equation:

$$d \sin \theta = n\lambda \quad [2]$$

where n is an integer.

As an atom readily acts as a scattering point, a diatomic molecule will also be expected to produce a scattering pattern similar to the pattern from the slits. Hence if the wavelength of the radiation is known, and the angle θ obtained from the pattern, one can find the separation of the atoms: i.e. the bond length.

A beam of electrons is the ideal form of radiation in structure determination because, firstly, the wavelength of the electrons gives the optimum number of rings on the photographic plate for common nozzle to plate distances and, secondly, the cross-section for diffraction of electrons is far greater than that for electromagnetic radiation, and as the total number of molecules in the gas phase is small compared to a solid, use of an electron beam allows one to get a satisfactory pattern in a reasonable time.

The resultant pattern is a combination of four scattering types. These are the coherent atomic scattering, the inelastic atomic scattering, extraneous scattering and finally the molecular scattering. The inelastic collisions do not lead to observable interference effects, but they do contribute to the overall scattered beam intensity. The inelastic scattering arises when an electron interacts with an atom and raises it to an excited electronic state. Generally, this constitutes a negligible effect on the overall pattern and atoms are all assumed to be in their ground state.

The extraneous scattering is due to multiple collisions, reflections from the chamber walls and collisions with residual gases. The multiple collisions are minimised by running the experiment at low sample pressures, maintaining as good a vacuum as possible, and keeping the area of interaction small. The exposure time should be determined such that the intensity of the plates is just sufficient. The atomic scattering is a monotonic rapidly declining function and can be computed and subtracted from the overall intensity function. This then leaves the molecular intensity component with the extraneous and inelastic scattering.

For a rigid system of atoms considered to be independent scattering centres, the intensity of electrons scattered elastically is

$$I = \frac{I_0}{R^2} \sum_{i=1}^m \sum_{j=1}^m f_i(s) f_j(s) \frac{\sin(r_{ij} \cdot s)}{r_{ij} \cdot s} \quad [3]$$

$$\text{where } s = \frac{4\pi \sin\theta/2}{\lambda} \quad [4]$$

in which f_i is the scattering factor for atom i , θ is the scattering angle, r_{ij} is the distance between atoms i and j , and R is the distance from point of scattering to the plate.

If it is assumed that the inelastically scattered intensity is completely coherent, then the total intensity is given by

$$I_{\text{TOT}} = I_{\text{m}}(s) + I_{\text{b}}(s) \quad [5]$$

where $I_{\text{b}}(s)$ is the background and contains the non-structure sensitive part of components inelastic, extraneous and atomic scattering. The structure dependent part $I_{\text{m}}(s)$ may be written for atoms i and j :

$$I_{\text{m}}(s) = \text{constant} \sum_i |f_i(s)|^2 + \sum |f_i| |f_j| \cos \left(\eta_i - \eta_j \right) \cdot \frac{\sin(s \cdot r_{ij})}{s \cdot r_{ij}} \quad [6]$$

assuming the molecule is rigid. Thus the molecular intensity curve will be superimposed on the smoothly varying background curve. Since atomic scattering amplitudes may be computed with reasonable confidence, the only unknown to reproduce the experimental diffraction intensities would be the set of internuclear distances r_{ij} . $f(s)$ is the scattering factor of an atom at point s , $(\eta_i - \eta_j)$ is the phase shift on scattering from atom pair ij at point s .

However, when the experimental and theoretical intensity curves are compared using the rigid model the fit is inadequate, and allowance must be made for molecular vibrations.

If the rigid model molecular intensity curve equation is transposed by Fourier Transform to the radial distribution curve a set of single lines at all the values of r_{ij} would be found. By vibrating the bonds, they will have

harmonic oscillations which have periods several orders of magnitude greater than the interaction time, and each electron will see a single length although these lengths will vary. The nature of the statistical distribution over all possible molecular configurations is available from quantum mechanics. Hence for any pair of atoms i and j there will be a probability function $P_{ij}(r)$ for the expected values between r and r_{ij} and the term $(\sin(r_{ij} \cdot s) / r_{ij} \cdot s)$ will vary and must be determined.

Now

$$I_m(s) = \text{const.} \sum |f_i| |f_j| \cos(n_i - n_j) \int P_{ij}(r) \frac{\sin(r_{ij} \cdot s) dr}{r_{ij} \cdot s} \quad [7]$$

$$\text{with } P_{ij} = \frac{1}{\sqrt{2\pi} u_{ij}} \exp \frac{(r - r_{ij})^2}{2u_{ij}^2}$$

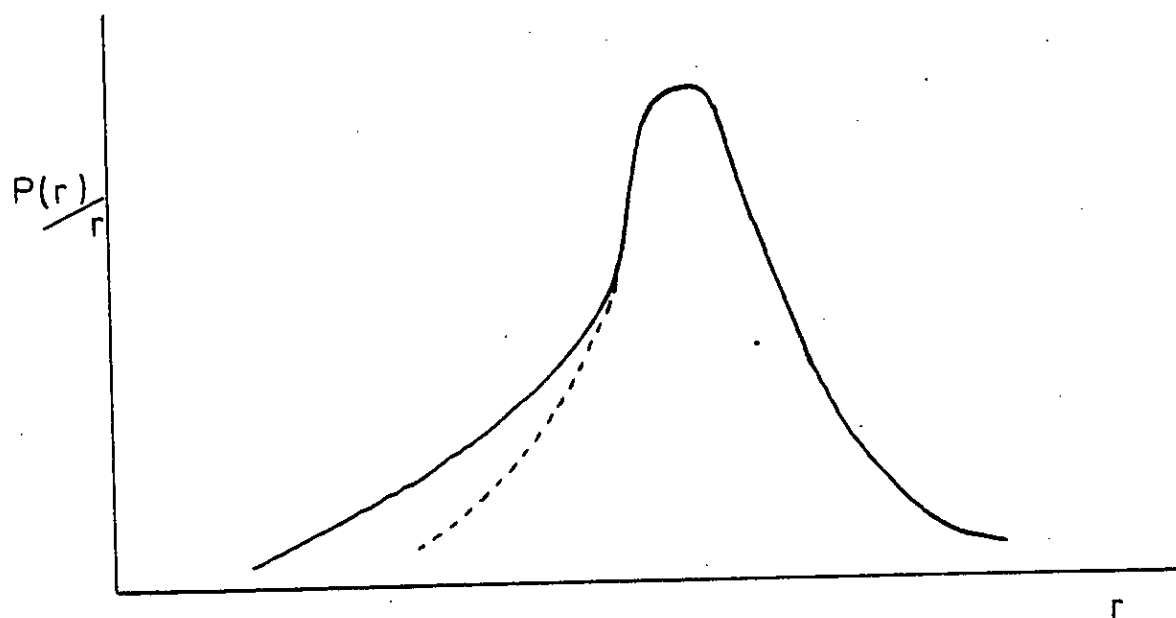
where u_{ij} is the root mean square of amplitude of vibration, and r_{ij} now denotes the mean distance between atoms i and j . At this stage the Fourier Transformed radial distribution curve would give a series of Gaussian distribution curves (with some overlap if the distances are close), where u_{ij} is equal to the width of the curve at half height. Expanding the probability term and only using the first term of the integrals gives:

$$I_m(s) = \text{const.} \sum |f_i| |f_j| \cos(n_i - n_j) \frac{\sin(r_{ij} \cdot s)}{r_{ij} \cdot s} \exp \left(\frac{-s^2 u_{ij}^2}{2} \right) \quad [8]$$

The last consideration to be included is the anharmonicity of the vibration a_{ij} , which is related to the constant \underline{a} in the morse potential and to the mean amplitude. To a first approximation the intensity curve is now represented by:

$$I_m(s) = \text{const} \sum |f_i| |f_j| \cos(\eta_i - \eta_j) - \frac{\sin(r_{ij}s - a_{ij}s^3)}{r_{ij} \cdot s} \exp \frac{-s^2 \cdot u_{ij}^2}{z} \quad [9]$$

The anharmonicity is assumed to be equal to $au^4/6$ and is set equal to 200 pm for bonded distances and zero for non-bonded distances. The anharmonicity accounts for the asymmetry of peaks in the radial distribution curve. See Figure 1.1.



————— curve with anharmonicity

----- curve without anharmonicity

Figure 1.1: Peak in radial distribution curve

1.3 Structure Determination

The molecular structure is determined by comparing the experimental intensity curves or radial distribution curves with the appropriate theoretical curves as produced by the equations above. From equation [7] the molecular scattering contribution can be simplified as:

$$I_m(s) = \sum_{ij} A_{ij}(s) \int \frac{\sin(r_{ij} \cdot s)}{r_{ij} \cdot s} P_{ij}(r) dr \quad [10]$$

which for a diatomic and using Fourier Transform theory can be converted to⁹

$$\frac{P_{ij}(r)}{r_{ij}} = \int_0^{\infty} \frac{s I_m(s)}{A_{ij}(s)} \sin(r_{ij} \cdot s) ds \quad [11]$$

$$\text{or} \quad = \int_0^{\infty} I(s) \sin(r_{ij} \cdot s) ds \quad [12]$$

At this stage an artificial damping function is included in the integrals to reduce the effect of a finite upper limit in the integration. The lack of data below s_{\min} will change the zero line of the curve. Thus

$$\frac{P(r)}{r} = \int_{s_{\min}}^{s_{\max}} I(s) \exp(-ks^2) \sin(rs) ds \quad [13]$$

In practice theoretical data are added from 0 to s_{\min} to correct the baseline of the radial distribution curve. The integration is performed by summation and consequently the interval Δs must be constant across the entire range of data. Also, Δs must be quite small relative to $2\pi/r_{ij}$. In

the experiments described in this thesis the s range is from 20 to 360 nm^{-1} , with a minimum Δs of 2 nm^{-1} . The damping factor included in the intensity equation, before performing the Fourier inversion, provides strong discrimination against data of higher s values because they are either unavailable or unreliable.

Clearly, for polyatomic molecules the equations will be more complex, with more interatomic distances, and the $P_{ij}(r)/r_{ij}$ of each atom will be weighted proportionally to the products of their atomic numbers. Also, since the r_{ij} is calculated from the centre of gravity of a peak in the $P(r)/r$ curve, the apparent average distances will be less than the true average - i.e. in $P(r)$ - because the lower end of the curve is weighted relative to the upper end. This distance is reduced by u^2/r (where u is amplitude of vibration). One effect of the damping function is to raise the apparent vibrational amplitudes in the radial distribution curve from u_{ij} to $(u_{ij}^2 + 2k)^{\frac{1}{2}}$, but this does not affect the structural analysis.

The structural analysis begins with assumed bond distances, angles and amplitudes of vibration for the predicted structure. With the more complicated structures estimates of the distance from the centre of peaks in the experimental radial distribution curve is inadequate because of the overlapping peaks corresponding to nearly equal distances. Then previous knowledge of the bond lengths from related structures can help solve the structure. The second stage is to try refining the parameters to obtain

optimum correlation between the experimental and theoretical curves. The programs used in this work refined the parameters to give the best fit to the molecular intensity curves. At any stage of the refinement the intensity curves and radial distribution curves could be plotted out and these included a difference curve between experimental and theoretical curves. The background could be subtracted by drawing a smooth curve through the difference curve and subtracting this from the total intensity plots. Once the baseline is equal (or almost equal) to the difference curve the intensity curves are fixed and all subsequent refinements are done on these curves. More recently Blair¹² has developed a program, based on spline functions, designed to subtract the background automatically. The program is not only fast and easy to use but is accurate and will not add a background that has a frequency of oscillation for s of more than 100 pm. Thus refined structures should not be altered by the background subtraction.

In most cases it is not possible to refine all the bond lengths and amplitudes of vibration as independent parameters. Based on an assumed molecular model, where the atomic coordinates are defined by the bond distances and angles, the dependent distances may be calculated from the independent distances and angles. Having done that, the structure found will be the r_a structure which does not take into account vibrational corrections or shrinkage factors. These are discussed below.

Early electron diffraction studies were done by comparing experimental and theoretical intensities or radial distribution curves calculated from a limited number of molecular models. The theoretical curves were in general assumed to be a superposition of Gaussian peaks according to the equation below.

$$\text{Theoretical function} = \text{const.} \sum_{ij} n_{ij} z_i z_j \frac{P_{ij}(r)}{r_{ij}} \quad [14]$$

Now the method of refinement is that of least squares refinement, in which the sum of the squares of the differences between experimental and theoretical curves is minimised. Since not all the data regions are equally reliable a suitable weighting procedure must be used which in fact gives less weight to the lowest s values and highest s values for each data set. Also there is an additional factor in the weighting procedures with the correlation of errors at neighbouring data points. This is particularly significant when the data relate to a continuous function. The number of data points (n) should be chosen so that essentially no new information is gained by increasing the number. Thereafter the standard deviations will be roughly proportional to $n^{-\frac{1}{2}}$ so that it would seem that increasing n reduced the standard deviation to small values, which is not correct. For small intervals between the intensity points, the data points become too close to remain as completely independent measurements. The first electron diffraction study which

included a correlation factor in the least squares refinements was carried out by Murato and Morino^{13,14}. The sum to be minimised in the least squares refinements can be expressed by

$$\sum_{j=1}^N w_j u_j^2 \quad [15]$$

where w_j is the weight attached to point j , u_j the difference between experimental and theoretical intensities at point j , and N is the number of points measured.

In this work the weighting points s_1 and s_2 , for the centre and edge of the photographic plates, were chosen by inspection. Then the weight applied to any points outside these limits was reduced as data was thought to be less reliable in these regions. However equation [15] does not make any allowance for the correlation between adjacent points and the edge of data plates and this can be done by using an off-diagonal weight matrix, w . We actually seek to minimise the expression

$$U' W U \quad [16]$$

where w is the square weighted matrix and u is the column matrix of differences between experimental and theoretical values.

The diagonal elements of the weighting matrix were therefore:

$$w_{ii} = (s_i - s_{\min}) / (s_1 - s_{\min}) \text{ where } s_{\min} < s_i < s_1$$

$$w_{ii} = 1 \text{ where } s_1 < s_i < s_2$$

$$w_{ii} = (s_{\max} - s_i) / (s_{\max} - s_2) \text{ where } s_2 < s_i < s_{\max}$$

and the off-diagonal elements were introduced to the weight matrix as follows:

$$w_{ij} = 0 \text{ where } i \neq j \pm 1$$

$$w_{ij} = 0.5(w_{ij} + w_{jj}) / (p/h)_R \text{ where } i = j \pm 1$$

The correlation parameter $(p/h)_t$ at the nozzle to plate distance R was calculated by the method of Murato and Morino¹³ and is a measure of how smooth the molecular intensity curve is. Thus if the curve is a smooth curve with a constant frequency the correlation will be near 0.5 value; a curve which fluctuates unevenly will have a low correlation. It has been shown¹⁴ that a simple diagonal matrix is inadequate because the observations of the intensity or radial distribution curves must be regarded as indirect. Despite the importance of the off-diagonal points in the weighting matrix, the elements need only be included for adjacent points since the degree of correlation between points falls off rapidly with separation.

Finally, a measure of the closeness of fit between the theoretical and experimental curves is given by the R-factor

which is calculated at the end of each refinement stage. The R_D values are simply a measure of the difference represented by

$$R_D = \frac{\sum (I_{\text{expt}} - I_{\text{theory}})^2}{\sum I_{\text{expt}}^2} = \frac{\sum D^2}{\sum I^2} \quad [17]$$

and do not include any account of correlation between adjacent points. In matrix form this can be expressed as

$$R_D = \frac{D' W D}{I' W I} \quad [18]$$

where W is the weight matrix containing only the diagonal elements. D is the intensity difference.

The R_G value is defined using the weighting matrix including the off-diagonal weighting elements. Thus

$$R_G = \frac{D' W D}{I' W I}^{\frac{1}{2}} \quad [19]$$

where D is again the observed value minus the value calculated from the estimates of the parameters but W is now the full weighting matrix, and I is the vector of intensities. The R_G value is a better estimate of the fit, although both values are quoted in the electron diffraction analysis chapters later.

1.4 Apparatus for Electron Diffraction Experiments

In this section the basic requirements of the electron diffraction experiments are given, with some additional information on the way the experiment is carried out on the apparatus installed at Edinburgh.

A stable electron beam is produced from an electron gun assembly and passed via a series of focussing magnetic lenses through an evacuated chamber to interact with a fine stream of sample vapour, from a nozzle, passed at right angles across the electron beam. The subsequent scattered pattern is then recorded on a photographic plate, positioned perpendicular to the undiffracted beam. It is important that a hard vacuum is maintained for two reasons. Firstly, air molecules will cause extraneous scattering and secondly, all the compounds studied in the project are extremely reactive with air and water vapour. Some electron diffraction workers¹⁵ now use a mass spectrometer which records the mass spectrum of the sample actually at the time of the diffraction experiment. This gives an indication of the purity of the sample.

It is necessary to know the wavelength of the electron beam and the nozzle to photographic plate distance. The area of interaction should be as small as possible and the volume the electron beam travels through should be a minimum to reduce scattering of the electron beam by more than one molecule and to ensure the scattering is from as near as possible to a single point. To achieve these requirements the experiment is carried out as follows.

1.5 The Electron Beam

A thin tungsten wire has a sufficient current passed through it to raise the temperature and boil off the electrons.

To obtain a higher temperature and thus provide a larger proportion of beam electrons, the filament is pinched in the centre to create regions of extra high resistance and provide a point source. See Figure 1.2.

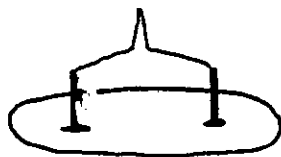


Figure 1.2: Tungsten filament

The electrons from the filament then enter the potential gradient and will be accelerated towards the anode using a voltage of between 40-45 kV. The anode will have a hole in it, to allow the electrons to pass through.

The potential difference accelerating the electrons is related to the wavelength by the following equations. Since the wavelength (λ) and momentum (p) are related by Planck's constant, and since equation [1] relates potential difference (V) to the momentum of a particle, the wavelength can be related to the accelerating voltage by equation:

$$\lambda = h/p \text{ De Broglie's hypothesis} \quad [1]$$

$$Ve = p^2/2m \quad [20]$$

$$\therefore \lambda = \frac{h}{(2meV)^{\frac{1}{2}}} \quad [21]$$

However this expression assumes the electrons are travelling at near the speed of light and the more accurate representation is from the relativistically correction expression¹⁶ where

$$\lambda = \frac{150}{V(V+9.834 \times 10^{-7})^{\frac{1}{2}}} \quad [22]$$

and V is the voltage specified in volts and λ in Å.

At a voltage of around 43 kV the wavelength of the electron beam is found to be between about 5-6 pm which is ideal for structure determination as the bond lengths and non-bonded distances will be between 10 and 100 times the beam wavelength.

The focussing and collimating of the beam is done by a series of small apertures and magnetic lenses, and the beam can be checked by observing the size of spot it makes on a small fluorescent screen behind the photographic plate. Once the spot is focussed the sample can be allowed to pass through the nozzle into the evacuated chamber.

The vacuum is maintained by three oil diffusion pumps, backed by a mechanical oil pump. Before any experiment is started the chamber is pumped out overnight. The operating

vacuum is 10^{-6} mm Hg.

1.6 The Gas Sample

Despite the necessity of keeping the vapour jet to a small diameter, the electrons must interact with a sufficient number of molecules to give a reasonable scattering pattern. The sample is injected into the chamber through a narrow metal nozzle positioned just below the electron beam.

The apparatus at Edinburgh has the facility to run the experiment at two nozzle to plate distances; one about 285 mm, one at 128 mm. The pressure and exposure time are calculated according to the times found suitable for compounds of similar volatility and molecular weight. All the compounds discussed in this thesis were run at room temperature as they are all of relatively low volatility. Thus the only variation possible is the exposure time. To reduce any build-up of gas pressure in the chamber, a cold trap cooled by liquid nitrogen is placed opposite the nozzle the other side of the electron beam.

For compounds that are particularly involatile, e.g. GeH_3NCS , with vapour pressures at room temperature less than 1 mm Hg a heated nozzle would be an advantage. However the option is not available on the Edinburgh apparatus. If the vapour pressure of the sample at room temperature is >20 mmHg, an appropriate pressure is

maintained by using solvent slush baths, and by control of the needle value between the nozzle and ampoule.

1.7 Detection of scattered beam

The apparatus in these experiments recorded the scattering pattern on Kodak Electron Image plates. Certain investigations have looked into possible counting techniques^{17,18} as is commonly employed in the field of X-ray crystallography. However the counting technique would be inadequate for this kind of work, because in most cases the total time involved in collecting the data may be several hours. While a single crystal is usually stable, for a gas sample you would need a much larger supply of sample than present techniques need, and it would be difficult to maintain stable operating conditions. The flow of vapour may not be constant and the sample may not condense immediately on the cold finger after leaving the nozzle. To obtain reasonable resolution on the plates a relatively small grain size emulsion must be used, the relationship between the density of developed emulsion to the time integrated beam intensity must be linear over as wide a range as possible.

A major problem in the early development of electron diffraction as a structural technique was that no photographic plate was available that would record the scattered beam over a suitable range because the intensity of the beam falls off as the fourth power of the scattering

angle. Thus either the narrow angle data was too dark, but wider angle pattern visible, or no outer pattern was observed if the inner pattern was measurable. This was solved by placing a rotating metal sector between the scattered beam and the photographic plate. The sector is usually a heart shaped plate with an angular opening that widens as the third or fourth power of the scattering angle and evens out the scattered electron intensity so that over substantially the whole photographic plate there is an accurately measurable relationship between the density of the developed emulsion and the intensity of the scattered electrons. See Figure 1.3.

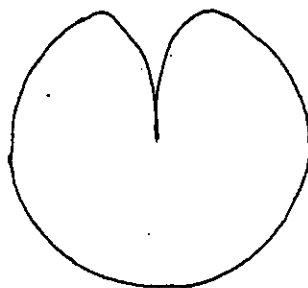


Figure 1.3: The sector

The centre of rotation of the sector should coincide with the centre of the diffraction pattern and the rotation speed should be large enough that it is immaterial whether the sector has completed an integral number of oscillations during the exposure or not. Clearly the shape of the sector must be known so that an allowance can be made for the true

scattering pattern. Having the correct equation is essential and it is believed that certain problems with the intensity curves giving spurious undulations can to some extent be attributed to the incorrect sector equation.

The acceptable range of scattering angles obtainable with any electron diffraction apparatus is limited by how close to the centre of the sector a narrow gap can be cut and then how well calibrated the inner region is. Clearly the wider the inner spacing is the wider the outer region must be. For these experiments, the intensity range that was reasonable to use was between s values $40\text{-}360\text{ nm}^{-1}$. To obtain an expansion of the inner region long distance plates were run, giving the scattering pattern from 20 to 140 nm^{-1} while the short distance contains useful data for 60 to 360 nm^{-1} . See Figure 1.4

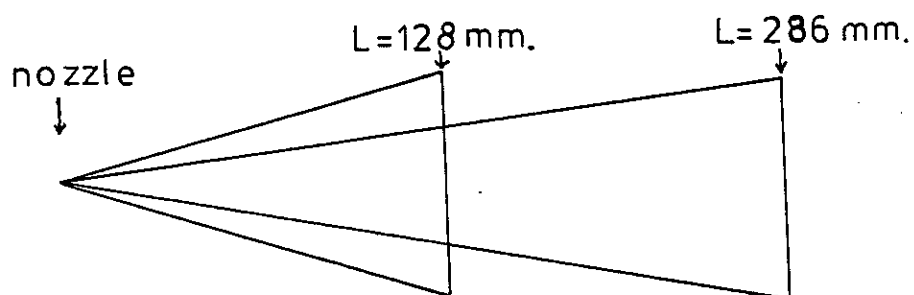


Figure 1.4:

The tracing of the plates and conversion to electron density at particular s values is done at the SERC Daresbury Laboratory using a Joyce-Loebl Microdensitometer 6. This is a computer controlled double-beam microdensitometer with x and y drives which has been programmed to trace the circular electron diffraction patterns to maximum advantage. The input to the computer consists of the coordinates of the centre of the pattern, the electron wavelength and camera distance used, and the required s intervals for the intensity data. The radii of rings are chosen to give intensities at integral multiples of Δs . The optical density is then measured five times at each of 1000 points equally spaced round each ring. As each density is measured with an uncertainty of ± 0.002 , after 5000 readings the mean density is accurate to better than ± 0.0001 D. After every five rings have been scanned, the density of a fixed region of the plate is checked so that any small correction for drift may be made. Also a fixed block of the exposed plate is checked for any drift. At the end of the run, a ring outside the pattern is scanned to give the optical density of unexposed plate. The final output consists simply of the average optical densities for the rings. The scanning technique also has the advantage that any flaws on the plate can be ignored by specifying the appropriate angular sector. The earlier tracing technique employed at Edinburgh involved finding the centre of the pattern and then spinning the plate and measuring the pattern radially from that position. This

meant that flaws were included and averaged over the whole pattern. Thus in many cases it was necessary to interpolate between data points traced, while the new tracing technique only scans the regions from which intensities are required and makes interpolations unnecessary. Also, this helps to reduce correlation between adjacent observations.

Data produced from the Daresbury microdensitometer ~~are~~ good, and the difference between intensities for several scans of one plate are of an order of magnitude less than differences between intensities from several plates of the same compound.

1.8 Sample Purity

The purity of the sample is very important, particularly as the likely hydrolysis products will have similar volatilities to the compound under study. In some cases allowance can be made for a percentage of impurity by including the known bond lengths and angles in the molecular model. This is then included in the fitting of the experimental and theoretical intensity and radial distribution curves. However the results are never as good as for a pure sample with the refineable parameters having larger esds.

1.9 The Diffraction Experiment

The sample is stored in a glass ampoule which can be attached by a ground glass joint to the entry to the nozzle. Once the electron beam is focussed the sector is set spinning by a small mechanical motor and the pressure of the sample raised to the required value. When the pressure is steady the electron beam shutter is pushed aside leaving the sample exposed to the beam. The exposure time is calculated according to the pressure attainable and the expected scattering power of the atoms. During the exposure a digital measure of the voltage is recorded and can be used to compare the relative voltage during the run of each plate. Three plates are run at each distance (128 and 285 mm) and on the same settings plates of benzene are run. The analysis of the benzene plates (of known structure) is used to find the plate to nozzle distance and the electron beam wavelengths for each plate.

1.10 Voltage and Wavelength Calculation

To analyse the benzene plates (two at long distance and two at short distance), it is initially assumed that the first plate will have the same wavelength as the last plate of the previous run. The other plates' wavelengths are then scaled by using the digital voltage reading. These are not actual readings but can be used as relative values. The high voltage V is calculated from the wavelength using equation [23].

$$V = \frac{\sqrt{\frac{5.91}{(100\lambda)^2} + 1} - 1}{197 \times 10^{-6}} \quad [23]$$

After analysis of the benzene plates a value of $r(C-C)$ should be obtained which will not necessarily be very close to the true value of 139.7 pm. A new wavelength for the first benzene plate is now calculated from the initial λ value, using the new $r(C-C)$ distance to scale by:

$$\lambda = \frac{\lambda_A \cdot 139.7}{r(C-C)} \quad [24]$$

This new wavelength has a corresponding digital voltage and this is now used to find the wavelength for each of the sample plates, as was done above with equation [22].

At the same time the nozzle to plate distances are calculated by scaling the input distances for benzene, with the $r(C-C)$ bond lengths obtained by refining with one data set at a time.

1.11 Data-Reduction and Refinement

All the calculations were carried out using an ICL 2972 computer at the Edinburgh Regional Computing Centre. The data reduction program was a version of an established program¹⁹, modified to handle data direct from Daresbury.

The least-squares refinement program is a new version of an established program²⁰ which uses an off-diagonal weight matrix to allow for correlation between data points.

Using this program it is possible in principle to refine all independent parameters, amplitudes of vibration and scale factors. In fact, usually not all the parameters were refineable and these were fixed at values found in related compounds. Groups of amplitudes of vibration could be refined as single parameters where the values within the groups were held at fixed ratios to one another.

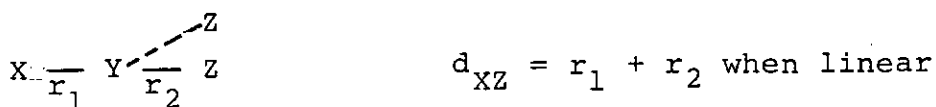
Also the program contains plotting routines to record the intensity and radial distribution curves, with the difference curves between theoretical and experimental functions. In all the calculations the complex scattering factors of Schäfer et al were used²¹.

Most of the problems that occur in the analysis of the diffraction patterns are discussed in the respective chapters as the problems arise. In all the compounds studied there are overlapping peaks in the $P(r)/r$ curves for similar distances and also problems of fixing the positions of the hydrogen atoms whenever the molecule has many heavier atoms which are much better scatterers. The area of the peaks is governed by the multiplicity of the distance (n_{ij}) and the atomic numbers of the atom (z_i) pair. The area is proportional to

$$\frac{n_{ij} z_i z_j}{r_{ij}} \quad [25]$$

where r_{ij} is the distance between atoms i and j .

The extent of the random errors in the parameters is measured in the least squares refinements of the data, but when quoting estimates of the reliability, the estimated standard deviations have been increased to allow for any systematic errors. All the final distances quoted are r_a which corresponds to the centre of the peaks in the $P(r)/r$ curves. The r_a structure does not take into account the vibrational motions that occur at the temperature of the experiments. In particular, no account is taken of the shrinkage effects for large amplitude low frequency bending motions. Since the electron diffraction experiment measures the average distance between atoms, the apparent structure of a linear group XYZ with a large amplitude bending motion will be bent because for a substantial time the distance between X and Z will be less than the sum of the bond distances XY and YZ.



It is possible to construct molecular models which take into account these vibrational motions and these show that the molecule should not be considered as a rigid structure. However in this work only the apparent angles were calculated from the average structures and they are discussed as such.

1.12 Characteristics of silicon, germanium and phosphorus that affect the structure of their compounds

The range of compounds studied in this thesis includes some methyl silyl pseudohalides $(\text{CH}_3)_n\text{SiH}_{3-n}\text{ps}$, [where $n = 1, 2$, $\text{ps} = \text{NCO}$, NCS and CN], silyl and germyl monothioacetates, and difluorophosphine monothio and monoselenoacetates. The electron diffraction study of difluorophosphine monothioacetates was not attempted, but the infra-red, Raman, and nuclear magnetic resonance data show how the PF_2 group is bonded.

The interest in the geometry of atoms and groups around silicon and germanium atoms stems in part from the availability of vacant d orbitals on silicon and germanium. Phosphorus also has a vacant d orbital although its effect is less pronounced than for silicon.

In contrast to carbon, silicon and germanium do not readily form $p\pi$ multiple bonds, but there is considerable evidence that in certain bonds to silicon, notably from oxygen and nitrogen, there is some double-bond character involving d orbital overlap; referred to as $(p-d)\pi$ bonding. Early evidence for this was that $(\text{SiH}_3)_3\text{N}^{22}$ differs from $(\text{CH}_3)_3\text{N}^{23}$ in being planar rather than pyramidal and in being a very weak Lewis base. These observations can be explained by supposing that nitrogen forms $(p-d)\pi$ bonds to silicon atoms. In the planar state of $(\text{SiH}_3)_3\text{N}$ the non-bonding electrons of nitrogen would occupy the $2p_z$ orbital if we assume that the Si-N bonds are formed using

the sp_xpy trigonal hybrid orbitals of nitrogen. Silicon has empty 3d orbitals which are of low enough energy to be able to interact appreciably with the nitrogen $2p_z$ orbital. See Figure 1.5

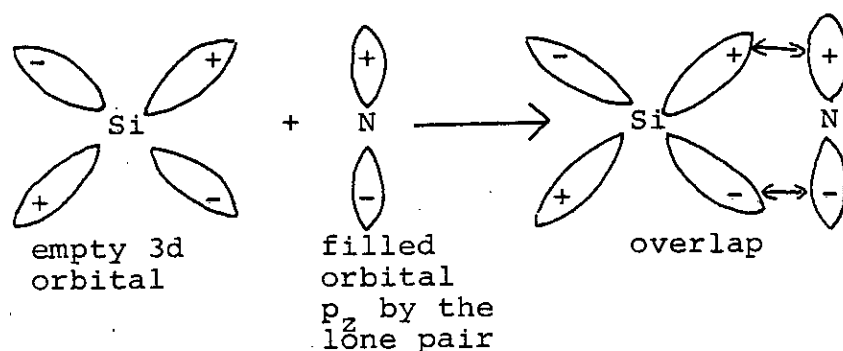


Figure 1.5:

The overlap should add additional bond strength, with a resulting shorter bond than predicted from the sum of the covalent radii. Also the delocalisation of the nitrogen lone pair allows the SiN_3 skeleton to adopt a planar configuration, whereas C has no vacant orbital, no delocalisation can occur and $(CH_3)_3N$ is pyramidal. Germanium also has a vacant d orbital, the 4d orbital, but this is a higher energy than the nitrogen $2p_z$ orbital and so interaction is less. However a number of germanium compounds do have relatively wide angles at N suggesting some overlap of orbitals is possible. For example trigermylamine is essentially planar with a simple valence force field calculation²⁴ based on the assignment of bands at 850 and 370 cm^{-1} as e and a_1 skeletal stretching modes of a

C_{3v} skeleton led to an angle at nitrogen of $116(2)^\circ$, and analysis of the gas phase electron diffraction data gave an angle of 120° ²⁵.

Similar wide angles are found in Si-O compounds; for example $(SiH_3)_2O$ is a much weaker base than $(CH_3)_2O$ and has an apparent angle at O of about 144° ²⁶, while the carbon equivalent is tetrahedral at O. If allowance is made for the large amplitude bending motion at O, the SiOSi angle is almost 180° . The related ether $(GeH_3)_2O$ ²⁷ is found to have a narrower angle of 125.6° but this is still wider than the tetrahedral angle. Also there is a shortening of the Si-O and Ge-O bonds.

The structural anomalies of silicon found in the amine and ether compounds have also been investigated for SiH_3NCO , SiH_3NCS and SiH_3NCSe . Again wide angles at nitrogen are found in the electron diffraction studies^{28,29} (with no allowance for shrinkage), and near linear configurations by microwave³⁰ and vibrational studies^{31,32} for the gas phase. Interestingly, the crystal structure of SiH_3NCO ³³ gives an SiNC angle of 159° with fairly strong Si...N and Si...O non bonded intermolecular interactions.

Despite the evidence for the structural characteristics of silicon being due to (p-d) π bonding there are three other explanations. Oberhammer and Boggs³⁴ have carried out a series of ab initio calculations for $(SiH_3)_2O$ and have found that their calculated and the recently published

experimental³⁵ geometric parameters are in very good agreement; in particular the short Si-O bond distance and the wide SiOSi angle. The calculations were done without attaching much importance to the d orbitals, and instead making the character of the Si-O bonds more ionic than would be estimated from the electronegativities, resulting in electronic repulsions between the strongly positive silicon atoms.

Secondly, Glidewell³⁶ has calculated the geometries of a number of silicon pseudohalides using a model designed to test the molecular geometry based upon the second-order Jahn-Teller effect. This is more fully explained in Chapter 5. Again wide angles at the nitrogen adjacent to silicon are found for all silicon isocyanate, isothiocyanates and azides. In contrast the methyl compounds had angles of 130-134° for isocyanates, and 150-155° for isothiocyanates. It was found that substituted silicon pseudohalides with C_s symmetry could be bent up to 170.5° (e.g. SiH₂ClNCO).

Lastly, there is an approach using the idea of hard sphere radii by Bartell³⁷ in which one considers the thermally averaged non bonded distances of the atoms either side of the central atom, and this has been successfully applied to silyl pseudohalides by Glidewell and Robiette³⁸.

The bonding of silicon to second row elements (3p) is more as would be predicted with a much smaller shortening of Si-M bond lengths (M = S,P) and narrower

angles of atoms adjacent to silicon. For example $(\text{SiH}_3)_3\text{P}^{39}$ is pyramidal and $(\text{SiH}_3)_2\text{S}^{40}$ has an angle at S of 97.4° , this is very close to the angle at S in $(\text{CH}_3)_2\text{S}^{41}$ (98.9°). Also the Si-S distance is very close to that predicted from $\text{C}_2\text{H}_6^{42}$, $\text{CH}_3\text{SiH}_3^{43}$ and $(\text{CH}_3)_2\text{S}^{41}$. Thus it seems that $(p-d)\pi$ bonding is of little importance in the bonding of silicon and 3p atoms possibly because the d-p orbital overlap is small.

Phosphorus, as a group V element, has three unpaired electrons in the outer 3p orbitals which are available for bonding, and hence phosphorus can be formally trivalent or pentavalent. The promotional energy of $3p \rightarrow 3d$ is small enough to allow the vacant d orbitals to participate in bonding. This is in contrast to nitrogen where the $2p \rightarrow 3d$ energy is too large for effective d bonding to take place. Generally $(p-p)\pi$ bonds are unknown, while $(d-p)\pi$ bonding is moderately strong, but less significant than for silicon. The most important factor for phosphorus is that valence expansion is possible.

The interest in the structure of the esters is to see how the difluorophosphine, silyl or germyl groups are bonded, and also to investigate any short non-bonded distances $\text{M} \dots \text{O}$ or $\text{M} \dots \text{S}$ (where $\text{M} = \text{P}, \text{Si}, \text{Ge}$). In earlier work $\text{SiH}_3\text{OOCCH}_3^{44}$ was found to have short $\text{Si} \dots \text{O}$ distances, not short enough to be considered as a bonded distance, but shorter than the sum of the Van der Waals' radii for the two atoms.

All the structure determination has been done by electron diffraction, and the compounds have been studied in the gas phase. This is the ideal phase to observe single molecules since intermolecular interactions should be negligible. The geometric parameters are complemented with infra-red, Raman and nuclear magnetic resonance data to confirm the atomic arrangement. Also the vibrational spectra obtained for gas, liquid and solid phases give an insight into intermolecular interactions resulting in shifts and enhanced intensity of the bands.

CHAPTER 2: EXPERIMENTAL TECHNIQUES

2.1 Introduction

This chapter contains descriptions of the various experimental techniques used in the course of this work. The first part describes the method of handling the samples, and the second part explains how the infra-red, Raman, and nuclear magnetic resonance experiments were run and instruments used. The last section deals with the preparation and purification of samples.

2.2 Vacuum Techniques

All components under study are volatile liquids or gases at room temperature and most are reactive with both air and water vapour. Hence the use of a vacuum line is essential and its employment is now widespread in many branches of chemistry.

The compounds that lend themselves to vacuum line work are those with sufficient vapour pressure at room temperature (>5 mmHg) but very small pressures at liquid nitrogen temperature (77 K). Moreover the apparatus is particularly suitable for working with small quantities of material, often fractions of a mmol, that are needed for spectroscopic studies.

The vacuum system used consisted of two trap sections,

used for storage of samples and for trap-to-trap vacuum distillation during purification. Also there were a number of ground glass 'take-off' points each with a tap which allowed the removal and addition of compounds to the system. All the taps on the vacuum line were greaseless 'sovirel' taps, which were extremely easy to clean and allowed the cleaning of traps individually. All the glass joints were sealed using Apiezon 'L' grease, and any ground glass taps sealed by 'N' grease.

The pumping system was a mercury diffusion pump backed by a rotary oil pump. This easily gave pressures down to 10^{-4} mm Hg. To monitor the pressure and hence measure the quantities of sample in the vacuum line a glass spiral gauge with a mirror and small lamp was used. This acted as a 'null instrument' by the introduction of air pressure to the other side of the spiral gauge through the 'back section'. The total volume of the apparatus permitted up to 12 mmol of sample to be expanded, without having a pressure greater than one atmosphere.

The vacuum line facilitates a number of special techniques. Gas phase infra-red spectra are easily obtained by attaching a 10 cm cell with KBr or CsI end plates, and vapour pressure measurements are obtained by freezing the sample into the spiral section 'cold finger' and reading the spiral deflection at a given temperature. Using a molecular weight bulb of known volume, measurement of pressure and weight of gas in the bulb give the

sample's molecular weight.

All the samples were stored at liquid nitrogen temperatures using Dewar flasks, and the different temperatures required for fractional distillation were obtained by mixing various organic solvents with liquid nitrogen or solid carbon dioxide. For example, toluene and nitrogen give a temperature of 177 K; acetone and carbon dioxide a temperature of 195 K.

For certain preparations an inert atmosphere can be introduced into the system by attaching an external cylinder. The solid phase infra-red spectra were run in a 10 cm cell with CsI plates, which also had a CsI plate inside, opposite a drawn glass nozzle. The inner plate could be cooled with liquid nitrogen and samples sprayed onto the plate via the nozzle. The final recorded spectrum was run after annealing the sample until no further band changes were found. The spectrophotometer employed was a Perkin-Elmer 577 grating one, over the range $200 \rightarrow 4000 \text{ cm}^{-1}$. Band positions were found by expanding the bands and using the wavemarkers positions calibrated from standard spectra. The accuracy of the positions depends on the sharpness of bands.

The Raman spectra were run on a Cary 83 spectrometer from about $100 \rightarrow 4000 \text{ cm}^{-1}$. The instrument has no expansion facility and band positions are only accurate to $\pm 4-8 \text{ cm}^{-1}$. The laser is produced by 488 nm argon excitation. The liquid phase spectra were run by condensing samples into

5 mm glass tubes and sealing off to a length of about 5 cm. The depth of sample was usually about 0.5 cm. This tube could then be positioned in the laser beam. The solid phase spectra were obtained by spraying samples onto a brass plate contained within an evacuated vessel, and cooled by liquid nitrogen. Again annealing was attempted until the bands sharpened appreciably.

Nuclear magnetic resonance spectra were run on either a Bruker WH360 (^1H , ^{13}C , ^{29}Si , ^{31}P) or Varian XL-100 (^{19}F) or Varian HA-100 (^1H) spectrometer. The nmr tubes were 5 mm in diameter and the solvent chosen for its availability, melting point and position of signal in the nmr spectrum. About 2.5 cm depth of solvent was used and the amount of sample was between 0.2-0.3 mmol. Thus the maximum concentration was about 0.75 M.

All the mass spectra were obtained from an AEI MS 902 machine.

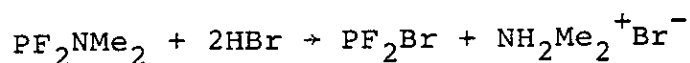
2.3 Preparation of Samples

Below are the preparations carried out in the course of this work. Many are standard reactions and in such cases a reference is given to the original work. More details are given for any new compounds prepared.

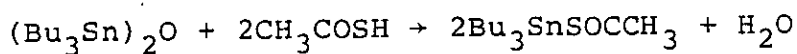
In all the preparations below, purification was achieved by separation of the compounds of different volatilities by low temperature fractional distillation

through one of the trap systems. The temperature of the slush baths used are only included for new preparations and are not given for the standard preparations.

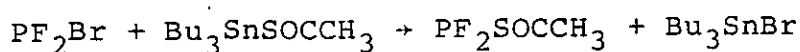
2.3.1 Bromodifluorophosphine: was prepared by condensing HBr and PF_2NMe_2 in the ratio 2:1 into a 3ℓ bulb and leaving at room temperature for ten minutes⁴⁵.



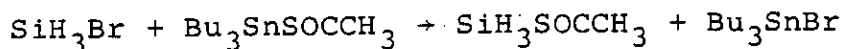
2.3.2 Tributyl tin monothioacetate was prepared by mixing 10 mmol of $(\text{Bu}_3\text{Sn})_2\text{O}$ with 20 mmol of CH_3COSH in 40 ml of toluene and shaking for one minute. The water was then boiled off and toluene removed with a hot water bath and rotary evaporator. The resulting yellow-orange liquid was dried by pumping for 2 hours on the vacuum line.



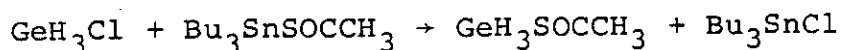
2.3.3 Difluorophosphino monothioacetate was prepared by condensing PF_2Br into dried $\text{Bu}_3\text{SnSOCCH}_3$ and warming to room temperature for one minute. The volatile products were removed by pumping through a 77 K trap for 2 hours and $\text{PF}_2\text{SOCCH}_3$ was found to pass 238 K but stopped in 209 K. The yield was 62%.



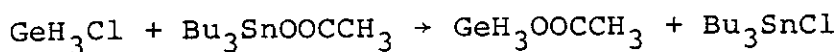
2.3.4. Silyl monothioacetate was prepared by condensing SiH_3Br into $\text{Bu}_3\text{SnSOCCH}_3$ and pumping out the volatile products. This is different from Drake's method³⁰. The product $\text{SiH}_3\text{SOCCH}_3$ was found to pass 258 K but stop in 209 K. Yield was up to 65%.



2.3.5 Germyl monothioacetate - as for silyl monothioacetate but using GeH_3Cl . Yield up to 70% and again not as originally prepared by Drake⁴⁶.



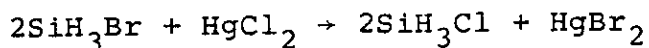
2.3.6 Germyl acetate was prepared by condensing GeH_3Cl on to solid $\text{Bu}_3\text{SnOOCCH}_3$, and removing by pumping. The product $\text{GeH}_3\text{OOCCH}_3$ was involatile at 227 K, and found in a yield of 70%. This is a modification of the method used by Srivastava and Onyszchuk⁴⁷.



2.3.7 Silyl bromide was prepared by a modification to the method of Fritz and Kummer⁴⁸. 50 mmol of phenyl silane and 100 mmol HBr were co-condensed into a 250 ml ampoule fitted with a sovirel tap and immersed in a 195 K bath overnight. Silyl bromide stops in 153 K, but passed 195 K.

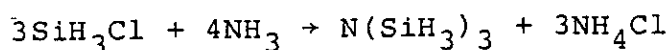


2.3.8 Silyl chloride was prepared by passing a stream of silyl bromide through an excess of HgCl_2 ⁴⁹.



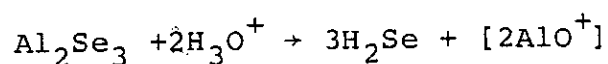
2.3.9 Ammonia was obtained from a cylinder and dried by storing over sodium metal at 195 K.

2.3.10 Trisilylamine was prepared by the reaction of ammonia being sprayed into silyl chloride⁵⁰ using a 2 bulb apparatus.

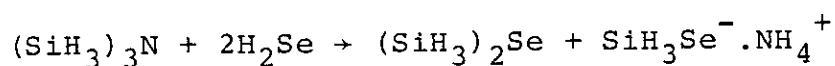


2.3.11 Hydrogen selenide was obtained by the reaction of aluminium selenide and dilute sulphuric acid⁵¹.

The volatile products were passed through a 177 K trap to stop any water but pass H_2Se .



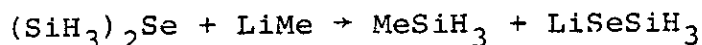
2.3.12 Ammonium silaneselenol is prepared by co-condensing trisilylamine and H_2Se in an ampoule at room temperature for 48 hours⁵². Sufficient material should be used to give a pressure of 2-4 atmospheres, with an excess of H_2Se present.



The volatile products were removed from the ampoule,

leaving white solid $\text{NH}_4\text{SeSiH}_3$ on the walls of the flask.

2.3.13 Lithium silylselenol can be obtained by reaction of the disilyl selenide obtained in 1.3.12 with MeLi ⁵³.



The volatile products were pumped away leaving LiSeSiH_3 in the ampoule as a white solid.

2.3.14 Silyl monoselenoacetate was prepared by condensing dry degassed acetyl chloride onto $\text{NH}_4\text{SeSiH}_3$ ^{52,53}.

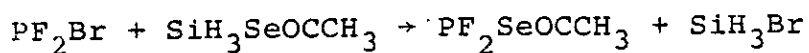
As the mixture is warmed to room temperature a yellow liquid forms which contains the $\text{SiH}_3\text{SeOCCH}_3$.



Alternatively the same product can be obtained by the reaction of the lithium silyl selenol and acetyl chloride⁵³.



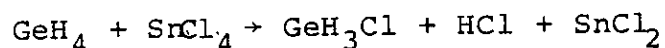
2.3.15 Difluorophosphine monoselenoacetate was first obtained in an nmr tube by the equimolar reaction of PF_2Br with $\text{SiH}_3\text{SeOCCH}_3$. The products, all observed in the ³¹P nmr spectrum, were initially only $\text{PF}_2\text{SeOCCH}_3$, but this rapidly decomposed to PF_3 , $\text{PF}_2\text{SeSiH}_3$, $(\text{PF}_2)_2\text{O}$, $(\text{PF}_2)_2\text{Se}$ and HPF_2O . See Chapter 3 for a further discussion of this reaction.



2.3.16 Germane was prepared by the reduction of a basic solution of germanium dioxide with KBH_4 in acetic acid⁵⁴.

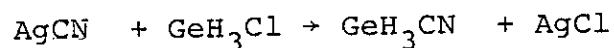


2.3.17 Germyl chloride was prepared by chlorination of germane using stannic chloride⁵⁵.



A slight excess of germane must be present to avoid dichlorogermane forming.

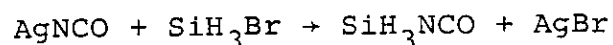
2.3.18 Germyl cyanide was prepared by condensing germyl chloride in 1-2 mmol portions onto dry silver cyanide in an ampoule⁵⁶.



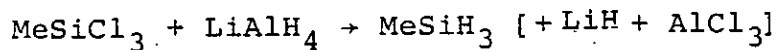
2.3.19 Germyl isothiocyanate was prepared by the reaction of germyl chloride on silver isothiocyanate⁵⁷.



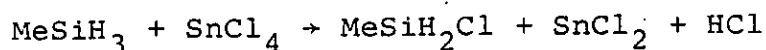
2.3.20 Silyl isocyanate was prepared by the reaction of silyl bromide with silver isocyanate⁵⁸.



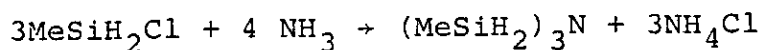
2.3.21 Methyl silane was prepared by the reduction of trichloromethyl silane with LiAlH_4 in the analogous reaction for the preparation of silane⁵⁹.



2.3.22 Methyl silyl chloride was obtained by the chlorination of methyl silane with stannic chloride⁶⁰.



2.3.23 Tris monomethyl silyl amine was prepared by streaming ammonia into a slight excess of methyl silyl chloride, and leaving overnight at room temperature⁶¹. Some $(\text{MeSiH}_2)_2\text{NH}$ was usually formed but need not be removed as it acts in all subsequent reactions, just as the tris amine.

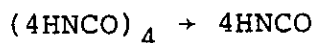


2.3.24 Methyl silyl bromide was obtained by reacting HBr with $(\text{MeSiH}_2)_3\text{N}$, and leaving at room temperature for 30 minutes.



Methyl silyl iodide can be obtained in the same way using HI instead of HBr.

2.3.25 Isocyanic acid was obtained by subliming $(\text{HNCO})_4$ at reduced pressure on the vacuum line.



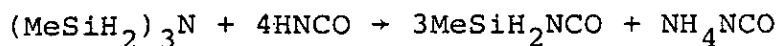
2.3.26 Silver cyanide was precipitated by mixing solutions of silver nitrate and potassium cyanide. After filtering the white solid was washed with water and then portions of ethanol followed by "blue" label ether. To fully dry the salt, it was placed in an ampoule and pumped out overnight. To reduce decomposition of the silver cyanide by sunlight, the salt was stored in a dark cupboard or surrounded by metal foil. It was found that washing with acetone severely reduced the subsequent yield of the methyl silyl cyanide.

2.3.27 Silver isocyanate and isothiocyanate were prepared in the same way as silver cyanide but starting with potassium isocyanate or potassium isothiocyanate.

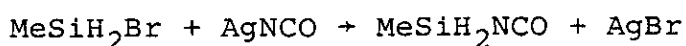
2.3.28 Methyl silyl isocyanate was prepared in two ways.

(i) The most successful route was by the reaction between tris(methylsilyl)amine and HNCO using a two-bulb apparatus streaming the HNCO into the amine. After two hours at room temperature the reaction was complete with all the amine reacted. Fractionation through a trap at 195 K stopped most of the methyl silyl isocyanate, and passed HNCO. However complete separation was difficult

and the final portion of HNCO was removed by the addition of small amounts of tin(methylsilyl)amine and leaving the reactants for 1½ hours. Yield was 90%.



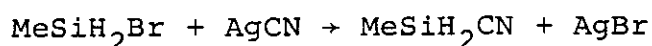
(ii) The reactions between AgNCO and MeSiH₂Br or MeSiH₂I all gave a mixture of mono and bis isocyanate with much H₂ formed, deduced from the quantity of involatile product formed. The bis product was identified from the infra-red spectrum and the high molecular weight value calculated. Separation of MeSiH₂NCO and MeSiH(NCO)₂ by fractional distillation proved difficult and was never complete. The characteristic band in the infra-red, assigned to MeSiH(NCO)₂ was the SiH deformation at 880 cm⁻¹, while the SiH₂ modes observed in that region should occur at 960 and 910 cm⁻¹.



2.3.29 Methyl silyl isothiocyanate was prepared by the reaction of methyl silyl bromide and silver isothiocyanate. A three-fold excess of AgNCS was placed in an ampoule and dried overnight by pumping. Portions of MeSiH₂Br were condensed in 1.5 mmol at a time, warmed to room temperature and then the volatile products were removed by pumping through a trap cooled to 77 K.

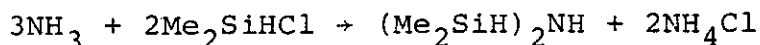
Fractionation through 209 K trap, passed MeSiH_3 and $(\text{MeSiH}_2)_2\text{O}$ and stopped MeSiH_2NCS . The final yield was 80%.

2.3.30 Methyl silyl cyanide was first prepared by Emeleus, Onyszchuk and Kuchen by condensing MeSiH_2I onto dry AgCN ⁶² but the yield can be vastly improved if MeSiH_2Br is used. Less HCN is formed and the yield was up to 70%.



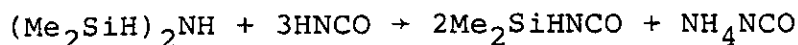
2.3.31 Dimethyl silyl chloride was obtained commercially and before using was degassed thoroughly, and passed through a 177 K slush bath to remove any HCl .

2.3.32 Bis(dimethylsilyl)amine was prepared by streaming ammonia into dimethyl silyl chloride⁶³ and leaving at room temperature overnight. Fractionation at 227 K passed unreacted Me_2SiHCl but stopped the amine.

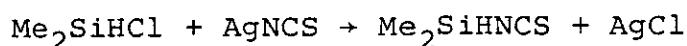


2.3.33 Dimethyl silyl isocyanate was prepared by streaming a slight excess of HNCO into bis(dimethylsilyl)amine using a 2-bulb apparatus. To achieve a greater dispersion of the relatively involatile amine it was necessary to tip the reaction bulb around and spread the amine over a larger surface area. The reaction was only complete after

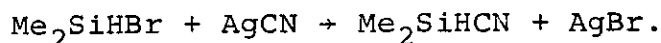
3-4 hours. Again separation of the Me_2SiHNCO and HNCO was difficult by fractionation and so the excess HNCO was removed by the addition of small portions of $(\text{Me}_2\text{SiH})_2\text{NH}$. The eventual yield was 80%.



2.3.34 Dimethyl silyl isothiocyanate was prepared by condensing Me_2SiHCl onto dry AgNCS and leaving at room temperature for $2\frac{1}{2}$ hours. When the volatile products were pumped out and passed through a trap at 227 K, unreacted Me_2SiHCl passed and Me_2SiHNCS stopped. The yield was about 65%.

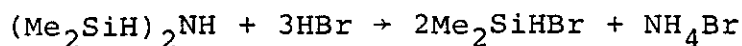


2.3.35 Dimethyl silyl cyanide was first prepared by Durig⁶⁴ from the reaction of Me_2SiHCl and AgCN in ether. The mixture was stirred for 36 hours and then fractionated. This gave a yield of 48%. However the reaction of Me_2SiHBr and dry AgCN gave almost complete conversion to the desired product and with a reaction time of 1-2 minutes.



2.3.36 Dimethyl silyl bromide can be obtained by the reaction of $(\text{Me}_2\text{SiH}_2)\text{NH}$ and HBr using a 2-bulb apparatus.

with a reaction time of 2-3 hours. Fractionation through a trap held at 195 K stopped the Me_2SiHBr but passed the excess HBr .



2.4 Physical Properties of the New Compounds Prepared

This section contains data for colour and physical appearance, vapour pressure, exact mass measurement from mass spectrum where possible, and calculated molecular weight of the compounds previously uncharacterised. A full discussion of the infra-red spectra is given in later chapters for each compound.

2.4.1 Difluorophosphino monothioacetate: This is a yellow liquid, white when frozen, with a vapour pressure of 39 mmHg at 273.K. The molecular weight was 142.8g (cf. theoretical value of 143.9g), and from the mass spectrum the parent ion was 143.961310g (error of 2 ppm).

2.4.2 Difluorophosphino monoselenoacetate: Very little information is available for this compound due to its instability. It appeared to be a reddish-yellow compound fairly involatile (a vapour pressure at 273 K <20 mmHg), and decomposed readily to leave selenium deposited on the glassware.

2.4.3 Monomethyl silyl isocyanate: A white compound observed to form long spindle-like crystals on the inside of the traps. These are likely to be due to formation of SiNCO chains between adjacent molecules. The vapour pressure at 273 K was 87 mmHg and the parent ion in the mass spectrum was at 87_g which excludes possible structures such as MeSiH(NCO)₂, but no exact mass measurement was made.

2.4.4 Monomethyl silyl isothiocyanate: This was also found to give long crystals; some up to 6 mm long, but had a much lower vapour pressure of 18 mmHg at 291 K. As a liquid and solid there was a faint yellow colour.

2.4.5 Dimethyl silyl isocyanate: This had a vapour pressure of 40 mmHg at 289 K and showed signs of some intermolecular interactions but the crystals were less well defined.

2.4.6 Dimethyl silyl isothiocyanate: This was the least volatile sample prepared and moved very slowly around the vacuum line. The measured vapour pressure was 7.7 mmHg at 289 K.

Accuracy of Results: For the more volatile compounds, molecular weight calculations were reasonably accurate because a greater amount of sample could be expanded into the bulb and so give a greater weight difference. Also since the pressure is accurate to ± 2 mmHg, the temperature to ± 0.5 K and zeroing the spiral to ± 1.5 mmHg, a small vapour pressure will be lost in the errors.

CHAPTER 3: DIFLUOROPHOSPHINO, SILYL AND GERMYL ESTERS

3.1 Introduction

Over the last few years some work has been done on a number of germyl and silyl acetates and monothioacetates. The interest in these studies has been to find out more about the bonding between the oxygen or sulphur atoms of the acetates and the silicon or germanium atoms. Drake⁴⁶ and co-workers found that germyl and trimethyl germyl monothioacetates were entirely in the form with germanium bonded to sulphur in contrast to the silyl and trimethylsilyl monothioacetates which were bonded through the oxygen in the thiono form.

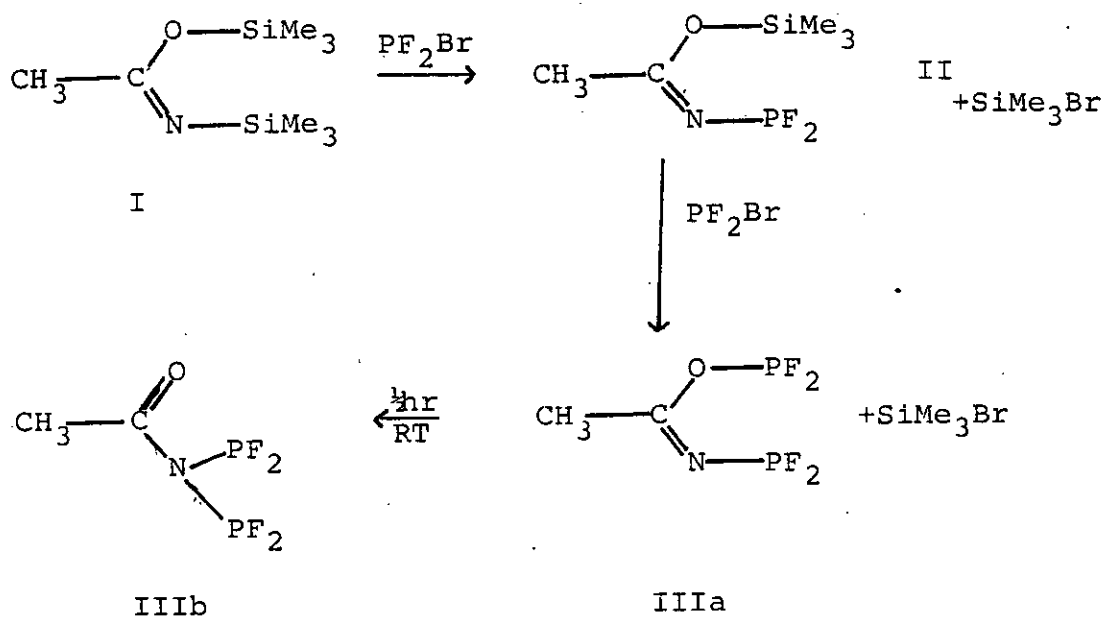
These investigations were carried out using infra-red, Raman and nmr techniques. More recently the structures of $\text{CH}_3\text{COOSiH}_3$ ⁴⁴ and HCOOSiH_3 ⁶⁵ have been studied in the gas and solid phases and it was found that there is a very short non-bonded distance between the silicon atom and oxygen of the carbonyl group; for example in $\text{CH}_3\text{COOSiH}_3$ the sum of the van der Waals' radii of Si and O is 350 pm, while the interatomic distance is 283.2 pm and 279.5 pm in the solid and gas phases respectively.

Hence it was decided that a further study of esters would be attempted, involving the monothioacetate and monoselenoacetate with silyl, difluorophosphino and germyl groups. The formation of these esters would be followed to

see if the short non-bonded distances of Si and Ge to S or O found in acetates and formates are found in monothioacetates.

When Drake studied the germyl and silyl thioacetates he found that a single isomer was formed in each case and he could see no evidence for exchange of bonding site. In this work the formation of the esters at low temperatures has been studied using nmr spectroscopy.

This technique was used to look at the reaction of PF_2Br and bis(trimethylsilyl)acetamide⁶⁶, by observing the shift of the signal in the ^{31}P spectrum as PF_2 shifted from O to N bonding. The steps in the rearrangement are shown below:



Structure (II) is formed with equimolar quantities of PF_2Br and (I). With excess PF_2Br the product is (IIIa) which when left at room temperature for half an hour



rearranges to (IIIb). The nmr spectrum indicated that there was about three times as much of (IIIb) as (IIIa) at equilibrium.

At room temperature there is rapid exchange of the trimethylsilyl groups of structure (I) between the O and N sites, while at low temperatures the exchange is slow enough on the ^1H nmr timescale for two separate resonances to be observed. However with the products II, IIIa and IIIb, no exchange of bonding site of the $-\text{PF}_2$ group from N to O was observed.

3.2 Difluorophosphino monothioacetate

3.2.1 Infra-red and Raman spectroscopy:

The first infra-red spectrum of observed $\text{CH}_3\text{C}(\text{OS})\text{PF}_2$ was run after a number of fractionations to remove PF_2Br and PF_3 . This showed a strong band in the carbonyl stretching region, seven bands between 1450 and 800 cm^{-1} and a number of weaker bands below 600 cm^{-1} . The presence of the carbonyl band is indicative of the phosphorus being bonded through the sulphur but does not exclude there being some isomer of phosphorus bonded to the oxygen. Further ir spectra were run using new freshly prepared $\text{CH}_3\text{C}(\text{OS})\text{PF}_2$, and these spectra show very weak carbonyl bands which over 30-40 minutes at room temperature increased in intensity. This suggests the $-\text{PF}_2$ group is initially bonded to the oxygen but exchanges site to give

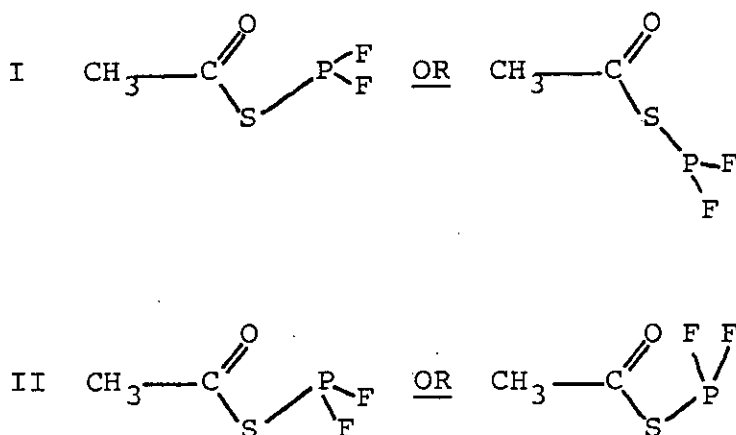
some sulphur bonded species. See section 3.2.2 dealing with the exchange of bonding site followed by ^{31}P nmr.

The assignment of the infra-red bands was done by comparison with other difluorophosphino compounds, thioacetic acid, and silyl and germyl monothioacetate. The bands at 1442 and 1377 cm^{-1} are characteristic of methyl deformations in all the esters, and those at 869 and 846 are the P-F asymmetric and symmetric stretches. The thioacetate skeletal modes are at 1131, 1004, 925 cm^{-1} (ρCH_3) and 977 cm^{-1} ($\nu(\text{C-C})$). These all appear in silyl esters and thioacetic acid. In the infra-red there are two strong bands between 1200-1300 cm^{-1} , which in the Raman appear as one strong band at 1265 cm^{-1} , and one weak band at 1210 cm^{-1} . By comparison with silyl and trimethylsilyl thioacetate³⁰, which are both O bonded species, the C-O stretch is found to be strong in the Raman spectrum but weaker in the infra-red and hence assigned to 1265 cm^{-1} , leaving the C=S stretch assigned to the band at 1210 cm^{-1} . Above 600 cm^{-1} , there are two bands unassigned. The band at 620 cm^{-1} appears to vary in intensity with the carbonyl band and is very strong in the liquid Raman spectra. A likely assignment is to the C-S stretch which is only present when conversion to S-PF₂ bonded species takes place, and this compares favourably with the position of the C-S band of thioacetic acid at 626 cm^{-1} , also of medium intensity in the infra-red but very strong in the Raman. Additionally, the germyl thioacetates⁴⁶ (which are S-

bonded) have C-S stretches at 625 and 637 cm^{-1} . Finally, the P-O stretch is assigned to the band at 692 cm^{-1} . This is a relatively intense band in the Raman spectrum, is present in $\text{CH}_3\text{COOPF}_2$ (although slightly higher at 770 cm^{-1}) and is in $(\text{PF}_2)_2\text{O}$ ⁶⁷ at 682 cm^{-1} .

Assignment below 600 cm^{-1} cannot be conclusive, although the bands at 461 and 370 cm^{-1} seem to be characteristic of the deformation and wagging modes of the $-\text{PF}_2$ group.

The solid phase infra-red spectra show a number of significant changes. The carbonyl bands now split to give bands at 1745 and 1680 cm^{-1} which are believed to be due to different conformations of the S-bonded species being frozen out. These could either be 2 conformers by a twist around the C-S bond (I) or by 2 conformers by a twist around the S-P bond (II).



With the data available it is not possible to say which set of conformers is present. However, in $\text{CH}_3\text{COOSiH}_3$ ⁴⁴ and $\text{CH}_3\text{C}(\text{OS})\text{SiH}_3$ ⁶⁸ only the cis conformers are found in the

solid phase so assuming the same applies to the more bulky -PF_2 groups, conformers II are more likely to be present. Also this would be consistent with a relatively strong P...O intramolecular interaction being present which would have to be broken in conformer I.

The bands at 461 and 370 cm^{-1} previously assigned to PF_2 deformation modes each split, which must be either due to two conformers freezing out or could be a crystal packing effect with molecules in different sites. Lastly the strong band at 855 cm^{-1} assigned to the P-F stretch in the gas phase is found to shift in the solid phase to 810 cm^{-1} . This shift of 30-40 cm^{-1} is found for many PF_2 compounds including $(\text{PF}_2)_2\text{O}$ ⁶⁷ and $(\text{PF}_2)_2\text{S}$ ⁶⁹.

All these assignments are listed in Table 3.1, for the gas and solid phase infra-red, and liquid phase Raman spectra and the spectra are shown in Figures 3.1, 3.2 and 3.3.

The conversion from entirely O-bonded thioacetate to some S-bonded species can be followed by infra-red spectroscopy. A portion of freshly prepared sample was expanded into a gas cell and a spectrum run immediately. Already on the first spectrum a weak band at 1750 cm^{-1} could be seen, and this could be observed increasing in intensity over 2 hours, while the gas cell was held at room temperature. Table 3.2 below gives the relative intensity of the band with respect to the methyl deformation band at 1370 cm^{-1} . The C-S stretch was found to increase in intensity with the carbonyl band, but no other significant

Table 3.1: Observed frequencies and assignments of $\text{CH}_3\text{C}(\text{OS})\text{PF}_2$

Ir gas/ cm^{-1}	Ir solid/ cm^{-1}	Raman (liquid)/ cm^{-1}	Assignment
3036 vw			$\nu(\text{C-H})$ asym
2982 vw		2940 m	$\nu(\text{C-H})$ sym
1747 s	1745 m	1720 broad w	$\nu(\text{C=O})$
	1680 s		$\nu(\text{C=O})$
1442 w	1427 m	1435 w	δCH_3 asym
1377 m	1364 m	1375 m	δCH_3 sym
	1314 w		δCH_3 sym
1271 s	1256 s	1265 vs	$\nu(\text{C-O})$
1207 s	1213 s	1210 w	$\nu(\text{C=S})$
1131 s	1143 s	1140 w	ρCH_3
1004 s	997 s	1005 m	ρCH_3
977 s	951 s		$\nu(\text{C-C})$
925 w	908 w		ρCH_3
892 w			PF_3 [impurity]
869 vs	849 vs (br)	860 broad s	$\nu(\text{P-F})$ asym
848 vs			$\nu(\text{P-F})$ sym
815 s	810 vs	810 m	CH_3 mode
784 w	749 w	745 vw	(combination?)
692 m	693 m	702 vvs	$\nu(\text{P-O})$
620 m	638 m	635 vs	$\nu(\text{C-S})$
513 w	519 w	530 w	
	511 w	510 s	
480 w			
461 m	466)m	[460 s]	skeletal modes (see text)
	457)m	[455 shoulder m]	
	430 w		
	395 w	400 w	
	{380 w	360 w	
370 m	(355 m	315 m	
		270 w	

w = weak, s = strong, m = medium, v = very

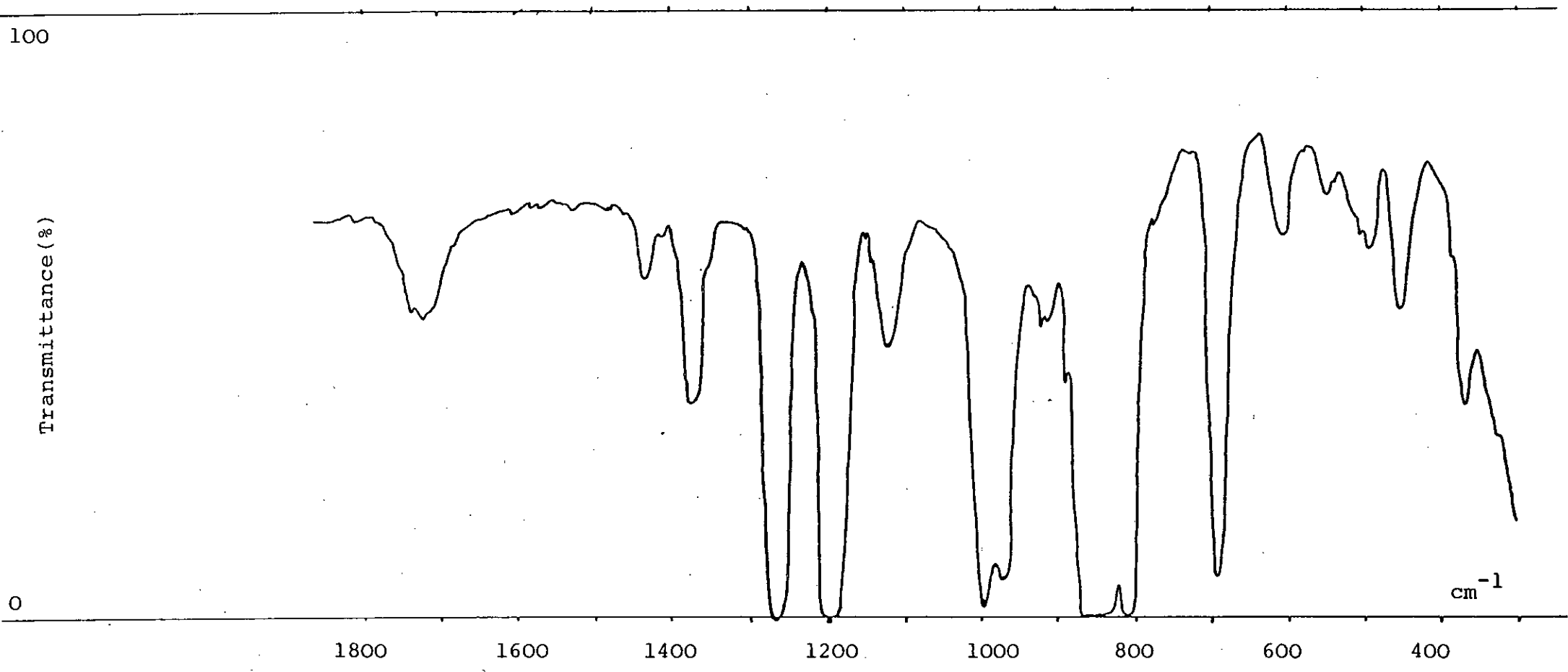


Figure 3.1: Infra-red spectrum of an equilibrium sample of $\text{CH}_3\text{C}(\text{OS})\text{PF}_2$ in the gas phase (25 mmHg pressure)

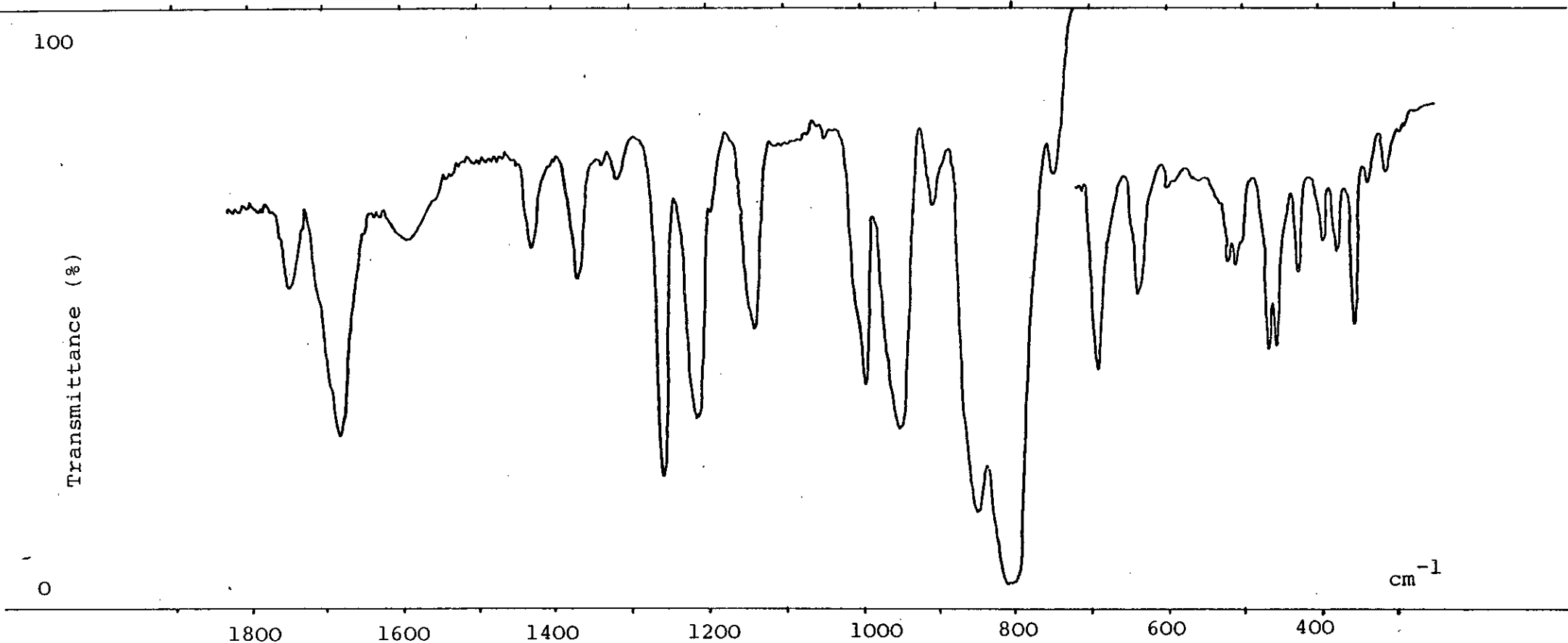


Figure 3.2: Infra-red spectrum of $\text{CH}_3\text{C}(\text{OS})\text{PF}_2$ in the solid phase, after previously being allowed to reach equilibrium between O and S bonded isomers in the gas phase

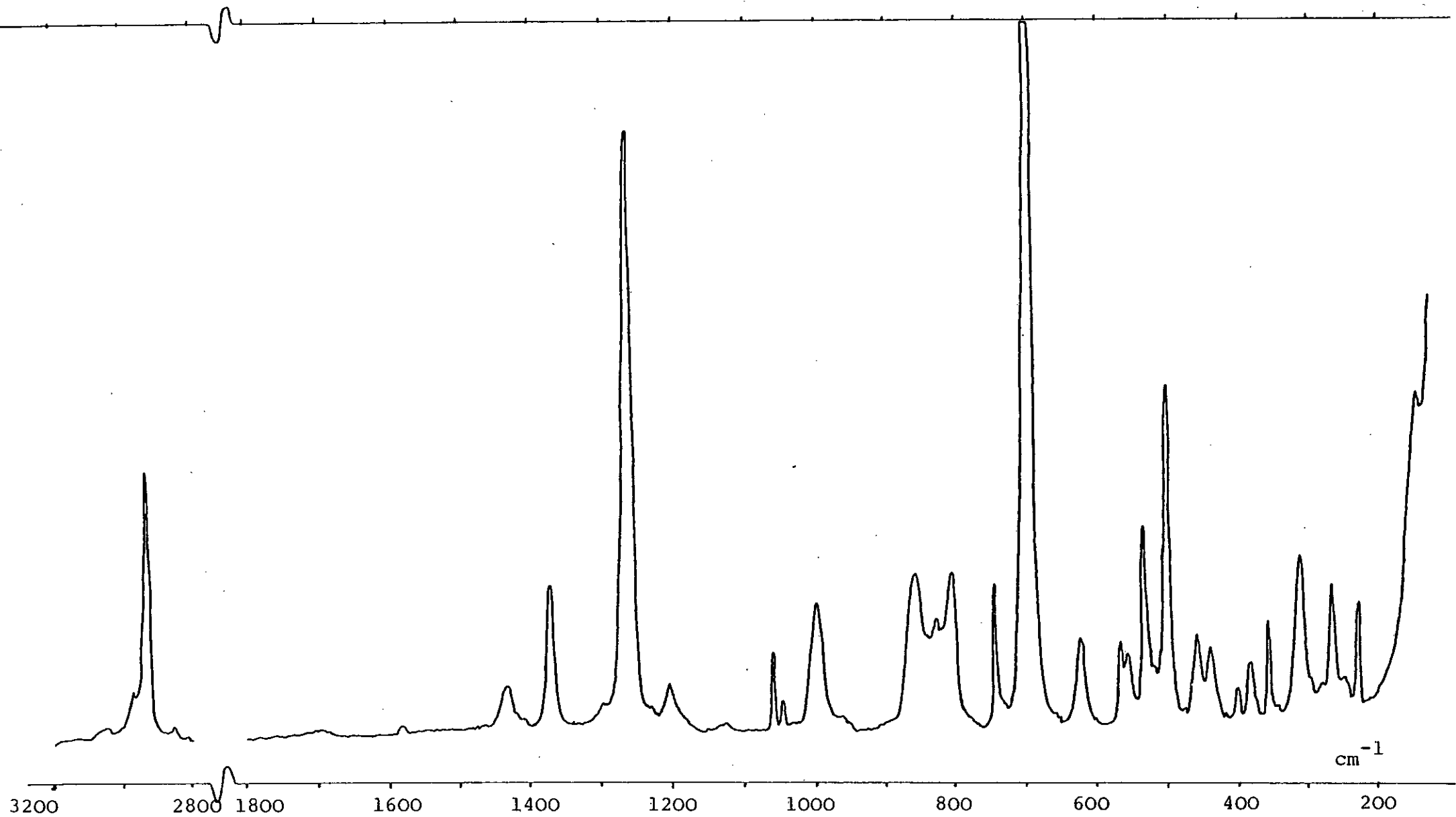


Figure 3.3: Raman spectrum of $\text{CH}_3\text{C}(\text{OS})\text{PF}_2$ in the liquid phase at equilibrium

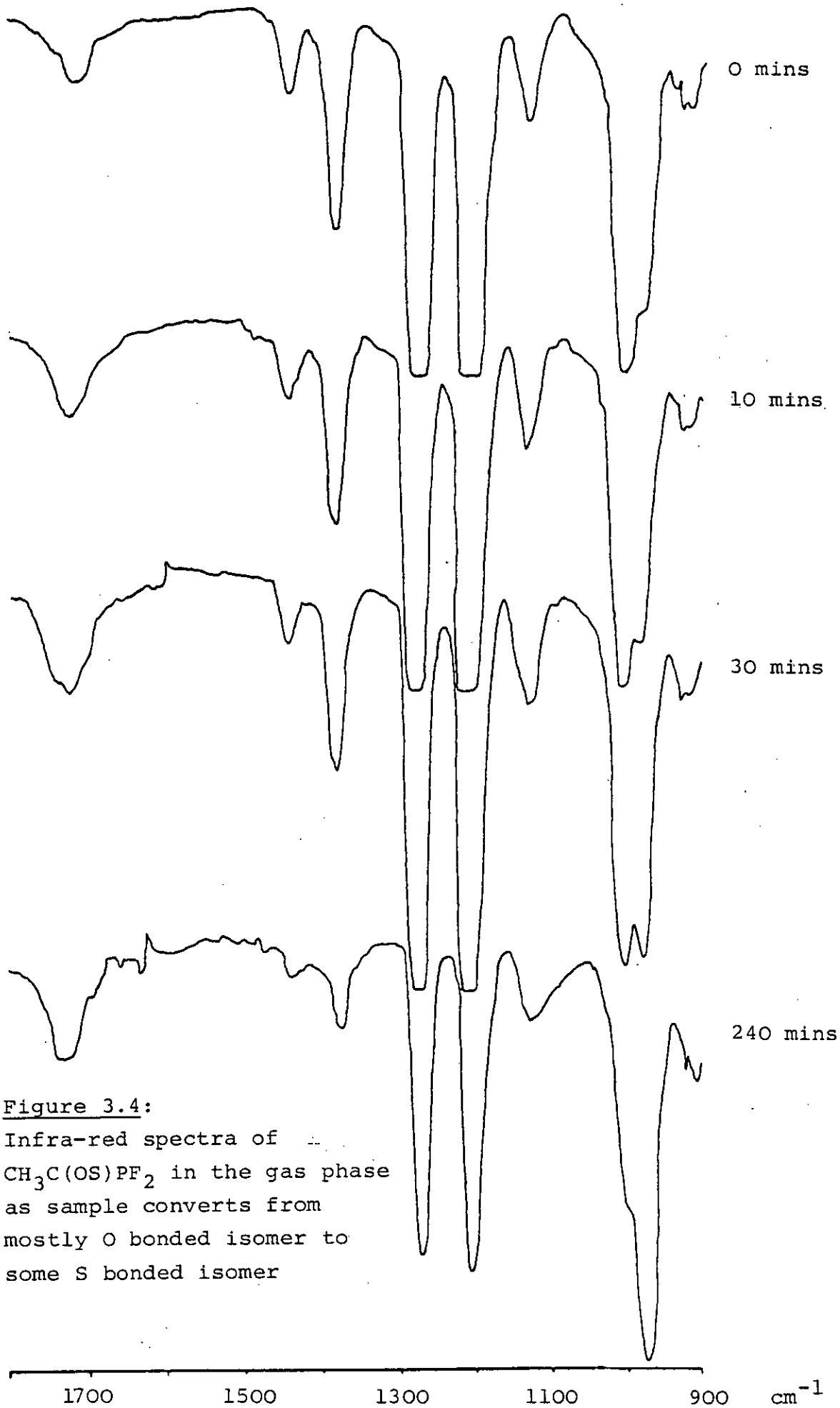


Figure 3.4:
Infra-red spectra of $\text{CH}_3\text{C}(\text{OS})\text{PF}_2$ in the gas phase
as sample converts from
mostly O bonded isomer to
some S bonded isomer

changes were found.

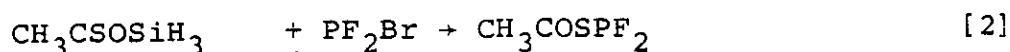
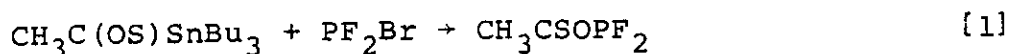
Table 3.2: Table of ratio of intensities of (C=O) band to δCH_3

Time at room temperature/ minutes	Intensity ^a		Ratio $\nu(\text{C=O})$: δCH_3
	$\nu(\text{C=O})$	δCH_3	
0	0.192	0.885	0.22 :1
3.5	0.231	0.847	0.273 :1
8	0.211	0.758	0.279 :1
30	0.292	0.754	0.388 :1
40	0.293	0.477	0.61 :1
120	0.297	0.585	0.51 :1
18 hrs @ 10°C	0.241	0.223	1.08 :1
Warmed to 20°C	1.44	0.693	2.0 :1

^aIntensity $\propto \log I/I_0$

3.2.2 Nuclear magnetic resonance spectra of $\text{CH}_3\text{C}(\text{OS})\text{PF}_2$

The formation of $\text{CH}_3\text{C}(\text{OS})\text{PF}_2$ has been studied by following two different reactions using ^{31}P nmr. It was found that a fresh sample made from tributyl tin monothioacetate gave an O-bonded species that slowly converted to some S-bonded, while the formation from $\text{CH}_3\text{C}(\text{OS})\text{SiH}_3$ gave an exclusively S-bonded species first which then converted to mostly O-bonded.



The sample from reaction 1 was run at 193 K initially and only one triplet was observed at 114.5 ppm ($^1J_{\text{PF}} = 1343$ Hz), which was assigned to the $\text{CH}_3\text{CSOPF}_2$ species, by comparison with $(\text{PF}_2)_2\text{O}$ ⁶⁷. No change in the spectrum was found until the tube reached 243 K, when a second triplet at 211.5 ppm ($^1J_{\text{PF}} = 1269$ Hz) appeared. The tube was then left to equilibrate at this temperature and the integrals of the triplets recorded. Further spectra were run from 243 to 308 K in steps of 10 K in order to watch the increase of the second isomer. The chemical shift of the second triplet is close to that of $(\text{PF}_2)_2\text{S}$ ⁵⁴ and is assigned to $\text{CH}_3\text{COSPF}_2$. Table 3.3 gives the positions of the triplets at the various temperatures and the relative integral values

Table 3.3: Relative intensities of O and S bonded $\text{CH}_3\text{C}(\text{SO})\text{PF}_2$ formed from $\text{CH}_3\text{COSSnBu}_3 + \text{PF}_2\text{Br}$

Temp/K	Chemical Shift ppm		Ratio	
	OPF ₂	SPF ₂	OPF ₂	: SPF ₂
193	114.5	n.o.	∞	: 1
243	115.1	211.5	19.0	: 1
253	115.2	211.7	11.9	: 1
263	115.3	212.0	6.3	: 1
263*	115.7	213.7	5.4	: 1
273	115.4	212.3	5.4	: 1
283	115.5	212.6	4.8	: 1
293	115.6	212.8	4.5	: 1
308	115.8	213.9	4.3	: 1

*left overnight at this temperature

n.o. not observed

The tube was held at 263 K overnight to see if equilibrium was being reached in the course of the experiment. As the table shows, there was no change in the relative proportions of the O and S bonded species after 10 hours. The compound appears to be fairly stable although when left overnight at room temperature some decomposition to PF_3 and $(\text{PF}_2)_2\text{O}$ was evident.

The reaction between PF_2Br and $\text{CH}_3\text{CSOSiH}_3$ (equation [2]) gave a product at 193 K showing a single triplet at 209.9 ppm ($^1J_{\text{PF}} = 1269$ Hz) in the ^{31}P nmr spectrum which is assigned to the S-bonded species. On warming to 213 K no exchange of site of $-\text{PF}_2$ group was observed but more PF_2Br was consumed. However at 228 K a second triplet appeared at 114.9 ppm ($^1J_{\text{PF}} = 1342$ Hz), which is assigned to the O-bonded species. No more PF_2Br was consumed because the ratio of PF_2Br to $\text{CH}_3\text{COSPF}_2$ at 213 K was the same as the ratio of PF_2Br to the sum of $\text{CH}_3\text{COSPF}_2$ and $\text{CH}_3\text{CSOPF}_2$ at 228 K.

As this reaction was warmed to room temperature the exchange of the $-\text{PF}_2$ site continued until the final equilibrium position was the same as for the sample prepared from the $\text{CH}_3\text{COSSnBu}_3$ derivative. Both tubes were left overnight at 263 K and the ratio of O-bonded to S-bonded species was about the same.

The assignment of the ^{31}P nmr is relatively straightforward as the chemical shift of the signal is very characteristic of the atom adjacent to the PF_2 group.

Figure 3.5a: $\text{CH}_3\text{C}(\text{OS})\text{PF}_2$

^{31}P spectrum of fresh sample at 193 K

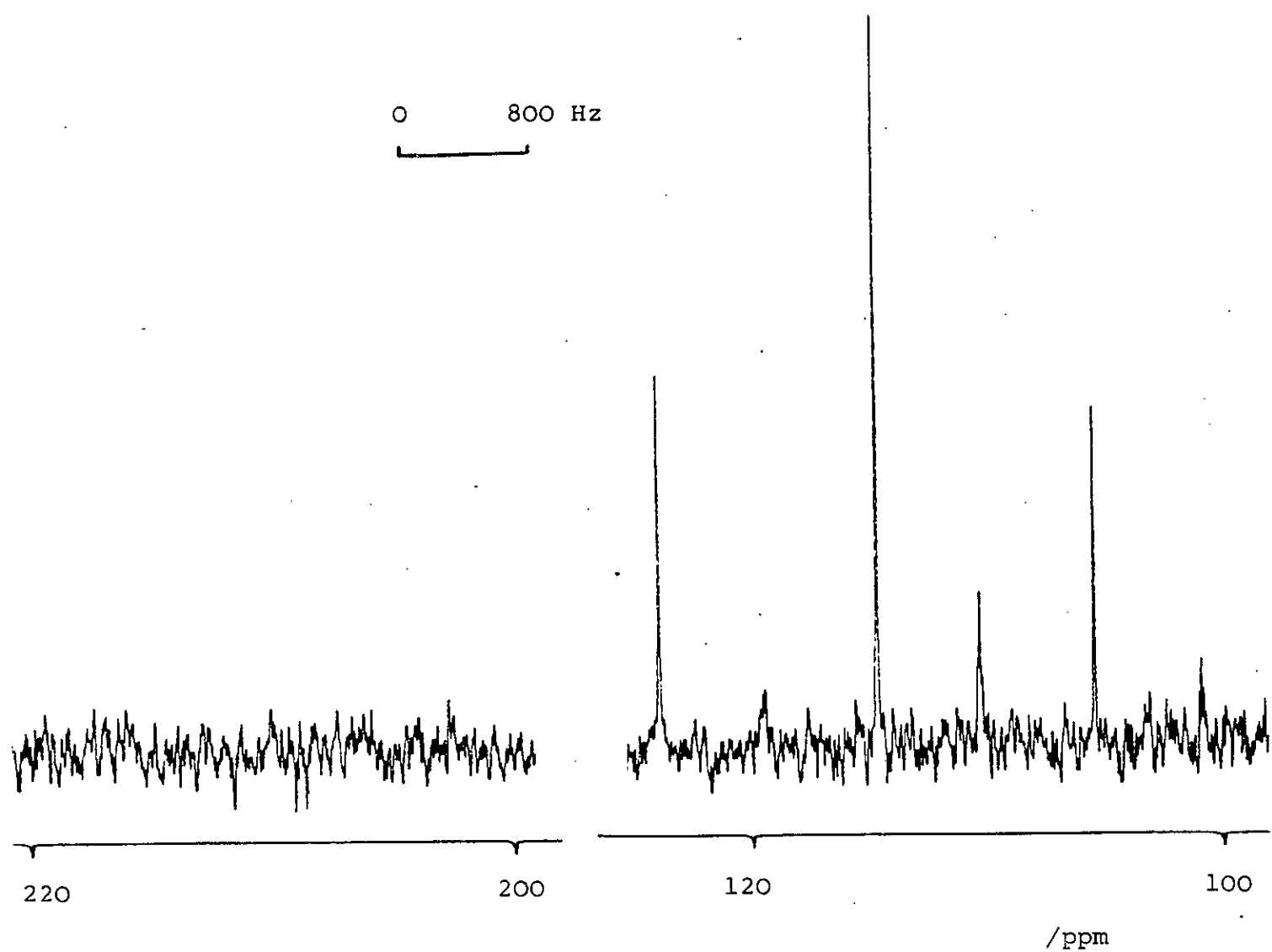


Figure 3.5b: $\text{CH}_3\text{C}(\text{OS})\text{PF}_2$

^{31}P nmr spectrum of fresh sample
warmed to 243 K.

* PF_2Br

+ $(\text{PF}_2)_2\text{O}$

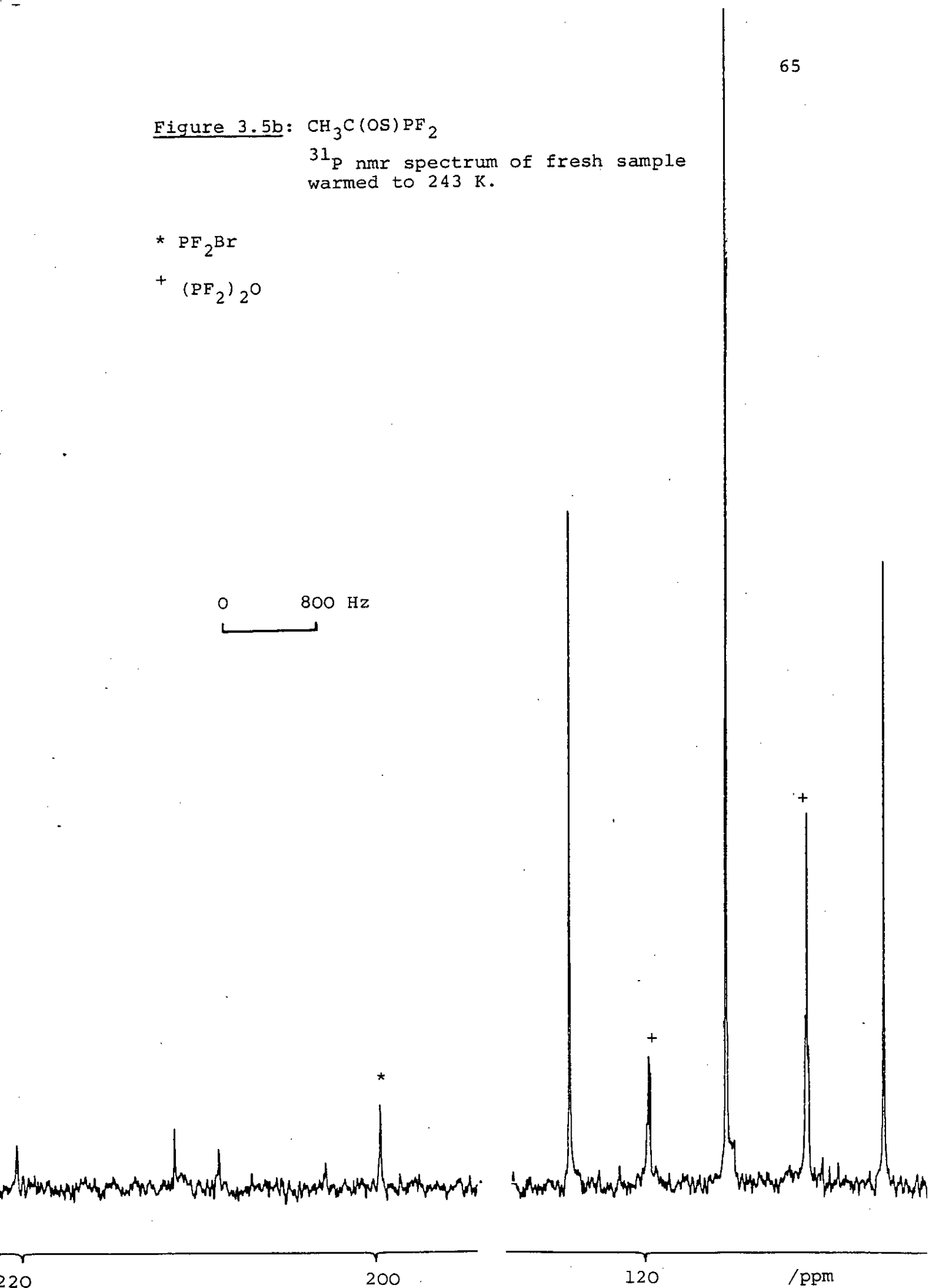


Figure 3.5c: $\text{CH}_3\text{C}(\text{OS})\text{PF}_2$

^{31}P nmr spectrum of fresh sample warmed to 283 K.

* PF_2Br

+ $(\text{PF}_2)_2\text{O}$

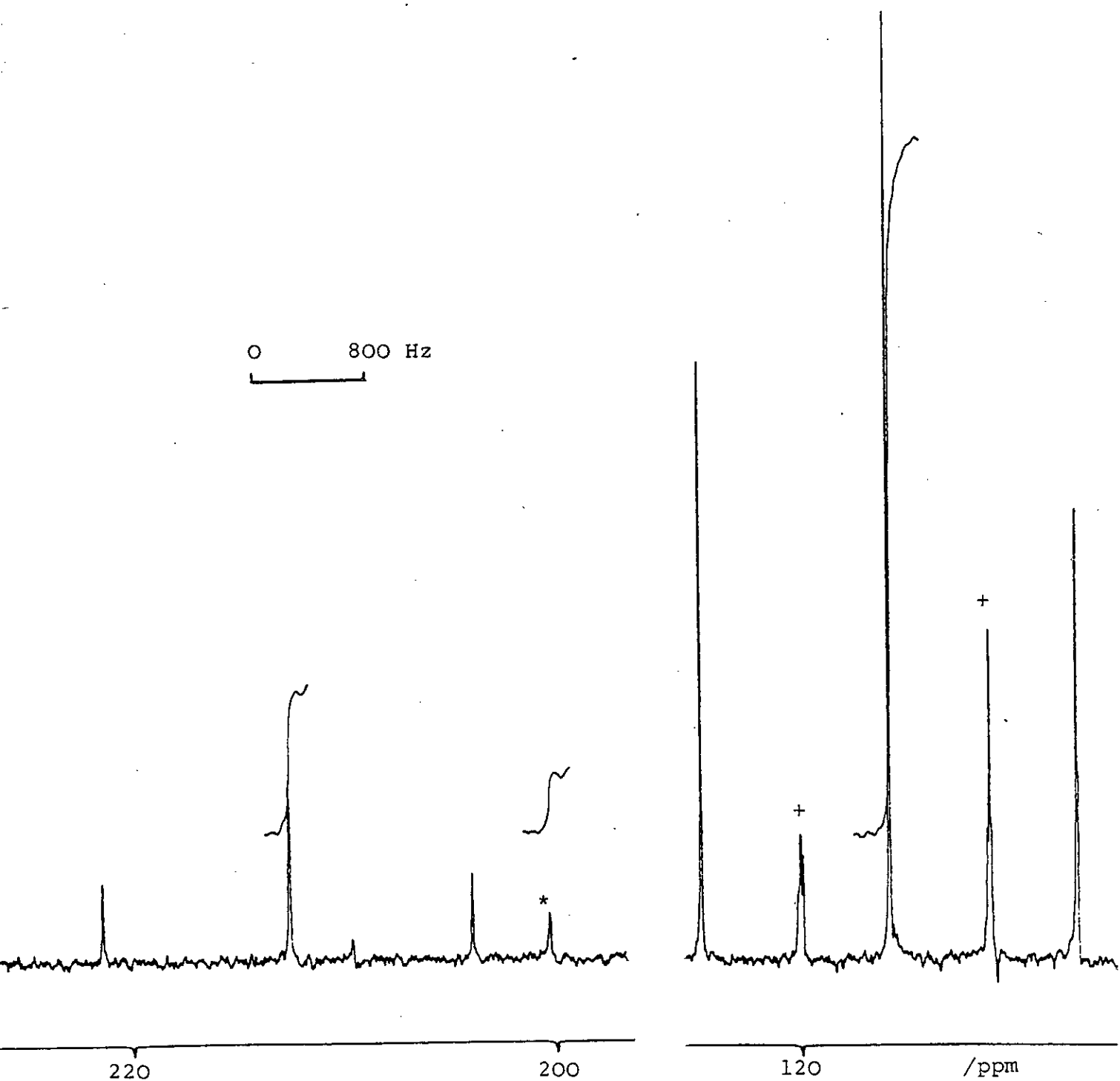


Figure 3.5d: $\text{CH}_3\text{C}(\text{OS})\text{PF}_2$

^{31}P nmr spectrum of fresh sample warmed to 298 K

* $(\text{PF}_2)_2\text{O}$

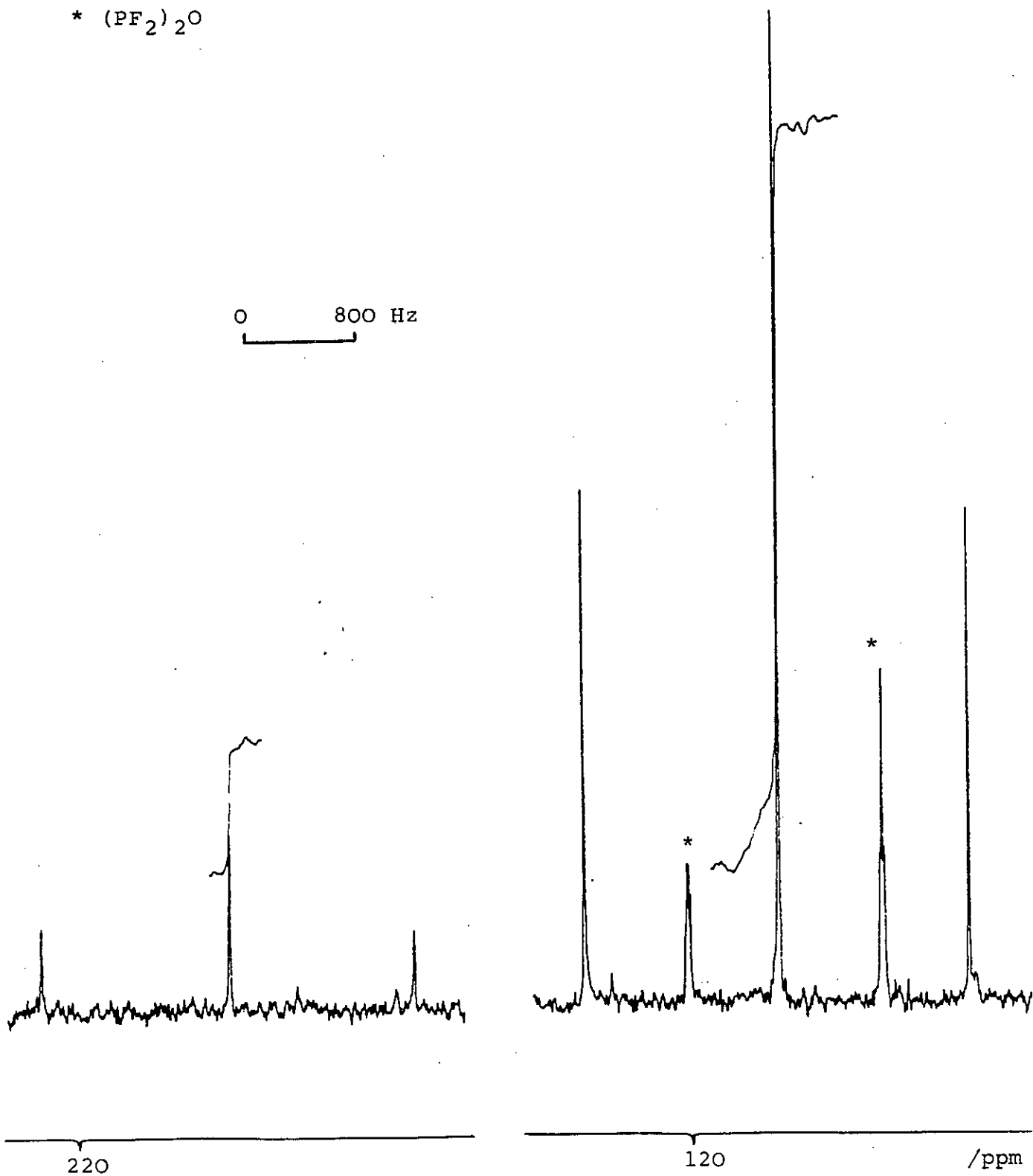


Figure 3.5e: $\text{CH}_3\text{C}(\text{OS})\text{PF}_2$

^{31}P nmr spectrum of fresh sample
warmed to 308 K

* PF_2Br

+ $(\text{PF}_2)_2\text{O}$

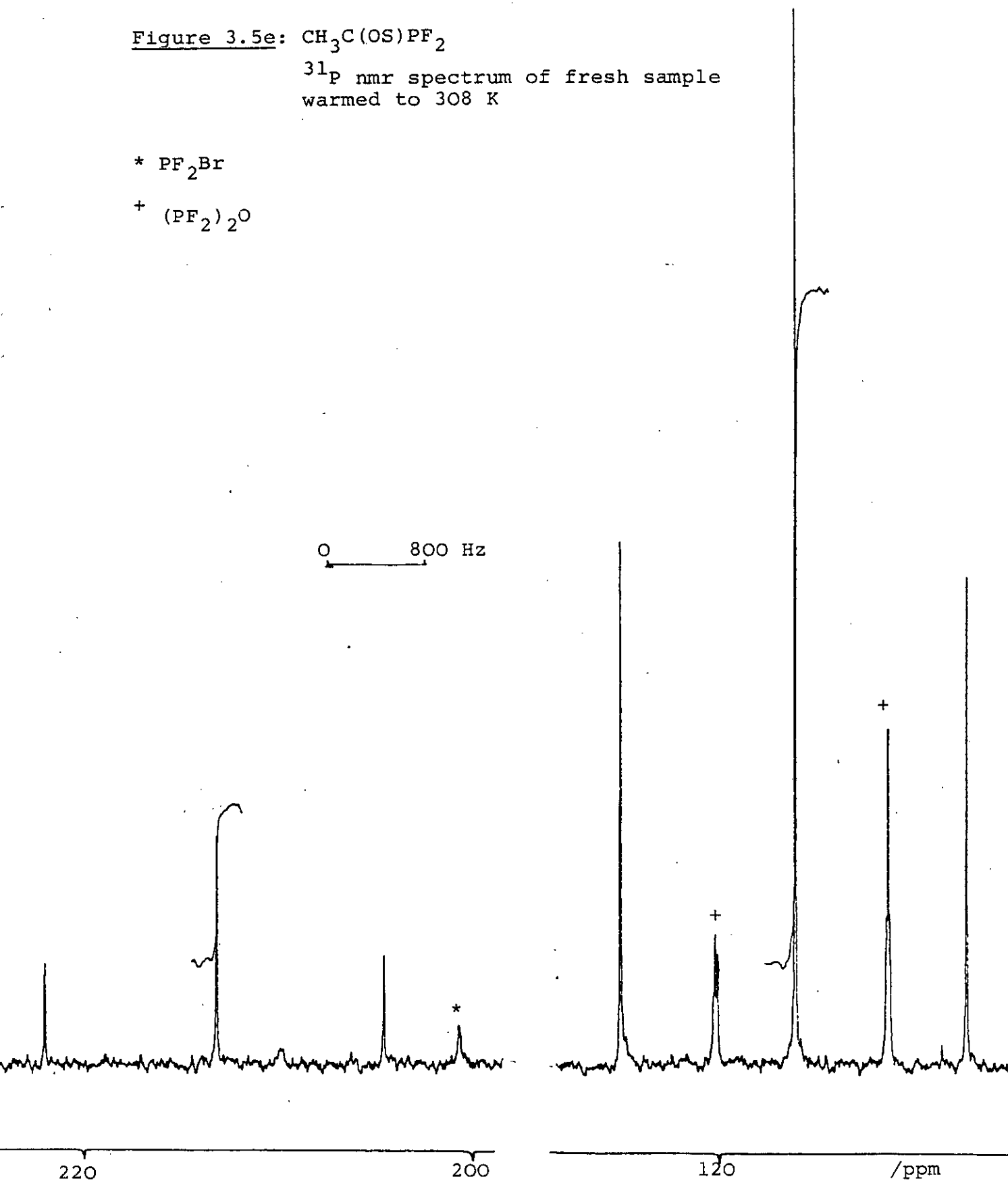


Table 3.4 shows how the chemical shifts of PF_2 bonded to O, N and S vary for a number of compounds.

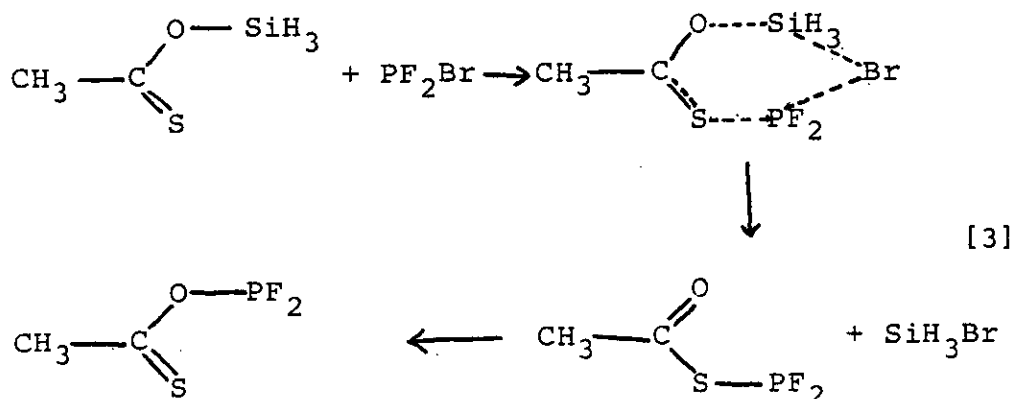
Table 3.4: Chemical shifts of some PF_2 derivatives

Compound	$\delta\text{P/ppm}$	$^1\text{J}_{\text{PF}}$	Ref
$(\text{PF}_2)_2\text{O}$	110.7	1355	This work
$\text{CH}_3\text{CSOPF}_2$	115.6	1343	This work
$\text{CH}_3\text{C}(\text{NPF}_2)\text{OPF}_2$	121.4	1340	50
$(\text{PF}_2)_2\text{S}$	219.4	1303	54
$\text{CH}_3\text{COSPF}_2$	212.9	1269	This work
PF_2NH_2	148.0	1200	55
$(\text{PF}_2)_2\text{NH}$	144.4	1253	56
$\text{CH}_3\text{C}(\text{OPF}_2)\text{NPF}_2$	148.5	1269	50

3.2.3 Mechanism of the exchange of bonding site:

The nmr data show that the PF_2Br binds initially to the vacant atom on the thioacetate derivative. Hence in the reaction with the Bu_3Sn derivative, which is S-bonded, the PF_2 bonds to the vacant O atom, while with $\text{CH}_3\text{CSOSiH}_3$ which is O-bonded, the product is initially S-bonded. Despite the different initial product the final equilibrium mixture of O- and S-bonded species at room temperature is the same, with a four-fold excess of O-bonded isomer.

For example,



There is no evidence for rapid exchange of sites by the PF_2 group at room temperature, which could be slowed down at low temperatures. This is unlike the exchange in bis(trimethylsilyl)acetamide⁵⁶ where the Me_3Si group moved from O to N sites. Also, one cannot be certain how the PF_2 exchanges its site once either the O or S bonded species is formed. The initial formation is likely to proceed via a six membered ring as drawn above with subsequent loss of SiH_3Br or Bu_3SnBr . In all other silyl and germyl esters studied by electron diffraction or X-ray crystallography short non-bonded distances between $\text{C}=\text{O}$ or $\text{C}=\text{S}$ and the silyl or germyl group have been found, i.e. $\text{CH}_3\text{COOSiH}_3$ ⁴⁴, HCOOSiH_3 ⁶⁵, $\text{CH}_3\text{COSSiH}_3$ (this work), $\text{CH}_3\text{COSGeH}_3$ (this work), and thus if similar short distances for $\text{P}\cdots\text{S}$ or $\text{P}\cdots\text{O}$ are present, exchange would be easier.

An electron diffraction study of $\text{CH}_3\text{C}(\text{OS})\text{PF}_2$ would be difficult because there are many distances which are close together and it would be difficult to allow for the two isomers present at room temperature as well as allowing

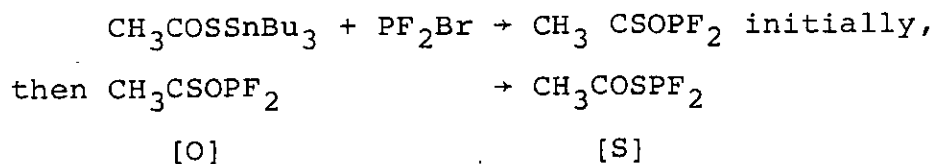
for all the PF₂ conformations. A solid phase structure by X-ray crystallography might be easier since below 230 K both O- and S-bonded species have been observed on their own.

3.2.4 Thermodynamics of the exchange process:

The integrals of the respective triplets in the ³¹P nmr spectra of the CH₃C(OS)PF₂ isomers were measured at each temperature at which a spectrum had been run. Hence the ratio of O- to S-bonded isomers can give the equilibrium constant. According to the Van't Hoff equation [5]:

$$\ln K = \frac{\Delta H}{R} \cdot \frac{1}{T} + \frac{\Delta S}{R} \quad [5]$$

where K is the equilibrium constant, T the temperature in K and R a constant. Therefore a plot of lnK vs ¹/T gives a straight line of slope -ΔH/R allowing the calculation of ΔH for the reaction.



See Table 3.5.

$$K = \frac{[S]}{[O]}$$

Table 3.5: Exchange of O- to S-bonded

T/K	$1/T \times 10^{-3}$	K	lnK
243	4.12	0.0525	-2.95
253	3.95	0.0845	-2.47
263	3.80	0.158	-1.84
273	3.66	0.185	-1.69
283	3.53	0.206	-1.58
293	3.41	0.223	-1.50
308	3.25	0.231	-1.46

These values are plotted on Figure 3.5. Note that the data points all lie on a straight line except the two at the lowest temperatures. This suggests that equilibrium had not been reached, for these points only. The slope found by least squares excluding the two lowest temperature points is -613.5 . Thus $\Delta H = 5.1 \text{ kJmol}^{-1}$ and $\Delta S = 4.6 \text{ Jmol}^{-1}\text{K}^{-1}$. These values indicate that exchange of O to S bonding sites is relatively easy and does not require a high energy intake.

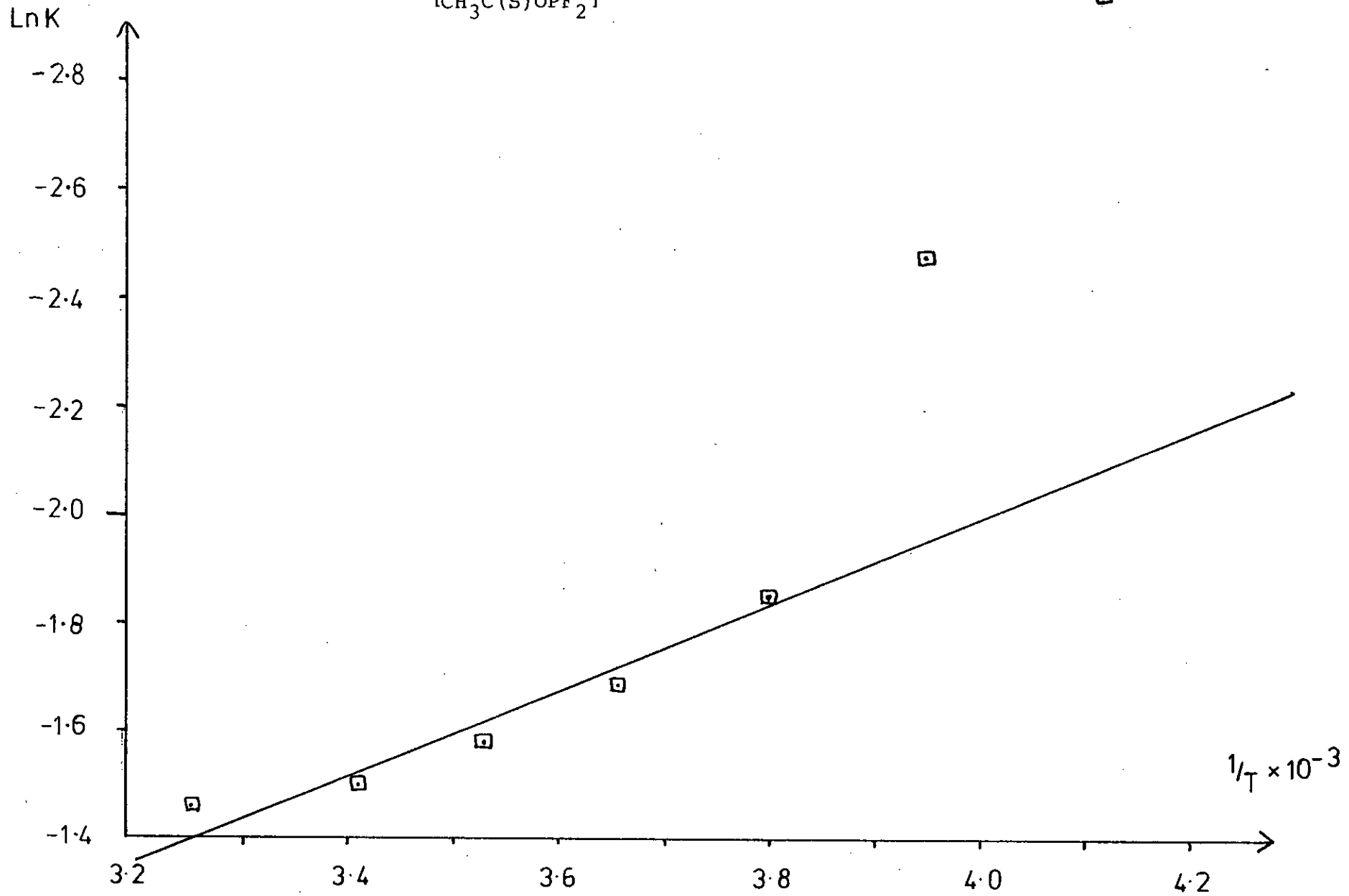
The value of ΔH for this exchange indicates that heat must be put in to push equilibrium to the right hand side of the equation, i.e. leading to formation of $\text{PF}_2\text{O(S)CCH}_3$ from $\text{PF}_2\text{S(O)CCH}_3$.

3.2.5 Nmr of other nuclei:

This section records the ^{19}F , ^{13}C and ^1H nuclear

Figure 3.5: Plot of $\ln K$ vs $\frac{1}{T}$ using data from Table 3.5.

$$K = \frac{[\text{CH}_3\text{C}(\text{O})\text{SPF}_2]}{[\text{CH}_3\text{C}(\text{S})\text{OPF}_2]}$$



magnetic spectra of $\text{CH}_3\text{C}(\text{OS})\text{PF}_2$. The ^{19}F nmr was observed from 213 K to room temperature on a relatively freshly prepared sample. At 213 K two doublets were found with large couplings, one at -78.2 ppm and the other, eight times the intensity of the first, at -58.3 ppm. On warming to room temperature the positions of the doublets did not change significantly but the relative intensity of the minor doublet increased slightly to a ratio of 1:5. By comparison of the relative intensities and the coupling constants to the ^{31}P nmr spectra, the doublet at -78.2 ppm ($^1J_{\text{PF}} = 1269.1$ Hz) was assigned to the $\text{CH}_3\text{COSPF}_2$ and the doublet at -58.3 ppm ($^1J_{\text{PF}} = 1342.5$ Hz) was assigned to $\text{CH}_3\text{CSOPF}_2$. It is noted that the chemical shift of the ^{19}F signal is not such a good indication of the atom bonded to the $-\text{PF}_2$ group unlike the ^{31}P chemical shift which is highly dependent on the adjacent atom, as is shown in Table 3.4. For example the chemical shifts of $(\text{PF}_2)_2\text{O}$ and $(\text{PF}_2)_2\text{S}$ are -37.94 ppm⁷¹ and -64.30 ppm⁷⁰ which are up to 20 ppm different from the appropriate shifts for $\text{CH}_3\text{COSPF}_2$, although the relative positions are the same with the $-\text{OPF}_2$ signal to high frequency of the $-\text{SPF}_2$ signal.

In spectra run on a narrower spectral width with the proton coupling in, the doublet signal was split to give a doublet of quartets. This must be due to the coupling through five bonds to the methyl protons. It was found that the O-bonded doublets had a smaller quartet coupling than the S-bonded doublet, with $^5J_{\text{PF}} = 0.75$ Hz (O-bonded)

and ${}^5J_{\text{PF}} = 1.0 \text{ Hz}$ (S-bonded).

The ${}^1\text{H}$ nmr spectrum was run for a sample that had already reached equilibrium and contained both O- and S-bonded $\text{CH}_3\text{C}(\text{OS})\text{PF}_2$. It was hoped that it would be possible to distinguish the proton signals of the methyl groups of the two isomers. The spectrum observed was two doublets of triplets with a relative intensity between the multiplets of about 4:1. The major isomer was assigned to the main multiplet at 2.649 ppm and the minor isomer to the signal centred at 2.514 ppm. As was found in the fluorine and phosphorus spectra the couplings to protons are not the same through oxygen and sulphur. The actual couplings are given in Table 3.6. For both ${}^4J_{\text{PH}}$ and ${}^5J_{\text{FH}}$ the couplings are less through oxygen than sulphur, and this trend has been found for a number of group VI compounds. For example $(\text{PF}_2)_2\text{O}$ ${}^2J_{\text{PP}} = 5\text{Hz}$ ⁷⁰ and $(\text{PF}_2)_2\text{S}$ ${}^2J_{\text{PP}} = 274 \text{ Hz}$ ⁷⁰.

The ${}^{13}\text{C}$ nmr spectrum was run with the proton coupling decoupled on a sample at equilibrium to give a spectrum with a singlet at 35.3 ppm, two equal but weaker intensity peaks at 219.1 and 219.0 ppm and a weak peak at 34.1 ppm. By comparison with the ${}^{13}\text{C}$ spectra of CH_3COSH ⁶⁴ and CH_3COOH ⁶⁴ the region around 20-35 ppm is characteristic of the methyl carbon signal and the carbonyl signal would be expected around 170-220 ppm. From the spectra it is not possible to assign the C=O, C=S signals because the peaks are of similar intensity but the methyl region can be assigned from the peak integral values.

The nmr parameters for the two $\text{CH}_3\text{C}(\text{OS})\text{PF}_2$ isomers have been summarised in Table 3.6 and the ^{19}F , ^{13}C and ^1H nmr spectra are given in Figures 3.6, 3.7 and 3.8 respectively for an equilibrium sample.

Table 3.6: Chemical shifts and coupling constants of $\text{CH}_3\text{C}(\text{OS})\text{PF}_2^{\text{a}}$

	$\delta\text{P}^{\text{c}}$	$\delta\text{F}^{\text{d}}$	$\delta\text{H}^{\text{e}}$	$\delta\text{C}_{\text{H}}^{\text{e}}$	$\delta\text{C}_{\text{O/S}}^{\text{b,e}}$	$^1\text{J}_{\text{PF}}$	$^4\text{J}_{\text{PH}}$	$^5\text{J}_{\text{FH}}$
$\text{CH}_3\text{COSPF}_2$	212.9	-78.2	2.514	34.0	219.1	1269	2.23	1.01
$\text{CH}_3\text{CSOPF}_2$	115.6	-58.3	2.649	35.3	218.9	1343	2.09	0.73

^arun in CD_2Cl_2 at room temperature, chemical shifts in ppm, couplings in Hz.

^bassignment may be reversed

^cppm to high field of 85% H_3PO_4

^dppm to high field of CCl_3F

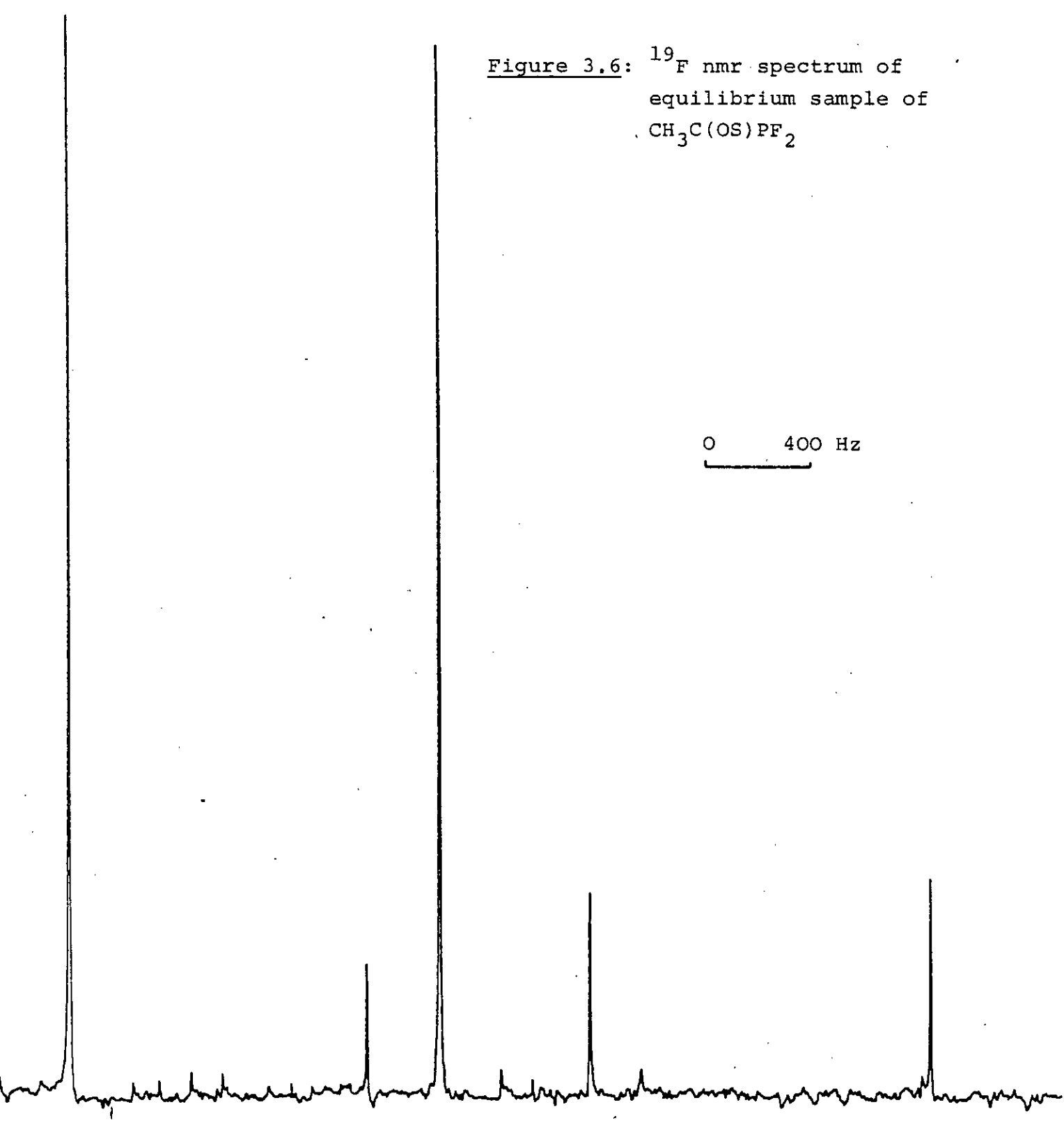
^eppm to high field of SiMe_4

3.2.6 Summary of nmr results:

The nmr results have been useful in observing the ratio of the O and S bonded isomers, which could not have been achieved by simply employing infra-red and Raman spectroscopy, and the chemical shifts were characteristic of O-or S-bonded $-\text{PF}_2$ groups and confirm that the derivatives contained tri-coordinate phosphorus⁷³. One problem with a possible structural study of $\text{CH}_3\text{C}(\text{OS})\text{PF}_2$ either by electron diffraction or X-ray crystallography is

Figure 3.6: ^{19}F nmr spectrum of
equilibrium sample of
 $\text{CH}_3\text{C}(\text{OS})\text{PF}_2$

0 400 Hz



The figure shows an NMR spectrum with a horizontal axis representing frequency. There are four distinct peaks: a very tall, narrow peak on the far left; a smaller peak to its right; a tall, narrow peak in the center; and a peak on the far right. A scale bar below the spectrum indicates a length of 400 Hz, starting from a point labeled '0'.

Figure 3.7: ^{13}C nmr spectrum of equilibrium sample of $\text{CH}_3\text{C}(\text{OS})\text{PF}_2$

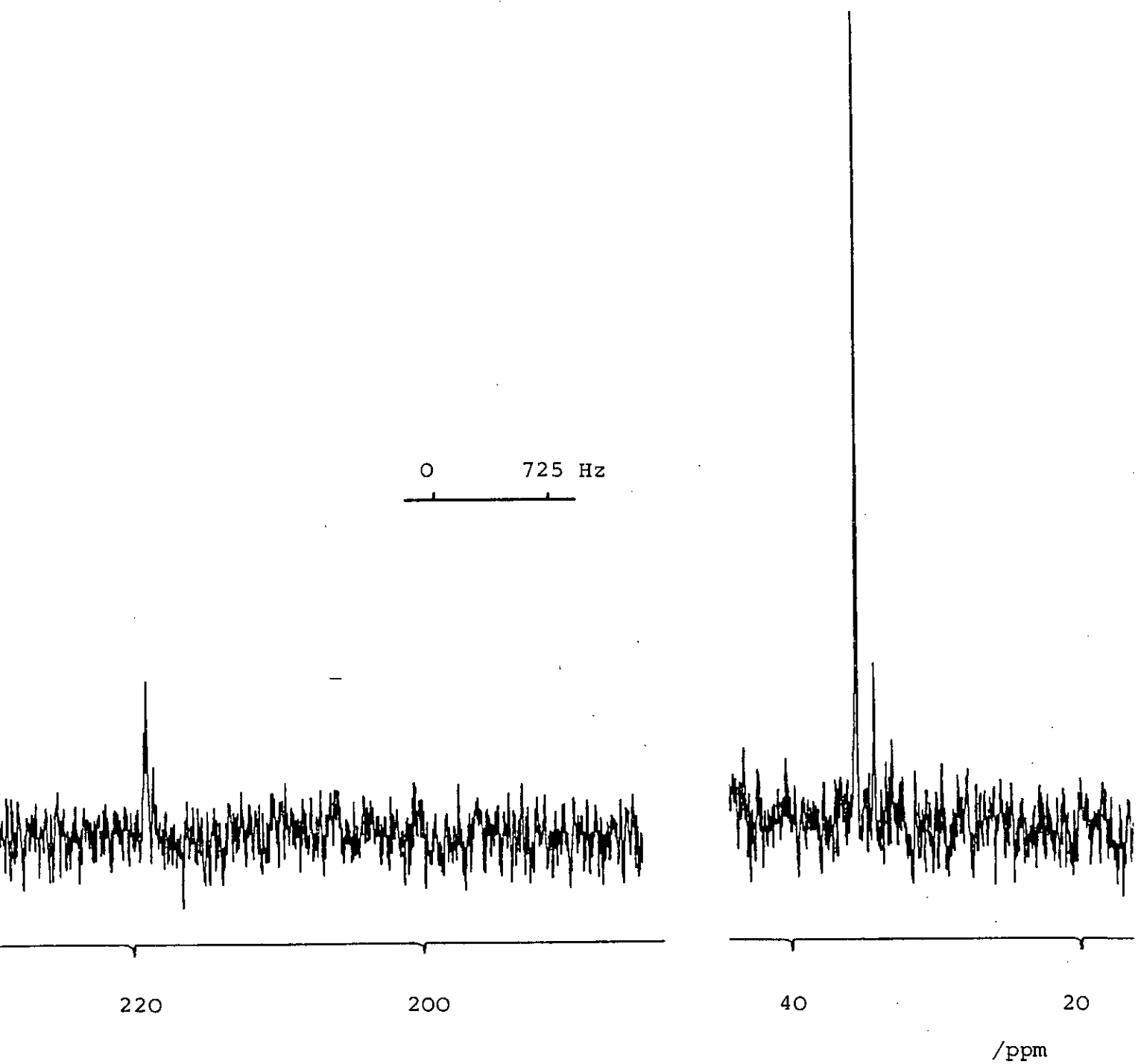
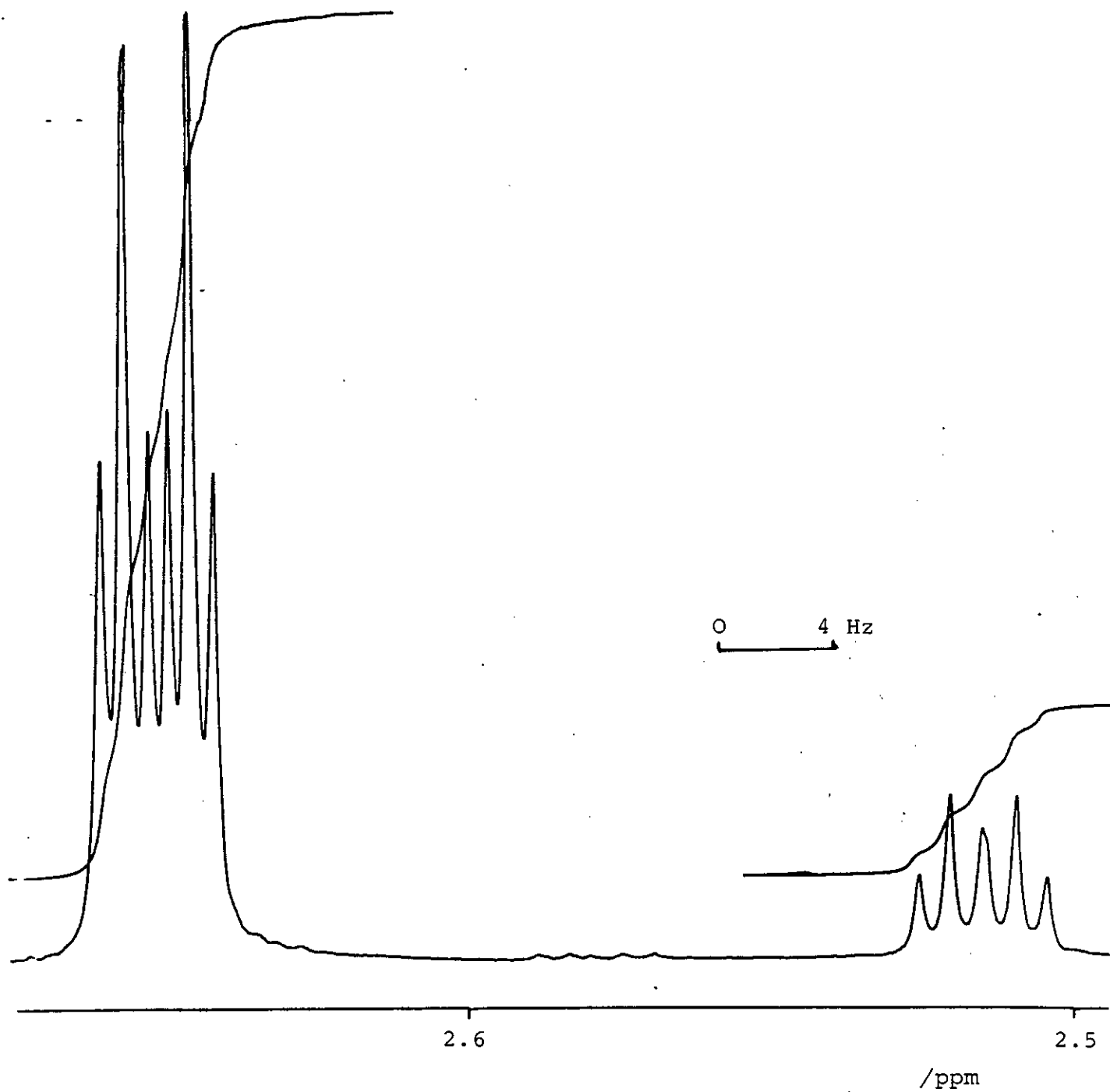


Figure 3.8: ^1H nmr spectrum of equilibrium sample of $\text{CH}_3\text{C}(\text{OS})\text{PF}_2$



that an equilibrium mixture is present. However, certain structural parameters could probably be obtained by liquid-crystal nmr, which can be employed for mixtures or impure samples.

3.2.7 Mass spectrum of $\text{CH}_3\text{C}(\text{OS})\text{PF}_2$:

In Table 3.7 are listed the ions observed in the mass spectrum of an equilibrium sample of $\text{CH}_3\text{C}(\text{OS})\text{PF}_2$, run with ionising voltages of 70 and 16 eV. At both voltages the $[\text{CH}_3\text{CO}]^+$ ion gave the strongest peak in the spectrum.

The fragment ions present in the spectrum confirmed the proposed atomic arrangement of $\text{CH}_3\text{C}(\text{OS})\text{PF}_2$, although at 70 eV, the parent ion was relatively weak and there was some impurity from hydrolysis products present. By reducing the ionising potential to 16 eV the parent ion was stronger and the hydrolysis products HPF_2O and $(\text{PF}_2)_2\text{O}$ relatively less intense. With all involatile compounds containing PF_2 groups it has been found difficult to exclude $(\text{PF}_2)_2\text{O}$ because of small leaks and trace moisture in the mass spectrometer ionising chamber. Despite the presence of some $(\text{PF}_2)_2\text{O}$, the fragmentation pattern shows that more of the ester was O-bonded than S-bonded, with peak ratios of 14:3 in the 20 eV spectrum.

The molecular weight of the parent ion peak was found to be 143.961310g [error of <2 ppm for $\text{C}_2\text{H}_5\text{OF}_2\text{PS}$].

Table 3.7: Mass spectrum of $\text{CH}_3\text{C}(\text{OS})\text{PF}_2$

M/e	Relative Abundances		Assignment
	at 70 eV	at 16 eV	
154	28	10	$[(\text{PF}_2)_2\text{O}]^+$
144	18	49	$[\text{CH}_3\text{COSPF}_2]^+$
106	3		$[\text{CH}_3\text{COSP}]^+$
104	7		$[\text{CHCOSP}]^+$
102	14		$[\text{HPF}_2\text{O}]^+$
101	3		$[\text{PF}_2\text{S}]^+$
92	71	54	$[\text{POCSH}]^+$
91	71	2	$[\text{POCS}]^+$
88	26		$[\text{PF}_3]^+$
86	28		$[\text{HPF}_2\text{O}]^+$
85	14		$[\text{PF}_2\text{O}]^+$
76	14	3	$[\text{CH}_3\text{COS}]^+$
69	100	5	$[\text{PF}_2]^+$
67	11		$[\text{HPFO}]^+$
66	13		$[\text{PFO}]^+$
65	11		
63	8		$[\text{SP}]^+$
61	20	2	
59	44	49	$[\text{CH}_3\text{CS}]^+$
50	28	4	$[\text{PF}]^+$
44	17	4	$[\text{PF}_3]^{2+}$
43	100	100	$[\text{CH}_3\text{CO}]^+$
42	27		$[\text{CH}_2\text{CO}]^+$
41	4		$[\text{CHCO}]^+$
32	16		$[\text{S}]^+$
31	17		$[\text{P}]^+$

3.3 Germyl monothioacetate

When germyl monothioacetate was first characterised, Drake⁴⁶ observed that in the proton nuclear magnetic resonance spectrum there is a germyl resonance close to that of $(\text{GeH}_3)_2\text{S}^{70}$ at 4.60 ppm but no resonance close to that of $(\text{GeH}_3)_2\text{O}^{70}$ whose chemical shift is about 5.30 ppm. On the basis of these results and from the infra-red spectrum he deduced that no O-bound isomer of germyl monothioacetate was formed.

In this work the reaction between silyl monothioacetate and germyl fluoride was studied at low temperature to see if an O-bound isomer could be detected as an intermediate in the formation of the S-bound isomer.

3.3.1 Proton nuclear magnetic resonance:

The quality of the proton resonance spectrum obtained at 180 K was poor, but sufficient to show that even at so low a temperature substantial reaction had occurred. Good quality spectra were obtained from 193 K upwards and no peaks were observed that could plausibly be assigned to the O-bound isomer. At 193 K reaction appeared to be complete and so if any of the O-bound isomer is formed it must rearrange too rapidly to be detected. The proton chemical shifts for $\text{CH}_3\text{COSGeH}_3$ in toluene solution at 183 K are $\delta\text{H}(\text{C})=1.89$, $\delta\text{H}(\text{Ge})=4.32$ ppm. See Figure 3.9 for proton resonance spectrum.

Table 3.8: Infra-red data of $\text{CH}_3\text{COSGeH}_3$

gas/cm ⁻¹	solid/cm ⁻¹	Assignment
2130 s	2128 s	$\nu(\text{GeH})$ asym
2108 s	2102 s	$\nu(\text{GeH})$ sym
1709 s	1678 vs	$\nu(\text{C=O})$
	1415 m	$\delta(\text{CH})$ asym
1361 m	1354 s	δCH sym
	1261 w	δCH
1132 s	1128 s	ρCH_3
1088 vw	1095 m	
1018 w	1019 vw	ρCH_3
955 m	955 s	$\nu(\text{C-C})$
874 m	854 s	δGeH_3
862 m		
817 vs	807 vs	δGeH_3
811 vs	793 vs	δGeH_3
625 s	629 s	$\nu(\text{C-S})$
585 w	593 m	ρGeH_3
466 w	471 m	skeletal CH_3COS
426 w	417 m	skeletal CH_3COS
291 w	296 m	$\nu(\text{Ge-S})$

s = strong, m = medium, w = weak, v = very

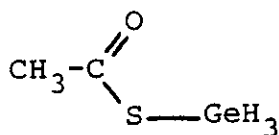
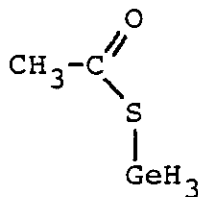
Spectra were recorded on a Perkin Elmer 577 spectrophotometer. Solid phase annealed until no further change in spectrum.

3.3.2 Infra-red spectrum of $\text{CH}_3\text{COSGeH}_3$:

The infra-red spectra of germyl monothioacetate in the gaseous and solid phases were determined to see whether there were any substantial shifts in frequency with change in phase, and also to see if any new bands appeared in the solid phase spectrum. The results are given in Table 3.8 with the assignment of bands.

In general there are shifts to low frequency from the gas to solid phase but these are quite consistent with the shifts observed in the spectra of other esters including methyl acetate. For example, the bands assigned to the deformations of the methyl and germyl groups shift by between 8 and 15 cm^{-1} . The largest shift is of the carbonyl stretch, from 1709 to 1678 cm^{-1} , although this is smaller than the shift of most silyl esters⁷⁴ as shown in Table 3.9.

It is thought that the stronger the intermolecular interactions in the solid phase, the greater the shift of the carbonyl stretching frequency. In fact, germyl monothioacetate has a smaller shift than methyl acetate which is known to have weak intermolecular interactions⁴⁴. There was no evidence from the infra-red spectrum for any change in structure from gas to solid, and there is no splitting in the CO stretch such as would have been expected if the solid contained both cis and trans isomers.

cistransTable 3.9: Carbonyl stretching frequencies in solid and gas phase

	gas phase/cm ⁻¹	solid phase/cm ⁻¹	shift
HCOOSiH ₃	1734	1695	39
CH ₃ COOSiH ₃	1750	1707	43
HCOOCH ₃	1754	1693	61
CH ₃ COOCH ₃	1774	1731	43
CH ₃ COSGeH ₃	1709	1678	31

3.3.3 The mass spectrum of germyl monothioacetate:

The mass spectrum was also recorded. The principal fragments with their approximate relative intensities are given in Table 3.10. The fragmentation pattern is consistent with the structure suggested by infra-red and nmr spectroscopy. No metastable peaks were observed.

3.4 Silyl monothioacetate

Early work on this compound suggested that a small proportion of the S-bound isomer may be present at low temperatures⁷⁵. However new ¹H nmr spectra were recorded

Table 3.10: Mass spectrum of $\text{CH}_3\text{COSGeH}_3$ ^a

Exact mass measurements of parent ion = 151.93573
(error 4 ppm)

Ion ^b	m/e	Relative Intensity
$[\text{}^{74}\text{GeH}_3\text{SOCCH}_3]^+$	152	20
$[\text{}^{74}\text{GeSC}]^+$	118	22
$[\text{}^{74}\text{GeS}]^+$	106	20
$[\text{}^{74}\text{Ge}]^+$	74	14
$[\text{COS}]^+$	60	2
$[\text{CS}]^+$	44	13
$[\text{CH}_3\text{CO}]^+$	43	100
$[\text{CCO}]^+$	40	11
$[\text{CO}]^+$	28	99
$[\text{CH}_3\text{C}]^+$	27	7
$[\text{GeO}]$	90	2

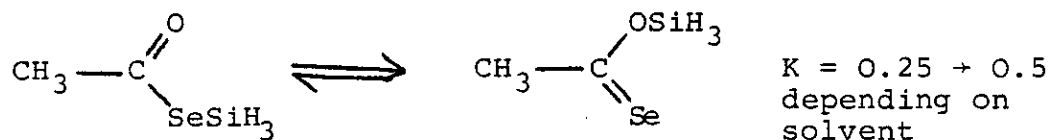
^aRecorded on an MS902 spectrometer, with ionising voltage of 70 eV.

^bFragments containing Ge all show a pattern reflecting the relative abundance of the Ge isotopes.

and there was no evidence of the singlet in the region close to the $(\text{SiH}_3)_2\text{S}^{77}$ signal. This therefore confirms Drake's⁴⁶ observation that only the O-bound isomer is present. The infra-red spectrum was not conclusive as the sample contained a small amount of $(\text{CH}_3\text{CO})_2\text{S}$ which has a very strong carbonyl band at 1720 cm^{-1} . Even so the electron diffraction study reported in Chapter 4 used a model which only allowed for one isomer, and the fit between experimental and theoretical data (at curves) was very good. A mass spectrum was obtained and this showed conclusively that the O-bound isomer predominates and no $[\text{SSiH}_3]^+$ fragments were observed.

3.5 Difluorophosphine monoselenoacetate

When silyl monoselenoacetate was first prepared⁵² the silyl group was found to be bound to Se or O giving an equilibrium mixture, with an excess of Se-bound. The same reaction was looked at in more detail⁵³ and the activation parameters determined for the exchange of Se to O bound.



Therefore it was of interest to prepare $\text{CH}_3\text{C}(\text{OSe})\text{PF}_2$ to observe how the $-\text{PF}_2$ group is bonded. Would it be less bound to O than $\text{CH}_3\text{C}(\text{OSe})\text{SiH}_3$ as in the thioacetate, or would the relative strengths and stabilities of the C=O and C=Se bonds influence the equilibrium mixture?

Table 3.9a: Mass spectrum of $\text{CH}_3\text{CSOSiH}_3$

<u>m/e</u> ^a	<u>Assigned species</u>	<u>Relative Abundance</u>
92	$[\text{HCSOSiH}_3]^+$	4
91	$[\text{CSOSiH}_3]^+$	4
89	$[\text{CSOSiH}]^+$	4
88	$[\text{CSOSi}]^+$	3
79	$[\text{SOSiH}_3]^+$	7
78	$[\text{SOSiH}_2]^+$	11
77	$[\text{SOSiH}]^+$	91
76	$[\text{SOSi}]^+$	43
75	$[\text{CH}_3\text{CSO}]^+$	57
74	$[\text{CH}_2\text{CSO}]^+$	11
73	$[\text{CHCSO}]^+$	32
72	$[\text{CCSO}]^+$	15
61	$[\text{HCSO}]^+$	21
60	$[\text{CSO}]^+$	13
47	$[\text{OSiH}_3]^+$	19
46	$[\text{OSiH}_2]^+$	3
45	$[\text{OSiH}]^+$	27
44	$[\text{OSi}]^+$	11
43	$[\text{CH}_3\text{CO}]^+$	100
42	$[\text{CH}_2\text{CO}]^+$	24
41	$[\text{CHCO}]^+$	5
40	$[\text{CCO}]^+$	5
33	$[\text{HS}]^+$	13
32	$[\text{S}]^+$	67
30	$[\text{SiH}_2]^+$	12
29	$[\text{SiH}]^+$	5
28	$[\text{Si}]^+$	7
27	$[\text{CH}_3\text{C}]^+$	100
26	$[\text{CH}_2\text{C}]^+$	21

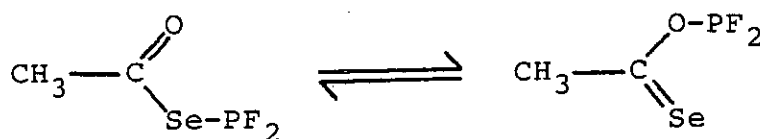
^aRun at 70 eV ionising voltage.

At 20 eV ionising voltage same peaks, and still no parent ion at 106 for $[\text{CH}_3\text{CSOSiH}_3]^+$.

3.5.1 Nuclear magnetic resonance spectra of $\text{CH}_3\text{C}(\text{OSe})\text{PF}_2$:

The formation of $\text{CH}_3\text{C}(\text{OSe})\text{PF}_2$ was followed by the reaction of PF_2Br and $\text{CH}_3\text{C}(\text{OSe})\text{SiH}_3$ using ^{31}P nmr and observing the chemical shifts of the signals. At 193 K a single triplet at 244 ppm was observed, with a large coupling of 1265 Hz. The chemical shift is close to that of $(\text{PF}_2)_2\text{Se}^{77}$ at 247 ppm and is to high frequency of the signal for $(\text{PF}_2)_2\text{O}$ and $\text{CH}_3\text{CSOPF}_2$ found in the 110-114 ppm region. Also, there was a triplet at 198 ppm which was assigned to unreacted PF_2Br . On leaving for 5 minutes at that temperature, six different triplets were produced all with large coupling, suggesting they are all due to PF_2 compounds, and when warmed to 223 K the triplet at 244 ppm had begun to decrease in intensity with respect to PF_2Br . By including proton coupling the triplet at 259 ppm split to a triplet of quartets, and the signal at 81.5 ppm split to a triplet of doublets. After another 10 minutes at 223 K all the triplets were less intense than the PF_2Br triplet, suggesting decomposition was taking place. Hence the signal at 244 ppm is assigned to $-\text{PF}_2$ bound to Se and four of the remaining five multiplets can be assigned to $\text{PF}_2\text{SeSiH}_3$, $(\text{PF}_2)_2\text{Se}$, PF_2Br and HPF_2Se . The unassigned signal is at 112.2 ppm ($^1J_{\text{PF}} = 1344$ Hz) and is close to the position for $(\text{PF}_2)_2\text{O}$, but does not have the second order pattern or a large enough coupling constant to be assigned to $(\text{PF}_2)_2\text{O}$. This is probably due to a small proportion of O-bound $-\text{PF}_2$ in the selenoacetate.

As the sample was warmed to 263 K further decomposition occurred leaving $(PF_2)_2Se$, HPF_2Se and a yellow solid. The relative intensity of the Se and O triplets varied little as the temperature was increased and at 263 K the ratio was 10:1 with excess Se bound PF_2 isomer. Hence the equilibrium constant for the exchange must be about 0.1.



These observations show that there is a preference for phosphorus bonded to Se rather than O, and that in the thioacetates and selenoacetates the silyl ester has a higher proportion of O bonded isomer than the $-PF_2$ ester. The factors involved in the bonding are discussed below.

3.5.2: Infra-red spectrum of $CH_3C(OSe)PF_2$:

An attempt was made to run the gas phase infra-red spectrum of $CH_3C(OSe)PF_2$. The bands observed not readily assignable to impurities and decomposition products are 1810 m ($\nu(C=O)$), 1210 m (δCH_3), 980 s ($\nu(C-C)$), 780 m (skeletal?) and 550 m (skeletal?). The bands associated with the PF_2 vibrations were obscured by the PF_2 impurities.

3.6. Discussion of Esters

The discussion is in two sections. The first section is a summary of the preferred bonding of PF_2 , SiH_3 and GeH_3 to O, S and Se, and the second section is a discussion of the factors affecting the mechanism of formation and subsequent rearrangement of the esters.

3.6.1: Bonding in the esters at equilibrium:

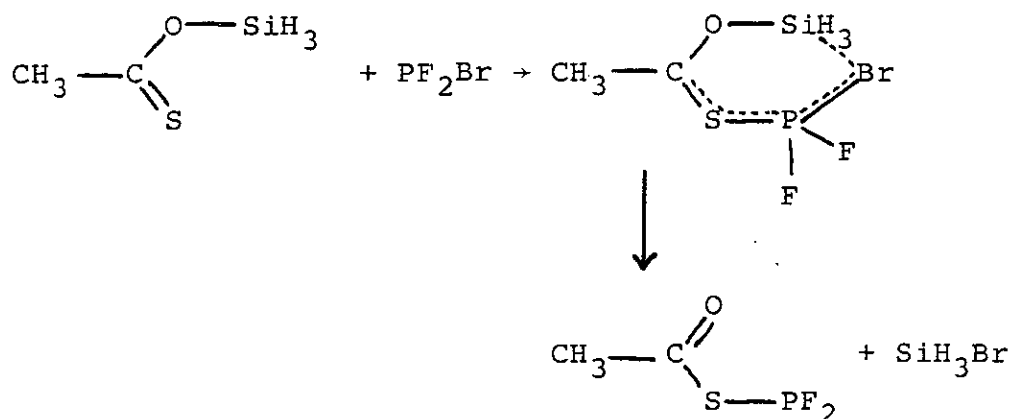
Earlier work had found that in the monothioacetates⁴⁶ the silyl group is exclusively bound to the oxygen, while the germyl group is bound to the sulphur: the new results reported here confirm this. The difluorophosphine now gives a mixture of O and S bound ester, with 80% in the $\text{CH}_3\text{CSOPF}_2$ form at room temperature. This trend can be interpreted according to soft and hard, acid and base theory. The silyl group can be considered as a hard acid while the germyl group is soft, and for the bases the O is hard and sulphur soft. Hence the more stable bonds should be the Si-O and Ge-S. It would also seem that $-\text{PF}_2$ is a harder acid than GeH_3 but softer than SiH_3 . In the monoselenoacetates, selenium would be expected to be softer than sulphur and so $\text{CH}_3\text{C}(\text{OSe})\text{SiH}_3$ also will be an O bound isomer. The fact that the isomer is largely Se bound suggests that an additional factor in the preferred bonding are the stabilities of the C=O and C=Se bonds. However within the selenoacetate group, as expected, the

PF₂ ester has a higher proportion of Se bound isomer than silyl selenoacetate because the PF₂ is a softer acid than SiH₃ and so would not form such a strong bond to oxygen as silicon does. The preferred bonding of silicon to oxygen and germanium to sulphur is exhibited in the syntheses of the ethers and sulphides. Disilyl ether is easily prepared and forms readily when any silyl compound reacts with traces of water vapour or air; in contrast, digermyl ether is comparatively difficult to make and does not form when germyl compounds react with air. Digermyl sulphide on the other hand is easily prepared. The stability of the Si-O bond was at first attributed to (p-d) π bonding. There are not many reliable measured values for E(Ge-O), but estimates suggest that E(Si-O) is very much greater, a conclusion reached from studies of the hydrolyses of chlorosilanes and chlorogermanes⁷⁸ and from studies of alkyl, silyl and germyl ethers⁷⁹. The latter study found bond energies for (M-O) in (Me₃Si)₂O and (Et₃Ge)₂O of 440 and 381 kJ mol⁻¹ respectively. In phosphorus compounds the P-S linkages tend to be less stable thermally and hydrolytically than the oxygen analogues. Common values⁸⁰ for E(P-O) are 360 kJ mol⁻¹ and for E(P-S) about 290 kJ mol⁻¹. As an alternative approach Pauling⁸¹ has suggested that the Si-O bonds are not any stronger than would be predicted by the view of electronegativity he has put forward. Comparing the experimental bond energies with those he calculates, the agreement is generally good and there are no discrepancies that can be accounted for by (p-d) π bonding.

Pauling's approach and the (p-d) π bonding approach, would both predict Ge-X bonds being weaker than Si-X bonds. Additionally, the bond energies of the C=O/S and C-O/S bonds must be considered in a full analysis of the most favourable isomer. In fact the difference between the total bond energies for C=O, C-S and P-S vs C=S, C-O and P-O is very small; about 10-20 kJ mol⁻¹ out of a total of 1250 kJ mol⁻¹.

3.6.2 Mechanism of exchange:

From the nmr spectra it was found that the initial bonding of the difluorophosphino group in CH₃C(OS)PF₂ is dependent on the position of the leaving group. In the reaction of PF₂Br and CH₃COSSnBu₃ the O-bound isomer is formed while with CH₃CSOSiH₃ the S-bound isomer is formed. Thus the -PF₂ group always adds to the vacant atom, whether it is O or S. This suggests the reaction is via a six membered ring intermediate.



The ability of phosphorus to expand from a 3-coordinate to 4-coordinate atom is well known and this change will lower the barrier to exchange taking place.

The mechanism of germyl bromide exchanging with $\text{CH}_3\text{C}(\text{O})\text{SSnBu}_3$ may be different. Firstly, no O-bonded species of $\text{CH}_3\text{COSGeH}_3$ was observed even in the fresh sample, perhaps because very fast intramolecular exchange took place. A more likely mechanism is via a two step process (S_N) with initial loss of $-\text{SnBu}_3$ to leave the monothioacetate species available for attack by GeH_3Br . The product of GeH_3F and $\text{CH}_3\text{CSOSiH}_3$ gave no evidence of O-bonded $\text{CH}_3\text{COSGeH}_3$ but in fact whichever mechanism is involved only the S-bound isomer would be expected. If it is via a 6 membered ring, only the S site is vacant, and if it is via a thioacetate anion (S_N) only the S-bound isomer is likely as this is the preferred isomer at equilibrium from 198 K upwards.

Also, the ease of formation of the six membered ring intermediate must be enhanced by the short non-bonded distances between $\text{Si}\dots\text{S}$ and $\text{Ge}\dots\text{O}$ found in the electron diffraction study (Chapter 4) and which are presumed to be present in $\text{CH}_3\text{C}(\text{OS})\text{PF}_2$. There is no evidence that the PF_2 group is bound equally to O and S as this would markedly alter the nmr spectrum giving a chemical shift not consistent with 3-coordinate phosphorus and only one signal.

Finally, the mechanism for reaction of $-\text{PF}_2$ with silyl monoselenoacetate is complicated by the fact that the silyl

ester is present in the form of the two isomers. However, since the ester is mostly Se-bound, one would expect at low temperatures that the major initial bonding site of the $-PF_2$ group would be oxygen while from the ^{31}P nmr at 193 K the only isomer observed initially is the Se-bound. This suggests that either the exchange is rapid with any initially O-bound PF_2 converting to Se-bound at 193 K before exchanging to a 10% proportion O-bound at higher temperatures, or that the mechanism is via loss of $-SiH_3$ from both O and Se sites before attack by the PF_2 group. This would not then be the same as the exchange in $CH_3C(OSe)SiH_3$ ⁵² which was thought to be intramolecular and fast on an nmr timescale at room temperature but slow at low temperatures (below 223 K). The exchange was presumed to be intramolecular because the spectrum was not affected by a substantial change in concentration of the ester, and because in all other esters studied the configuration has been cis, and thus the $-SiH_3$ group was sufficiently close to the C=Se or C=O group for rearrangement to take place.

CHAPTER 4: THE GAS PHASE STRUCTURES OF SILYL MONOTHIOACETATE
AND GERMYL MONOTHIOACETATE

4.1 Introduction

The molecular structures of silyl formate⁶⁵ and silyl acetate⁴⁴ in the gas phase have recently been determined and in each case the heavy atom skeleton is planar, with the Si-O and C=O bonds mutually cis. The arrangement is associated with an unusually short intramolecular Si...O distance of about 280 pm which is considerably less than the sum of the van der Waals' radii of 360 pm. In the solid phase, the molecular structure is little altered, although there is in addition an intermolecular Si..O contact of 272 pm. The short intramolecular distance and cis configuration are also found in methylacetate⁴⁴ and methylformate⁸² with C...O distances of 261 pm (crystalline phase) and 268 pm (gas phase), respectively. The sum of the van der Waals' radii for C and O atoms is 320 pm indicating that the discrepancy between the M...O distances where M = C, Si, and the sum of the van der Waals' radii is more pronounced in silyl esters. Despite the short intramolecular distances there is no evidence that there is any exchange of bonding site.

Hence these observations have prompted the study of other silyl esters, and some germlyl esters; in particular those of monothioacetate. The monothioacetates present additional structural possibilities with the substitution of one oxygen by a sulphur introducing variations in atomic size and donor-acceptor properties. Also there is the

Choice of bonding to oxygen or sulphur, and studies of the infra-red and nuclear magnetic resonance data⁴⁶ suggest that the silyl group is O-bound, and the germyl is S-bound.

Lastly, there is interest in how the Si-O, Ge-S distances, and SiOC and GeSC angles compare with the parameters found for $(\text{SiH}_3)_2\text{O}$ and $(\text{GeH}_3)_2\text{S}$. The angle at oxygen in disiloxane²⁶ is abnormally wide while the angle for GeSGe²⁷ is about normal, and these are coupled with a short Si-O bond and a normal Ge-S bond.

4.2 Structure Refinement

4.2.1 The molecular model:

During refinement of the structures of the two monothioacetates it was assumed that the OSiH_3 , SGeH_3 and CCH_3 groups each had local C_{3v} symmetry and that the three bonds to the central carbon atom were coplanar. The molecular geometry was then defined by 6 bond lengths, 5 valence angles and 3 torsion angles. The $\text{SiH}_3(\text{GeH}_3)$ and CH_3 torsion angles were defined as zero when one M-H bond (M=Si, Ge, C) was staggered with respect to the C=S(O) bond, while the angle describing the twist about the C-O(C-S) bond was defined to be zero when the C=S or C=O and Si-O or Ge-S bonds were cis with respect to each other; i.e. when the torsion angle for the C-O or C-S bond equalled zero all the heavy atoms were coplanar.

4.2.2: Refinement of silyl monothioacetate structure:

The refinement required care since there are several sets of overlapping peaks in the radial distribution curve (see Figure 4.1). The main features are a peak at 165 pm with a shoulder at 145 pm, and a non-bonded distance peak at 265 pm. Within these peaks are the C-C, C-O, Si-H at 145 pm, the Si-O and C=S under the 165 pm peak, and between 230 to 270 pm the C...Si, C...O, C...S and S...O non bonded distances.

The Si-H distance was fixed to permit refinement of the C-C distance and the three torsion angles were optimised by considering variations of R-factor as the angles were fixed at different values. The bonded distance amplitudes all refined to acceptable values except the $u(\text{Si-H})$ which was fixed and the $u(\text{Si-O})$ and $u(\text{C-O})$ which were constrained in appropriate ratios to $u(\text{C-S})$ and $u(\text{C-C})$ respectively. However this model still gave a rather high R-factor of about 0.16. On further inspection of the radial distribution curve there was a significant peak at 210 pm not accounted for in the O-bound silyl monothioacetate model. A dramatic improvement was possible when an allowance was included in the model for contamination of the sample with disilyl sulphide ($r(\text{Si-S}) = 214$ pm) which is known to be formed in a disproportionation reaction. The model was expanded to include (fixed) distances and amplitudes for Si-S, Si...Si, Si-H, Si...H and S...H distances with values taken from reference 40.

The proportion of $(\text{SiH}_3)_2\text{S}$ present was varied and a minimum R_G value was obtained for 3.2% impurity (mole to mole basis) for the plates at the short camera distance and 11.5% impurity for the plates at the long distance. With these extra factors in the model the final R factors were $R_G = 0.102$ and $R_D = 0.078$.

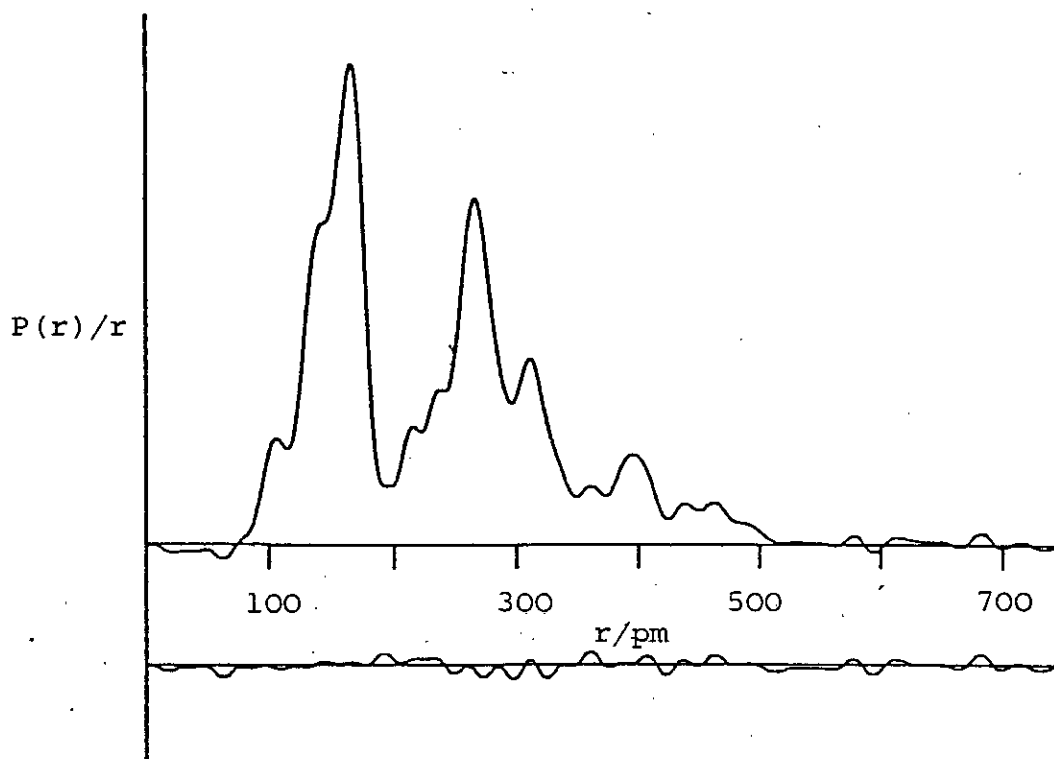
The final independent and dependent parameters are given in Table 4.3 and the observed and final difference molecular scattering curves are shown in Figure 4.2. Details of the least squares correlation matrix are given in Table 4.2. The errors in Table 4.3 are estimated standard deviations obtained from the least squares analysis increased to allow for any systematic errors.

The presence of small quantities of $(\text{SiH}_3)_2\text{S}$ means that the refined parameters are not to as high a precision as is usually possible. However, the results are quite good enough for sensible comparison with other esters in the gas and solid phases.

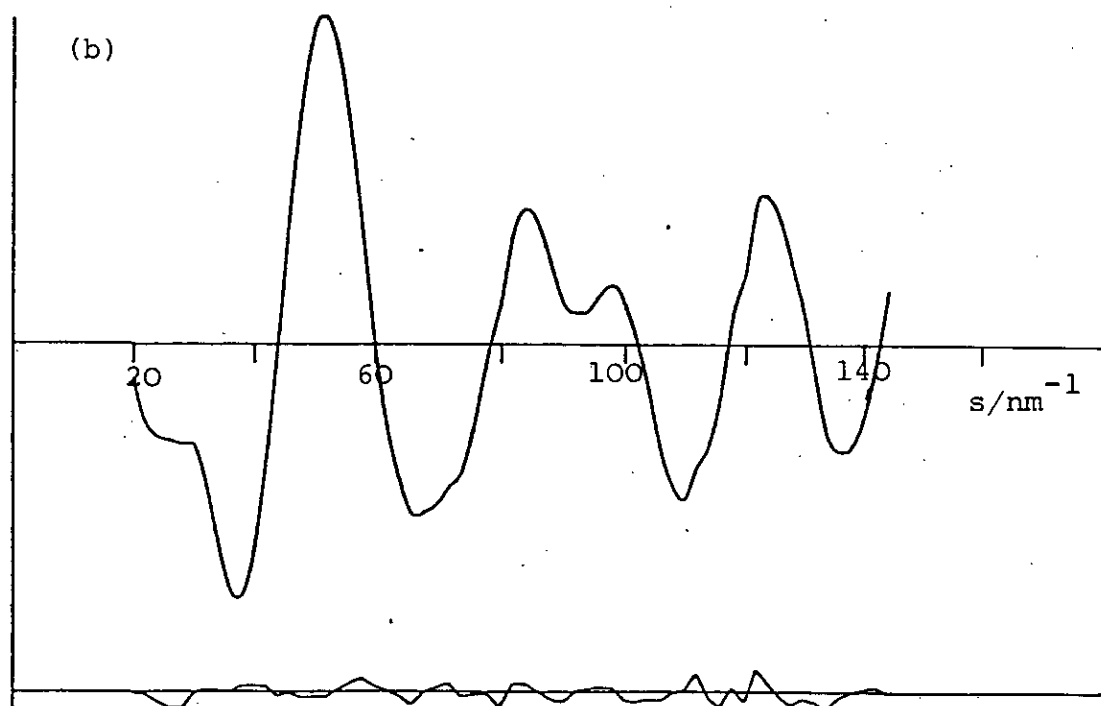
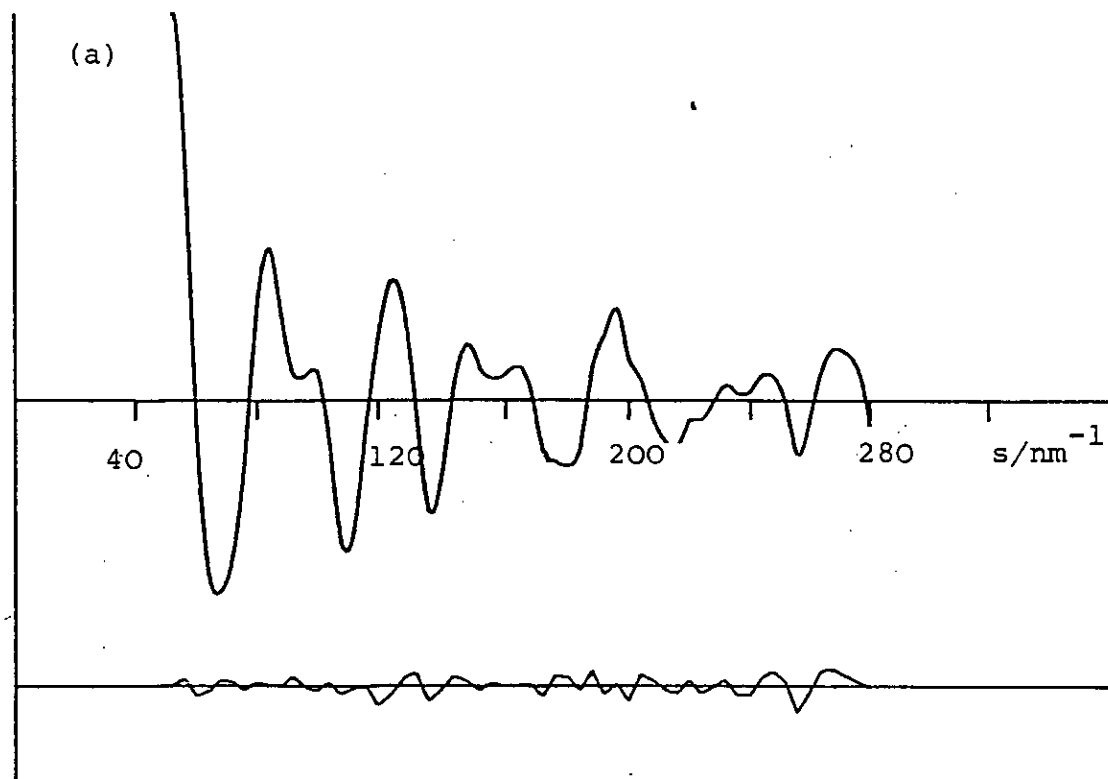
4.2.3: Refinement of geryl monothioacetate structure:

Although the radial distribution curve (Figure 4.3) was dominated by the large Ge-S peak at 220 pm, there were 3 other peaks in the region associated with bonded distances and it was possible to refine all bonded distances except Ge-H. In a series of refinements with this parameter fixed at various values, the lowest R

Figure 4.1: Observed and final difference radial distribution curves, $P(r)/r$, for $\text{CH}_3\text{CSOSiH}_3$



Before Fourier inversion the data were multiplied by
 $s \cdot \exp \left[-0.000015 s^2 / (Z_{\text{Si}} - F_{\text{Si}}) (Z_{\text{O}} - F_{\text{O}}) \right]$



Observed and final weighted difference molecular scattering intensities at nozzle-to-plate distances of (a) 128 and (b) 286 mm.

Table 4.1: Weighting functions, correlation parameters and scale factors for electron diffraction structure of $\text{CH}_3\text{CSOSiH}_3$

<u>Camera height</u> mm	Δs	s_{\min}	sw_1	sw_2	s_{\max}	<u>Correlation parameter</u>	<u>Scale Factor</u>
286.34	2.0	20	35	125	144	0.2939	0.651(16)
128.40	4.0	52	70	220	280	0.0045	0.521(21)

Table 4.2: Electron diffraction analysis : portion of the least-squares correlation matrix showing all the off-diagonal elements greater than 50%.

	Angles						
r_5	1	2	3	u_2	u_3	u_7	
	-57	67	-64	86		54	r_1
-83					91		r_3
	-50				-85		r_5
		-59	59	53	52		1)
			-96	-52) Angles
							2)
						56	u_2

Table 4.3: Gas phase molecular parameters of $\text{CH}_3\text{CSOSiH}_3$

(a) Independent parameters

	<u>Distance (pm)</u> <u>or angle (°)</u>	<u>Amplitude</u>
r_1 (C-H)	104.8 (10)	6.1 (15)
r_2 (C-C)	148.4 (14)	5.9 (25)
r_3 (C=S)	161.5 (8)	3.2 (24)
r_4 (C-O)	134.5 (7)	5.5 ^b
r_5 (Si-O)	171.7 (6)	3.4 ^c
r_6 (Si-H)	148.0 (fixed)	8.8 (fixed)
Angle 1 (C-C-O)	111.4 (8)	
Angle 2 (O-C=S)	127 (2)	
Angle 3 (Si-O-C)	118 (2)	
Angle 4 (H-Si-O)	110 (fixed)	
Angle 5 (H-C-C)	110 (fixed)	
Torsion 1 (Si-O-C-S)	10 ^a	
Torsion 2 (H-Si-O-C)	35 ^a	
Torsion 3 (H-C-C-S)	70 ^a	

(b) Dependent distances (pm) and amplitudes (pm)

d_7 (C...S)	207.5 (15)	10.3 (7)
d_8 (C...O)	233.9 (10)	6.0 (18)
d_9 (C...H)	208.8 (18)	9.9 (45)
d_{10} (C...Si)	263.2 (22)	10.3 ^d
d_{11} (S...O)	265.2 (20)	10.3 ^d
d_{12} (Si...C)	394.8 (15)	9.2 (15)
d_{13} (Si...S)	314.3 (9)	13.8 (9)

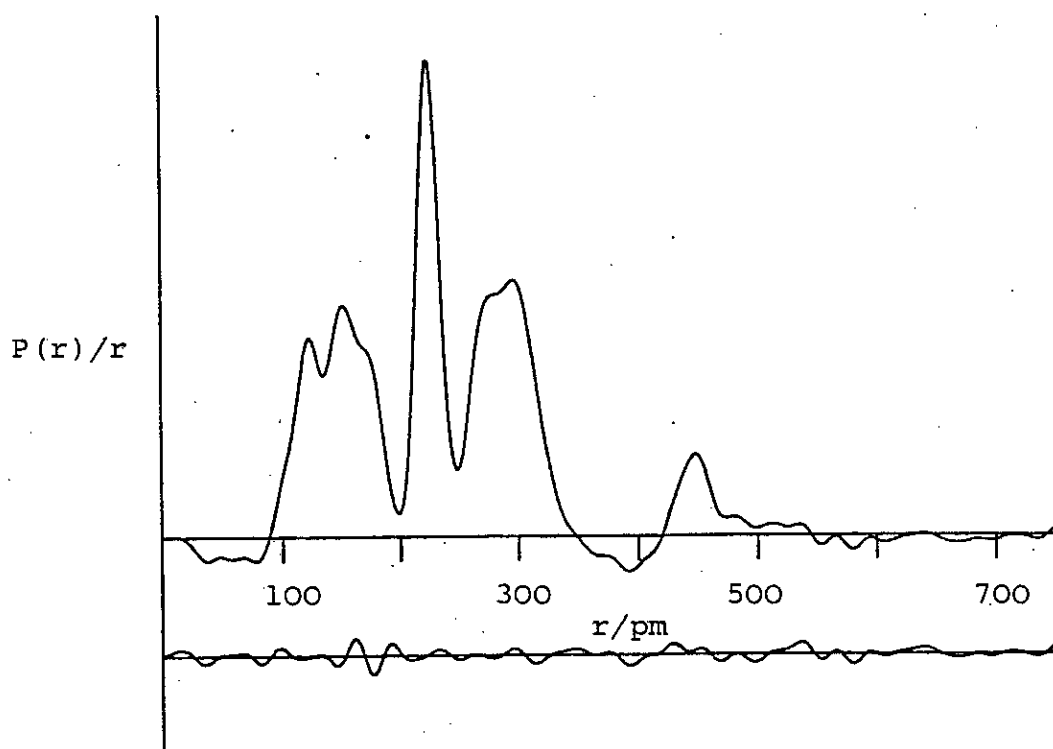
^atorsion angles optimised by R factor minimisation (see text);
^bproportional to u_2 (see text); ^cproportional to u_3 (see text);
^dtied to u_7 (C...S).

factor was found when the bond length was fixed at 152.5 pm and this was the value set in all subsequent refinements. Similar methods were used to find optimum values of the three angles describing the conformation of the molecule. The three valence angles involving the heavy atoms all refined normally but the SGeH and CCH angles would not refine satisfactorily and were therefore fixed at 110° .

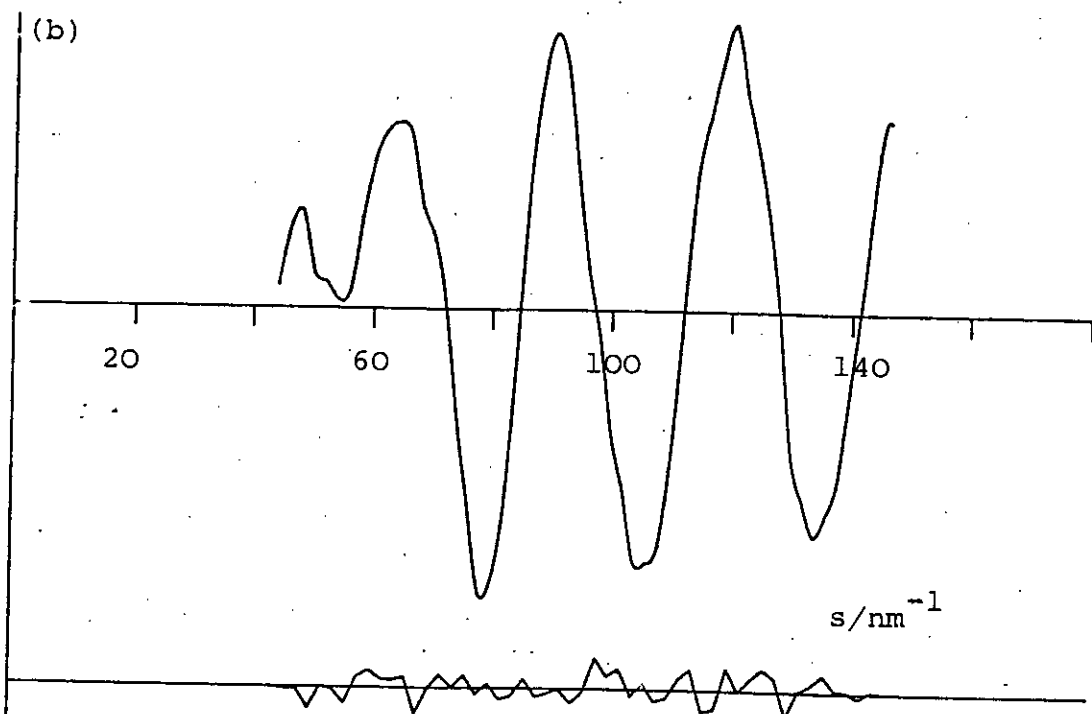
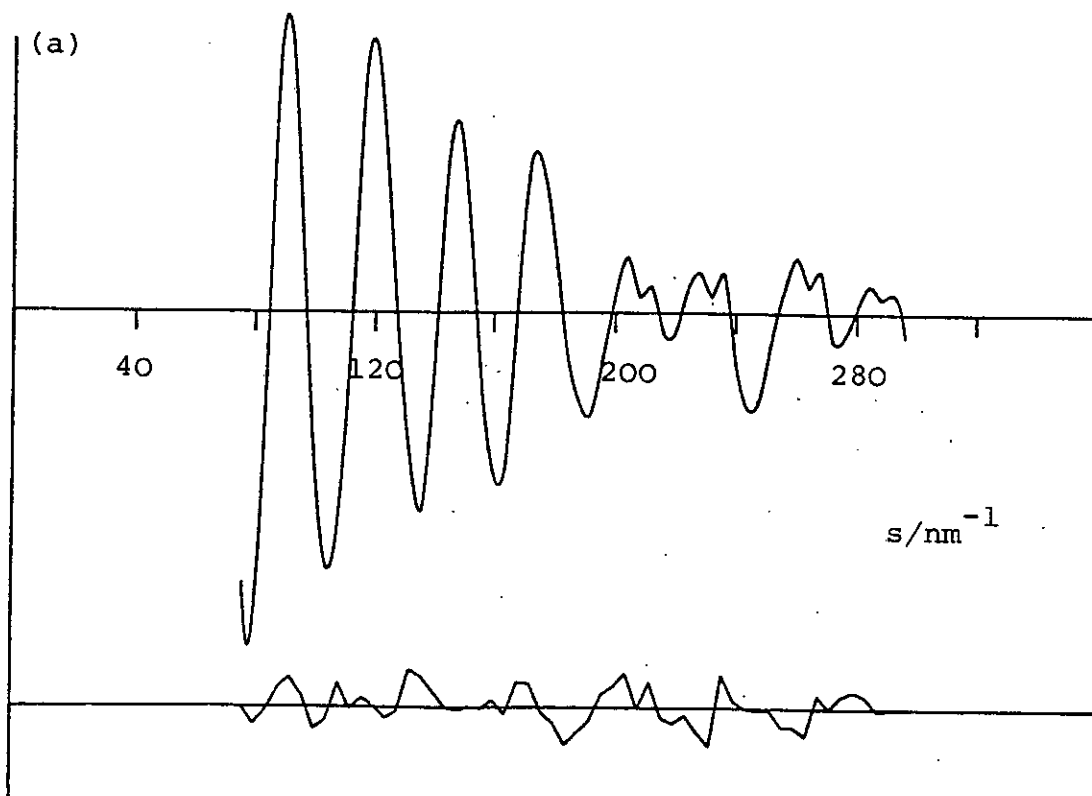
The bonded distance amplitudes generally did not refine well and were fixed at normal values found in other acetates and germyl compounds. The S...C and S...O amplitudes were constrained to be equal and refined satisfactorily. Part of the least squares correlation matrix is given in Table 4.5 and from it one can see that the most significant correlations are between the three refined angles, which are defined by the non-bonded distances which lie between 260-330 pm. This region of the radial distribution curve appears as one fairly strong broad peak, containing the Ge...C, O...S and Ge...O distances. The refined data provides clear evidence that germyl monothioacetate exists completely as the S-bound isomer in the gas phase. No attempt was made to allow for small proportions of the O-bound isomer because the radial distribution difference curve (Figure 4.3) showed no features attributable to a Ge-O distance unaccounted for in the model.

The intensity curves are illustrated in Figure 4.4, together with the difference curves for the final refinement for which the R factors were $R_G = 0.116$ and

Figure 4.3: Observed and final difference radial distribution curves, $P(r)/r$, for $\text{CH}_3\text{COSGeH}_3$.



Before Fourier inversion the data were multiplied by $s \cdot \exp[-0.00002 s^2 / (Z_{\text{Ge}} - F_{\text{Ge}})(Z_{\text{S}} - F_{\text{S}})]$.



Observed and final weighted difference molecular scattering intensities at nozzle-to-plate distances of (a) 128 and (b) 286 mm

Table 4.4: Weighting functions, scale factors, and correlation parameters for electron diffraction structure of $\text{CH}_3\text{COSGeH}_3$

<u>Camera height</u> mm	<u>Δs</u>	<u>s_{\min}</u>	<u>sw_1</u>	<u>sw_2</u>	<u>s_{\max}</u>	<u>Correlation parameter</u>	<u>Scale factor</u>
			nm^{-1}				
128.29	4	76	84	220	296	0.328	0.883(30)
286.11	2	44	58	120	146	0.042	0.923(16)

Table 4.5: Portion of least-squares correlation matrix showing off-diagonal elements greater than 30% for $\text{CH}_3\text{COSGeH}_3$

r_2	r_5	<1	<2	<3	u_8	k_1	
34	30	-62	48	-40			r_1
		-43				36	r_4
					-38		r_5
			-58	-73	-67		<1
				-70	53	-32	<2
					-56		<3
						55	u_5

Table 4.6: Molecular parameters of $\text{CH}_3\text{COSGeH}_3$

	<u>Distance (pm)</u>	<u>Amplitude (pm)</u>
(a) Independent distances		
r_1 (C-C)	149.3(10)	5.0 ^a
r_2 (C-H)	108.7(12)	6.5 ^a
r_3 (C=O)	122.4(8)	3.9 ^a
r_4 (C-S)	176.5(7)	4.8 ^a
r_5 (Ge-S)	223.3(4)	5.7(4)
r_6 (Ge-H)	152.5 ^b	8.8 ^a
(b) Dependent distances		
d_7 (C...O)	235.1(18)	8.0 ^a
d_8 (S...C)	277.3(14)	7.3(14)
d_9 (S...O)	265.3(12)	
d_{10} (Ge...C)	300.4(8)	10.9(13)
d_{11} (Ge...C)	445.6(10)	8.5(12)
d_{12} (Ge...O)	297.2(14)	15.0 ^a
(c) Angles ($^\circ$)		
<1 (CCO)	116.4(13)	
<2 (SCO)	124.1(10)	
<3 (GeSC)	96.7(4)	
<4 (SGeH)	110.0 ^a	
<5 (CCH)	110.0 ^a	
<6 (twist GeH_3)	5.0 ^b	
<7 (twist CH_3)	40.0 ^b	
<8 (dihedral GeSCO)	5.0 ^b	

^afixed^bsee text

$R_D = 0.114$. The final independent and dependent distances, angles and amplitudes are given in Table 4.6. The errors are estimated standard deviations obtained from the least-squares analysis, increased to allow for systematic errors.

4.3 Results and Discussion

The geometrical parameters for the monothioacetate part of the molecules are much as would be expected by comparison with $\text{CH}_3\text{COOSiH}_3$ ⁴⁴, HCOOSiH_3 ⁶⁵ and $\text{CH}_3\text{COOCH}_3$ ⁴⁴ and the low R factors for both structures show that the models assuming silyl monothioacetate in the completely O-bound isomer, and germyl monothioacetate in the completely S-bound isomer are correct.

The C-C and C-H distances are entirely consistent with earlier structures. Similarly, the C-O bond length in $\text{CH}_3\text{CSOSiH}_3$ is the same (within estimated error) as in related esters in the gaseous phase, although there is a distinct widening of the COSi angle by 1.5° from 116.5° to 118° compared to $\text{CH}_3\text{COOSiH}_3$. The Si-O bond length is rather long for many Si-O compounds, but is close to values reported in other silyl esters^{65,44,83}. For example in $(\text{SiH}_3)_2\text{O}$, Si-O = $163.4(2)$ pm²⁶, but in $\text{CH}_3\text{CSOSiH}_3$ it is $171.7(6)$ pm. The widening of these angles on substitution of sulphur for oxygen is probably an effect of the increased steric bulk of sulphur. There is also a slight increase of the torsion angle along the C-O bond, raising the SiH_3 group out of the CCOS plane. This

apparent twist from planarity may only be due to shrinkage.

As shown in Table 4.7, the Si...S distance is considerably shorter than the sum of the van der Waals' radii for silicon and sulphur, although the distance is too long to be considered as a bonded distance. The sum of the radii is 390 pm, and the reduction in distance to 314 pm is quite close to the decrease found in $\text{CH}_3\text{COOSiH}_3$ ⁴⁴ and HCOOSiH_3 ⁶⁵, but is twice the decrease found for the C...O distance in $\text{CH}_3\text{COOCH}_3$ ⁴⁴ (solid and gas phase). The close contact of the Si and S atoms is almost certainly an electrostatic attraction with the positive charge on the silicon atom greater than on carbon, explaining the greater attraction between Si to O, and Si to S, than C to O. Interestingly, the shortening of the distance between Si and S is almost the same as the shortening between Si and O, indicating that it is the silicon atom that has the main influence on the interatomic distances.

It is also noteworthy that the substitution of sulphur for oxygen does not alter the C...Si 2-bond distance, which is consistently shorter than the sum of Bartell's³⁷ hard sphere radii for silicon and carbon. Additionally, the shortening of the Si...C is greater than the shortening of the C...C distance in HCOOCH_3 ⁸² as shown in Table 4.7. This interaction would also appear to be an electrostatic attraction; the Si...C contact in silyl formate⁶⁵ (260 pm) is distinctly shorter than that observed in methoxysilane⁸⁴ (266 pm) or silyl dimethyl amine⁸⁵ (276 pm) while the C...C

Table 4.7: Non-bonded distances in esters in the gas phase (pm)^a

	2 bond distance		3 bond distance	
	M...C M=C,Si	Hard sphere radii	M...O or S M=C,Si	Van der Waals' radii
HCOOCH ₃	235.2	250[15]	268.7	300[31]
HCOOSiH ₃	260.1	282[22]	286.5	350[64]
CH ₃ COOSiH ₃	259.3	282[23]	279.5	350[71]
CH ₃ CSOSiH ₃	263.2	282[19]	314.3	390[76]

^aThe numbers in square brackets are the differences between the experimental distances and the sum of the hard-sphere radii or Van der Waals' radii.

contact in methyl formate⁸² (233 pm) is very close to that found in dimethyl ether⁸⁶ (234 pm). This may be because the attractive interaction between the silicon and carbonyl oxygen shortens the Si...C distance in the esters, but in $\text{CH}_3\text{COOCH}_3$ ⁴⁴ and HCOOCH_3 ⁸², which have small C...O=C interactions, the C...C distance is not reduced to less than in dimethyl ether.

There are also certain differences between the solid⁸⁷ and gas phase structures of silyl monothioacetate, and these are listed in Table 4.8 below. The Si-O bond length and C=S remain the same for both phases but the C-O length and COSi angle both change. The result is a longer C-O bond in the gas phase but a narrower angle resulting in the C...Si non-bonded distance remaining about the same. Similar changes were observed in the gas and solid phases of $\text{CH}_3\text{COOSiH}_3$ ⁴⁴ and are attributed to the relatively strong intermolecular interactions in the solid. There is a widening of the OCS angle from the solid phase [$123.0(2)^\text{a}$] to gas phase [$127(2)^\text{o}$]. However the gas phase angle has a large error and the difference may be of small significance. The crystal structure study of $\text{CH}_3\text{CSOSiH}_3$ ⁸⁷ has shown that as well as short Si...S intramolecular distances, there is a similar short intermolecular distance of 338.2(10) pm with an S...Si-O angle of $166.3(3)^\text{o}$. This attractive interaction may explain why the silyl group is bent further away from the C=S in the solid than the gas phase. In the crystal structure of $\text{CH}_3\text{COOSiH}_3$ there is an intermolecular C=O...Si distance of 272.1(4) pm and an O-Si...O angle of

Table 4.8: Comparison of certain bond lengths and angles in gas and solid phase

	Si-O ^a	C-O	COSi	Si...C	Si...O/S	Ref
CH ₃ COOSiH ₃ gas	168.5(3)	135.8(4)	116.5(7)	259.3(9)	279.5(13)	44
CH ₃ COOSiH ₃ solid	169.9(4)	131.2(6)	120.9(3)	262.6	283.2(4)	44
CH ₃ CSOSiH ₃ gas	171.7(6)	134.5(7)	118(2)	263.2(22)	314.3(9)	This work
CH ₃ CSOSiH ₃ solid	169.9(2)	131.9(3)	125.1(2)	268.4	318.5(1)	87

^abond lengths in pm; angles in degrees; errors in brackets

173.1(2)^o, while CH₃COOCH₃, studied as a reference structure, has no short intermolecular contacts.

The arrangement of four short and one long bond to silicon is entirely analogous to, although more striking than, the situation in crystalline disiloxane, which has intermolecular Si...O contacts of 311.5(5) pm.

The intermolecular Si...O interaction also appears to cause a slight narrowing of the OSiH angle as the silicon becomes nearer five coordinate. The angle in crystalline CH₃CSOSiH₃ is 100.3(17) while the gas phase angle is 110^o. This is similar to the OSiH angle in CH₃COOSiH₃⁴⁴ [106^o], and other silyl compounds involving short Si...M (M=N,O) intermolecular interactions; e.g. SiH₃NCO⁸⁸. Despite the known inaccuracy in finding the position of hydrogen atoms these angles are clearly distorted from the tetrahedral shape.

The molecular structure of gaseous germyl monothioacetate was refined assuming that only the S-bound isomer was present and this was found to be adequate. The CH₃-C portion of the molecule gave parameters consistent with other esters and the C=O bond length appears to be lengthened relative to other silyl and methyl esters although the effect is small; most esters have C=O bond lengths in the range 120.9(7) → 121.4(4) pm, while the bond in GeH₃SOCCH₃ is 122.4(8) pm. The OCS angle [124.1(10)^o] is very similar to the angle in SiH₃O(S)CCH₃ despite the double bond being a carbonyl rather than thionyl. As with other related esters the heavy atom skeleton is planar with the small

apparent deviation from planarity [5°] almost certainly due to a shrinkage effect.

The remaining geometrical parameters show small differences to those reported for related compounds but they may be significant. The C-S distance [176.5(7) pm] is shorter than in dimethyl sulphide [180.2(2) pm]⁴¹, but the difference (3.7 pm) is only half as great as that between C-O distances in methyl acetate⁴⁴, silyl acetate⁴⁴ and silyl monothioacetate, and that in dimethyl ether⁸⁶. Table 4.9 gives the differences between these distances.

Table 4.9: C-O and C-S bond lengths in esters, ethers and sulphides.

	C-O/pm	C-S/pm	Difference/ pm	Ref
CH ₃ COOSiH ₃	135.8(4)	-	5.8	44
CH ₃ COOCH ₃	133.7(4)	-	7.9	44
CH ₃ CSOSiH ₃	134.5(7)	-	7.1	This work
CH ₃ COSGeH ₃	-	176.5(7)	3.7	This work
(CH ₃) ₂ O	141.6(3)	-	-	86
(CH ₃) ₂ S	-	180.2(2)	-	41

The Ge-S bond length [223.3(4) pm] is greater than in digermyl sulphide⁸⁹ [220.9(4) pm], and associated with this, there is a narrowing of the angle at sulphur from $98.9(1)^\circ$ to $96.7(4)^\circ$. These changes are in the same direction as, but much smaller than, changes in the Si-O bond length and angles at oxygen when comparing disiloxane²⁶ to silyl

esters^{44,65}. By comparison with ethane⁴², methyl silane⁴³ and dimethyl ether⁸⁶, the Si-O bond length would be predicted to be 174.9 pm, and the Si-S bond length, predicted from ethane, methyl silane and dimethyl sulphide⁴¹ would be 213.5 pm. In fact it is found that Si-O in $(\text{SiH}_3)_2\text{O}$ is much shorter [163.4(2) pm], while the Si-S bond in $(\text{SiH}_3)_2\text{S}$ is almost as predicted [213.6 pm]⁴⁰. Coupled with the short Si-O bond in $(\text{SiH}_3)_2\text{O}$ is a wide SiOSi angle of $144.1(8)^\circ$. In the silyl esters the angle at oxygen is narrower and the Si-O bond longer with values of $116.5\text{-}118^\circ$, and $168.5\text{-}171.7$ pm respectively.

Prediction of the Ge-O and Ge-S bond lengths from ethane, dimethyl ether, dimethyl sulphide and methylgermane⁹⁰, gives values of 182.7 and 221.3 pm respectively, and again there is a shortening of the M-O bond in $(\text{GeH}_3)_2\text{O}$ to $176.6(4)$ pm²⁷ [GeOGe angle $126.5(3)^\circ$], but the difference is only half the shortening of the Si-O bond. The Ge-S bond length is shortened by only 0.4 pm in $(\text{GeH}_3)_2\text{S}$ ⁸⁹ [GeSGe angle is $98.9(1)^\circ$]. In both the germyl and silyl esters the shortening of Si-O or Ge-S bond is less than in the respective oxide or sulphide, particularly for Ge-S which is almost as predicted and the factors involving shortening have most influence on the Si-O bond. One explanation is that the lone pair of electrons on the oxygen atom is delocalised to the vacant d orbitals on silicon. This would also contribute to a widening of the angle at oxygen. Alternatively, there is greater ionic character of silicon with an increase in

electrostatic attraction to oxygen as explained by Oberhammer and Boggs³⁴ which would cause shortening of the bond. The predicted values of course assume the atoms retain their covalent character. The COSi angle is narrower than SiOSi since there is only one silicon adjacent to oxygen to influence the angle and there is the short Si...S attraction. The lack of shortening of the bonds involving germanium and sulphur or oxygen is as expected since germanium does not tend to contribute to (p-d) π bonding, and would not have as strong electrostatic attraction to oxygen as silicon.

Finally, the Ge...O non-bonded distance in $\text{GeH}_3\text{S(O)CCH}_3$ is observed to be significantly shorter [297.2(14) pm] than the sum of the Van der Waals' radii for Ge and O ca 360 pm. The shortening is not as great as those observed for silyl esters (ca 80 pm) but must nevertheless indicate that there is a strong non-bonded interaction between germanium and oxygen. This attractive interaction could account for the narrowing of the CSGe angle compared to the GeSGe angle and slight lengthening of the Ge-S bond length.

No good crystals were obtained of germyl monothioacetate so no study of intermolecular Ge...O contacts in the crystalline phase was possible. However, the crystal structure of $\text{CF}_3\text{COOGePh}_3$ ⁹¹ has very recently been published,

and this was also found to have a cis configuration with a short Ge...C distance of 277 pm close to the limiting contact distance for germanium and carbon, and a short Ge...O distance of 309 pm (sum of Van der Waals' radii 360 pm). Unlike silyl acetate and monothioacetate there were no intermolecular interactions.

Clearly a consistent pattern in the bonding of Si-O and Ge-S and the angles at O and S is emerging and a further study of $\text{GeH}_3\text{OOCCH}_3$ and $\text{SiH}_3\text{SSCCH}_3$ would be interesting, to gain a greater understanding of the factors that influence the ester structures.

CHAPTER 5: THE GAS PHASE STRUCTURES OF MONOMETHYLSILYL
ISOCYANATE AND DIMETHYLSILYL ISOCYANATE

5.1 Introduction

Silyl isocyanates have been the subject of many structural studies, with particular interest in the SiNC angle. Electron diffraction studies of $(\text{CH}_3)_3\text{SiNCO}^{92}$, $\text{Cl}_3\text{SiNCO}^{93}$ and $\text{F}_3\text{SiNCO}^{94}$ all require molecular models with non-linear SiNCO chains, while the microwave spectra^{95,96,97} of SiH_3NCO were all analysed for the molecule in its ground vibrational state by equations that were essentially based on the standard symmetric top expression.

Electron diffraction results for $\text{SiH}_3\text{NCO}^{28}$ indicate an apparent angle at nitrogen of 152° , and this is ascribed to the shrinkage effect from the low frequency, large amplitude bending motion at nitrogen. The same study went on to look in more detail at the Si...O peak in the radial distribution curve and deduced that the potential energy function for the bending motion had a low hump at the linear configuration, the height of which approximated to the energy of the lowest vibrational level, i.e. about 20 cm^{-1} . This was obtained from an expression for the potential of $v(\text{cm}^{-1}) = -300 \theta^2 + 1090 \theta^4$ (θ = bend from linear configuration) which has more recently⁹⁷ been slightly modified but the same double minimum trough is found. The same work on the gas-phase microwave spectrum⁹⁷ concluded that the potential surface in the SiNC skeletal bend had a minimum that can be described in the form of a circular

valley at a configuration of $\theta = 22^\circ$ with a maximum at linear SiNC configuration some 20 cm^{-1} higher in energy. The ground vibrational state is within 1 cm^{-1} of this maximum and the first vibrational interval is about 22 cm^{-1} . The infra-red spectrum of SiH_3NCO contains some rotational detail suggestive of C_{3v} symmetry and the low frequency region of the infra-red has confirmed the nature of the p.e. function⁹⁸, with ν_{10} (SiNC bend) assigned to 64 cm^{-1} in the gas phase.

Therefore all the above gas phase electron diffraction and microwave spectroscopy results indicate a linear molecule for SiH_3NCO with a low frequency, large amplitude, bend at nitrogen, causing an apparent angle of about 152° . However in the solid phase the infra-red⁹⁹ and X-ray diffraction³³ results indicate a bent configuration. The unit cell of SiH_3NCO was found to be a zig-zag chain of SiNCO linked from O to adjacent Si, with angles of NCO $176.4(6)^\circ$ and SiNC $158.4(5)^\circ$. The closeness of the apparent electron diffraction derived angle and the solid phase angle is probably coincidental. The other geometric parameters of the solid phase molecule are similar to gas phase except for a lengthening of the Si-N bond attributed to intermolecular interaction to surrounding molecules in the unit cell. The solid phase vibrational spectra⁹⁹ of SiH_3NCO have been studied for the molecule in a number of matrices, and all were interpreted from normal coordinate analysis in terms of C_s symmetry.

Less work has been done on trimethylsilyl isocyanate

but the studies completed indicate a linear SiNCO chain¹⁰⁰ in the gas phase but an apparent angle of $150(3)^\circ$ at nitrogen in the electron diffraction work⁹².

More recently MNDO calculations³⁶ on a large range of silyl and substituted silyl isocyanates showed that the SiNC chain is linear or very near linear. Those showing the greatest deviation from linearity were those with C_s symmetry. For example SiH_2ClNCO with an angle of 170° . In contrast the methyl and substituted methyl isocyanates were calculated to have bent configurations of up to 130° . The NCO angle remained at 180° in all silyl compounds but around 167° in the methyl isocyanates.

Since the silyl and trimethylsilyl isocyanates are symmetric tops when linear, it was felt that a study of monomethyl and dimethylsilyl isocyanate would be interesting. The methyl groups lower the symmetry of the molecule, giving it C_s symmetry whether bent or linear. Also the effect of the methyl groups on certain bonds, in particular the Si-N bond which one would expect to be influenced by the electron-donating methyl groups, will be noted. Lastly, if the SiNC group is bent, there will be a preferred configuration of methyl groups to the NCO group. No detailed analysis is possible of the Si...O peak in the radial distribution curve because in the methylsilyl compounds this distance overlaps into the long C...C distance.

5.2 Refinements and Models

5.2.1 Model of MeSiH₂NCO:

The subroutine was written describing the atomic coordinates by six bond distances, five bond angles and three torsion angles. The Si-N bond torsion angle was defined to be zero when the NCO group was trans to the methyl group. The torsion angle of the methyl group viewed along the C-Si bond was at zero when one hydrogen was in the CSiN plane and bisecting the HSiH angle. Local C_{3v} symmetry was assumed for the SiCH₃ group.

Hence the independent parameters are the Si-N, Si-C, C-H, Si-H, N=C, C=O bonds, the NSiC, HSiH, HCSi, SiNC and NCO angles, and the torsion angles are along the Si-C, Si-N, and N=C bonds, and the torsion along the N=C bond was defined to be zero when oxygen lay in the SiNC plane.

5.2.2 Model of Me₂SiHNCO:

This molecule was described by six bond lengths, six bond angles and three torsion angles. The two methyl groups were assumed to have local C_{3v} symmetry and the NCO group was trans to the bisector of the CSiC angle when the torsion angle along Si-N was zero. The six bond lengths are Si-C, Si-N, Si-H, C-H, N=C, C=O, the angles are CSiN, CSiC, SiCH, NSiH, NCO and SiNC, and the three torsion angles are one along the Si-C bond, rotating one methyl

group; one along the Si-N bond rotating the $\text{Si}(\text{CH}_3)_2$ group; and one along the N=C bond. The methyl twist angle is a clockwise movement of one H on one methyl group from a plane parallel to the SiNC plane (when $\tau(\text{Si-N}) = 0$), whilst the second methyl group remained fixed.

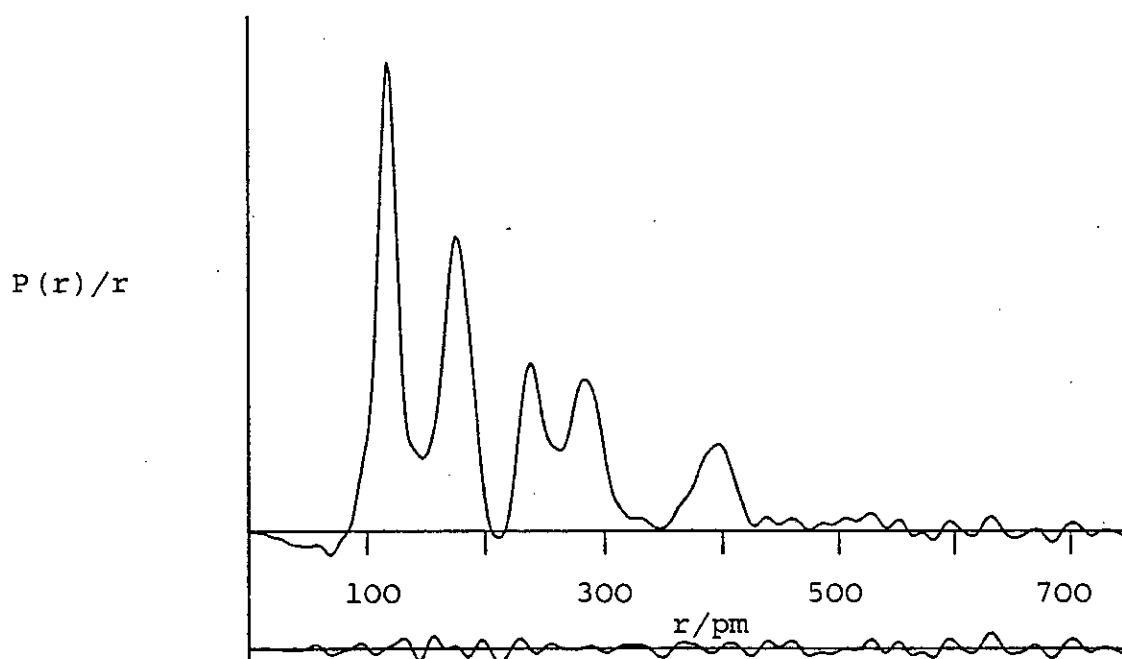
5.2.3 Refinement stages of MeSiH_2NCO structure:

In the refinement of these two structures it was anticipated that there might be problems distinguishing the C=O and N=C distances, and the Si-C and Si-N distances because in each case the two bond lengths are under the one peak in the radial distribution curve (see Figure 5.1). In fact in both compounds all four distances were refined to give sensible values, with the N=C bond remaining longer than the C=O and the Si-C bond longer than the Si-N bond. The preferred orientation of the methyl group to the NCO along the Si-N is defined by the C...C and C...O distances, and the twist angle was found by a series of refinements varying the twist angle stepwise. The angle giving the lowest R-factor was then used in subsequent refinements. The minimum R-factor was found to be when the C=O group eclipsed one Si-H bond. There was strong correlation between the amplitudes of vibration of N=C and C=O distances and so these were constrained to be equal in all refinements. The amplitudes of Si-N and Si-C were initially tied to be equal, but refined to rather high values. However when $u(\text{Si-C})$ was fixed to 5.2 pm, and

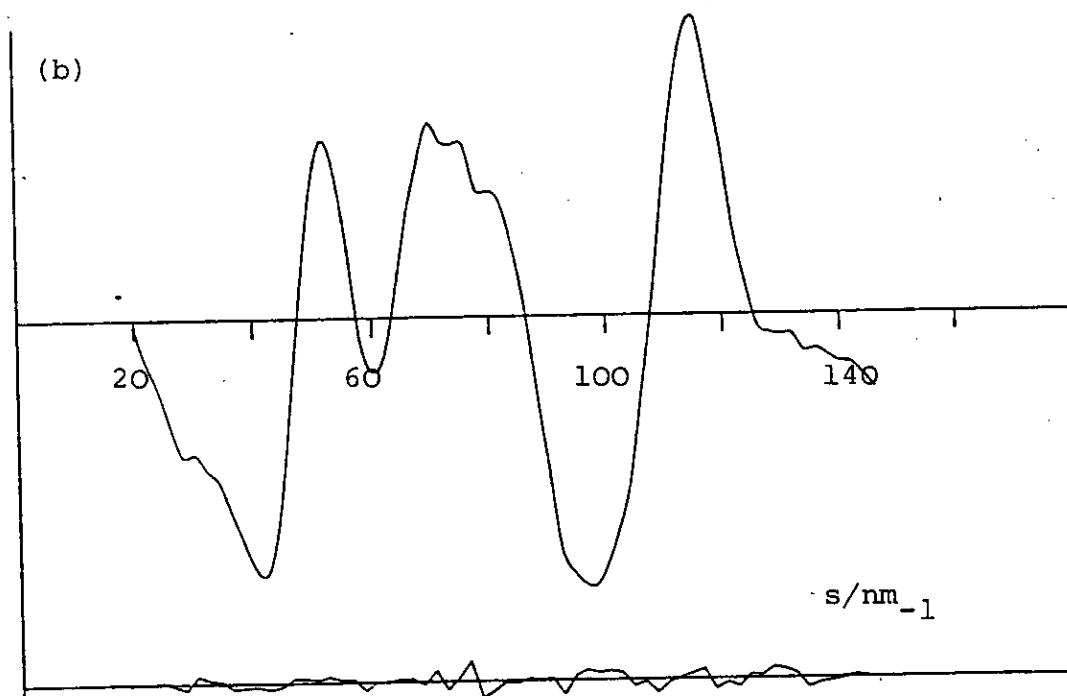
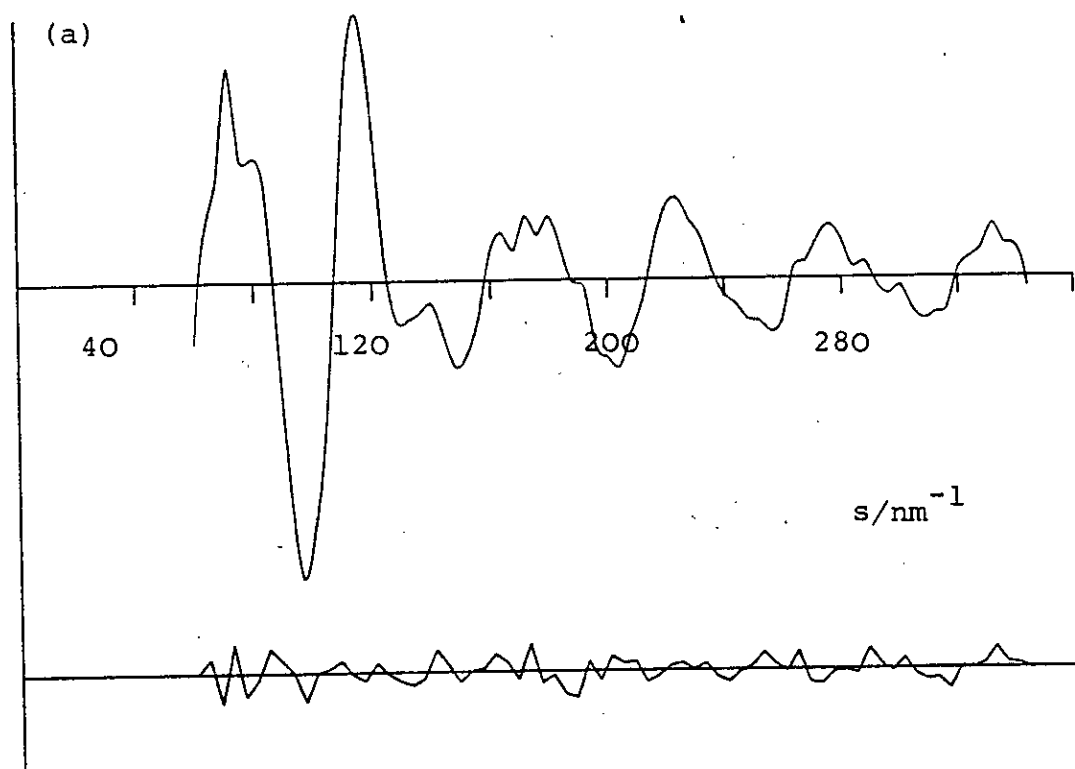
$u(\text{Si-N})$ refined, the amplitude emerged as a value equal to $u(\text{Si-C})$. All the angles at methyl and SiH_2 refined to values close to the tetrahedral angle or were fixed. The NSiC angle refined to a slightly wider angle than tetrahedral, $111.6(8)^\circ$ and the SiNC angle refined to $148.0(15)$ and this is discussed later. Rotation of the methyl hydrogens about the Si-C bond gave a minimum R-factor when the hydrogens were staggered with respect to the silicon hydrogens. The angle of the NCO group when refined, went to a value of 175° with a large estimated standard deviation; so this was then fixed at that angle. With a bent angle at carbon, the oxygen atom could be rotated about the N-C bond. This had very little effect on the R-factor but the final angle is included for completeness. The only bond distances not refined were the C-H and Si-H . The C-H distance lies under the same peak in the radial distribution curve centred at 120 pm as the C=O and N=C bond lengths and tended to refine to unreasonably high values. The Si-H bond length should give a weak peak independent of the other distances, but no feature was observed in the radial distribution curve and the distance when refined went to very high values.

All the heavy atom non-bonded distance amplitudes were refined independently. The $\text{C}\dots\text{H}(d_9)$ and $\text{N}\dots\text{H}(d_{12})$ distances contributed significantly to the area of peaks in the curve, but their amplitudes of vibration did not refine well, so were fixed. All the other amplitudes for interatomic distances involving two hydrogens, or one

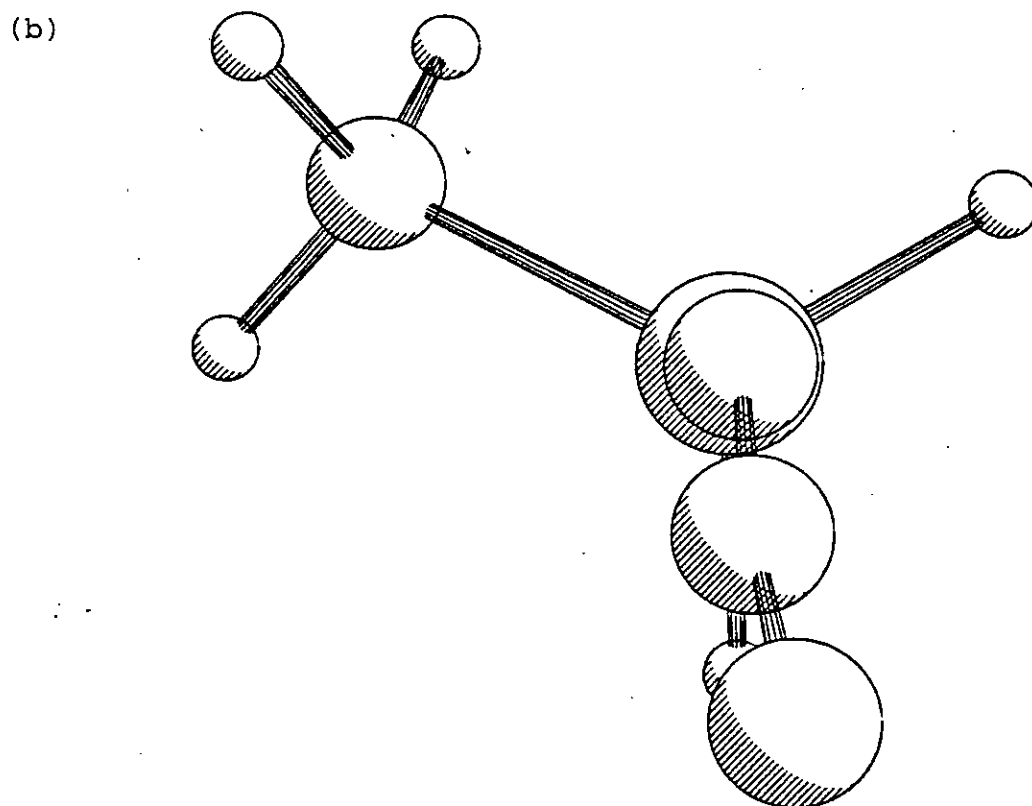
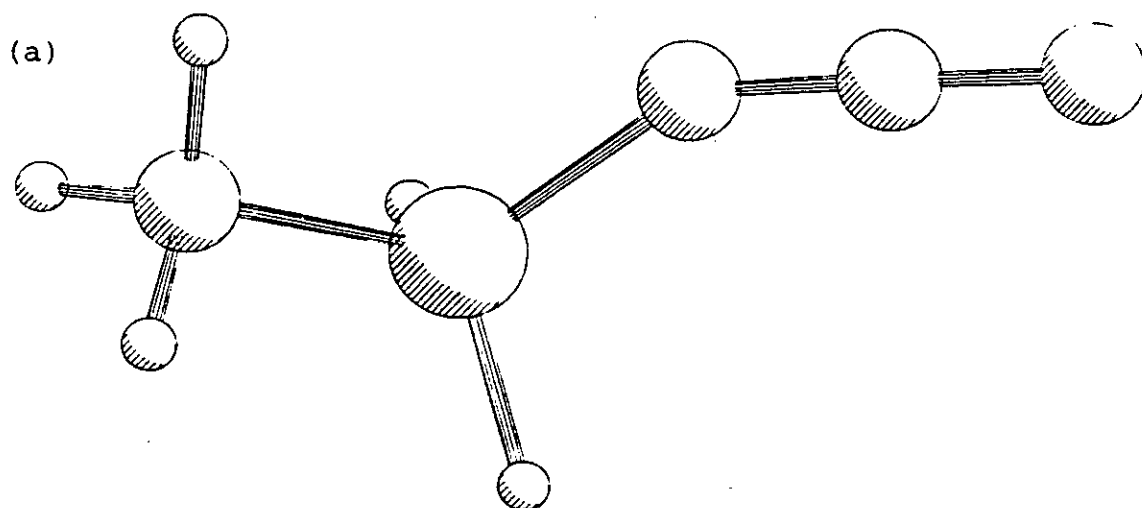
Figure 5.1: Observed and final difference radial distribution curves, $P(r)/r$, for $\text{CH}_3\text{SiH}_2\text{NCO}$.



Before Fourier inversion the data were multiplied by $s \cdot \exp[-0.000015 s^2 / (Z_{\text{Si}} - F_{\text{Si}})(Z_{\text{N}} - F_{\text{N}})]$.



Observed and final weighted difference molecular scattering intensities at nozzle-to-plate distances of (a) 128 and (b) 286 nm



Molecular structure of $\text{CH}_3\text{SiH}_2\text{NCO}$
(a) general view
(b) viewed along bond from N to Si

Table 5.1: Scale factors, weighting functions and correlation parameters

Compound	Camera distance mm	Δs	s_{\min}	s_1 nm	s_2 nm	s_{\max}	p/h	Scale factor	Wavelength nm
$\text{CH}_3\text{SiH}_2\text{NCO}$	285.73	2	20	40	120	146	0.0740	0.811(9)	5.676
$\text{CH}_3\text{SiH}_2\text{NCO}$	128.37	4	60	80	320	344	-0.0939	0.846(16)	5.676
$(\text{CH}_3)_2\text{SiHNCO}$	285.59	2	20	40	120	146	0.334	0.866(15)	5.681
$(\text{CH}_3)_2\text{SiHNCO}$	128.36	4	60	90	290	336	-0.0211	0.866(19)	5.682

Table 5.2: Least squares correlation matrix for $\text{CH}_3\text{SiH}_2\text{NCO}$ multiplied by 100.

r_3	r_5	r_6	Angles		u_1	u_5	u_8	u_{10}	u_{15}	u_{16}	
			1	4							
100					-42						r_3
	100	-98		-79	-94		44			-45	r_5
		100		78	+94					45	r_6
			100					-48	-68		1)
				100		75)Angles
					100				-40	62	u_1
						100					u_5
							100			-44	u_8
								100			u_{10}
									100	-62	u_{15}
										100	u_{16}

Only correlations with absolute values greater than 0.4 are included.

Table 5.3: Molecular parameters for $\text{CH}_3\text{SiH}_2\text{NCO}$

(a) Independent geometrical parameters:

	<u>Distance/pm</u>	<u>Amplitude/pm</u>
r_1 (Si-N)	171.8(4)	5.2(4)
r_2 (Si-H)	148.0(fixed)	8.8(fixed)
r_3 (Si-C)	185.3(5)	5.2(fixed)
r_4 (C-H)	109.0(fixed)	7.0(fixed)
r_5 (N=C)	120.5(15)	3.1(8)
r_6 (C=O)	116.9(13)	3.1(tied to u_5)
	<u>Angle/°</u>	
Angle 1 NSiC	111.6(8)	
Angle 2 HSiH	109.0(fixed)	
Angle 3 HCSi	110.2(14)	
Angle 4 SiNC	148.0(15)	
Angle 5 TCH ₃	45.0(fixed) ^a	
Angle 6 TSi-N	60.0(fixed)	
Angle 7 NCO	175.0(fixed) ^a	
Angle 8 T(C-N)	-80.0(fixed) ^a	

(b) Dependent distances

	<u>Distance/pm</u>	<u>Amplitude/pm</u>
d_8 (Si...H)	245.2(18)	11.7(17)
d_9 (C...H)	272.2(5)	13.0(fixed)
d_{10} (N...C)	295.5(13)	6.1(18)
d_{12} (N...H)	260.8(5)	13.0(fixed)
d_{13} (Si...C)	281.4(8)	7.2(10)
d_{14} (N...O)	237.2(5)	4.6(8)
d_{15} (Si...O)	393.1(13)	11.3(10)
d_{16} (C...C)	402.4(16)	20.3(50)
d_{17} (C...O)	514.4(15)	33.9(12)

^aangle found by R-factor plot.

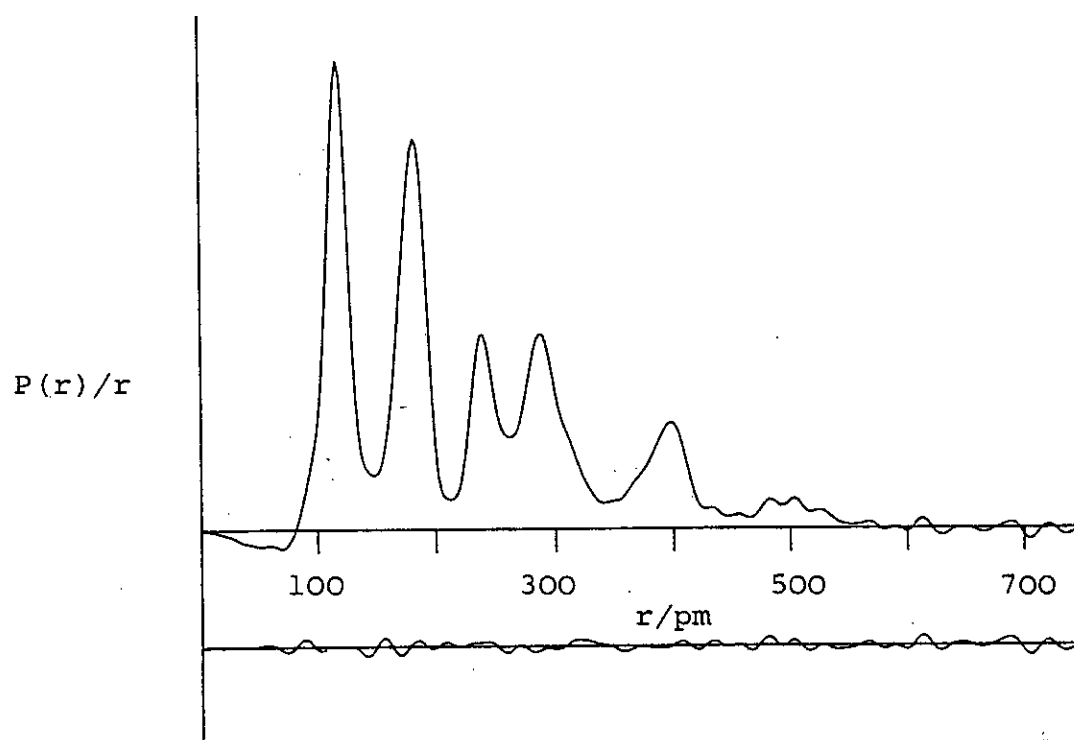
hydrogen and one heavier atom, were fixed at reasonable values. The final list of parameters and amplitudes is given in Table 5.3, corresponding to the values giving the lowest R-factors ($R_G = 0.094$, $R_D = 0.092$). The intensity curves are shown in Figure 5.2 and the pictures of the molecule are in Figure 5.3.

5.2.4 Refinement stages of $(CH_3)_2SiHNCO$ structure:

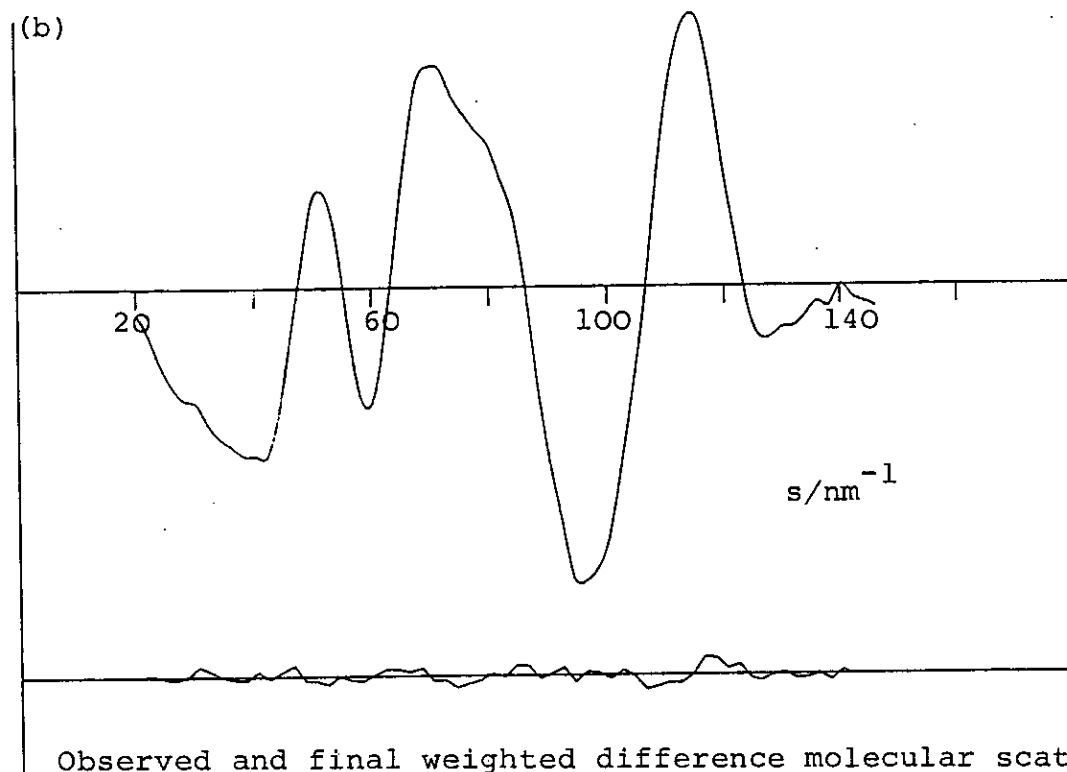
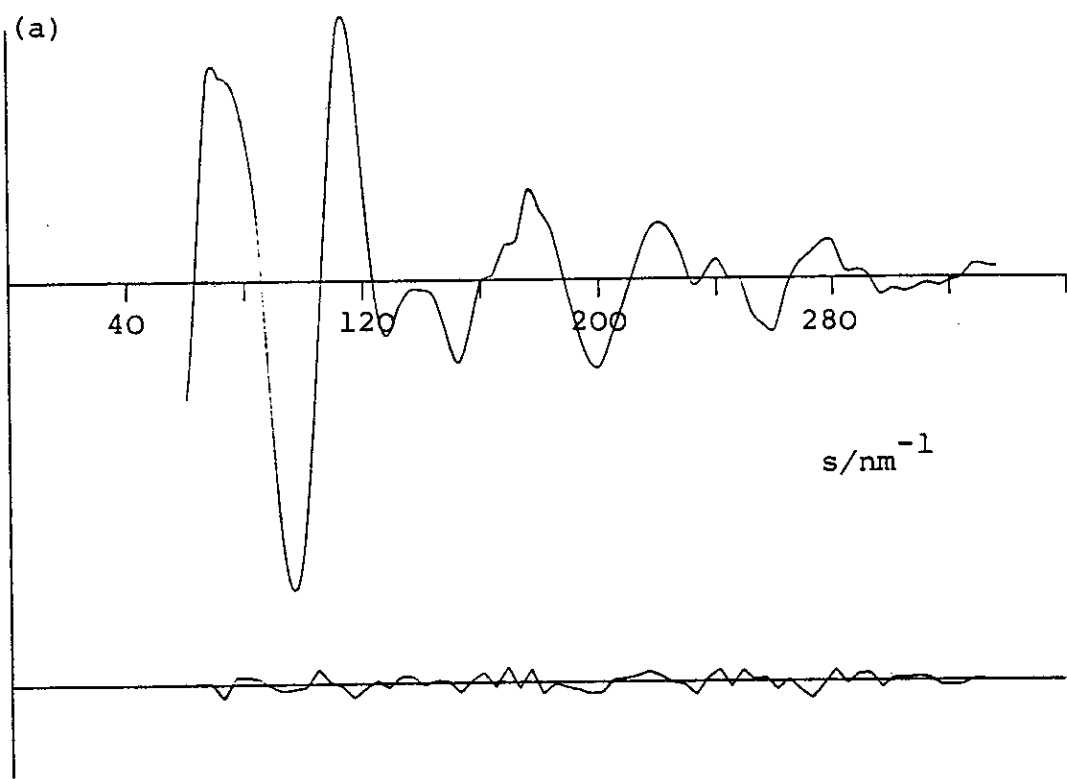
The radial distribution curve for $(CH_3)_2SiHNCO$ is similar to that for the monomethyl compound, with two main peaks at 120 and 180 pm, and smaller, broader peaks at 240, 290 and 400 pm. The Si-N and Si-C bond distances under the 180 pm peak again refined easily, and their amplitudes were refined whilst constrained to be equal. Under the peak at 120 pm are the N=C, C=O and C-H distances, and in this refinement all three distances refined although the final C-H bond is perhaps slightly long.

Again the Si-H distance did not refine and was fixed at 148.0 pm. It was found that when the NSiC and CSiC angles were refined independently one went to a high value, and one to a low value, although the average remained close to 110° . However by constraining the angles to be equal and refining NSiC, an acceptable angle was obtained. The torsion angle along the Si-N bond, rotating the NCO group with respect to the $(CH_3)_2Si$ group, was found from an R-factor plot from 0 to 180° and the angle giving the minimum R-factor was used

Figure 5.4: Observed and final difference radial distribution curves $P(r)/r$ for $(\text{CH}_3)_2\text{SiHNCO}$



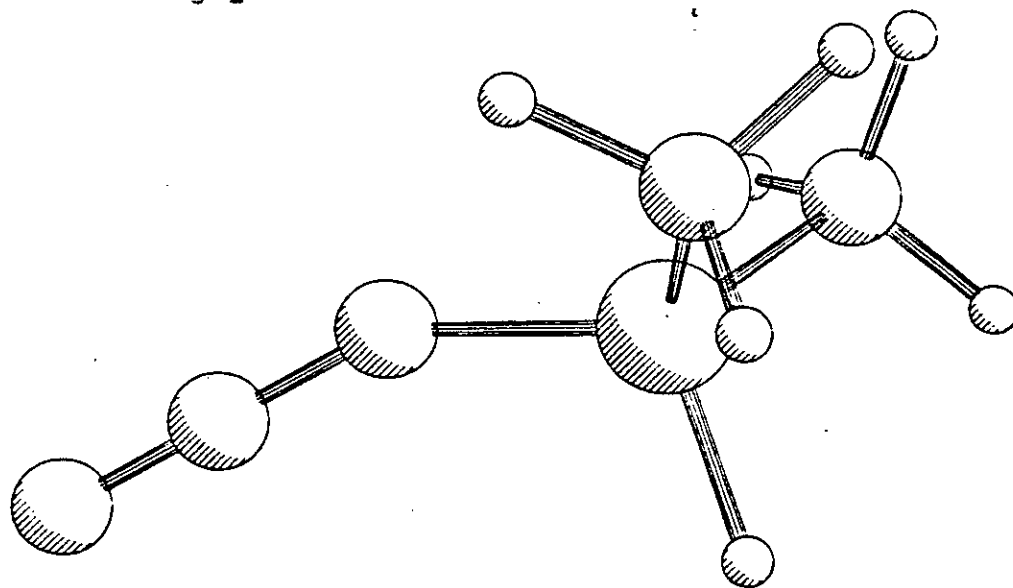
Before Fourier inversion the data were multiplied by $s \cdot \exp[-0.000015 s^2 / (Z_{\text{Si}} - F_{\text{Si}})(Z_{\text{N}} - F_{\text{N}})]$.



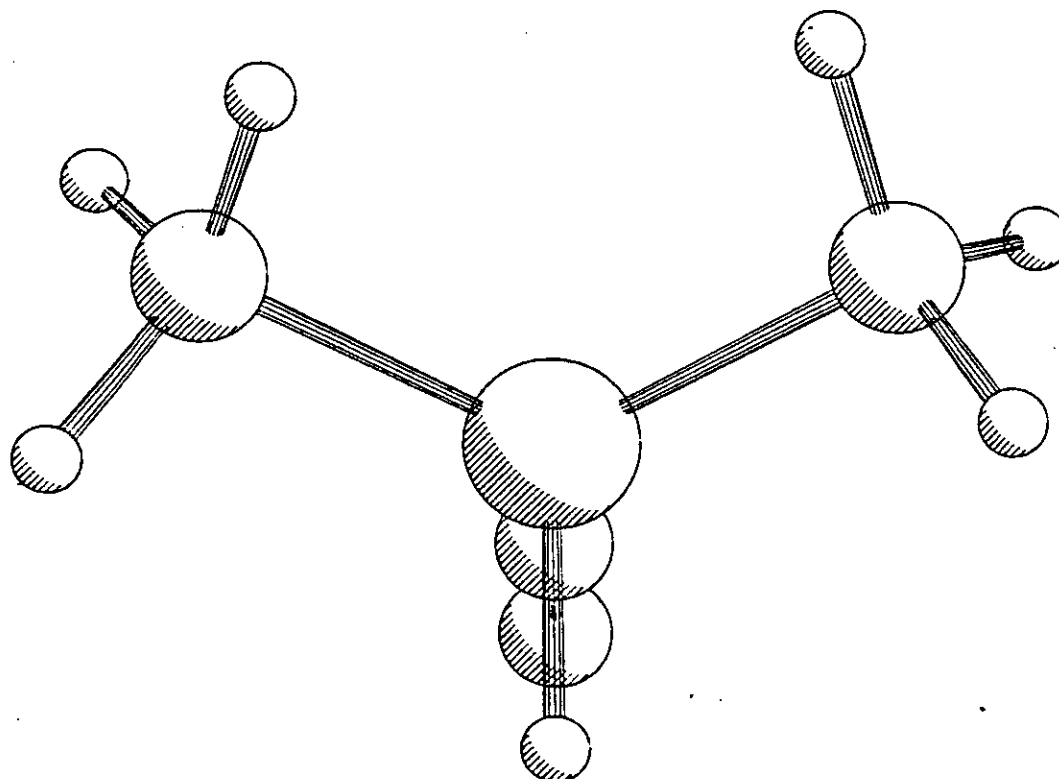
Observed and final weighted difference molecular scattering intensities at nozzle-to-plate distances of (a) 128 and (b) 285 mm

Figure 5.6: $(\text{CH}_3)_2\text{SiHNCO}$

(a)



(b)



Molecular structure of $(\text{CH}_3)_2\text{SiHNCO}$
(a) general view
(b) viewed along bond from Si to N

Table 5.4: Least squares correlation matrix for $(\text{CH}_3)_2\text{SiHNCO}$ multiplied by 100^a

<1	<2	r_3	r_4	r_5	<3	u_2	u_3	u_6	u_8	u_{10}	u_{11}	k_1	k_2	
100	53				-80				60					<1
	100								-51					<2
		100		-62										r_3
			100								44			r_4
				100		-41						-40	-47	r_5
					100									<3
						100						43	49	u_2
							100					60	64	u_3
								100				-50	-46	u_6
									100					u_8
										100				u_{10}
											100			u_{11}
												100	73	k_1
													100	k_2

^aOnly correlations with absolute values greater than 0.4 are included.

Table 5.5: Molecular parameters of $(\text{CH}_3)_2\text{SiHNCO}$

(a) Independent parameters

	<u>distance/pm</u>	<u>amplitude/pm</u>
r_1 (Si-N)	172.1(4)	6.1(tied to u_2)
r_2 (Si-C)	185.9(2)	6.1(4)
r_3 (C-H)	113.3(8)	9.4(10)
r_4 (N=C)	121.7(4)	3.5(fixed)
r_5 (C=O)	115.8(4)	3.5(fixed)
r_6 (SiH)	148.0(fixed)	7.7(20)
	<u>Angles/$^\circ$</u>	
Angle 1 (NSiC)	111.5(11)	
Angle 2 (SiCH)	107.2(7)	
Angle 3 (SiNC)	152.7(10)	
Angle 4 (CSiC)	111.5 ^a	
Angle 5 T(CH ₃)	10.0 ^b	
Angle 6 T(Si-N)	0.0 ^b	
Angle 7 (NSiH)	109.0(fixed)	
Angle 8 (NCO)	180.0(fixed) ^c	

(b) Dependent distances

	<u>distance/pm</u>	<u>amplitude/pm</u>
d_7 (C...C)	307.3(30)	15.5(tied to u_8)
d_8 (C...N)	296.0(20)	15.5(12)
d_9 (Si...C)	285.7(6)	6.8(6)
d_{10} (N...O)	237.5(4)	4.2(6)
d_{11} (Si...H)	244.6(10)	14.5(10)
d_{12} (C...C)	404.0(16)	27.6(35)
d_{13} (C...C)	404.0(16)	27.6(tied to u_{12})
d_{14} (Si...O)	398.3(8)	10.1(9)
d_{15} (C...O)	512.5(14)	26.0(26)
d_{16} (C...O)	512.5(14)	26.0(tied to u_{15})

^atied to be equal to NSiC - see text^bR-factor plot - see text^crefined to $180 \pm 3^\circ$, therefore fixed - see text.

for subsequent refinements. When the NCO angle was refined it remained at 180° with a large estimated standard deviation and so was fixed at that value. Similarly, the twist of the methyl groups was found by successive refinements with systematic variation of the angle. The remaining angles refined to acceptable values, except the NSiH, which was fixed at 109.0° .

The heavy atom non-bonded distance amplitudes were all refined with the pairs of C(H)..C and C(H)...O amplitudes constrained to be equal when refining. Also $u(\text{C(H)...C(H)})$ and $u(\text{C...N})$ were constrained to be equal. All the other amplitudes not refined were fixed at values compatible with other methylsilyl compounds. The final parameters giving the minimum R-factors [$R_G = 0.0749$, $R_D = 0.0597$] are given in Table 5.6, and the radial distribution curves and intensity curves are given in Figures 5.4 and 5.5. Figure 5.6 is a perspective picture of the molecule.

5.3 Results and Discussion

The interpretation of the structures of pseudohalides has always been difficult in view of the problems of shrinkage and the unknown extent of (p-d) π bonding. Molecular orbital calculations have predicted a linear structure even without the use of silicon 3d orbitals⁹³. Thus the precise angle at SiNC may be a fine balance of a

a number of factors, steric and electronic. On the other hand, the bond lengths may reflect mainly electronic factors.

The Si-C bond lengths of 185.3(5) and 185.9(2) are slightly shorter than in many methylsilyl compounds but the difference is only 2-3 pm. For example $\text{Si}_2(\text{CH}_3)_6$ ¹⁰² (187.9(3) pm), $\text{Si}(\text{CH}_3)_4$ ¹⁰² (187.6(2)), $(\text{SiH}_3)_2\text{CH}_2$ ¹⁰³ (187.4(2) pm), $(\text{CH}_3)_3\text{SiC}\equiv\text{Cl}$ ¹⁰⁴ (186.8(4) pm), Me_3SiNCO ⁹² (189(1)).

It is also noted that the Si-C bond is not shorter than the predicted value calculated from the covalent radii of Pauling⁸¹, and making an allowance for the difference in electronegativities introduced by Schomaker and Stevenson¹⁰⁵. This suggests that there is little, if any, π bonding between carbon and silicon, as would be expected as there is no lone pair unlike the Si-N and Si-O bonds which are up to 16 pm shorter than predicted. Alternatively it can be considered that the electrostatic attraction between silicon and carbon is small and the bond remains covalent with no ionic character.

The Si-C amplitudes are consistently higher than calculated by Cyvin¹⁰⁶, but are close to the values obtained for Me_3SiNCO ⁹², and other methylsilyl compounds studied recently¹⁰⁷ (i.e. $(\text{MeSiH}_2)_2\text{O}$, $(\text{Me}_2\text{SiH})_2\text{O}$ and $(\text{MeSiH}_2)_2\text{NH}$). The increase may arise in these compounds because the Si-C distance overlaps with either the Si-N or Si-O distances in the radial distribution curve,

although similar values have been observed for $\text{CH}_3\text{SiH}_2\text{Cl}$ and $\text{CH}_3\text{SiH}_2\text{Br}$ ¹⁰⁷, which do not have any distances overlapping with Si-C.

Considerable interest has been shown in the significance of the changes in length of the Si-N bond. The sum of the covalent radii (Pauling)⁸¹ is 187 pm but the observed value is much shorter. The shortening was first observed in $(\text{SiH}_3)_3\text{N}$ ¹⁰⁸, and explained as due to donation of the nitrogen lone pair into the vacant d orbitals of the silicon atom. The shortening of the bond also appears to be related to the number of silicon atoms around nitrogen as Table 5.6 shows:

Table 5.6: Variation of Si-N bond with number of silicon atoms around nitrogen

Compound	Si-N/pm	Ref
$(\text{SiH}_3)_3\text{N}$	173.5(2)	108
$(\text{SiH}_3)_2\text{NH}$	172.7(3)	109
$(\text{SiH}_3)\text{N}(\text{CH}_3)_2$	171.6(4)	110
$[\text{Si}(\text{CH}_3)_3]_2\text{NH}$	173.7	111

With more silyl groups around the nitrogen the lone pair will be donated over more Si-N bonds, and so will have less shortening effect, giving a longer bond. Additionally, one can see from the table above that replacement of hydrogen by methyl groups on the silicon causes an increase in bond length. This would suggest there must be a reduction in the electron acceptor ability of silicon by the electron donating effect of

methyl groups. For instance, if the Si-N bond contains some (p-d) π bonding, the methyl groups would appear to donate electrons along Si-C σ -bond towards the silicon atom, decreasing the acceptor-ability of the d-orbitals, resulting in less shortening of the Si-N bond length. Listed in Table 5.7 are the Si-N bond lengths of a number of silyl isocyanates including monomethyl and dimethyl studied in this work, and showing the variation of Si-N to number of methyl groups. Also in the table are parameters for trihalosilyl compounds.

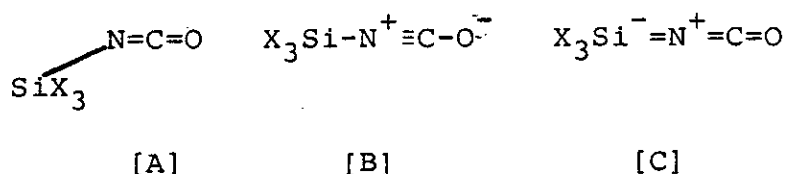
Table 5.7: Certain parameters of silyl isocyanates (bond length/pm, angles/ $^{\circ}$)

Compound	Si-N/pm	C=O	N=C	SiNC	Ref
SiH ₃ NCO	170.3	116.4	121.6	151.7	28
MeSiH ₂ NCO	171.8	116.9	120.5	148.0	This work
Me ₂ SiHNCO	172.1	115.8	121.7	152.7	This work
Me ₃ SiNCO	176	118	120	150	92
F ₃ SiNCO	164.8	118 ^a	118 ^a	161	94
Cl ₃ SiNCO	162.6	113.9	121.9	138	93
(SiH ₃) ₃ N	173.5	-	-	-	108

^amean value of bond lengths.

The further shortening of the Si-N bond in the halosilyl isocyanates can be explained as an inductive electron withdrawing effect by the halide atoms, causing increased (p-d) π bonding between silicon and nitrogen and delocalisation of electrons on the halide.

This change in bond length can also be interpreted in terms of simple valence bond structures:



Structures [A] and [B] will be adequate for HNCO and substituted methyl isocyanates, but the third structure [C] is necessary for the structures of silicon isocyanates to seem reasonable. This structure allows for a negative charge to reside on the silicon, possibly delocalised into the d orbitals. It explains the shortening on the Si-N bond, and will be stabilised by SiCl₃ and SiF₃ groups, but destabilised by SiMe₃, SiHMe₂ and SiH₂Me groups. The methyl substituted silyl group will stabilise structure [B] by electron donation to the nitrogen.

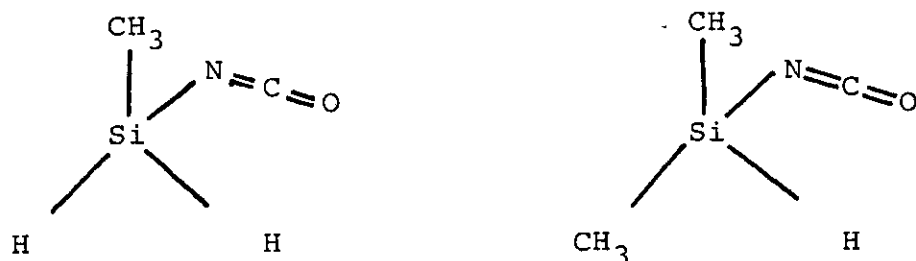
The bond lengths of N=C and C=O in MeSiH₂NCO and Me₂SiHNCO are both in accord with the valence bond structures. Thus the C=O bond should be short relative to the N=C bond when the X group is electron releasing (structure A) or when structure [C] is stabilised and it is found that the C=O bond is longer in the methylsilyl isocyanates than in the trihalosilyl isocyanates^{93,94}.

The heavy atom angles of NSiC and CSiC are slightly wider than tetrahedral but this may be simply attributed to the increased steric bulk compared to hydrogen atoms, and the HCSi angle in both compounds remains exactly tetrahedral (within one estimated standard deviation). The most interesting geometric parameters of the methylsilyl

isocyanates are in the SiNC angle and the torsion angle between the NCO and methyl groups along the Si-N bond. The apparent SiNC angle in MeSiH_2NCO is $148.0^\circ(15)$ and in Me_2SiHNCO is $152.7^\circ(10)$. Firstly, it is noticed that these angles are close to the angles found for $\text{SiH}_3\text{NCO}^{28}$ (151.7°) and $\text{Me}_3\text{SiNCO}^{92}$ ($150^\circ(3)$), even though the structural analysis by microwave^{95,96,97} and theoretical calculations³⁶ indicate linear configurations. The rationalisation of this disparity for SiH_3NCO is that the low frequency large amplitude bending mode at N causes a shrinkage effect, giving an apparent bent configuration. The infra-red and Raman spectroscopic data for these compounds (see Chapter 8) suggest that both dimethyl and monomethyl silyl isocyanates have low frequency bending modes below 100 cm^{-1} , assigned to SiNC bends, and hence the same explanation could apply to these structures.

When the configuration of methyl groups to NCO was established there was a clear minimum R-factor when the NCO was eclipsing an Si-H bond and trans to the bisector of CSiC (in Me_2SiHNCO) or at 120° to the methyl group (in MeSiH_2NCO).

Therefore the relative position of the methyl groups to the NCO is the same for both structures, and it would appear that most steric influence is exerted by the lone pair of electrons on the nitrogen. Without the lone pair the steric interaction between CH_3 and NCO would be expected to give the monomethyl compound a trans configuration. Hydrogen bonding between the C=O and SiH is unlikely as



the interatomic distance is too large. The configuration in trimethylsilyl isocyanate⁹² was thought to be staggered, with the C=O trans to one methyl group. This is as predicted considering bulk steric influences and would leave the nitrogen lone pair eclipsing one methyl group, suggesting that the C=O:CH₃ repulsive interaction is greater than the CH₃:lone pair interaction, which in turn is greater than the C=O:SiH interaction.

The fact that there is a clearly preferred configuration of the methylsilyl isocyanates suggests that the SiNC must be bent or is bending at a low frequency in a particular orientation with a large amplitude. The potential function for SiH₃NCO was described as a circular valley for the ground vibrational state, with a

slight hump at the linear configuration⁹⁷ and the same description can be used for the substituted silyl isocyanates, except that within the circular valley will be small humps corresponding to the methyl groups. The proton barrier has been determined for SiH_3NCO , with a value of about 2 cm^{-1} .

The mean amplitudes of vibration also give an insight into the bending motion of SiNC . Calculated mean amplitudes^{111a} of $\text{Si}\dots\text{O}$ for a rigid molecule refinement in SiH_3NCO give a value about half the magnitude of the experimental magnitude and the experimental values for the methylsilyl isocyanates amplitudes compare well with the values for SiH_3NCO . The same similarities are found for $\text{Si}\dots\text{C}$ (see Table 5.8).

Table 5.8: Amplitudes of vibration (pm)

Atomic Distance	Calculated values ^{111a} at 273 K for				
	SiH_3NCO	SiH_3NCO	MeSiH_2NCO	Me_2SiHNCO	Me_3SiNCO
$\text{Si}\dots\text{C}$	3.4	6.8(12)	7.2(10)	6.8(6)	6.5(fixed)
$\text{Si}\dots\text{O}$	5.1	9.6(9)	11.3(10)	10.1(9)	7.5(fixed)

Using these experimental amplitudes and comparing the change of mean amplitudes and shrinkage with assumed SiNC bending frequency ν_{10} , the plot that best reproduced the experimental results for SiH_3NCO was for $\nu_{10} = 69 \text{ cm}^{-1}$. Subsequently the band has been observed at 64 cm^{-1} in the gas phase⁹⁸. Since the amplitudes across the nitrogen atom are all close for this range of isocyanates, the model

applied to SiH_3NCO for shrinkage and a low frequency large amplitude bending mode is likely to be applicable to dimethyl and monomethyl silyl isocyanate.

The valence bond structures on page 141 are useful in explaining the linearity at nitrogen. It has already been established that structure [C] is favourable for silicon pseudohalides and this clearly will be linear. However the addition of methyl groups around the silicon will stabilise structure [B] (also linear) and to some extent structure [A] (non-linear). Thus there must be competing structures, with the methyl groups stabilising one that is linear and one that is bent. Also, of course, the linearity can be explained without the valence bond structure as being due to $(p-d)\pi$ bonding between silicon and nitrogen. This has been discussed earlier and is a very plausible explanation for linear SiNCO groups.

It is possible to attribute the structural anomalies at nitrogen without the use of the d orbitals on silicon. The second order Jahn-Teller effect¹¹² has been used to predict the angle in a number of silyl pseudohalides³⁶ in which the linearity of XYZ group was predicted in examples where the valence orbitals of X and Z were much less tightly bound than those on Y. If the X and Z orbitals were more tightly bound than those on Y the structure of XYZ should be bent. Therefore taking the values for SiNCO where XYZ is SiNC, the binding energy of the orbitals for N is greater than for Si and C and so a linear structure would be expected, without resorting to using $(p-d)\pi$ bonding.

According to calculations by Glidewell³⁶ the pseudohalides with the biggest deviation from linearity at nitrogen are the asymmetrically substituted silyl compounds, e.g. SiH_2Cl , 170.5° ; SiHCl_2 , 174.7° ; SiH_2F , 172.7° ; but from the electron diffraction evidence there is not a significant difference in the apparent SiNC angle to show that $(\text{CH}_3)_2\text{SiHNCO}$ and $\text{CH}_3\text{SiH}_2\text{NCO}$ were more bent than the symmetric SiH_3 and $(\text{CH}_3)_3\text{Si}$ isocyanates.

An alternative approach is to consider the thermal average Si...C distance using the "hard sphere" radii proposed by Bartell³⁷. It was found³⁸ that the Si...C distance is remarkably constant in a range of silicon compounds with totally different bond lengths; for example SiH_3NCO ²⁸ (283 pm), $\text{SiH}_3\text{NCNSiH}_3$ ³⁸ (281 pm), $\text{SiH}_3\text{N}(\text{CH}_3)_2$ ⁸⁵ (276 pm), $(\text{CH}_3)_2\text{SiHNCO}$ (285.7 pm), and $\text{CH}_3\text{SiH}_2\text{NCO}$ (281.4 pm), and it is suggested that the angle is determined more by the Si...C interaction than the Si-N, N=C bonds and presence of a nitrogen lone pair.

Finally, as can be seen from the pictures of the molecules in Figures 5.7 and 5.8, the hydrogens of the methyl groups adopt a staggered configuration to the silyl hydrogens in $\text{CH}_3\text{SiH}_2\text{NCO}$, and to each other and the Si-H in $(\text{CH}_3)_2\text{SiHNCO}$.

Thus this study of the methyl substituted analogues of SiH_3NCO has helped to support the earlier structural work. The structures are remarkably similar to that of SiH_3NCO although there is a clear lengthening of the Si-N.

bond, while the change in the apparent SiNC angle is probably insignificant. The adoption of a preferred configuration of NCO to methyl groups, with the lone pair on nitrogen governing the final shape, suggests that MeSiH_2NCO and Me_2SiHNCO may be slightly bent in the ground vibrational state with a small hump in the potential function of the SiNC bending mode at the linear configuration.

Further work in the far infra-red region would probably be useful but the methyl bends and torsions may complicate this region of the spectra. Also, the photoelectron spectra may help to identify how important the nitrogen lone pair is.

CHAPTER 6: THE GAS PHASE STRUCTURES OF MONOMETHYLSILYL
ISOTHIOCYANATE AND DIMETHYLSILYL ISOTHIOCYANATE

6.1 Introduction

The spectra and structures of silyl and trimethylsilyl isothiocyanates have been investigated by a number of researchers. The Raman spectra of the liquid phase and the infra-red spectra of the gas phase of silyl isothiocyanate¹¹³ were interpreted on the basis of C_{3v} molecular symmetry which requires the SiNCS to be linear. Microwave data¹¹⁴ confirmed this structure, but with a large amplitude SiNC bending vibration, the frequency of which was estimated to be 54 cm^{-1} . In the most recent infra-red and Raman study¹¹⁵ it was observed that the band assigned to the SiNC bend does not show appreciable broadening due to hot-band transitions and it was suggested that this was a good indication that the vibration was harmonic. The electron diffraction study of SiH_3NCS ²⁸ found that the SiNC angle was not linear but explained this as a result of shrinkage and characterised the bending potential function with a purely harmonic potential with $V(\text{cm}^{-1}) = 2400 \alpha^2$. In the same work SiH_3NCO was found to have a very anharmonic potential function with $V(\text{cm}^{-1}) = 1090 \alpha^4 - 300 \alpha^2$.

Other workers have looked at the gas phase structure⁹² and infra-red and Raman spectra of trimethylsilyl isothiocyanate¹⁰⁰. The structure analysis showed an apparent angle at nitrogen of $154(2)^\circ$, but in all the parameters there are large esds and the determination is not

as reliable as more recent structural work. The spectroscopic study¹⁰⁰ concluded, particularly in the light of work on SiH_3NCS , that the experimental angle is smaller than the true equilibrium angle because of the large shrinkage effect arising from the large amplitude low frequency bending mode. The fundamental was observed at 45 cm^{-1} in the Raman spectrum as a very broad and depolarised band, and no overtone was found.

Evidence for a linear SiNCS chain was that only one band was observed for the NCS bend (an e mode for C_{3v} symmetry, but a' and a'' for C_s symmetry), while the related structure Me_3SiN_3 has two bands for the NNN bend. Clearly the analysis of the Si...S peak²⁸ in the radial distribution curve, as had been done for SiH_3NCS , was not possible for Me_3SiNCS because of the overlap with the C...C distance peaks.

Additionally, the spectroscopic data for $\text{Si}(\text{NCS})_4$ ^{116,117,118} has been interpreted on the basis of T_d symmetry around the silicon, implying a linear structure for the four SiNCS groups. In contrast the infra-red data for $(\text{CH}_3)_3\text{CNCS}$ ¹¹⁸ indicated C_s symmetry and the electron diffraction study of CH_3NCS ¹¹⁹ gave a CNC angle of 141.6° , which is more bent than any silyl pseudohalide. The linearity of the silicon compounds, and the bent carbon compounds, has been rationalised in a number of ways. One factor may be the delocalisation of the nitrogen lone pair into the vacant d orbitals on the silicon atom. This is obviously not possible in the carbon compounds. Also the possible valence bond structures are more stabilised by

silicon than carbon.

There is interest in the Si-N bond length and how the distance varies with substituents on the silicon. In all cases the Si-N distance is shorter than the sum of the covalent radii^{63,81} while the C-N bond length is much closer to the predicted value and this observation is used to support the interpretation of delocalisation in silicon but not carbon.

Finally, it was of interest to compare the molecular structures of the methylsilyl isothiocyanates with the predicted structures of a number of halosilyl pseudohalides³⁶. The calculations were designed to test quantitatively a model of molecular geometry based upon the second order Jahn-Teller effect, in which ligands of low electronegativity lead to stereochemical inactivity on lone pairs of electrons on a central atom. The overall model envisaged three major cases: according to whether the ligand's electronegativity is greater than, comparable with, or less than the electronegativity of the central atom, then the force constant for skeletal deformation from linear coordination is negative, close to zero, or positive, giving rise to, respectively, distortion with stereochemical activity of lone pair, or to large amplitude, low frequency skeletal vibration, or undistorted skeletons with no lone pair on the central atom. From these calculations the force constant for all silyl isothiocyanates were between 2.7 to $6.9 \times 10^{-3} \text{ Nm}^{-1}$ (i.e.

v.small) and hence it was predicted that the shape at nitrogen should be linear. The silyl isocyanates had values of -3.8 to $+8.08 \text{ Nm}^{-1}$, giving angles bent by up to 10° , and the methyl pseudohalides had force constants of -10 to -2 Nm^{-1} , giving clearly bent configurations.

A crystal structure of SiH_3NCS is not available and, although there have been attempts to grow crystals¹²¹, these have been unsuccessful, or the crystals have suffered X-radiation damage. However the infra-red spectra in various matrices¹²² have all been interpreted in terms of C_{3v} symmetry molecules with a linear chain of SiNCS . This is not the same as SiH_3NCO which was found to be linear in the gas phase (like SiH_3NCS) but bent in the solid phase, and bent in various matrices.

It is therefore of interest to study the mono- and dimethyl-silyl isothiocyanates. These should have C_s symmetry, whether the configuration is linear or bent at nitrogen, and one would hope that comparison of the apparent angle in the methyl isothiocyanates with SiH_3NCS will give some idea of whether the angle is more bent when the silicon atom is asymmetric, as predicted by Glidewell³⁶ for halosilyl pseudohalides. Also there is interest in the configuration of the methyl groups to the NCS group, particularly in the light of the shapes adopted by the isocyanates described in Chapter 5.

6.2 Refinement and Models

6.2.1 Model of $\text{CH}_3\text{SiH}_2\text{NCS}$:

For the purposes of the refinement, it was assumed that the methyl group had local C_{3v} symmetry: the molecule can then be described by six bond lengths, five bond angles and three torsion angles. The bond distances chosen were Si-N, Si-H, Si-C, C-H, N=C and C=S; the angles were NSiC, HSiH, SiCH, SiNC and NCS; and the three torsion angles are along the Si-N bond, along the C-N bond, and the twist of the methyl hydrogen about the Si-C bond. The initial conformation of the NCS group was trans to the methyl group and the methyl group torsion was at zero when one hydrogen was in the heavy atom plane, and trans to the SiH_2 group. It was also assumed that the bisectors of the HSiH and NSiC angles coincided.

6.2.2 Model of $(\text{CH}_3)_2\text{SiHNCS}$:

This molecule was described by six bond lengths, six bond angles and three torsion angles. The two methyl groups were assumed to have local C_{3v} symmetry and the NCS group was initially assumed to be trans to the bisector of the CSiC angle. The six bond lengths were the Si-N, Si-C, C-H, Si-H, N=C and C=S; the angles were NSiC, CSiC, SiCH, NSiH, SiNC and NCS; and the torsion angles were of one methyl group, one along the N=C bond and one along the Si-N bond, rotating the $\text{HSi}(\text{CH}_3)_2$ group with respect to

Table 6.1: Scale factors, weighting functions and correlation parameters

Compound	Camera Height mm	Δs	s_{\min}	s_1	s_2	s_{\max}	p/h	Scale Factor	Wavelength/pm
MeSiH ₂ NCS	285.65	2	20	40	120	146	0.4225	0.885(20)	5.682
MeSiH ₂ NCS	128.36	4	60	90	290	328	0.4417	0.826(41)	5.682
Me ₂ SiHNCS	285.67	2	24	40	120	146	0.2789	0.908(19)	5.681
Me ₂ SiHNCS	128.36	4	60	90	280	340	0.0426	0.907(27)	5.681

the NCS group. The methyl twist was a clockwise movement relative to that in which one hydrogen lay in the CSiN plane. The nozzle to plate distances and operating wavelengths are given in Table 6.1 for mono- and dimethylsilyl isothiocyanates.

6.2.3 Refinement of the $\text{CH}_3\text{SiH}_2\text{NCS}$ structure:

In the refinements of the structures of these compounds it was anticipated that there might be problems distinguishing the C-H and N=C lengths and the Si-N and Si-C lengths. In fact most of the bond distances were refined to give reasonable values.

The main features of the radial distribution curve were one peak at 120 pm, a broad peak at 170, one large peak at 280 pm and minor peaks at 245, 380, 410 and 440 pm.

The peak at 120 pm contains the C-H and N=C bond distances and it was found necessary to fix the C-H, and refine N=C, to obtain acceptable values. The broad major peak at 170 pm contains the C=S, Si-N and Si-C distances, and all refined. The main bond angles of the molecule were defined by the C...N, Si...C and N...S non-bonded distances, all of which overlap under the peak at 280 pm. In fact NSiC and NCS were fixed at 109 and 180 respectively leaving the SiNC angle to refine to 168° . The position of the methyl group relative to the NCS group was defined by the C...C and C...S peaks, both of which are relatively small. The optimum torsion angle was found by varying the

angle in a series of refinements and recording the minimum R-factor. Then for subsequent refinements the torsion angle was fixed at this value. A similar method was used to find the twist angle for the methyl group - giving a staggered conformation with respect to the SiH_2 group. In all the monomethylsilyl compounds studied so far the HSiH angle was not refineable and so it was fixed at 110° , while the HCSi angle did refine to 110.2° . The amplitudes of vibration for the bonded interatomic distances in the $\text{CH}_3\text{SiH}_2\text{-N}$ group did not refine well and so were fixed at values found in other methylsilyl and isothiocyanate compounds but the N=C and C=S amplitudes refined satisfactorily.

Once most of the bonded amplitudes were fixed the non-bonded amplitudes refined reasonably, and compare well with those for $\text{CH}_3\text{SiH}_2\text{NCO}$. The final molecular parameters are given in Table 6.2. Allowance has been made in the quoted uncertainties for possible systematic errors, and these have been added to the random errors obtained by the least squares analysis. The least squares correlation matrix is presented in Table 6.3, and it can be seen that the refineable parameters and amplitudes were those that had relatively low correlation. The parameters quoted are those that gave the lowest R-factor ($R_G = 0.168$ and $R_D = 0.123$). This is not a particularly good fit between the theoretical and experimental intensity curves, and the radial distribution curve (Figures 6.1 and 6.2) shows that the main region of poor fit is between 90 and 130 pm. Since the C-H and N=C bonds are at reasonable values, and

Table 6.2: Molecular parameters for monomethyl silyl isothiocyanate

(a) Independent parameters

	<u>Distance</u>	<u>Amplitude</u>
r_1 (Si-N)	171.0(6)	5.0(fixed)
r_2 (Si-H)	148.0(fixed)	9.0(fixed)
r_3 (Si-C)	184.8(7)	5.0(fixed)
r_4 (C-H)	109.0(fixed)	8.0(fixed)
r_5 (N=C)	118.7(6)	4.6(10)
r_6 (C=S)	156.8(5)	4.5(7)

	<u>Angles</u>
Angle 1 NSiC	109.0(fixed)
Angle 2 HSiH	110.0(fixed)
Angle 3 HCSi	110.2(1.8)
Angle 4 SiNC	168.4(1.6)
Angle 5 τ (CH ₃)	10.0(fixed) ^a
Angle 6 τ (Si-N)	0.0(fixed) ^a
Angle 7 NCS	180.0(fixed)
Angle 8 τ (C-N)	0.0(fixed) ^a

^afixed by R-factor plot - see text

Distances and amplitudes of vibration are given in pm.
Angles are given in degrees, and angles 5, 6, and 8 are
torsion angles along the given bond or of the group.

/..

Table 6.2 (contd)

(b) Dependent parameters

	<u>Distance</u>	<u>Amplitude</u>
d_7 (Si...H)	244.8(26)	12.0(fixed)
d_8 (N...C)	289.7(6)	6.5(fixed)
d_9 (N...H)	260.8(4)	13.0(fixed)
d_{10} (Si...C)	288.3(5)	6.7(12)
d_{11} (N...S)	275.6(6)	5.2(9)
d_{12} (Si...S)	444.4(6)	9.1(6)
d_{13} (C...C)	400.2(15)	19.1(50)
d_{14} (C...S)	551.4(23)	30.7(55)

(c) Other amplitudes kept fixed

	<u>Amplitude</u>
$H_C \dots H_C$	14.0
$C \dots H_{Si}$	13.0
$H_{Si} \dots H_{Si}$	12.0
$H_C \dots H_{Si}$	17.0
$N \dots H_C$	15.0
$C \dots H_{Si}$	19.0
$C \dots H_C$	20.0
$S \dots H_C$	25.0
$S \dots H_{Si}$	20.0

Table 6.3: Least squares correlation matrix x100 for CH₃SiH₂NCS

r ₁	r ₃	r ₅	r ₆	A3	A4	u ₅	u ₆	u ₁₀	u ₁₁	u ₁₂	k ₁	k ₂		
100		-35			-41		-33							r ₁
	100										36			r ₃
		100	-33					32						r ₅
			100		-33									r ₆
				100							-41			A3
					100									A4
						100						32		u ₅
							100					31		u ₆
								100	66		31	37		u ₁₀
									100		30	37		u ₁₁
										100		48		u ₁₂
											100	33		k ₁
												100		k ₂

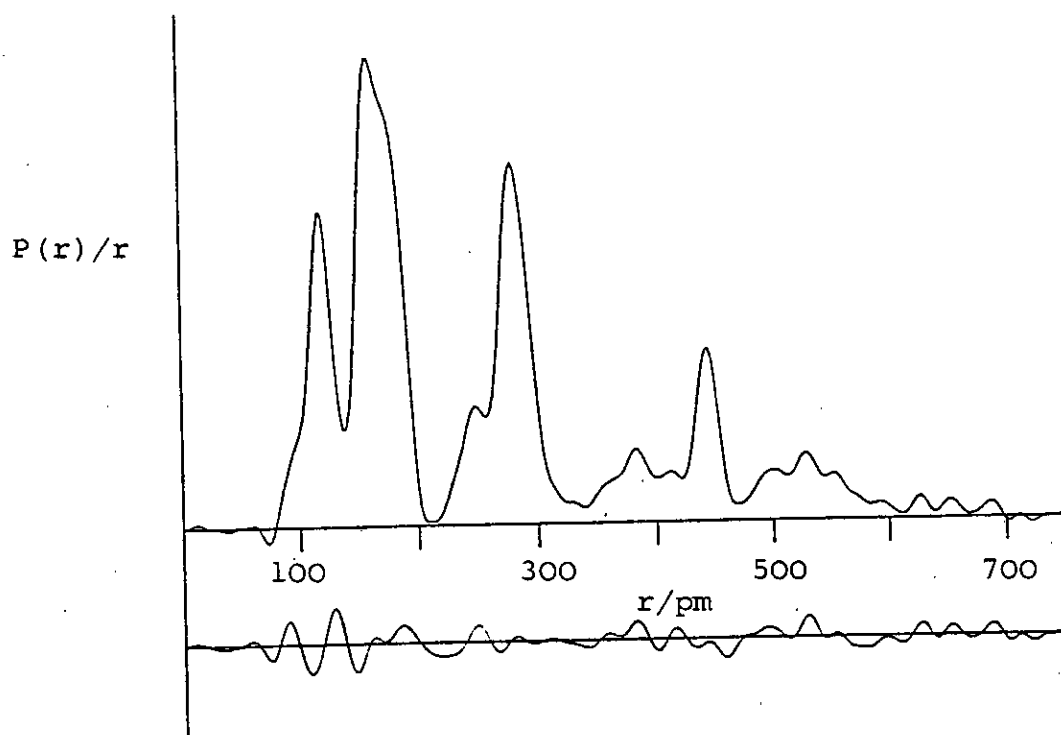
r - bond distance

A - Angle

u - amplitude of vibration

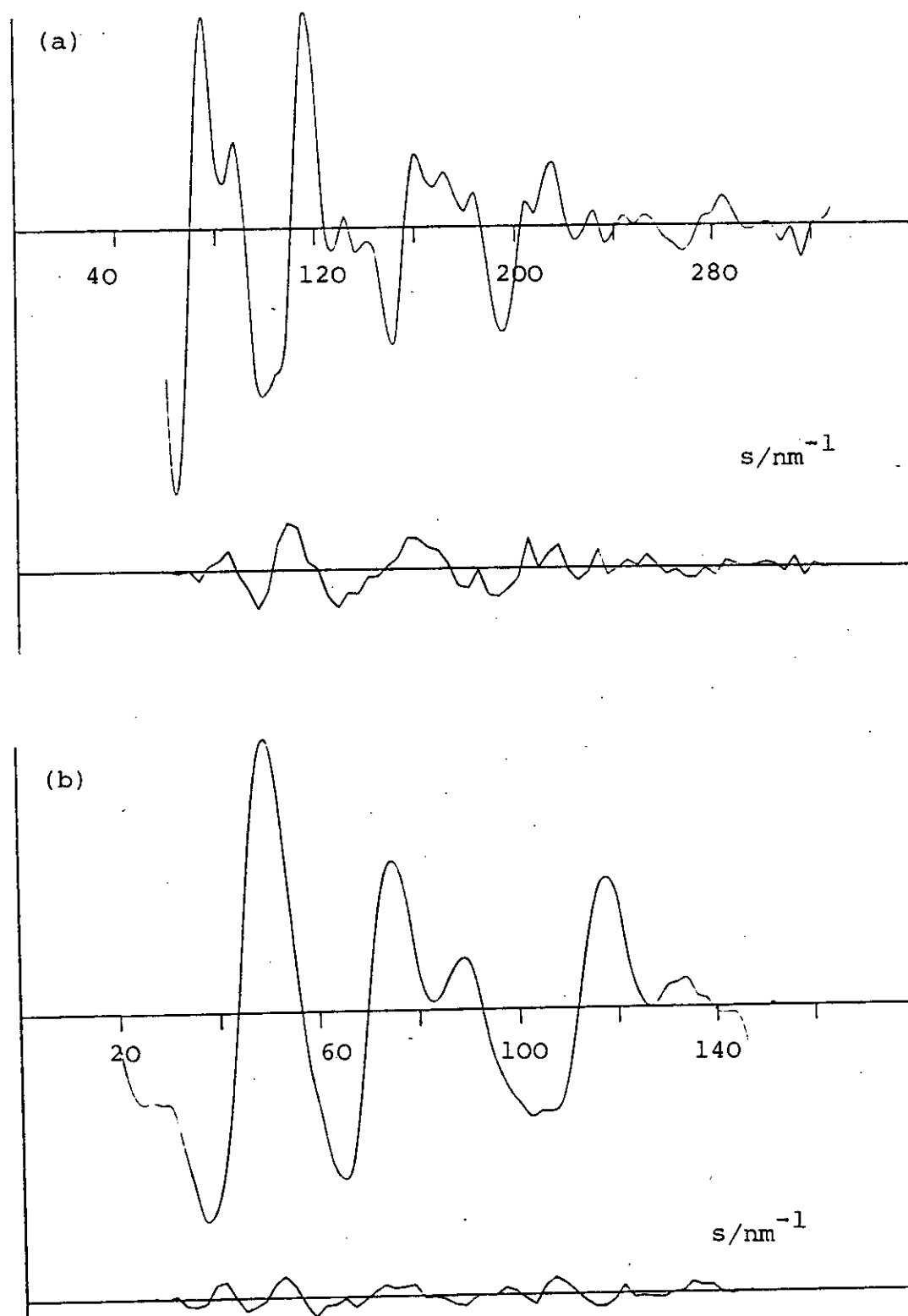
Only values greater than 30 are given

Figure 6.2: Observed and final difference radial distribution curves, $P(r)/r$, for $\text{CH}_3\text{SiH}_2\text{NCS}$



Before Fourier inversion the data were multiplied by $s \cdot \exp[-0.000015 s^2 (z_{\text{Si}} - F_{\text{Si}})(z_{\text{N}} - F_{\text{N}})]$.

Figure 6.1: $\text{CH}_3\text{SiH}_2\text{NCS}$



Observed and final weighted difference molecular scattering intensities at nozzle-to-plate distances of (a) 128 and (b) 286 mm

the poor fit cannot be explained by an impurity (e.g. $(\text{MeSiH}_2)_2\text{O}$), so the problem must arise from the experiment. Possible explanations are that the sector equation is not adequate or that the photographic plates were very dark and insufficient detail could be made out from them. From the intensity curves it can be seen that the short nozzle to plate distance has the poorest agreement: short distance $R_G = 0.277$, $R_D = 0.264$, long distance $R_G = 0.121$, $R_D = 0.08$.

6.2.4 Refinement of the $(\text{CH}_3)_2\text{SiHNCS}$ structure:

The data for this compound gave a much more satisfactory refinement and the agreement between experimental and theoretical curves is good, suggesting that the sector equation is quite adequate. The radial distribution curve is similar to the curve for $\text{CH}_3\text{SiH}_2\text{NCS}$ except that the C=S bond distance is now distinct from the peak containing the Si-N and Si-C distances. All the bonded distances except the Si-H refined, although the N=C is longer than in any other related isothiocyanate compounds. Again the heavy atom internal angles were defined by the non-bonded distances contained under a broad peak between 265-300 pm. The CSiC angle tended to widen on refinement, while the NSiC angle stabilised at around 107° . However by constraining the angles to be equal the result was more acceptable. The SiNC angle refined to 157.9 which compares well with the angle in SiH_3NCS and $(\text{CH}_3)_3\text{SiNCS}$. The SiCH

angle refined well, probably because the Si...H distance was well defined and isolated in the radial distribution curve at 245 pm.

The conformation of the $\text{Si}(\text{CH}_3)_2\text{H}$ group relative to the NCS group was found by a series of refinements, with the torsion angle varied from 0 to 180° . The C...C and C...S distances define this angle, and the minimum R-factor was when the NCS group was twisted 20° from trans to the CSiC bisector. This now means that there are two different C...C distances and two different C...S distances, contained under the relatively broad peaks at 400 and 550 pm in the radial distribution curve. It was found that the NCS angle refined to 180° with a large esd and so was fixed at 180° and not refined subsequently. This made the torsion along the C-N bond redundant and so is not included in the final parameter list. The non-bonded amplitudes of vibration were all in accord with those for $(\text{CH}_3)_2\text{SiHNCO}$, except $(\text{C}\dots\text{C}_\text{N})$ which is very small, and refined well. The Si-N, Si-C and N=C bonded amplitudes were also refined. The remainder were fixed at normal values.

The final parameters giving the minimum R-factor ($R_G = 0.114$, $R_D = 0.091$) are given in Table 6.4 and the radial distribution and intensity curves are given in Figures 6.3 and 6.4. The estimated deviations quoted in Table 6.5 include the random errors, determined in the least squares analysis, and allowances have been made for systematic errors and for the constraints applied during

Table 6.4: Molecular parameters for Me₂SiHNCS

(a) Independent parameters

	<u>Distance</u>	<u>Amplitude</u>
r ₁ (Si-N)	172.1(6)	6.6(10)
r ₂ (Si-C)	184.9(5)	5.8(7)
r ₃ (C-H)	112.5(8)	8.0(fixed)
r ₄ (Si-H)	148.0(fixed)	7.6(fixed)
r ₅ (N=C)	121.2(6)	4.7(8)
r ₆ (C=S)	157.9(5)	4.5(fixed)

Angles

Angle 1 NSiC	110.7(5)
Angle 2 CSiC	110.7 ^a (tied equal to A1)
Angle 3 SiCH	109.7(10)
Angle 4 NSiH	109.0(fixed)
Angle 5 twist (CH ₃)	0.0(fixed) ^b
Angle 6 SiNC	155.6(14)
Angle 7 twist (Si-N)	20.0(fixed) ^b
Angle 8 NCS	180.0(fixed)

r - bond distance

a - Angle

d - non-bonded distance

^asee text^bfixed by R-factor plot - see text.

/..

Table 6.4 (contd)

(b) Dependent distances

	<u>Distance</u>	<u>Amplitude</u>
d_7 (C...C)	304.3(7)	16.8(14)
d_8 (C...N)	293.8(6)	16.8(tied to u_7)
d_9 (Si...C)	286.9(7)	9.5(13)
d_{10} (N...S)	279.1(7)	6.7(7)
d_{11} (Si...H)	246.7(12)	12.1(10)
d_{12} (C...C)	394.9(7)	7.9(20)
d_{13} (C...C)	407.9(8)	7.9(tied to u_{28})
d_{14} (Si...S)	441.5(8)	9.9(6)
d_{15} (C...S)	539.2(7)	24.8(27)
d_{16} (C...S)	561.0(10)	24.8(tied to u_{53})

(c) Other amplitudes of dependent distances (all fixed)

	<u>Amplitude</u>
(C...H _{Si})	13.0
(N...H _{Si})	13.0
(H _C ...H _C)	14.0
(N...H _C)	15.0
(H _C ...H _{Si})	17.0
(C...H _{Si})	19.0
(C...H _C)	13.0
(C...H _C)	23.0
(H _C ...H _C)	20.0
(S...H _{Si})	23.0
(S...H _C)	25.0

Table 6.5: Least squares correlation matrix x100 for $(\text{CH}_3)_2\text{SiHNCS}$

r_1	r_2	r_3	A7	A10	r_5	r_6	u_2	u_1	u_5	u_7	u_9	u_{12}	k_1	k_2		
100	-49			65		52	77	71								r_1
	100			-38		-42	-50	-76								r_2
		100	-39		-35				53							r_3
			100						-30		-31		-54			A7
				100	34	58	57	58			32	-41				A10
					100					45	39			38		r_5
						100	43	61								r_6
							100	79		34			35			u_2
								100								u_1
									100					31		u_5
										100			44			u_7
											100		33			u_9
												100				u_{12}
													100	40		k_1
														100		k_2

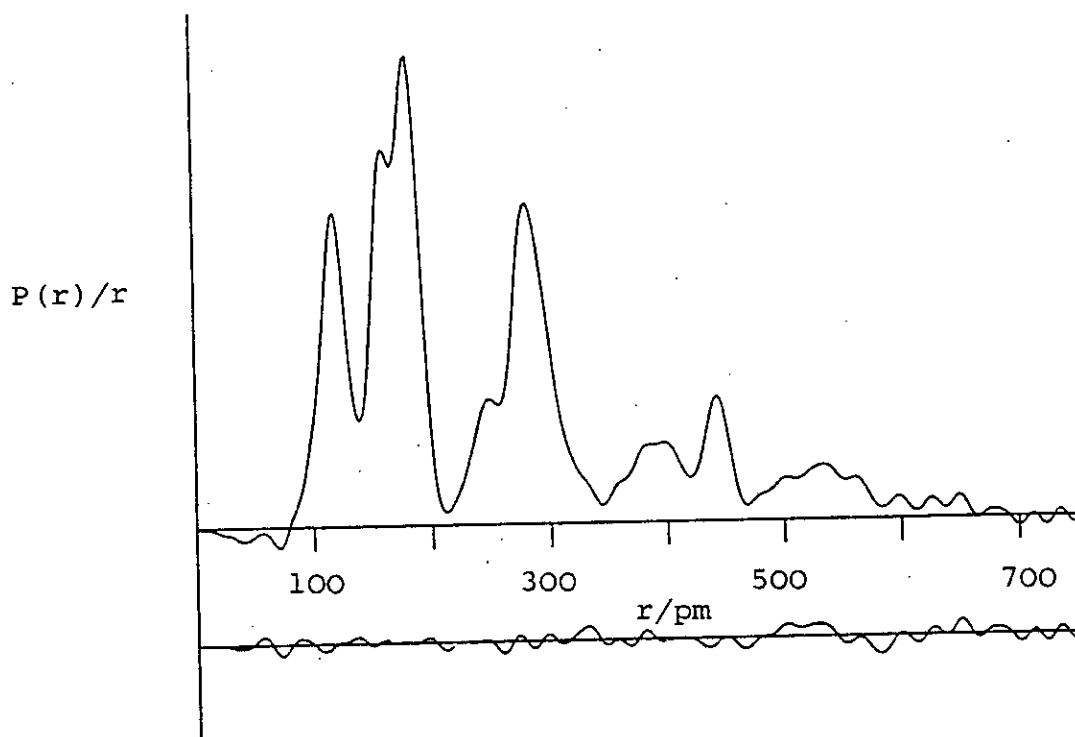
r - bond distance

A - Angle

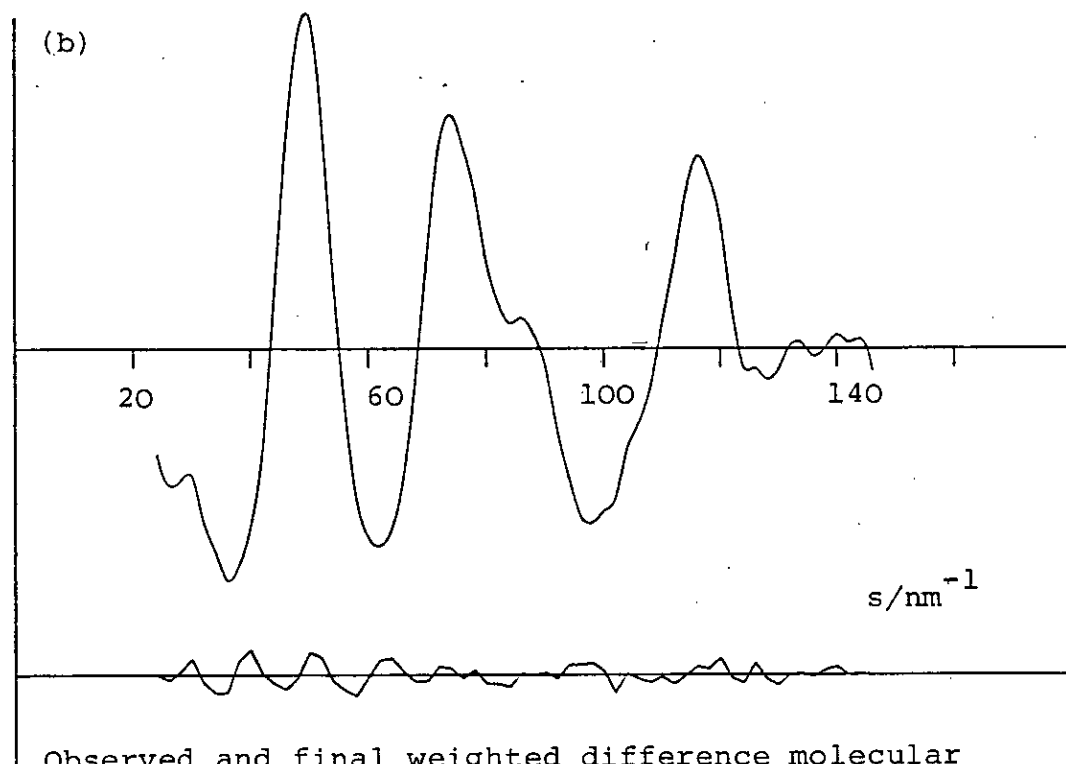
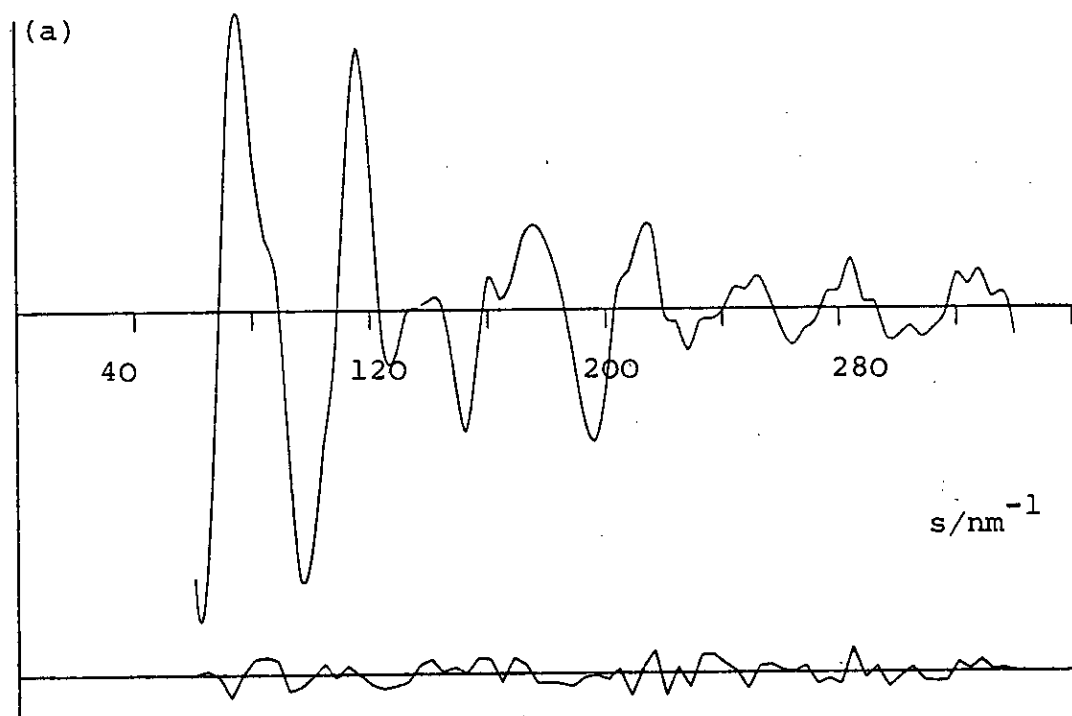
u - amplitude of vibration

Only values greater than 30 are given.

Figure 6.3: Observed and final difference radial distribution curves, $P(r)/r$, for $(\text{CH}_3)_2\text{SiHNCS}$.



Before Fourier inversion the data were multiplied by $s \cdot \exp[-0.000015 s^2 / (Z_{\text{Si}} - F_{\text{Si}})(Z_{\text{N}} - F_{\text{N}})]$.

Figure 6.4: $(\text{CH}_3)_2\text{SiHNCS}$ 

Observed and final weighted difference molecular scattering intensities at nozzle-to-plate distances of (a) 128 and (b) 286 mm.

the refinement. The final least squares correlation matrix is given in Table 6.5.

6.3 Results and Discussion

As with the methylsilyl isocyanates discussed in Chapter 5, the interpretation of the structures of the isothiocyanates was complicated by the problems of shrinkage and the unknown extent of (p-d) π bonding between the silicon and nitrogen atoms.

The molecular parameters found for monomethyl and dimethyl silyl isothiocyanates do not differ greatly from other methylsilyl compounds and other isothiocyanates. However there are small but significant changes which run in parallel with trends observed in the methylsilyl isocyanates.

Firstly, the Si-C bonds were found to be of equal length in $\text{CH}_3\text{SiH}_2\text{NCS}$ and $(\text{CH}_3)_2\text{SiHNCS}$ (within 1 esd), but were slightly shorter than those in methylsilyl isocyanates (see Table 6.6).

Table 6.6: Si-C bond lengths (pm) in methylsilyl isocyanates and isothiocyanates

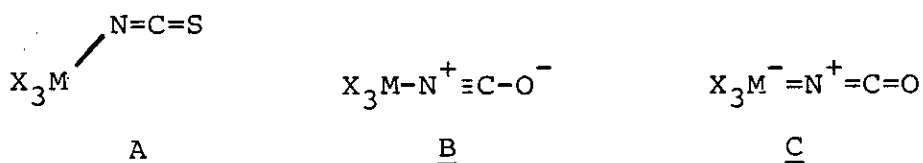
Compound	r(Si-C)		Ref
	Y=O	Y=S	
$\text{CH}_3\text{SiH}_2\text{NCY}$	185.3(5)	184.8(7)	This work
$(\text{CH}_3)_2\text{SiHNKY}$	185.9(2)	184.9(5)	This work
$(\text{CH}_3)_3\text{SiNKC}$	189(1)	187(1)	92

The data for the trimethylsilyl derivatives were less reliable, with large uncertainties, but the data do consistently show that the Si-C bond is shorter in isothiocyanates than in isocyanates, although there is no immediately apparent reason for this. Despite these small changes in the Si-CH₃ bond, it is not significantly shorter than predicted from the sum of the covalent radii^{63,81}.

In the trimethylsilyl derivative⁹², the isothiocyanate was found to have a long Si-N bond with respect to the silyl, monomethyl, and dimethylsilyl derivatives which all refined to give almost identical Si-N bonds (see Table 6.7). The Si-N bond length predicted by the Schomaker-Stevenson equation⁶³ is 180 pm, and the observed bond length is up to 9 pm shorter. It would appear that there may be considerable (p-d) π donation in this bond which should influence the SiNC angle, and this is discussed later. The length of the Si-N bond depends on the substituents on the silicon atom such that an electron withdrawing group should shorten the bond by permitting increased lone pair donation from nitrogen, while electron donating groups such as a methyl group, should tend to increase the bond length, probably by the inductive effect from the methyl groups towards silicon, reducing lone pair donation from nitrogen. There is no evidence of the methyl groups donating electrons into the vacant d orbitals as this would result in Si-C bond shortening. From this structural study the methylsilyl isothiocyanates do follow this trend. Hence the respective bond lengths are

SiH₃NCS²⁸, 170.4(6) pm; CH₃SiH₂NCS, 171.0(6) pm;
 (CH₃)₂SiHNCS, 172.1(6) pm; and (CH₃)₃SiNCS⁹², 178(2) pm.
 These values can be compared to trichlorosilyl isocyanate⁹³
 which has a very shortened Si-N bond of 164.6 pm.

The possible valence bond structures can also be used to explain the Si-N bond length variation. The bond lengths of HNCS and CH₃NCS¹¹⁹ can be explained in terms of the two forms A and B given below, but for the structures of silicon isothiocyanates these are insufficient and form C has to be included.



If there is an electron withdrawing group for X, or the M has vacant d orbitals, form C is stabilised and structure A becomes more favourable than B. The presence of silicon at M will favour C and the halogen groups at X will further stabilise this form, which has a M=N double bond which will therefore be short.

Conversely, the methyl groups will destabilise the structure C, lengthening the Si-N bond, in favour of structure A or B. In fact structure B is the only form that the methyl groups will actually stabilise, possibly resulting in a shortening of the N=C bond and a lengthening of the C=S bond. Table 6.7 shows how the Si-N does vary consistently with the number of methyl groups, but the N=C,

C=S bond length change is less clear.

Table 6.7: Si-N, N=C and C=S bond lengths in isothiocyanates

Compound	Bond Lengths/pm			Reference
	Si-N	N=C	C=S	
HNCS	-	121.7	156.0	123
SiH ₃ NCS	170.4(6)	119.7(7)	156.3(6)	28
CH ₃ SiH ₂ NCS	171.0(6)	118.7(6)	156.8(5)	This work
(CH ₃) ₂ SiHNCS	172.1(6)	121.2(6)	157.9(5)	This work
(CH ₃) ₃ SiNCS	178(2)	118(1)	156(1)	92

The bond angles NSiC, HSiC, HCSi and HSiH were all close to tetrahedral values, with a slight widening for the more bulky groups, and do not warrant further comment. The NCS angle was fixed at 180° which was consistent with the calculated skeletal bond angles³⁶ and with other isothiocyanates^{28,92,119,123}.

However the SiNC angle is more important, and should be more influenced by the electron-donating effect of the methyl groups, the valence bond structures, and the steric effect of the methyl groups. Firstly, there is not a definite consistent trend of this angle through the methyl-silyl series, although all the angles are wider than in germyl¹²⁴ and methyl isothiocyanates¹¹⁹, and with more methyl groups SiNC is generally more bent. Additionally the angles in the isothiocyanates are wider than in the comparable isocyanates (see Table 6.8).

Table 6.8: SiNC angles in methylsilyl isocyanates and isothiocyanates

	SiNC($^{\circ}$)	
	NCO	NCS
SiH ₃ -	151.7(12)	163.8(26)
CH ₃ SiH ₂ -	148.0(15)	168.4(16)
(CH ₃) ₂ SiH-	152.7(10)	155.6(14)
(CH ₃) ₃ Si-	150(3)	154(2)

By the analysis of the Si...S peak in the radial distribution curve of SiH₃NCS²⁸ it was found that the shape of the peak was best fitted to a purely harmonic function for the bending vibration and the apparent bent angle accounted for by considering the shrinkage due to the low frequency bending mode. Since the SiNCS chain was shown to be linear in SiH₃NCS and since the methyl substituted silyl isothiocyanate SiNC angles are quite close to the angle in SiH₃NCS it is likely that they also are near linear. However it is noticeable that the dimethyl and trimethyl derivatives do have narrower (by 10 $^{\circ}$) apparent angles, suggesting that they may be bent by a few degrees, or may be more easily bent by a bending motion.

Glidewell³⁶, in a series of MNDO calculations for pseudohalides of the type RNCS where R = SiH₃, SiF₃, SiCl₃, SiF₂Cl and SiFCl₂, has shown that the RNCS compounds should be linear at nitrogen in all cases, while the RNCO compounds deviate from linearity by a few degrees if the R group did not have local C_{3v} symmetry. In contrast methyl isothiocyanates were calculated to have CNC angles of between 130-150 $^{\circ}$, and these agree with experimental results¹¹⁹.

Attempts to fit the Si...S peak to a probability function for the methylsilyl compounds could not be done because of the overlap with the C...C distance, obviously not present in SiH_3NCS .

The possible valence bond structures could also be used to explain the linearity of the SiNC group (see page 170). Forms B and C have linear chains and although C will be destabilised by the presence of the methyl groups, form B will be stabilised. Hence there is likely to be a fine balance between the steric and electronic influences. It should be noted that there will be conflicting tendencies in these forms, because when M has a vacant d orbital forms A and C are possible, one with a wide SiNC angle, and the other with a narrow angle. It is known from the study of germyl pseudohalides^{124,125} that the GeNC angles are narrower than in the related silyl derivatives and this is commonly attributed to the weaker overlap of the nitrogen 2p orbitals with the germanium 4d orbitals, which allows delocalisation of the nitrogen lone pair. As explained in earlier chapters the overlap of the silicon and nitrogen (3d-2p) orbitals is an acceptable way of explaining the angles at nitrogen.

Without more detailed spectroscopic study of the region below 200 cm^{-1} , analysis of the bending motion at nitrogen could not be done. Only in $\text{CH}_3\text{SiH}_2\text{NCS}$ could a band be found that could possibly give an indication of the fundamental bending frequency (an overtone at 156 cm^{-1}).

Comparing the amplitudes of vibration of the

isothiocyanates it is clear that the refined values for the methyl substituted derivatives are close to the values for SiH_3NCS and hence it is reasonable to suggest that the structure of the SiNCS group and pure harmonic potential for the bending motion, calculated from the amplitudes for SiH_3NCS , are applicable to the substituted silyl isothiocyanates. However the methyl groups have been shown to affect the bond lengths and so it is likely they will also affect the bending motion to some extent. Again spectroscopic data from $0\text{-}200\text{ cm}^{-1}$ would help clarify this. Table 6.9 gives the non-bonded amplitudes of vibration.

Because the SiNC group was found to be bent in the electron diffraction structure, the NCS group could be rotated about the Si-N bond with respect to the methyl groups. The optimum fit was found to be exactly trans in monomethylsilyl isothiocyanate, and 20° from trans to the bisector of the CSiC angle in dimethylsilyl isothiocyanate. Thus it appears that the steric influence of the C=S group is greater than the electrostatic influence of the nitrogen lone pair (see Figure 6.9).

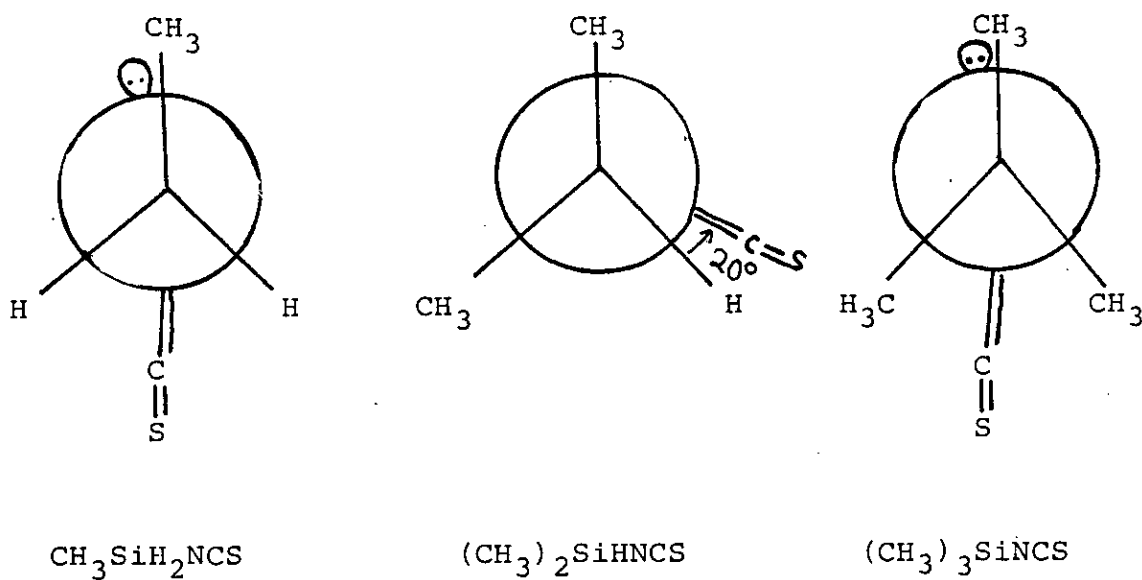
This is in contrast to the isocyanates discussed in Chapter 5 in which the lone pair had the greater steric influence. Therefore the apparent widening of the SiNC angles in the isothiocyanates noted in Table 6.8 must be real, with increased delocalisation of the lone pair in the isothiocyanate compounds. The configuration of trimethylsilyl isothiocyanate was not well defined but it was reported that the staggered arrangement was most likely.

Table 6.9: Amplitudes of vibration in silyl isothiocyanate/pm

Distance	SiH_3^-	$\text{CH}_3\text{SiH}_2^-$	$(\text{CH}_3)_2\text{SiH}$	$(\text{CH}_3)_3\text{Si}$
N...S	4.1 ^a	5.2(9)	6.7(7)	4.5
Si...C	6.8(12)	6.7(12)	9.5(13)	5.5
Si...S	9.6(9)	9.1(6)	9.9(6)	7.5
Reference	28	This work	This work	92

^aerrors are given in brackets after the refined value. When no error is given the value was fixed during refinement.

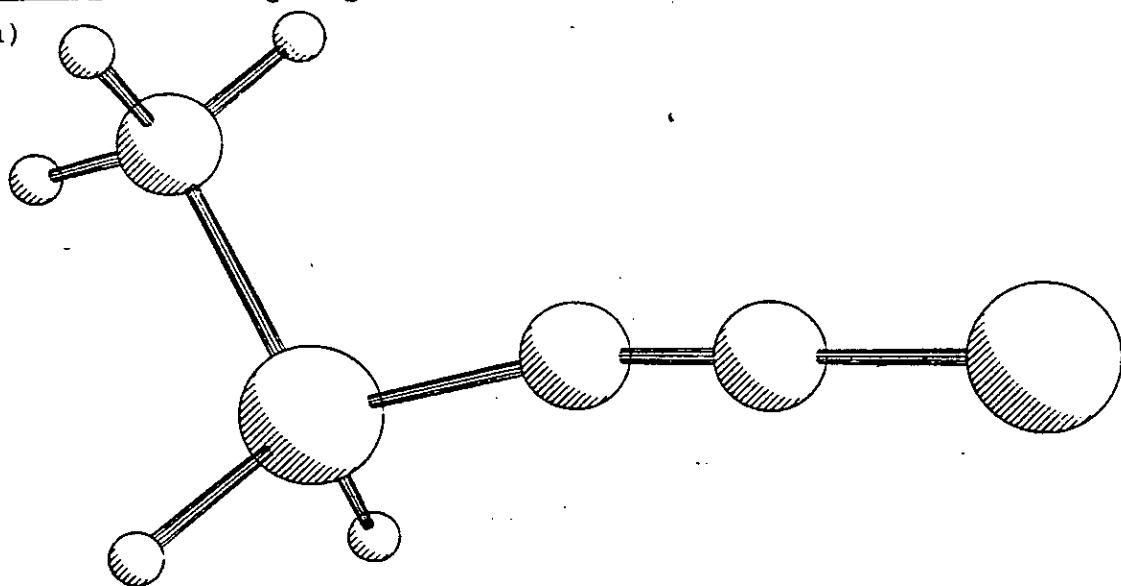
Figure 6.9: Conformation adopted by methylsilyl isothiocyanates



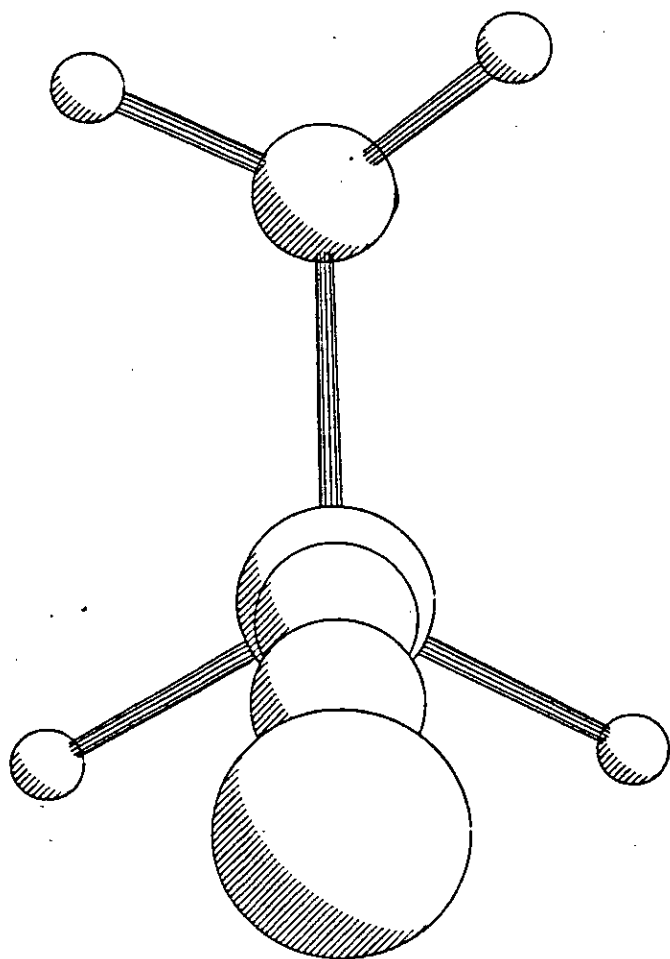
The greater repulsive interaction of H or CH₃ to C=S than H or CH₃ to a lone pair was also found in CH₃NCS¹¹⁹ with the nitrogen lone pair eclipsing one hydrogen. The slight twist of 20° from exactly trans position along the Si-N bond in dimethylsilyl isothiocyanate must either be due to the repulsive interaction between the C=S group and the hydrogen, or may just be a shrinkage effect.

Finally, it was found that there was a staggered configuration of the methyl group with respect to the SiH₂ group in the monomethyl derivative, and a small twist of one methyl group with respect to the other in the dimethyl derivative (see Figures 6.10 and 6.11).

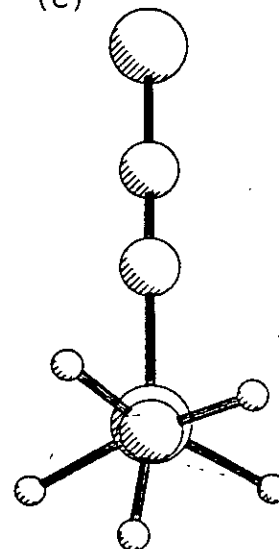
(a)



(b)

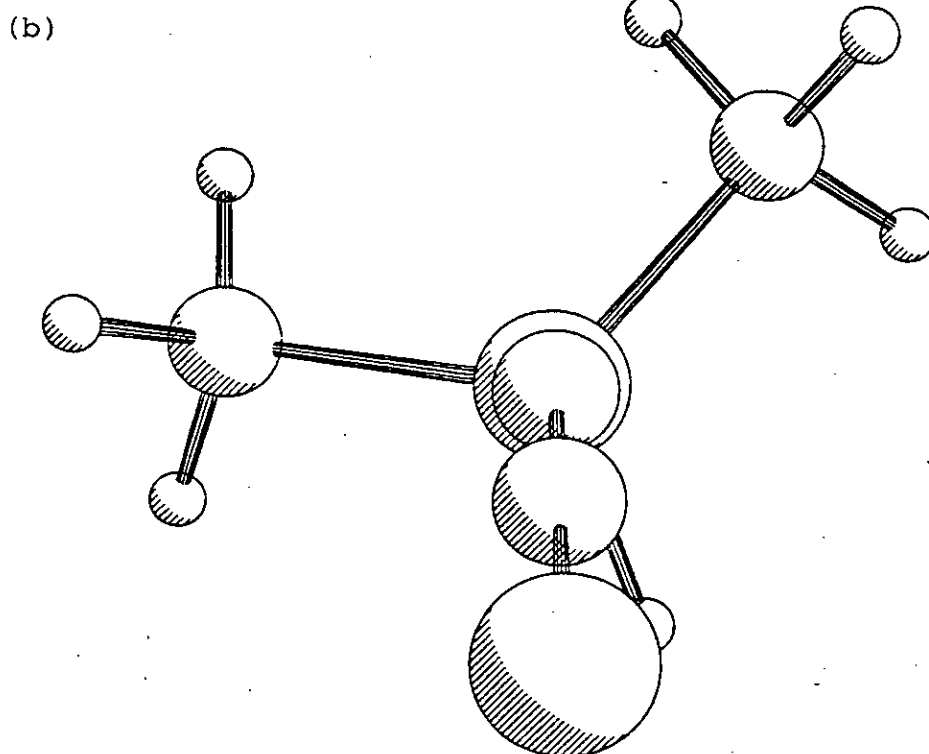
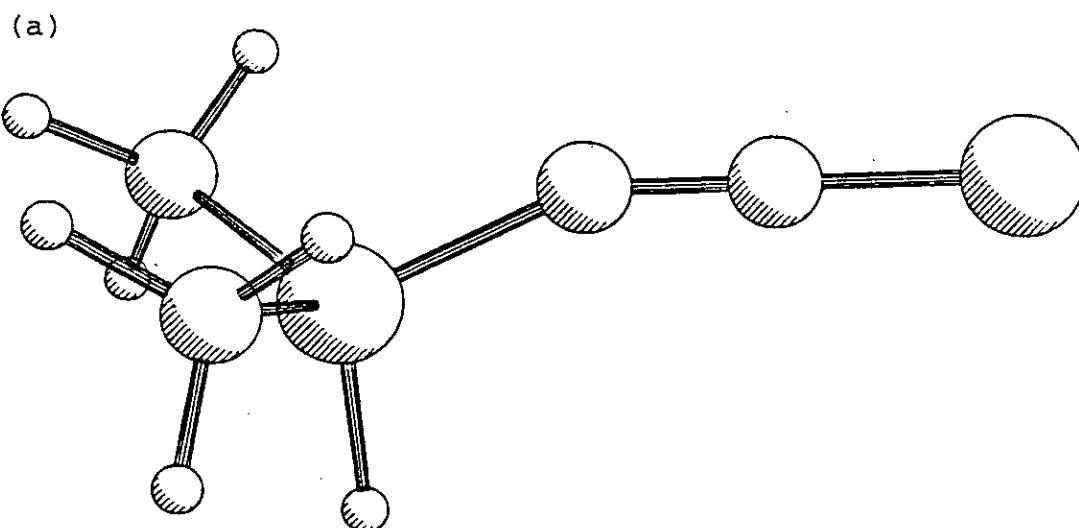


(c)



Molecular structure of $\text{CH}_3\text{SiH}_2\text{NCS}$
(a) general view; (b) viewed along bond from N to Si; and
(c) viewed along bond from C(H) to Si.

Figure 6.11: $(\text{CH}_3)_2\text{SiHNCS}$



Molecular structure of $(\text{CH}_3)_2\text{SiHNCS}$

(a) general view; (b) viewed along bond from N to Si

CHAPTER 7: THE GAS PHASE STRUCTURE OF MONOMETHYLSILYL
CYANIDE

7.1 Introduction

The electron diffraction studies of the structures of methylsilyl isocyanates and isothiocyanates have shown that there is a lengthening of the Si-N bond when the number of methyl substituents on the silicon atom is increased. Also when the silyl group is attached to a nitrogen^{28,92,126} or oxygen^{26,111,95} atom the Si-N and Si-O bonds are appreciably shorter than predicted from the sum of the covalent radii^{81,105}, and these observations have been interpreted in terms of (p-d) π bonding between silicon and first row atoms. However, although similar π -interaction between silicon and the carbon of a cyanide group should be possible the observed Si-C bond lengths^{127,128} are no shorter than would be expected after making allowance for the effect of the sp hybridisation of the carbon atom (see Table 7.1).

Table 7.1: Predicted Si-C bond length from Schomaker and Stevenson¹⁰⁵ and Pauling⁸¹ predictions/pm

	Schomaker/Stevenson	Pauling	Experimental
Si-N	180.2	187	169-172
Si-O	175.7	183	163-165
Si-C ^a	187.7	187	182.5-185
Si-C ^b	194	194	186-187

^awith allowance for sp hybridisation, i.e. in cyanide or acetylene compounds

^bfor sp³ hybridisation, i.e. Si-CH₃

Thus the structural study of monomethylsilyl cyanide should show whether the methyl groups have the same effect on the Si-CN bond as they have on the Si-N bond in isocyanates and isothiocyanates. Also there is interest in the electron-withdrawing effect of the CN group on the molecular structure and there exists the possibility of bonding through nitrogen of the CN group to form the isocyanide isomer. Some recent work on $(\text{CH}_3)_3\text{SiCN}$ ¹²⁹ by Durig et al suggested the presence of an appreciable amount of the isocyanide at ambient temperature but a more detailed study by nmr¹³⁰ and microwave spectroscopy¹³¹ has shown no isocyanide was present. It was believed the rotational spectrum assigned to isocyanide should have been assigned to $(\text{CH}_3)_3\text{SiCl}$.

Lastly the amplitudes of vibrations are of interest, when compared to related compounds as they can be indicative of the shape of the molecule, and the bending motion of apparently linear groups.

7.2 Refinement and Model

7.2.1 Model of $\text{CH}_3\text{SiH}_2\text{CN}$:

A subroutine was written which described the atomic coordinates in terms of five bond lengths, five bond angles and one torsion angle. The bond distances were the Si- CH_3 , Si-CN, C-H, Si-H and C=N; the angles were SiCN, SiCH, HSiH, CSiC and the angle between the HSiH

bisector and the Si-CN bond. The torsion angle was along the Si-CH₃ bond, rotating the methyl hydrogens with respect to the silyl hydrogens. The methyl was assumed to have local C_{3v} symmetry and a torsion angle along the Si-CN was not necessary because the SiCN angle in fact proved to be 180°.

7.2.2 Refinement of CH₃SiH₂CN structure:

The radial distribution curve (Figure 7.1) shows three main peaks: one at 120 pm containing the C≡N and C-H distances; one at 180-190 pm containing both Si-C distances; and one at 300 pm containing Si...N and C...C non bonded distances. Two smaller broader peaks are present at 400 pm for C...N, and at 250 for the three Si...H distances. Initially the heaviest atom bond distances were refined and it was found that the Si-CH₃ and Si-CN distances did separate and refine independently even though they are under the same peak and just 3 pm apart. Then the C≡N distance was refined to 116 pm. There was some uncertainty whether the amplitudes of the Si-CN and Si-CH₃ bonds should be refined separately or constrained to be equal. However when refined separately, they gave almost equal but high values with large uncertainties, while when constrained the values were reasonable and uncertainties low. In subsequent refinements the amplitudes were constrained to be equal.

The non-bonded amplitudes C...C and C...N both refined to acceptable values, as did the Si...N and C...C,

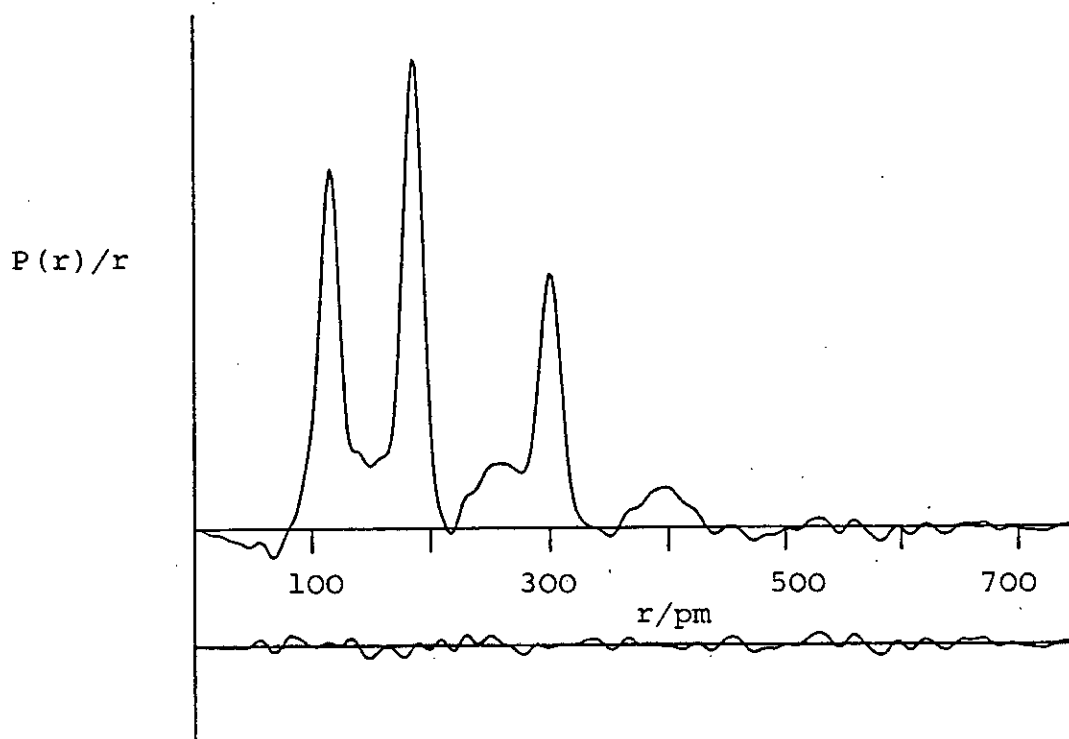
when constrained at various ratios from 0.60 to 0.75. The ratio giving the lowest R-factor was then fixed in all following refinements.

The positions of the methyl hydrogen atoms were defined by the angle HCSi (which refined to 110.9°) and the twist angle along the Si-C bond. The optimum twist angle was obtained by varying the angle systematically and noting the R-factor. The angle giving the lowest R-factor was then taken as the optimum value providing the parameters and amplitudes remained reasonable. This method was also used to find the bend angle of the SiH_2 plane.

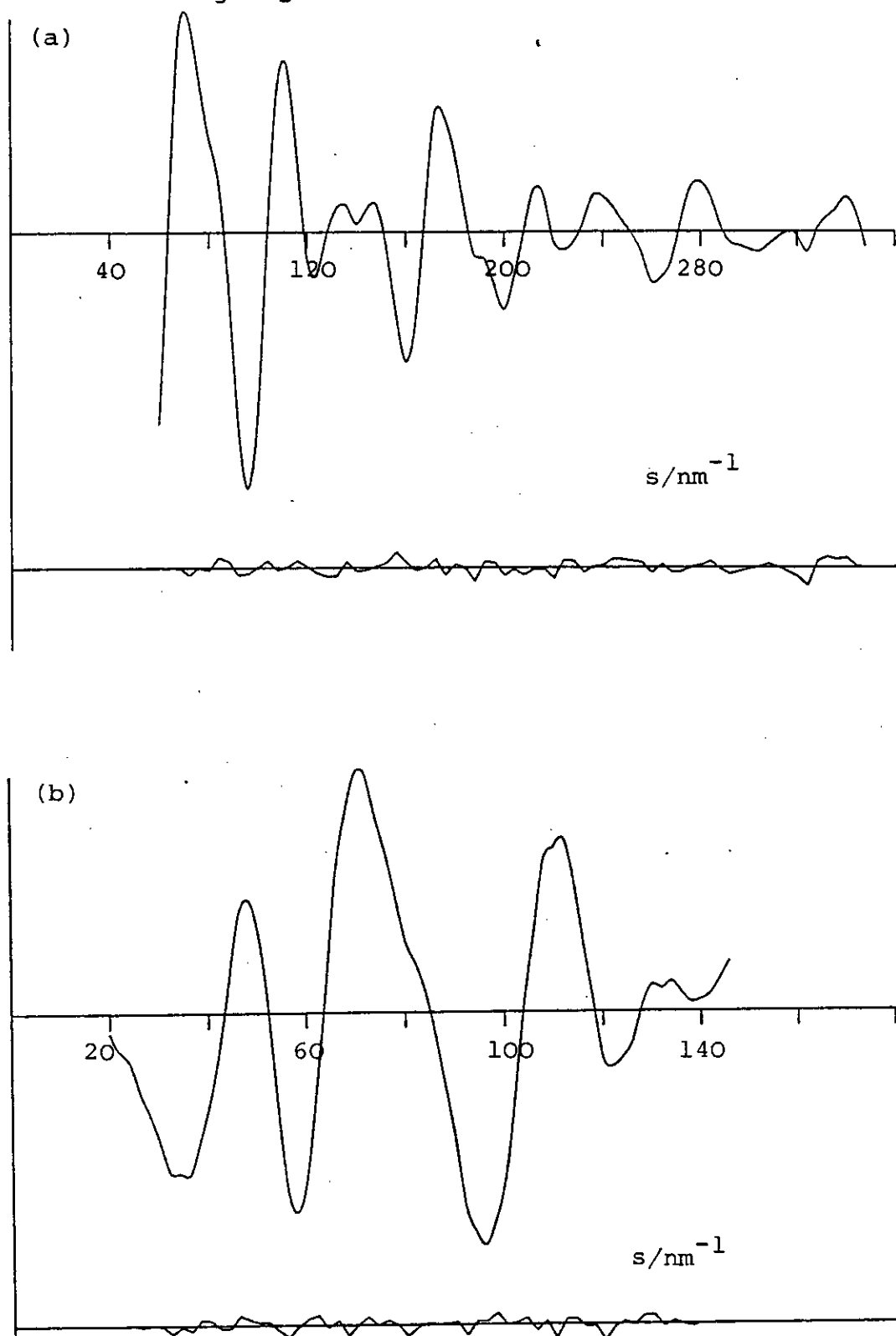
Allowance for $(\text{CH}_3\text{SiH}_2)_2\text{O}$:

When most of the refinement was complete, there was still a significant peak in the difference curve of the radial distribution curve at 164 pm and a wave of frequency 4 nm^{-1} running through the intensity curve. Since all the parameters had already been refined to reasonable values this strongly suggested that another compound was present which had not been allowed for in the model program. The most likely impurity was $(\text{CH}_3\text{SiH}_2)_2\text{O}$ which readily forms when the cyanide reacts with any trace of air or moisture. Thus the model program was modified to allow for a small percentage of impurity by including the Si-C, Si-O, Si...Si and C...O distances. The radial distribution difference curve then lost

Figure 7.1: Observed and final difference radial distribution curves,, $P(r)/r$, for $\text{CH}_3\text{SiH}_2\text{CN}$



Before Fourier inversion the data were multiplied by $s \cdot \exp[-0.000015 s^2 / (Z_{\text{Si}} - F_{\text{Si}})(Z_{\text{C}} - F_{\text{C}})]$.

Figure 7.2: $\text{CH}_3\text{SiH}_2\text{CN}$ 

Observed and final weighted difference molecular scattering intensities at nozzle-to-plate distances of (a) 128 and (b) 286 mm

the peak at 164 pm, and the R-factor decreased for the short distance plates, but increased for the long distance plates. Therefore a second model was written only allowing for $(\text{CH}_3\text{SiH}_2)_2\text{O}$ in the short distance plates and this proved to give the lowest R-factor. Having allowed for the impurity it was now possible to refine the Si-H distance to an acceptable value although the amplitude of vibration remained fixed.

The final parameters giving the minimum R-factor ($R_G = 0.072$, $R_D = 0.069$) are given in Table 7.2 and the final radial distribution curves and intensity curves are given in Figures 7.1 and 7.2. The errors are estimated standard deviations obtained from the least squares analysis and increased to allow for systematic errors. Table 7.3 is of the least squares correlation matrix and Table 7.4 contains the nozzle to plate distances, wavelength, and the s range for the intensity curves, with the weighting points.

7.3 Results and Discussion

It is unfortunate that the electron diffraction data for dimethylsilyl cyanide were not available to be discussed in this chapter. A paper describing the microwave spectrum of $(\text{CH}_3)_2\text{SiHCN}^{64}$ only gave the Si-CN bond length and the angle between the CSiC plane and Si-CN bond, for which values of 184.0 pm and 123.97° respectively were obtained, assuming the CSiC angle was 112.25° .

Table 7.2: Molecular parameters of $\text{CH}_3\text{SiH}_2\text{CN}$

(a) Independent parameters

	<u>Distance/pm</u>	<u>Amplitude/pm</u>
	<u>Angle/°</u>	
r_1 Si- CH_3	187.5(6)	6.2(3)
r_2 C-H	108.6(7)	7.8(fixed)
r_3 Si-H	148.3(9)	11.4(9)
r_4 Si-CN	183.9(6)	6.2(tied to u_1) ^c
r_5 C \equiv N	116.7(4)	3.7(3)
Angle 1 HCSi	112.5(14)	
Angle 2 HSiH	109.0(fixed)	
Angle 3 CSiC	108.8(7)	
Angle 4 SiCN	180.0(fixed)	
Angle 5 τCH_3	39.0(fixed) ^a	
Angle 6 B(SiH ₂)	55.5(fixed) ^{a,d}	
%(CH_3SiH_2) ₂ O	8.0(fixed) ^b	

^a angle by R-factor loop - see text^b percentage of (MeSiH_2)₂O allowed for in short plates^c $u_1 = u_4$ ^d angle between HSiH bisector and Si-CN bond - see text

(b) Dependent distances

	<u>Distance/pm</u>	<u>Amplitude/pm</u>
d_6 (C...H)	274.6(9)	13.0(fixed)
d_7 (Si...H)	250.1(17)	19.0(13)
d_8 (Si...N)	300.6(6)	5.7(3)
d_9 (C...C)	302.1(10)	8.1(tied to u_8) ^a
d_{10} (C...N)	402.4(12)	16.5(14)

^a tied to u_8 - $u_8 = 0.7 * u_9$

Table 7.3: Least squares correlation matrix x 100 for CH₃SiH₂CN

r ₁	r ₂	r ₃	r ₄	r ₅	A1	A3	u ₁	u ₃	u ₅	u ₇	u ₈	k ₁	k ₂	
100			-89	41		56	-54		43					r ₁
	100	46		39										r ₂
		100								-37				r ₃
			100	-43	32	-72	50							r ₄
				100									33	r ₅
					100			31						A1
						100								A3
							100				33	34	45	u ₁
								100				-57	-34	u ₃
									100				31	u ₅
										100				u ₇
											100	41	44	u ₈
												100	52	k ₁
													100	k ₂

r - bond distance

A - Angle

u - amplitude of vibration

Only correlations with values greater than 0.3 are included.

Table 7.4: Weighting functions, correlation parameters and scale factors for MeSiH₂CN

Distance mm	Δs	s_{\min}	s_1 nm ⁻¹	s_2	s_{\max}	Correlation	Scale Factor
285.73	2	20	40	120	146	0.0022	0.670(8)
128.36	4	60	80	320	348	0.1762	0.862(16)

Wavelength = 5.679 pm

In monomethylsilyl cyanide the bond distances for C-H and Si-H and the angles HCSi and CSiC are at expected values and do not warrant further discussion. The Si-CH₃ distance (187.6(6) pm) in methylsilyl cyanide was found to be slightly longer than the Si-C distance in most other methylsilyl compounds (about 186 pm), but this is likely to be due to the high negative correlation (see Table 7.3) between Si-CN and Si-CH₃ bond lengths resulting in a separation of the distances during refinement. Thus the Si-CN bond length is shorter than the same bond in SiH₃CN¹³², but is very close to the bond length in (CH₃)₂SiHCN⁶⁴, although not significantly shorter than predicted from the sum of the covalent radii, with allowance for sp hybridisation of the carbon atom.

Since the 2s orbital of carbon has a smaller radius than the 2p orbitals, it would be expected that the greater the s character of a hybrid orbital, the shorter the internuclear distance, at which the best overlap and repulsion would occur in the σ bonds. It has been estimated that the single bond radii for a carbon atom in the several states of hybridisation are: sp³, 77 pm, sp², 74 pm and sp 70 pm. Hence at least part of the decrease of the Si-CN with respect to the Si-CH₃ must be attributable to this effect rather than to any π -bonding. Table 7.5 lists a number of compounds containing Si-C bonds, with the C atom in sp³, sp² and sp hybridised states.

Table 7.5: Si-C bond length for sp^3 , sp^2 and sp hybridised carbon atoms

	Hybridisation	Si-C/pm	Method of Determination ^a	Reference	
SiH_3CH_3	sp^3	186.7	ed	43	
$SiH_3CH=CH_2$	sp^2	185.3	ed	136	
$SiH_3C\equiv CCl$	sp	181.2	ed	137	
$SiH_3C\equiv CCH_3$	sp	180.2	ed	138	
$SiH_3C\equiv CH$	sp	182.6	mw	128	
$SiH_3C\equiv N$	sp	185.1	ed	132	
$CH_2SiH_2C\equiv N$	sp	183.9	ed	This work	
$(CH_3)_2SiHCN$	sp	184.0	mw		64
$(CH_3)_3SiC\equiv N$	sp	184.4	ed		139

^aed electron diffraction, mw microwave spectroscopy

As confirmation that the shortening of the Si-C bond is due to the carbon orbital hybridisation rather than an explanation involving (p-d) π bonding (as for Si-O and Si-N bonds), it is found that the decrease in the length of Si-CH₃ bond to Si-CN bond is quite similar to, although actually less than, the decrease for the C-C bond from CH₃CH₃⁴² to CH₃CN¹³³. The shortening is about the same as that observed for the C-C bonds in isopropyl cyanide (150.1 pm)¹³⁴ and propane (152.6 pm)¹³⁵.

Also noticeable from Table 7.5 is that the Si-C \equiv bond is much shorter in the acetylene derivatives than the cyanide derivatives and this is believed to be because the cyanide is a much stronger electron withdrawing group, and so could decrease electron density in the Si-CN bond. Also the length of the Si-CH₃ bond does not appear to be affected by the cyanide group as the distance was found to be almost equal to the Si-C bond length in Si(CH₃)₄¹⁰² (187.6(2) pm).

The effect of the methyl groups on the Si-CN bond is not clear, but appears to be small. As is shown in Table 7.6 the bond in the methyl substituted cyanides is only 1 pm shorter than in SiH₃CN and this, as explained above, is quite likely to be due to the high correlation between Si-CH₃ and Si-CN bond length during refinement, exaggerating the difference which is not very significant anyway. The lack of influence of the methyl groups on the Si-CN bond is in contrast to the situation in

Table 7.6: Molecular parameters of methylsilyl cyanides in the gas phase^a

	SiH ₃ CN ^b	CH ₃ SiH ₂ CN ^b	(CH ₃) ₂ SiHCN	(CH ₃) ₃ SiCN ^b
Si-H	148.1	148.3	[148.3]	-
Si-CN	185.1	183.9	184.0	184.4
C≡N	116.5	116.7	[115.6]	117.0
HSiC>	109.9	112.5	[109.16]	109.16
SiCN>	177.0	[180.0] ^c	[180]	-
Si-CH ₃	-	187.5	[186.7]	187.1
Reference	132	This work	64	139

^adistances in pm, angles in degrees

^bstructure without any vibrational corrections

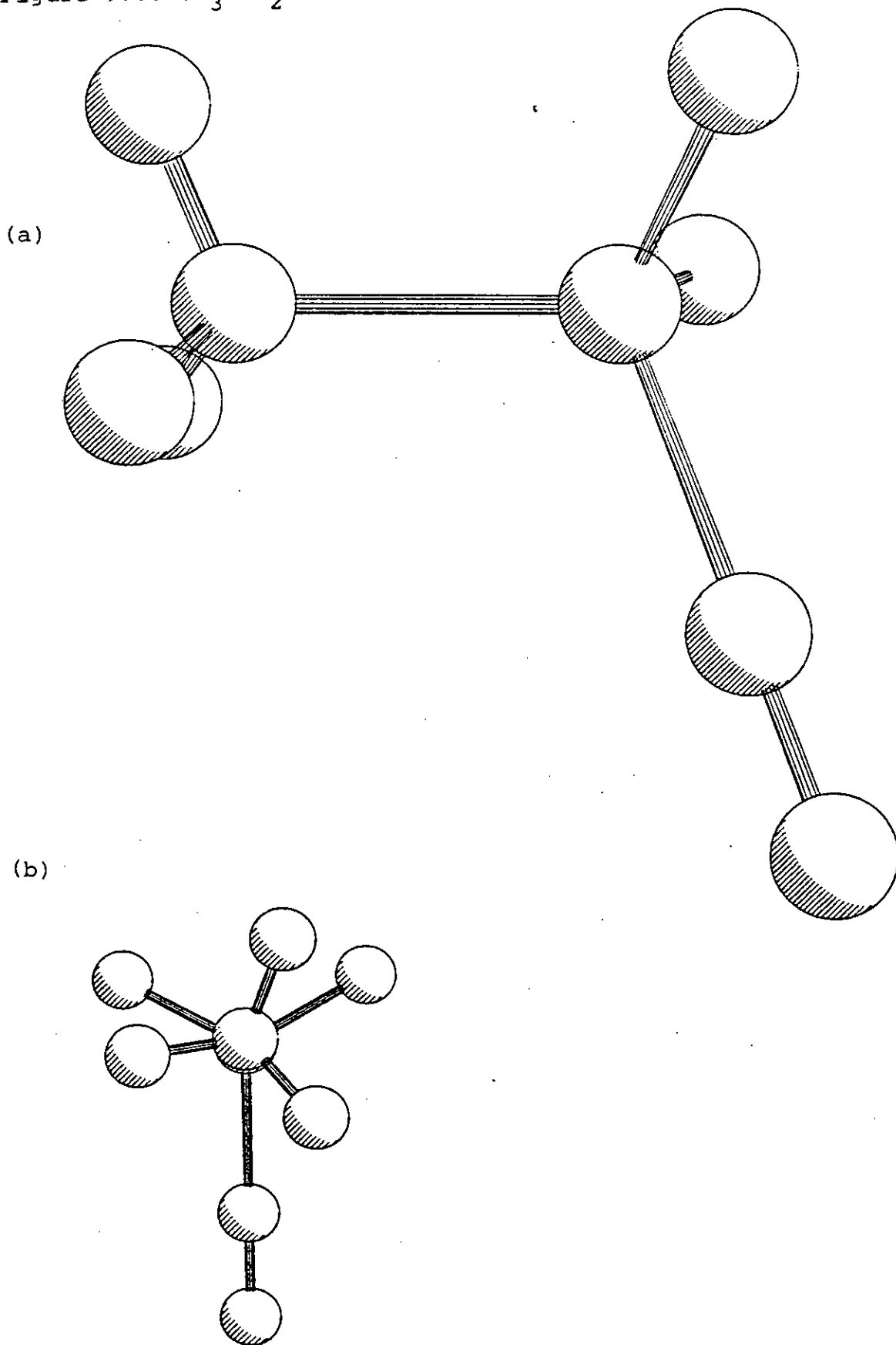
^cparameters in square brackets were fixed - the data for Me₂SiHCN was from microwave spectroscopy

methylsilyl isocyanates and isothiocyanates, in which the addition of methyl groups lengthened the Si-N bond. This was thought to be due to the decrease of (p-d) π bonding, or through the methyl groups influencing the preferred valence bond structure. The lack of change of the Si-CN bond suggests very little (p-d) π bonding can be involved.

In all the cyanide compounds studied the C \equiv N bond length appears to be almost constant and unaffected by the methyl substituents.

Finally, the conformation of the methyl hydrogens relative to the silyl hydrogens was found to be staggered, as is shown in Figure 7.3.

Further work on methylsilyl cyanides should include the gas phase structure of dimethylsilyl cyanide which so far has only been studied by microwave spectroscopy⁶⁴ which gave one bond length dependent on other assumed parameters. Data have now been collected, and the structure should soon be known.



Molecular structure of $\text{CH}_3\text{SiH}_2\text{CN}$
(a) general view
(b) viewed along bond from C(H) to Si

CHAPTER 8: VIBRATIONAL, NMR, AND MASS SPECTRA OF METHYLSILYL
PSEUDOHALIDES

8.1 Introduction

An essential part of the characterisation of a new compound is a study of its vibrational spectra, and in this work in addition to the gas phase infra-red spectrum, the solid phase infra-red and solid and liquid phase Raman spectra have been recorded. For each compound it is of interest to record the change in frequencies and the changes in the relative intensities for the three phases. Also there are certain differences in position for the equivalent vibration in the cyanide, isocyanate and isothiocyanate.

The assignment of the bands has been done by comparison with the appropriate methylsilane, the pseudohalide acid, and also the trimethylsilyl¹⁰⁰ and silyl pseudohalides^{99,122,140,141}. From all these it was found that the C-H stretches were found between 2980-3000 cm^{-1} , methyl deformations at 1250 and 1380-1430 cm^{-1} and the Si-H stretches around 2200 cm^{-1} . The silyl deformations and methyl rocking modes occur between 800-950 cm^{-1} and tend to overlap, making distinguishing the modes more difficult. The Si-C stretch in monomethyl derivatives was found at 760 cm^{-1} , and the dimethyl derivatives had two bands at 750 and 780 cm^{-1} for the symmetric and asymmetric Si-C stretches. Also the Si-CH₃ and Si-CN stretches appear to be distinguishable, with the Si-CN stretch occurring at a lower frequency.

Between 600 and 400 cm^{-1} the SiH_2 rock, Si-N stretches, and SiH_2 twist are usually found. The vibrations related to the pseudohalide groups occur at 2200 cm^{-1} for $\text{C}\equiv\text{N}$ stretch (overlapping with Si-H stretch), the NCO asymmetric stretch slightly higher at (2250 cm^{-1}) and symmetric stretch at 1400 cm^{-1} (overlapping with methyl deformation modes), and for isothiocyanate at 2100 and 1000 cm^{-1} . The bending modes of NCO and NCS are less predictable but usually around 600 and 480 cm^{-1} respectively.

Below 400 cm^{-1} the skeletal and methyl torsions are expected and it is often difficult to make definite assignments. Commonly the assignments of the pseudohalides have been made easier by comparison with the spectra of the related isotopically labelled samples. However in more complicated spectra, substitution of H for D merely shifts the SiD deformations from overlapping with the methyl rocking modes to overlapping with the Si-C and Si-N stretches.

The assignment of the bands in the gas phase is often not clear because the bands are broad, containing rotational detail in bands 20-30 cm^{-1} wide. However when the sample is observed in the solid phase, much of the broadening can be removed and the bands are more easily distinguished. For example the NCO symmetric stretch and methyl asymmetric deformation overlap in the gas phase in a broad band at 1400-1450 cm^{-1} . However on freezing the sample the bands sharpen and separate, giving the methyl deformation at 1420 cm^{-1} and the NCO stretch at 1450 cm^{-1} . Both bands are only 3-5 cm^{-1} wide. Similarly, between 800-950 cm^{-1} in the

solid the SiH_2 deformations and methyl rocking modes separate to leave distinct sharp bands.

The infra-red spectrum was used in this work as an indication of the purity of the sample. The usual impurities were the bis(methylsilyl)ether, and the pseudo-halide acid. Obviously there is a great deal of overlap between the bands of the impurities and the desired product, but all the ether compounds have a band at around 1100 cm^{-1} (Si-O stretch) and HCN a sharp Q-branch at 714 cm^{-1} , and HNCO an N-H stretch at 3500 cm^{-1} . None of these bands coincides with the sample bands and can be used to check purity.

By observing the nuclear magnetic resonance spectra one is able to confirm the predicted atomic arrangement. For example CH_3CN can be prepared as either the cyanide or isocyanide and nmr spectroscopy should show if any $\text{CH}_3\text{SiH}_2\text{CN}$ exists in this form as well as the normal SiCN arrangement. Also nmr can be used to confirm that the methylsilyl isocyanate really is $\text{CH}_3\text{SiH}_2\text{NCO}$ and not $\text{CH}_3\text{SiH}(\text{NCO})_2$, which would not be easily distinguishable by infra-red spectroscopy.

Much work has been done analysing the gas and solid infra-red and Raman spectra of SiH_3NCO and SiH_3NCS to decide if the SiNC group is bent or linear. If it is bent the molecule will have C_s symmetry while if the group is linear the molecule will have C_{3v} symmetry. Much of the analysis is based on whether the NCO or NCS bend have two

components, a' and a'' for C_s symmetry, or whether there is one band for the degenerate e mode for C_{3v} symmetry. In all the methylsilyl molecules the symmetry will be at most C_s , whether the SiNC chain is bent or linear. However it will be interesting to compare the splitting (if any) for the symmetry species a' and a'' with the splitting found for other bent pseudohalides. The infra-red spectrum of solid SiH_3NCO ⁹⁹ in various matrices shows the silyl rock to have a doublet splitting of up to 34 cm^{-1} and the NCO bending mode splits by up to 27 cm^{-1} . Although the solid phase spectra of the methylsilyl pseudohalides were not run in a matrix, in many cases it was possible to see the splitting for the in and out of plane modes.

The Raman spectra are often found to be useful in observing the low frequency modes which are often weak in the infra-red spectra but medium to strong in the Raman spectra. In molecules with an inversion centre it can be shown that a mode active in the infra-red will be inactive in Raman, and if inactive in the infra-red will be active in the Raman. For less symmetrical molecules there is not the complete mutual exclusion of activity but often bands strong in the infra-red are weak in the Raman and vice versa. For example the symmetric stretch of the NCO group at 1450 cm^{-1} is weak in the infra-red but strong in the Raman while the asymmetric stretch of the NCO group, particularly strong in the infra-red, is weak in the Raman.

By studying the liquid phase Raman spectra one has an additional aid in the assignment of bands, by observing

whether the band is polarised or not. Totally symmetric vibrations give rise to completely polarised Raman lines whereas the asymmetric vibrations give depolarised lines. Hence if a piece of polaroid is put into the scattered radiation first with its polarising axis at right angles to the incident beam and then parallel to the beam, the degree of polarisation can be estimated by noting how the intensity of the band changes.

For less symmetrical molecules, such as the methylsilyl pseudohalides under investigation, the polarised/depolarised effect may be less pronounced but in many cases a change in intensity can be observed. A symmetric vibration gives rise to a polarised band that decreases in intensity with the polarizing filter, while an asymmetric vibration maintains its intensity. For example the C-H stretching region in all spectra showed two bands around 2970 and 2920 cm^{-1} . The band to lower frequency was polarised (changed intensity) and so was assigned as the symmetric stretch, and the higher frequency band assigned to an asymmetric stretch which actually contains two components, a' and a'' .

The shift in vibrational frequency from the gas to solid phase is in many cases indicative of intermolecular interaction. The following spectra were all run after annealing the samples, and this should allow the molecules to align themselves according to any intermolecular attractions that may exist. For example in infra-red studies of $\text{SiH}_3\text{CN}^{142}$ the SiCN chain was found to align by

strong Si...N interactions resulting in shifts in the Si-C band vibrations and an increase in the number of Si-H stretching bands as the molecules aggregate and molecules are constrained in different crystal sites in the unit cell¹³².

As all the molecules under study were observed to form relatively long spindle-like crystals on the cold traps of the vacuum system, it would appear there are considerable intermolecular attractions in these molecules as well. The crystal structure of SiH_3NCO ³³

has strong Si...N and also Si...O interactions, resulting in short interatomic distances between these atoms.

The band shapes in the infra-red are significant and can sometimes be useful in making assignments. An early paper on the mono-methylsilyl halides¹⁴³ described the band shapes expected for these compounds. A vibration with a dipole change parallel to the axis with the greatest moment of inertia gives a C-type band (Q branch), a vibration with a dipole change parallel to the axis of intermediate moment of inertia gives a B-type band (PR branches), and lastly a vibration parallel to the axis of least moment of inertia gives an A-type band (PQR branches). In fact for C_s symmetry the band shapes may not be completely clear as two of the types will mix. These will probably be the B and C types.

Finally, the mass spectra of the pseudohalides are

recorded. These are largely inconclusive because the mass-spectrometer is not scrupulously dry and all the silyl compounds react with any traces of moisture and air to form the related ethers. However in most cases the parent ion peak was observable.

8.2 Vibrational Spectra of Monomethyl Silyl Cyanide

The infra-red and Raman spectra of $\text{CH}_3\text{SiH}_2\text{CN}$ are shown in Figures 8.1-8.4. The molecule was first prepared in 1956⁶² but not fully characterised, and the proton nuclear magnetic spectrum¹⁴⁴ was published later. The molecule belongs to the symmetry group C_s and therefore has 13a' and 8a" modes of vibration. The methyl motions should give 9 fundamentals, the SiH_2 motions another 6 and motions of CSiCN should account for the remaining 6 vibrations. The complete vibrational assignment is presented in Table 8.1.

The asymmetric C-H stretches are assigned to the bands centred at 3002, 2986 cm^{-1} (a' and a") in the solid ir and the symmetric stretch, usually lower in frequency, is assigned to the band at 2930 cm^{-1} in the gas phase. Distinguishing between the Si-H stretch and the $\text{C}\equiv\text{N}$ stretch is more difficult. In trimethylsilyl cyanide a strong line at 2190 cm^{-1} was observed in the liquid phase Raman spectrum, and in SiH_3CN ¹⁴² in a nitrogen matrix a medium strong line at 2200 cm^{-1} is observed, and these have been assigned to the $\text{C}\equiv\text{N}$ stretch. Since one would expect the $\text{C}\equiv\text{N}$

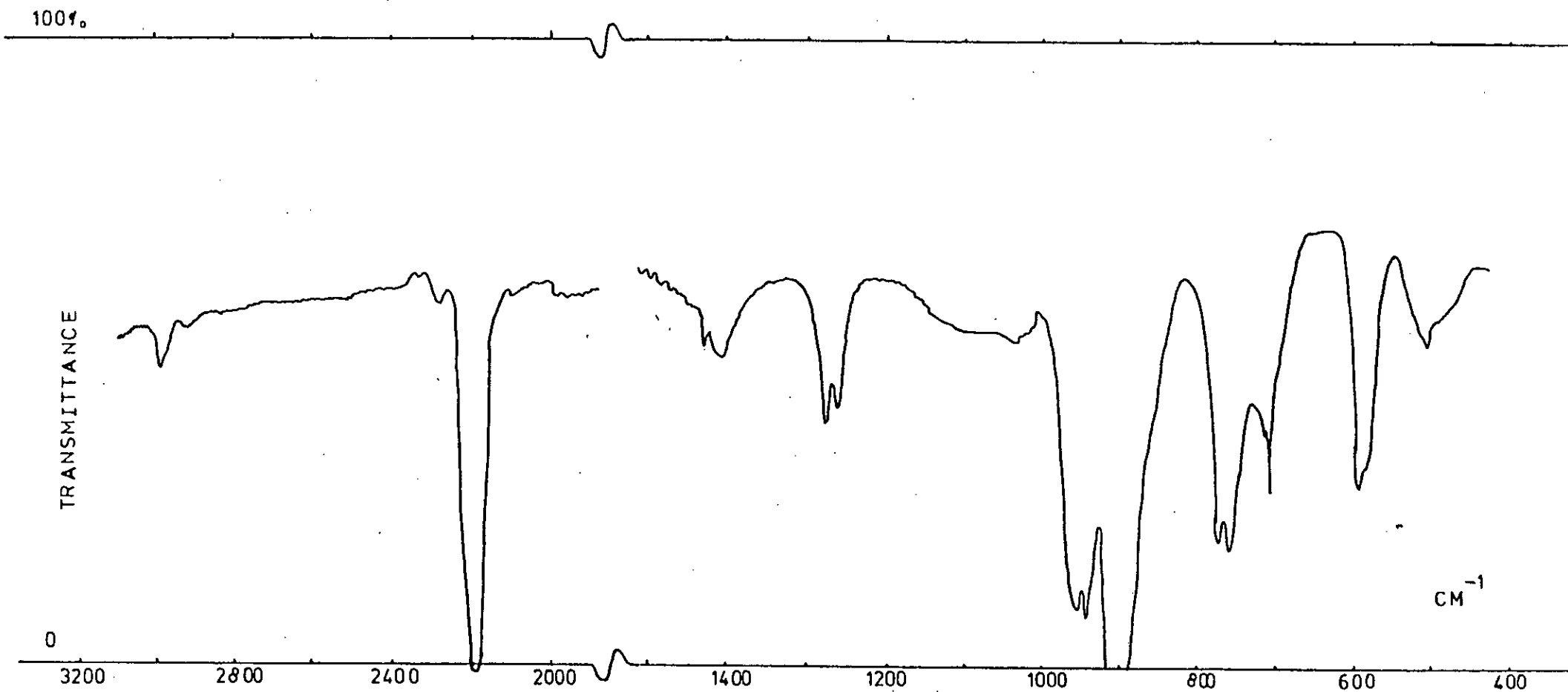


Figure 8.1: Infra-red spectrum of $\text{CH}_3\text{SiH}_2\text{CN}$ in the gas phase
[20 mmHg pressure]

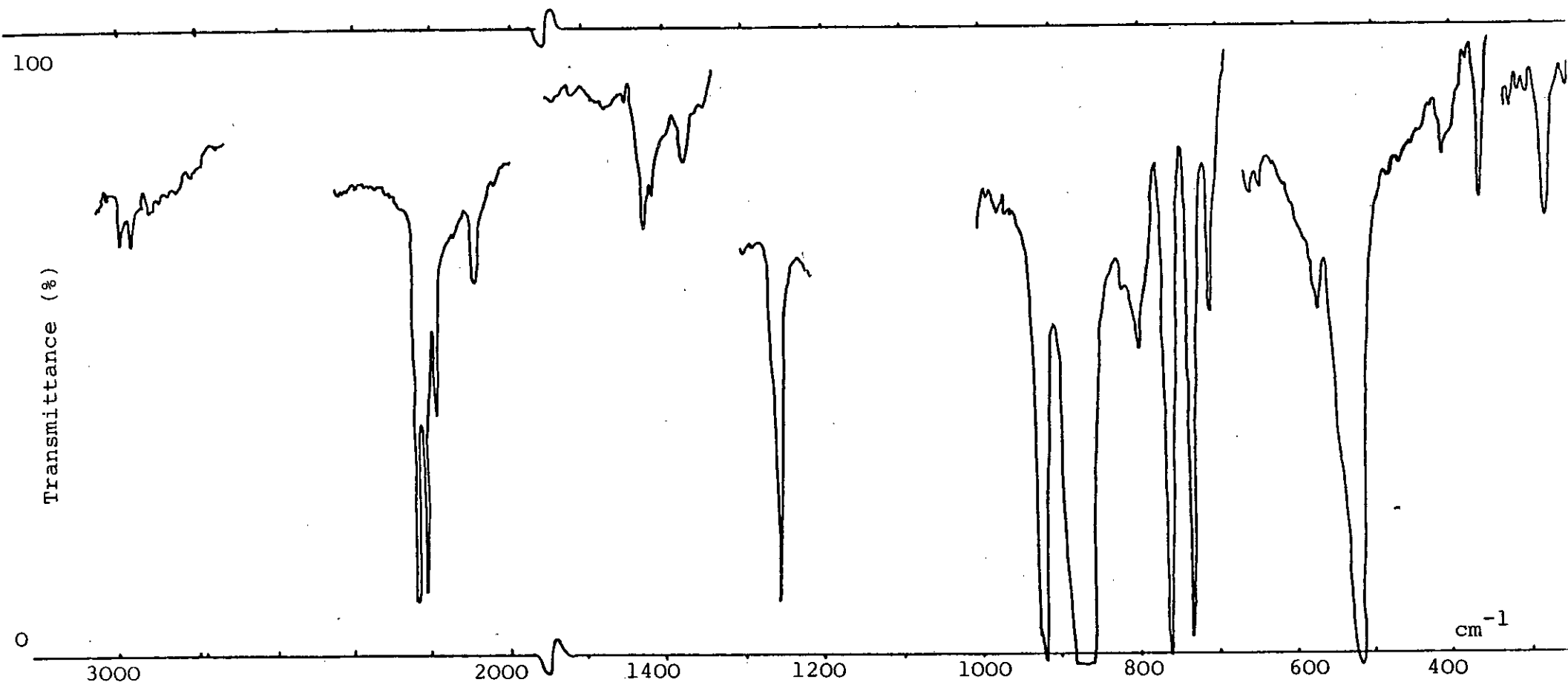


Figure 8.2: Infra-red spectrum of $\text{CH}_3\text{SiH}_2\text{CN}$ in the solid phase.

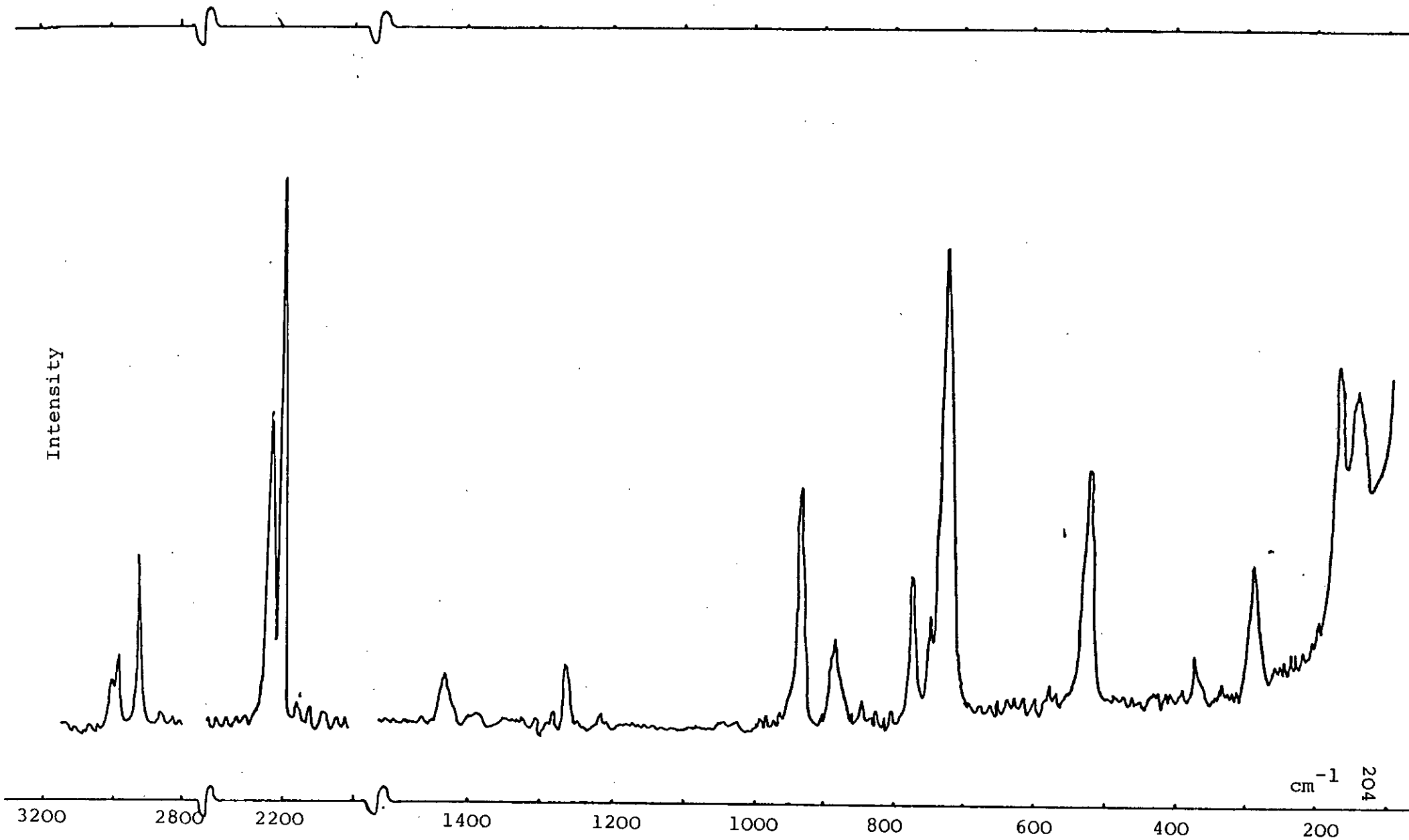


Figure 8.3: Raman spectrum of $\text{CH}_3\text{SiH}_2\text{CN}$ in the solid phase

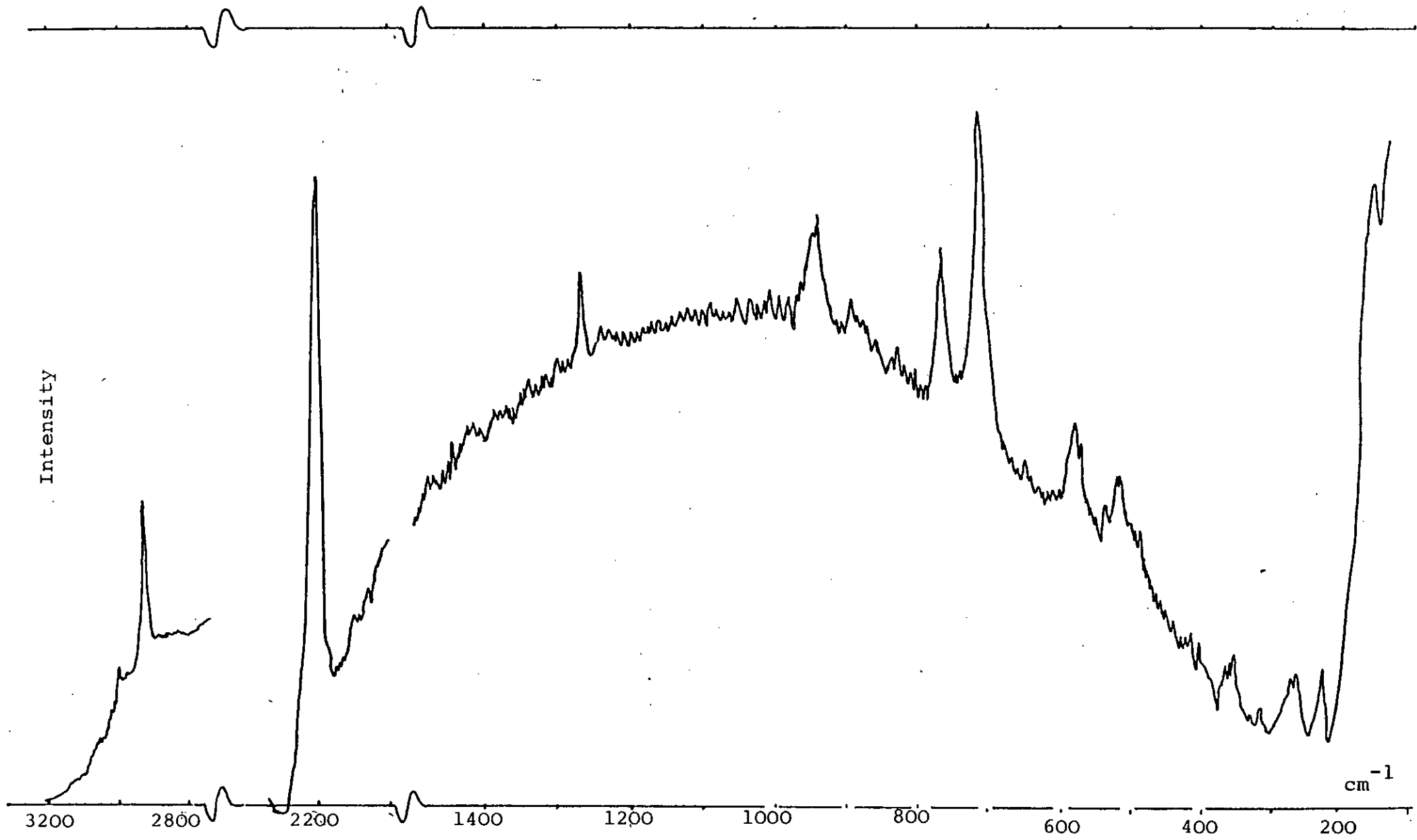


Figure 8.4: Raman spectrum of $\text{CH}_3\text{SiH}_2\text{CN}$ in the liquid phase

Table 8.1: Observed frequencies (cm^{-1}) and assignments for monomethyl silyl cyanide

<u>Raman</u>		<u>Infra-red</u>		<u>Assignment</u>
<u>Liquid</u>	<u>Solid</u>	<u>Solid</u>	<u>Gas</u>	
		3140		
3000 vw,dp	3005 w 2985 w	3002 w 2986 w	2992 w	(a''+a') ν (C-H) asym a' ν (C-H) sym
2935 m,p	2915 m		2930 w	(a') ν (C-H) sym
		2246 s	2280 w	
	2225 br.m	2220 s	2209 s	a'a'' ν (Si-H) asym & sym
2200 vvs,p	2195 vs	2198 m	2198 s	a_1 ν (C \equiv N)
2100 w,p		2093 m		ν (C \equiv N) in HCN
			1650 w	
1420 vvw	1425 w	1430 m	1430 mw	a'' CH ₃ asym def
		1415 w	1410 mw	a' CH ₃ asym def
		1377 w		
1265 m(p)	1258 w	1258 s	1271 m	a' CH ₃ sym def
945m,dp	928 s 878 m	923 s 870 vs	958 s 904 vs 880 m	a' SiH ₂ bend a'' SiH ₂ wag a' or a'' ρ CH ₃
765m,p	768 m 743 w	764 s 738 s	768 s	a' ν (Si-CH ₃) a' or a'' ρ CH ₃
720s,p	723 vs	714 m 575 m	709 m	a'' SiH ₂ twist
580m,p	518 s	522 vs	590 m	a' (Si-CN)
515w			506 w	a' SiH ₂ rock
360 w(dp)	370 w	364 m	340 w,br	CSiC bend
270 w,dp	283 m	284 m		a'' SiCN bend
160 m,dp	166 m 136 m			a' SiCN bend

stretching frequency to be relatively insensitive to the substitution of a hydrogen for a methyl group, the band at 2198 cm^{-1} in the solid infra-red spectrum is assigned to this vibration in $\text{CH}_3\text{SiH}_2\text{CN}$. This band is relatively strong in the solid phase Raman, but weaker in the infra-red. The Si-H stretches can then be assigned to the band at 2220 cm^{-1} which is very strong in infra-red but only of medium intensity in the Raman. These frequencies are close to those found for other monomethyl silyl compounds¹⁴³. In the solid phase infra-red spectrum after much annealing the band at 2210 cm^{-1} splits to two equal intensity bands which could be the symmetric and asymmetric modes of the SiH_2 group. However the separation of 26 cm^{-1} is perhaps rather high. For example the separation of the a' and e modes for SiH_3 stretches in SiH_3CN ¹⁴² was 16 cm^{-1} . A more likely assignment is that the bands are due to crystal splitting for molecules in different sites of a crystal lattice.

The relatively weak band at 2093 cm^{-1} only observed in the solid infra-red and liquid Raman spectra is likely to be due to the impurity HCN. This is a common decomposition product when the sample was left at room temperature, and only becomes more evident on annealing.

The asymmetric methyl deformations (a' and a'') are assigned to the bands around 1415 cm^{-1} . These are weak in the liquid phase Raman spectra and so one cannot confirm their assignment to an asymmetric vibration by observing the depolarisation. The band at 1271 cm^{-1} in

the gas phase is assigned to the methyl symmetric deformation (a'). This band shifts to low frequency by 13 cm^{-1} and sharpens in the solid phase, and appears to be slightly polarised in the liquid phase, as would be expected.

In the gas phase, the two strong bands at 958 and 904 cm^{-1} and the shoulder at 880 cm^{-1} are assigned to the SiH_2 bend, SiH_2 wag and methyl rock respectively. When the spectrum for the solid phase was observed the SiH_2 vibrations shifted to lower frequency covering the methyl rocking band. The polarised band at 765 cm^{-1} is assigned to the Si-CH_3 stretch and does not shift significantly between gas, liquid and solid phases. The second methyl rocking mode is assigned to the band at 738 cm^{-1} in the solid phase infra-red spectrum as a sharp band that is hidden under the broad Si-CH_3 stretch in the gas phase. On annealing the intensity of this band increases to equal that of the Si-CH_3 stretching band. The sharp band at 709 cm^{-1} in the gas phase is assigned to the SiH_2 twist and this would be expected to be relatively weak in the infra-red as it must involve only a small dipole change. However in the Raman spectra this mode gives rise to a very strong band at 723 cm^{-1} in the solid and 720 cm^{-1} in the liquid.

In the region $600\text{-}400\text{ cm}^{-1}$ only two bands were found in the gas phase spectrum. The weaker band at 506 cm^{-1} is assigned to the SiH_2 rocking mode, after comparison with

related methylsilyl compounds, e.g. $(\text{CH}_3)_2\text{SiH}_2$ 470 cm^{-1} , $\text{CH}_3\text{SiH}_2\text{Cl}$ 510 cm^{-1} , $\text{CH}_3\text{SiH}_2\text{Br}$ 495 cm^{-1} and $\text{CH}_3\text{SiH}_2\text{I}$ 480 cm^{-1} ¹⁴³. This leaves the stronger band at 590 cm^{-1} to be assigned to the Si-CN stretch. Comparison with the solid infra-red and Raman spectra shows the intense band is now at 522 cm^{-1} (see Figure 8.5) and it is suggested that the large shift must be due to constraining intermolecular interactions between adjacent methylsilyl cyanide molecules. Similarly, there is a shift of the Si-CN stretch in $(\text{CH}_3)_2\text{SiHCN}$ (30 cm^{-1}) ⁶⁴ when the sample is frozen, coupled with an increase in intensity in the infra-red spectrum. The strong Si...N interactions have been observed in the crystal structure of SiH_3CN in which chains of $\text{Si-C}\equiv\text{N}\dots\text{Si-C}\equiv\text{N}\dots$ link up, and give SiH_3CN certain physical properties such as a high melting point in the vacuum systems. Monomethyl silyl cyanide was also observed to melt with some difficulty.

The shift of the Si-CN stretch to lower frequency causes an overlap with the SiH_2 rocking band which is not observed in the solid phase. However in the liquid phase a decrease in the intermolecular attraction causes the bands to shift to positions much closer to the gas phase positions than the solid phase. The band at 580 cm^{-1} was found to be polarised and the band at 515 cm^{-1} slightly polarised, confirming the assignments of Si-CN stretch (a') and SiH_2 rock (a') respectively. The band at 575 cm^{-1} in the solid phase infra-red spectrum decreased in intensity on annealing and is probably an extra band

600

400

 cm^{-1}

210

Infra-red (gas)

Infra-red (solid)

Figure 8.5:

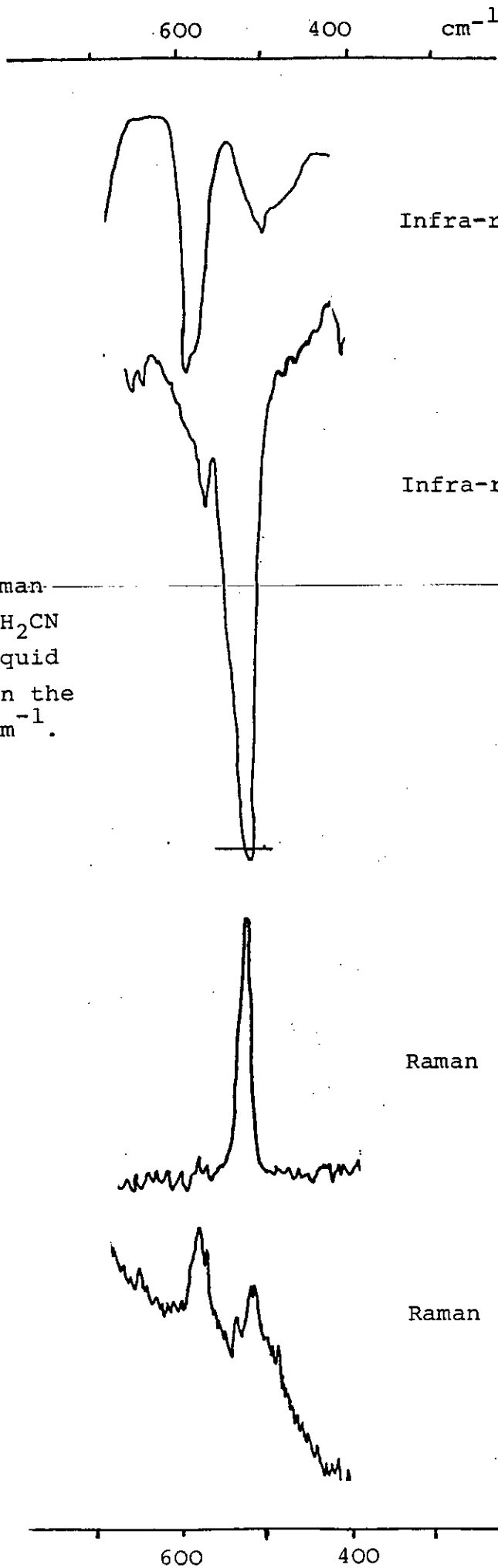
Infra-red and Raman spectra of $\text{CH}_3\text{SiH}_2\text{CN}$ in the solid, liquid and gas phases in the region $600\text{-}400\text{ cm}^{-1}$.

Raman (solid)

Raman (liquid)

600

400

 cm^{-1} 

assigned as arising from molecules in different crystal sites.

Below 400 cm^{-1} the assignments are less certain. Silyl cyanide has one band in this region at 246 cm^{-1} which can only be due to the SiCN bending motion, and this has an overtone at 475 cm^{-1} . For $\text{CH}_3\text{SiH}_2\text{CN}$ one would expect four bands in this region: the CSiC bend (a'), two SiCN bends ($a' + a''$) and one methyl group torsion. In the solid phase Raman spectrum of $\text{CH}_3\text{SiH}_2\text{Cl}^{145}$ a band at 225 cm^{-1} was assigned to the CSiCl bend, and since CSiC would be expected at higher frequency than this the band at 340 cm^{-1} gas phase is assigned to the CSiC bend. Also the CH_3 is probably very weak and not seen, leaving the bands at 283 and 166 cm^{-1} to be assigned to the SiCN bends. These two bands average to 220 cm^{-1} which is close to the SiH_3CN bend at 246 cm^{-1} . Lastly, the splitting of the 160 cm^{-1} band in the solid phase Raman spectra is most likely due to intermolecular couplings.

In all spectroscopic studies of cyanides evidence for the isocyanide has been looked for, e.g. $\text{CH}_3\text{SiH}_2\text{NC}$. None has been found for this compound as it is thought that the band at 2093 cm^{-1} (often assigned to isocyanide) is due to the impurity HCN present. In support of this is the sharp band at 714 cm^{-1} (the HCN bend) and at 3308 cm^{-1} (the NC-H stretch).

8.3 Vibrational Spectra of Monomethyl Silyl Isocyanate

The molecule should have C_s symmetry, and so the 10 atoms should give rise to 24 fundamentals, 15a' and 9a" modes. The methyl group hydrogen motions will take up 5a' and 4a", while the SiH_2 hydrogens take 3a' + 3a". The remaining modes are heavy atom vibrations, with 4a' due to bond stretches and 3a' + 2a" due to bending motions in and out of the plane.

The one a" C-H asymmetric stretch is assigned to the depolarised band at 2985 cm^{-1} and the two a' C-H symmetric stretches to the bands at 2900 and 2850 cm^{-1} . It is also possible the band at 2850 is a combination or overtone band. The relatively strong band at 2400 cm^{-1} only observed in the gas phase infra-red spectrum, is probably the combination of the NCO asymmetric stretch and a low frequency bend, as a similar band was observed for $(CH_3)_3SiNCO$ (but left unassigned)¹⁰⁰, and for $(CH_3)_2SiHNCO$ (see Section 8.4). The NCO asymmetric stretch is assigned to the very strong band at 2300 cm^{-1} in the infra-red which is weak in the Raman. This contrast in intensities between the infra-red and Raman spectra is found for all silyl isocyanates. The solid phase Raman spectrum was found to give two strong bands 10 cm^{-1} apart at 2210 cm^{-1} and these are best assigned to the symmetric and asymmetric Si-H stretches. This leaves two more bands above 2000 cm^{-1} , one which is observed in the solid phase Raman spectrum at 2150 cm^{-1} which could be assigned either as a difference band, although this is unlikely for a

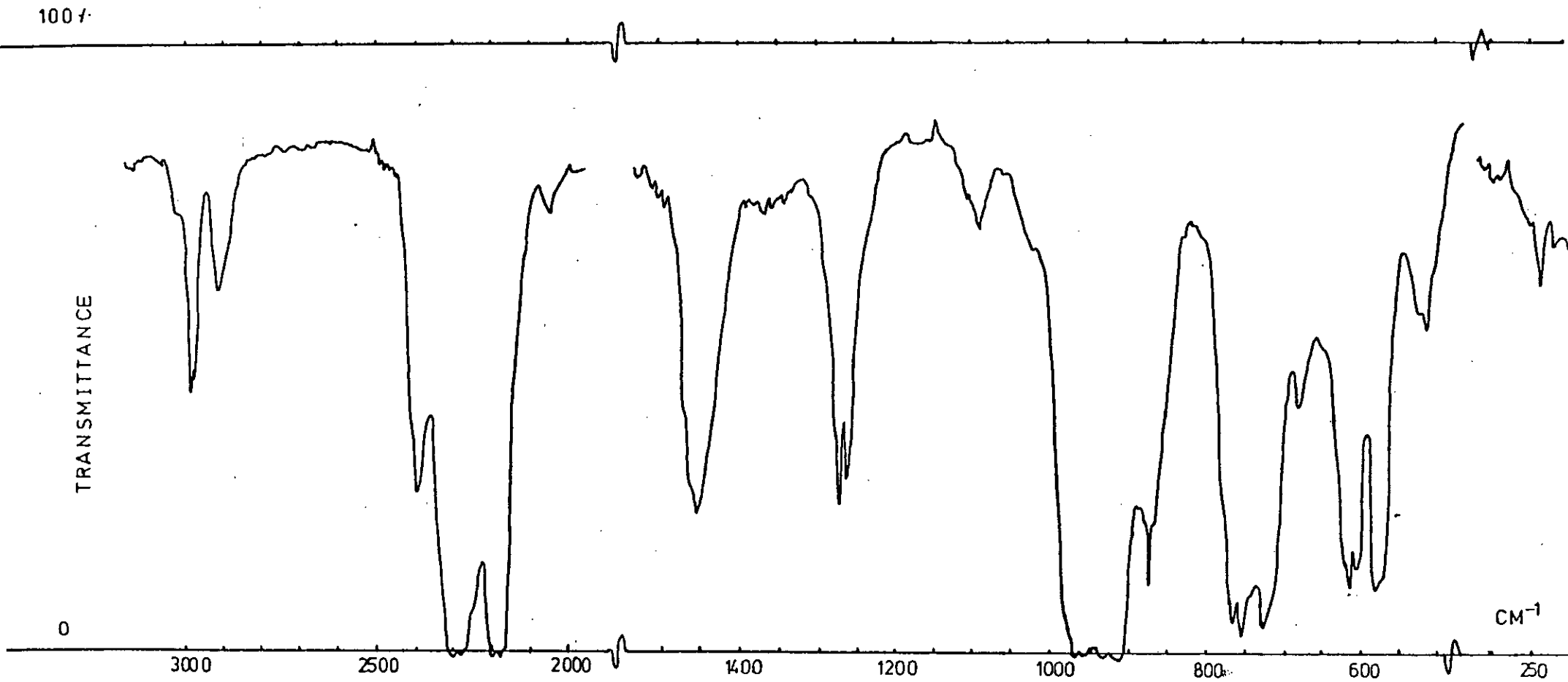


Figure 8.6: Infra-red spectrum of $\text{CH}_3\text{SiH}_2\text{NCO}$ in the gas phase (35 mmHg pressure)

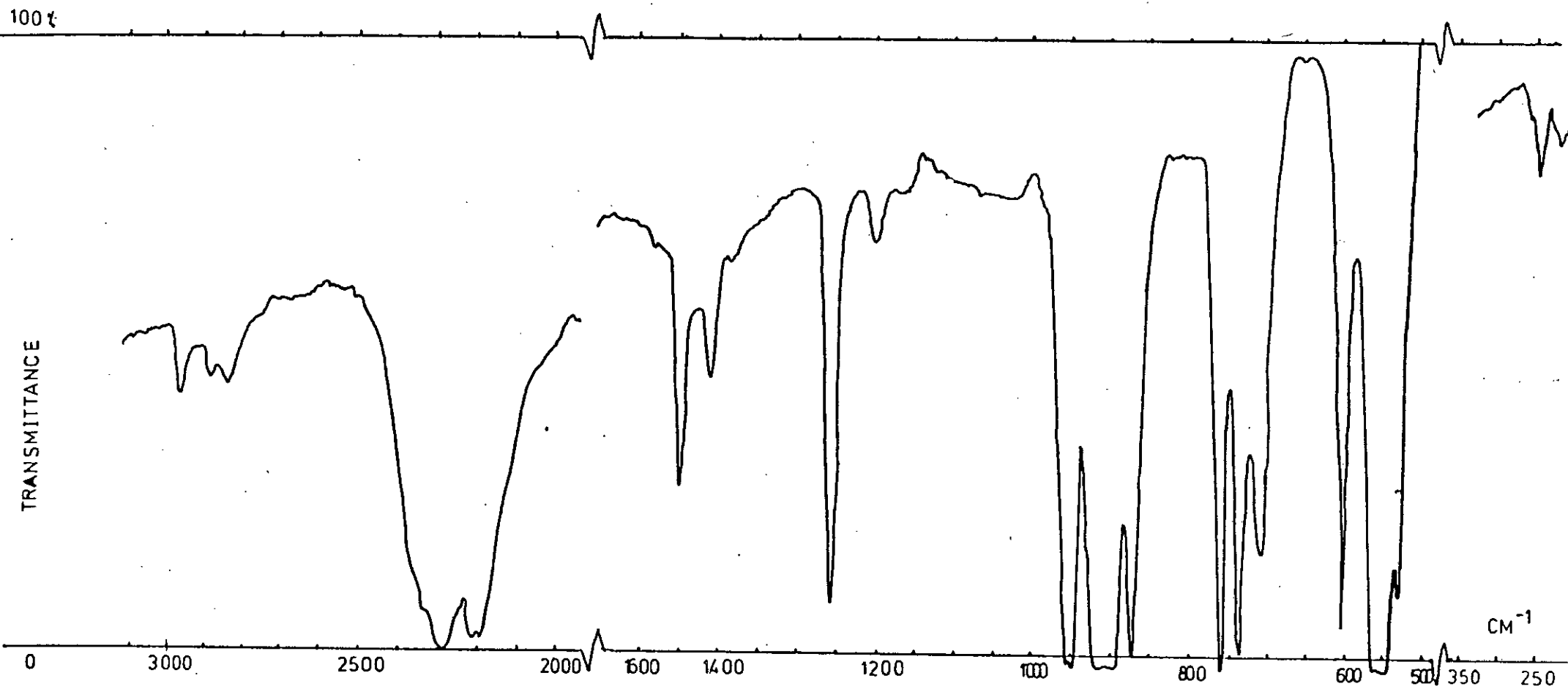


Figure 8.7: Infra-red spectrum of $\text{CH}_3\text{SiH}_2\text{NCO}$ in the solid phase

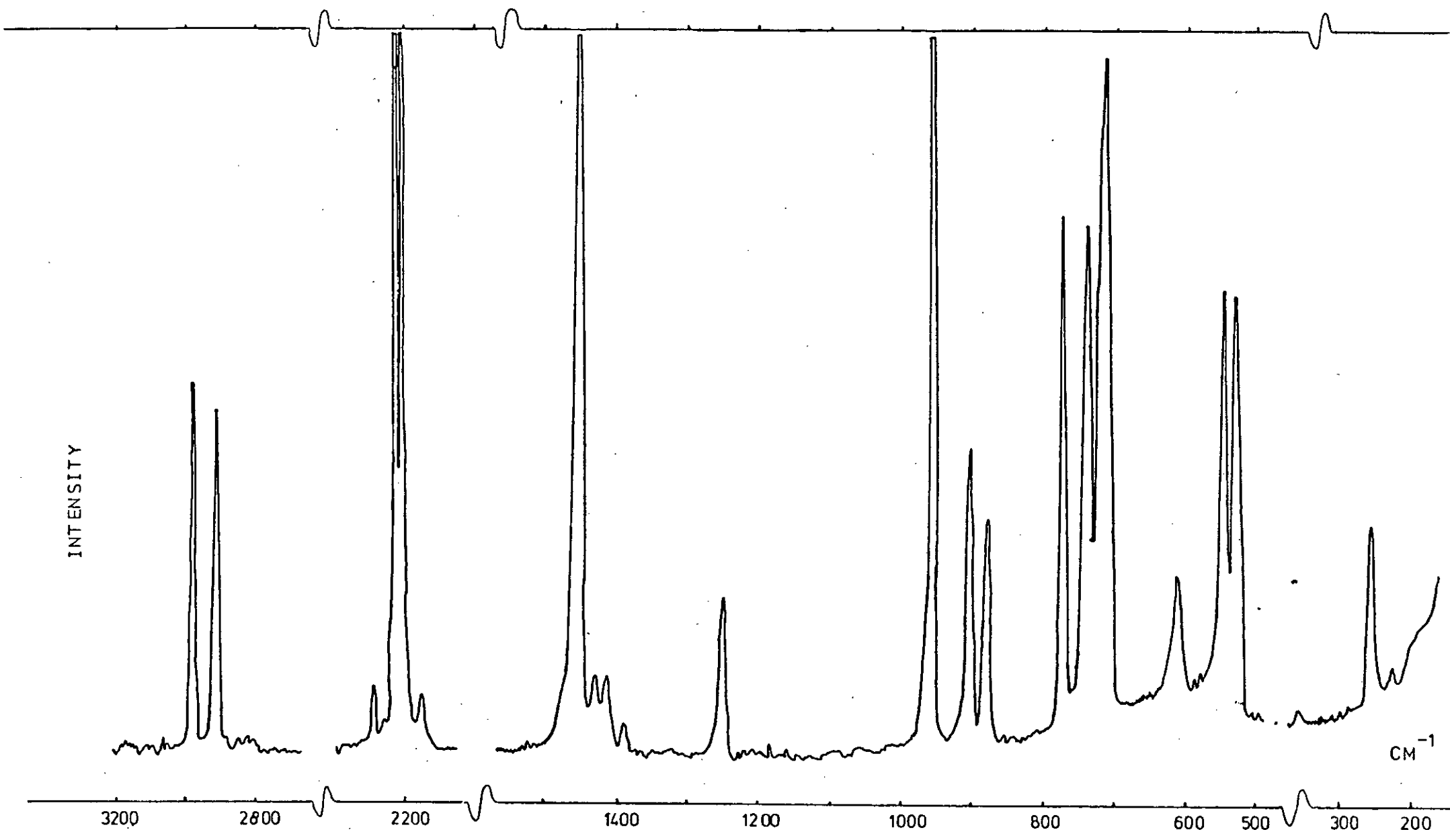


Figure 8.8: Raman spectrum of $\text{CH}_3\text{SiH}_2\text{NCO}$ in the solid phase

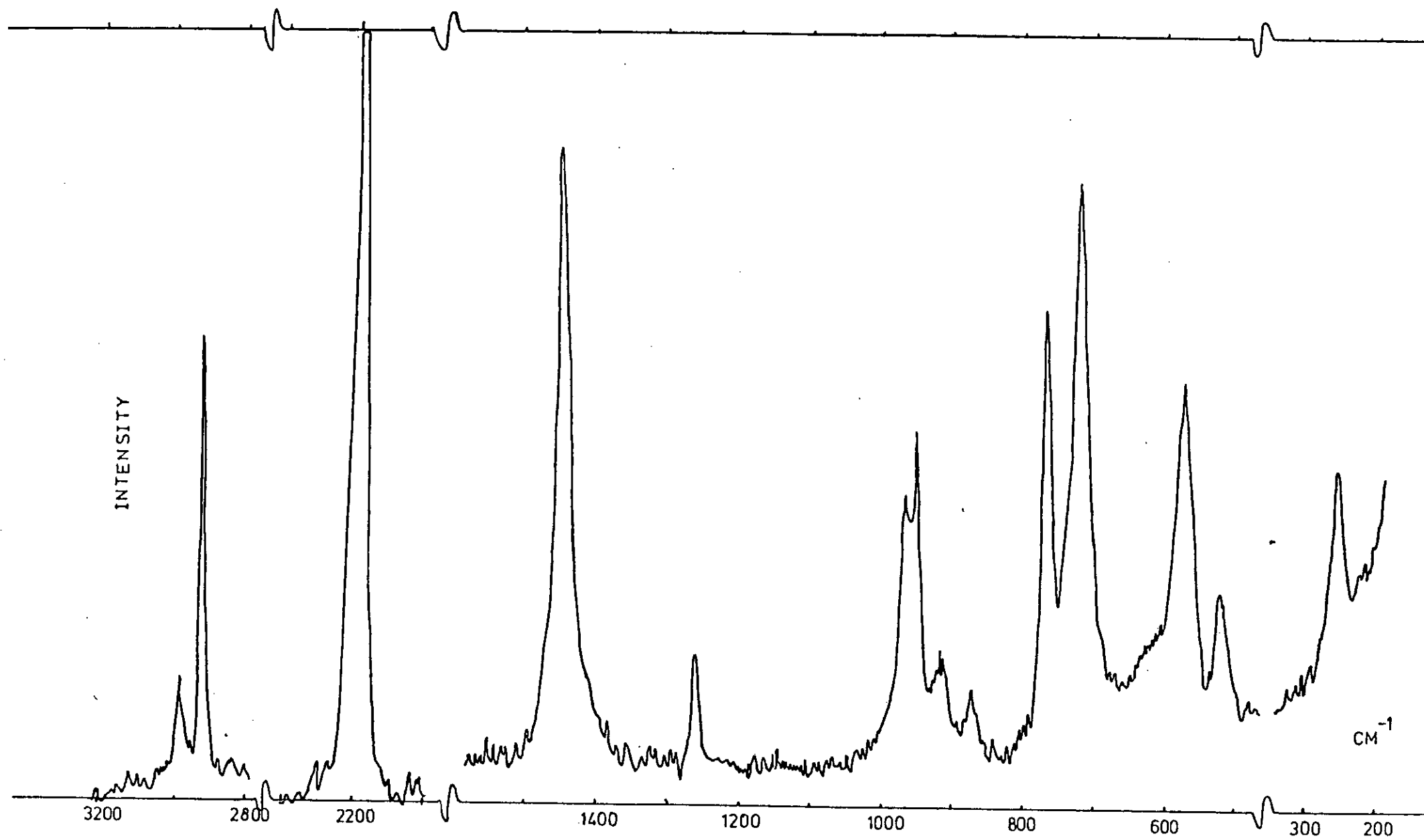


Figure 8.9: Raman spectrum of $\text{CH}_3\text{SiH}_2\text{NCO}$ in the liquid phase

Table 8.2: Observed bands in infra-red and Raman spectra and assignments for methylsilyl isocyanate (cm^{-1})

<u>Raman</u>		<u>Infra-red</u>		<u>Assignment</u>
<u>Liquid</u>	<u>Solid</u>	<u>Solid</u>	<u>Gas</u>	
2985 w,dp	2990 m	2990 w	3754 w 2986 m	$\nu(\text{NCO})$ sym and asym $a''(\text{C-H})$ asym stretch
2915 s,p	2920 m	2900 w 2850 w	2920 w 2400 s	$a'(\text{C-H})$ sym stretch $a'\nu(\text{C-H})$ sym stretch combination
2310 w	2290 w 2215 vs	2295 vs,b 2200 vs,b	2304 vvs 2188 vvs	$a'\nu(\text{NCO})$ asym stretch $a''\nu(\text{Si-H})$ asym stretch
2190 vs,p	2205 vs 2150 w		2060 vw	$a'\nu(\text{Si-H})$ sym stretch comb. $\nu(\text{NCO})+\text{SiH}_2$ twist comb. NCO sym+ NCO bend
1445 s,p	1452 vs 1422 w 1402 w 1381 w	1450 s 1410 m	1457 s	a' NCO sym stretch $a'a''$ CH_3 deform.asym.
1258 m,p	1250 m	1255 s	1269 s 973 vs	a' CH_3 sym deform.
960mp	957 vs	955 vs	962 vs	a' SiH_2 bend
915 w,dp	900 m	905 vs	925 vs	a'' SiH_2 wag
870 w(dp)	872 m	880 s	876 s	a'' CH_3 rock
766 m,p	770 s	760 s	766 s	a' Si-C stretch
735 m,sh,p	730 s	735 s		a' CH_3 rock
716 s,p	706 vs 603 m	710 s 605 s	728 s 685 m 606 s	a'' SiH_2 twist a'' ρCH_3 rock NCO bend
570 m,p	540 s	550 vs	571 s	a' Si-N stretch
518 w,dp	520 s 470 vw	530 s	530 m	a' SiH_2 rock 2 x CSiN bend
250 m,dp	245 m 145 vw	245 w	238 w	a'' CSiN bend 2 x SiNC bend

Abbreviations used:

s strong, m medium, w weak, v very, b broad, p polarised,
dp depolarised, sh shoulder, asym, asymmetric, sym, symmetric.

sample at 80 K or as a combination band of the NCO symmetric stretch and the SiH_2 twist. The other band is at 2060 cm^{-1} and is assigned to the combination of the NCO symmetric stretch and NCO bend.

In the gas and liquid phase one band is found at 1457 cm^{-1} . However in the solid phase, the broad band splits to give a band in the Raman spectrum at 1450 cm^{-1} and much weaker bands at 1422 , 1402 and 1381 cm^{-1} . The former is assigned to the NCO symmetric stretch a' and the latter bands as the methyl asymmetric deformations ($a'+a''$) although they are too weak to observe whether they are depolarised as would be expected. However the band at 1258 cm^{-1} is clearly polarised and assigned to the symmetric (a') methyl deformation. This band sharpens on annealing and shifts by 15 cm^{-1} to low frequency in the solid phase.

The three bands between 800 and 1000 cm^{-1} are assigned to the SiH_2 bend and wag and one methyl rock, and the relative intensities in the infra-red and Raman compare well with the SiH_3 deformations in SiH_3NCO ^{99,122,146} and the methyl rocks in $(\text{CH}_3)_3\text{SiNCO}$ ¹⁰⁰. The assignment is then: SiH_2 bend at 960 cm^{-1} , the SiH_2 wag at 915 cm^{-1} and the methyl rock at 870 cm^{-1} . Unfortunately the polarisation data are unclear because the band at 950 cm^{-1} is broad but the methyl band does appear to lose intensity with the polariser filter so is assigned to the out-of-plane rocking mode (a'').

The Si-C stretch at 766 cm^{-1} appears to vary very little for all the methylsilyl compounds, and stays constant in the three phases. The band at 735 cm^{-1} , only observed in the liquid and solid phases, is likely to be in-plane methyl rock (a'). The last band above 700 cm^{-1} is then the very strong band in the solid phase Raman spectrum at 716 cm^{-1} which shifts to 728 cm^{-1} in the gas phase, and is assigned to the SiH_2 twist, even though the band appears to be polarised (a') and the twisting mode would be expected to be a'' .

Since the molecule has C_s symmetry the NCO group should have two bending modes ($a' + a''$). For SiH_3NCO and $(\text{CH}_3)_3\text{SiNCO}$ in the gas phase (C_{3v} symmetry) the NCO band is at 620 cm^{-1} and medium intensity in the infra-red but weaker in the Raman. A similar band is found for $\text{CH}_3\text{SiH}_2\text{NCO}$ at 606 cm^{-1} in the gas phase which is sharp and strong in the solid infra-red, and weak in the Raman. Phenylisocyanate¹⁴⁷, which has C_s symmetry, has two NCO bending modes assigned to bands at 569 and 632 cm^{-1} . Hence if the band positions are similar in $\text{CH}_3\text{SiH}_2\text{NCO}$ the second NCO bend should overlap with the very strong Si-N stretching band centred at 550 cm^{-1} and is unlikely to be seen.

Between 500 and 600 cm^{-1} the two bands that are observed are assigned to the Si-N stretch and SiH_2 rock; both a' species. The Si-N stretching vibration is relatively strong in the gas phase infra-red but has greatly enhanced intensity in the solid phase, and shifts by 20 cm^{-1} to lower frequency. This must be because of strong intermolecular

interaction, between Si and O and N atoms in adjacent molecules allowing linking of SiNCO chains. The drop in frequency is identical to that found for SiH_3NCO ¹⁴⁶, which has already been studied in the crystal state by X-ray diffraction³³ and the close Si...O and Si...N contacts observed. The weaker band at 530 cm^{-1} is assigned to the SiH_2 rock.

This leaves only two bands below 400 cm^{-1} . The strongest is at 245 cm^{-1} and appears to be depolarised. Since the SiNC bending frequency for SiH_3NCO and $(\text{CH}_3)_3\text{SiNCO}$ is found below 100 cm^{-1} , this band is most likely to be the CSiN bend. In $(\text{CH}_3)_3\text{SiNCO}$ the SiC_3 asymmetric and symmetric deformations are assigned to bands at 278 and 246 cm^{-1} respectively so this assignment does not seem unreasonable. The very weak band at 145 cm^{-1} , only observed in the solid phase Raman spectrum, could be the first overtone of the SiNC bend. When SiH_3NCO was studied in the gas phase in the far-infra-red region⁹⁸ two bands were observed at 64 and 134 cm^{-1} , and so if this assignment is correct one can predict the SiNC bending fundamental of $\text{CH}_3\text{SiH}_2\text{NCO}$ to be at about 72 cm^{-1} .

The full table of bands observed and their assignments is given in Table 8.2, and the spectra are given in Figures 8.6 to 8.9.

8.4 Vibrational Spectra of Dimethylsilyl isocyanate

The molecule belongs to the point group C_s , and so from group theory one can predict that the molecule should have 19 a' and 14 a'' modes of vibration. The methyl group motions should give rise to 18 of the fundamental modes, 6 of them are C-H stretch, 10 are deformations and rocking modes, and 2 are torsions along the Si-C bonds. The Si-H group should have 1 bond stretch and 2 bending modes, and the heavy atom skeleton should give rise to 12 modes, 5 bond stretches, and 7 modes assigned to bends, deformations and torsions.

The spectra that were obtained are shown in Figures 8.10 to 8.13 and the band positions and assignments are given in Table 8.3.

The C-H stretching bands are relatively strong in the infra-red and Raman spectra, and the assignments are the asymmetric stretches ($2a' + 2a''$) to the bands at 2983 and 2918 cm^{-1} , with the weaker band at 2862 cm^{-1} assigned to the symmetric stretches ($a' + a''$). The characteristic NCO asymmetric stretch, strong in the infra-red and weak in the Raman is assigned to the band at 2270 cm^{-1} , and the Si-H stretch is found 100 cm^{-1} lower in frequency at 2172 cm^{-1} in the gas phase, and slightly lower still in the solid phase.

In the region 1400-1500 cm^{-1} only one broad band is observed in the gas phase, infra-red, but in the solid phase

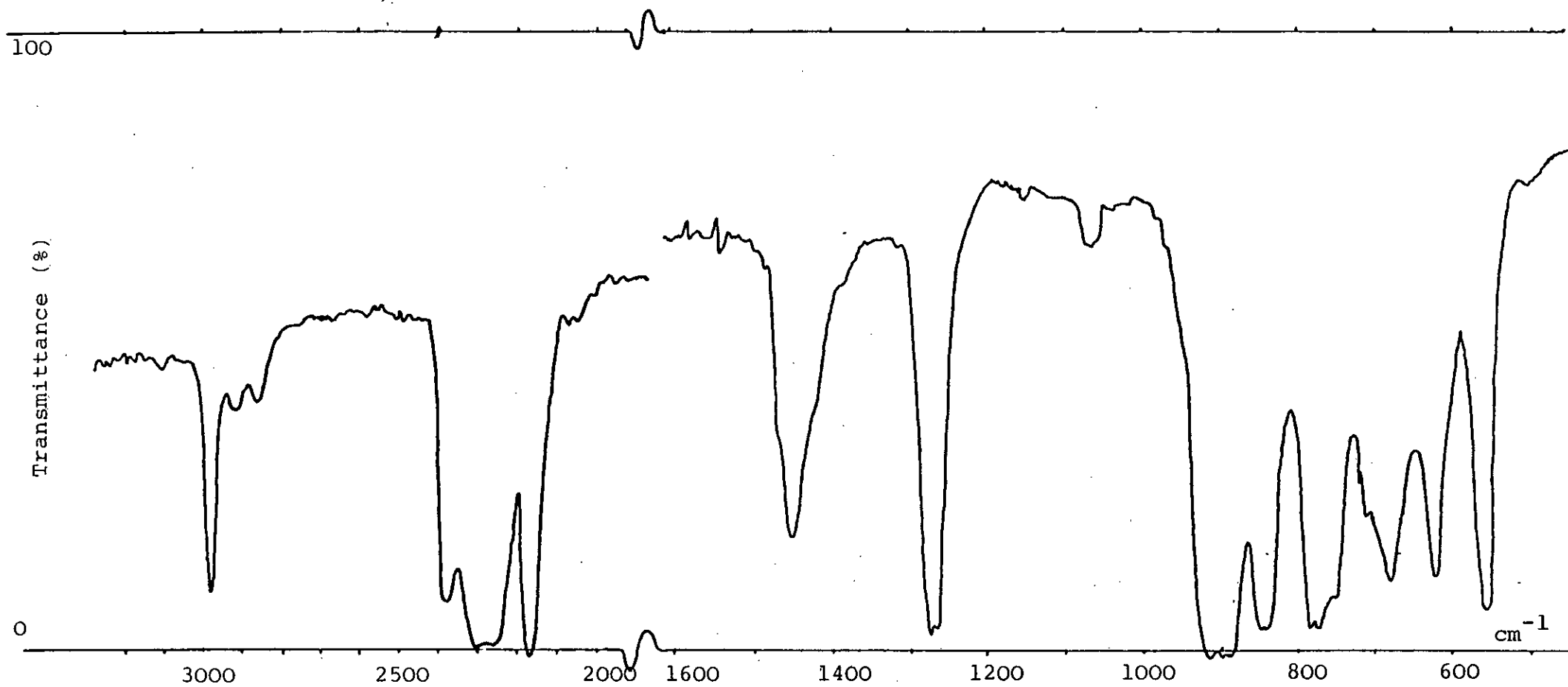


Figure 8.10: Infra-red spectrum of $(\text{CH}_3)_2\text{SiHNCO}$ in the gas phase (60 mmHg pressure)

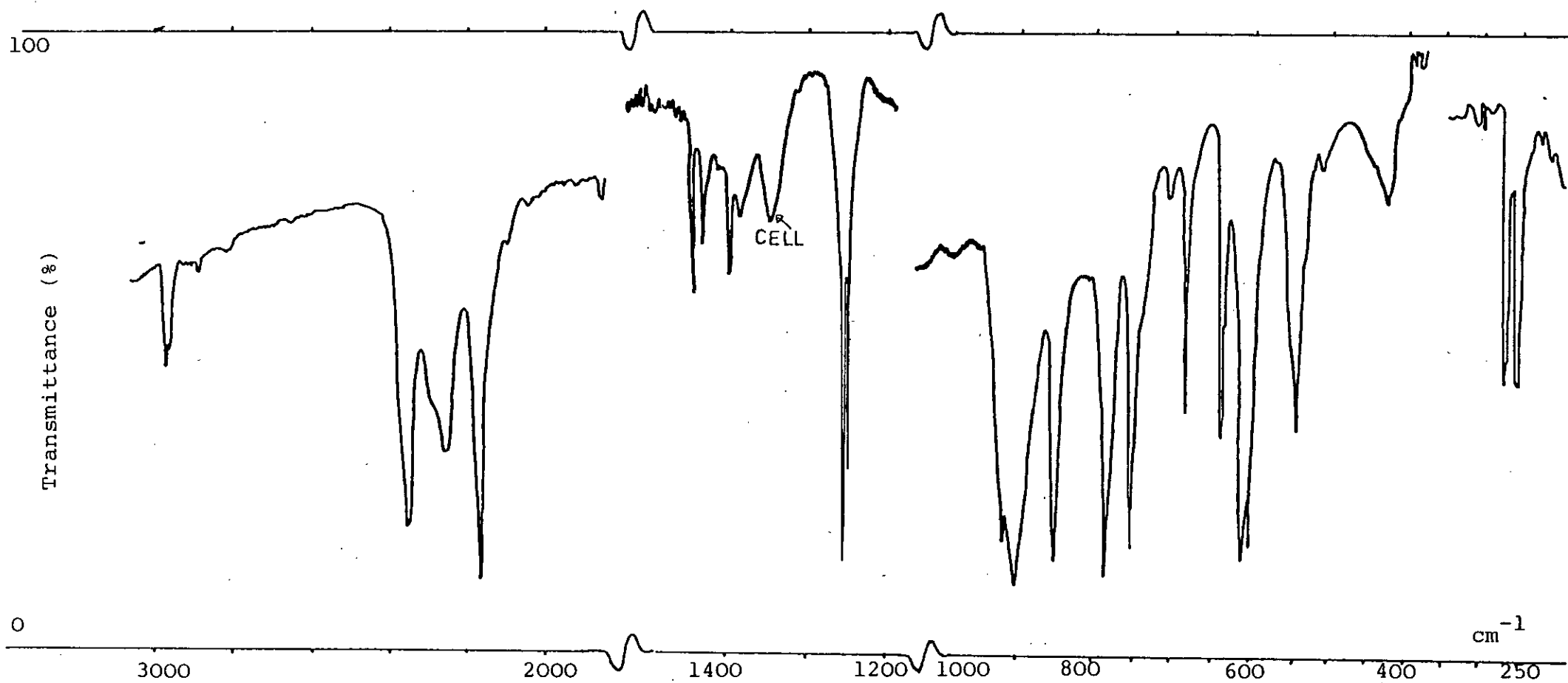


Figure 8.11: Infra-red spectrum of $(\text{CH}_3)_2\text{SiHNCO}$ in the solid phase

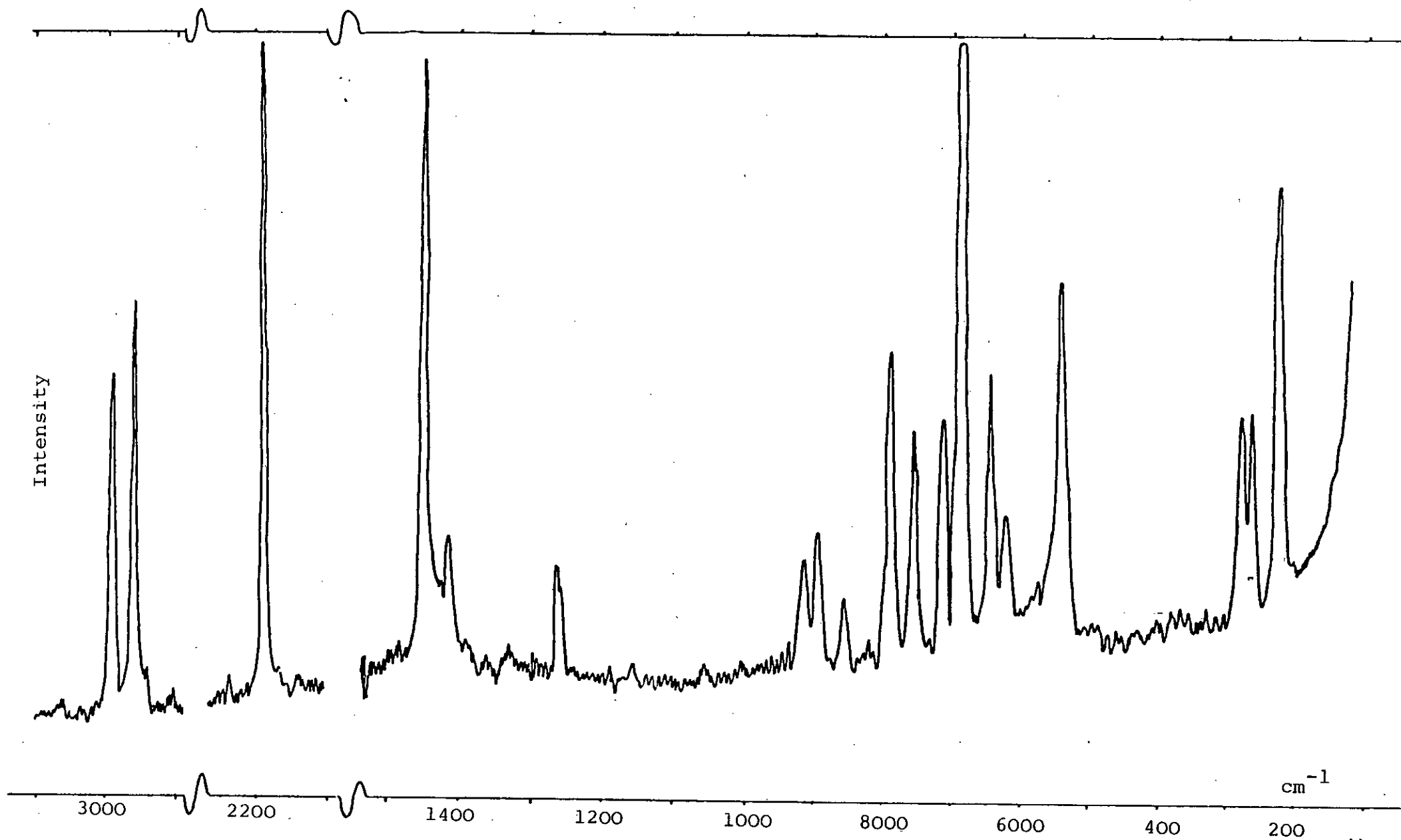


Figure 8.12: Raman spectrum of $(\text{CH}_3)_2\text{SiHNCO}$ in the solid phase

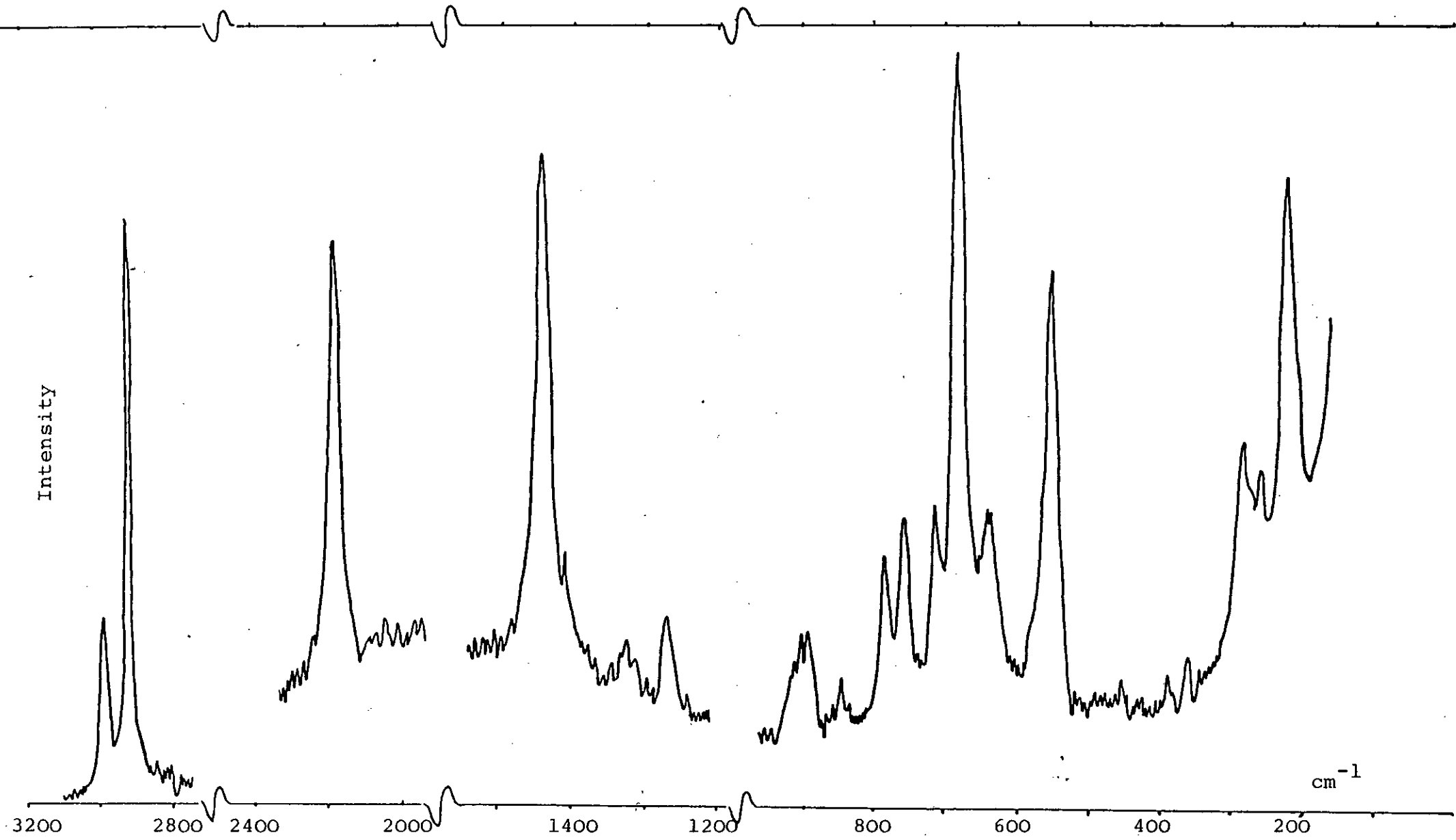


Figure 8.13: Raman spectrum of $(\text{CH}_3)_2\text{SiHNCO}$ in the liquid phase

Table 8.3: Observed frequencies (cm^{-1}) and assignments for dimethylsilyl isocyanate

<u>Raman</u>		<u>Infra-red</u>		<u>Assignments</u>
<u>Liquid</u>	<u>Solid</u>	<u>Solid</u>	<u>Gas</u>	
			3720 w	asym+sym NCO stretch
2970 m,dp	2965 m	2981 m	2983 s	a'+a" C-H asym stretch
2910 vs,p	2900 m		2918 w	a' a" C-H asym stretch
2860 vw			2862 w	a'+a" C-H sym stretch
		2360 vs	2383 s	NCO asym +I.F. bend
	2255 vw	2257 s,br	2270 vs	a' asym NCO stretch
2160 vs,p	2155 vs	2171 vs	2172 vs	a' Si-H stretch
1437 vs,p	1444 s	1446 m	1451 m	a' sym NCO stretch
		1434 m		a" CH ₃ deform asym
1400 w,dp	1410	1400 m		a" asym CH ₃ def
		1386 w		a" asym CH ₃ def
1262 m,p	1260 m	1258 vs	1269 vs	a' sym CH ₃ def
	1254 w	1252 vs		a"
910 w,dp	912 w	919 s	917 s	a" CH ₃ rock
890 w,p	890 m	900 s	901 vs	a' CH ₃ rock
840 w,p	852 w	850 s	845 s	a' Si-H bend
777 m,dp	784 m	780 s	780 s	a" Si-C asym stretch
752 m,p	750 m	750 s	750 s	a' Si-C sym stretch
710 m,p	709 m	706 w	710 m	a" CH ₃ rock
690 vvs,p	682 vvs	682 m	685 s	a' CH ₃ rock
632 m,br,dp	640 m	635 m	625 s	a" Si-H bend
	620 w,m	609 s	610m,sh	NCO bend
		600 s		NCO bend
		551 s		2 x 274
550 s,p	540 s	544 s	563 s	a' Si-N stretch
				2 x 256
		510 w		
		424 w		
277 m,dp	274 m	274 m		a' SiC ₂ scissors
255 w,dp	259 m	256 m	255 w	a" CSiN bend
222 s,dp	222 s			a' CSiN bend

Abbreviations:

s strong, v very, m medium, w weak, p polarised, dp depolarised, asym asymmetric, sym symmetric, sh shoulder, br broad.

on annealing this splits into four sharp but relatively weak bands. The liquid phase Raman spectrum has a very strong polarised band at 1437 cm^{-1} , and a weaker band at 1410 cm^{-1} . From the position and intensity of the Raman band at 1437 cm^{-1} , this is assigned to the NCO symmetric stretch (a') and the lower frequency bands at 1434, 1400 and 1386 cm^{-1} to the methyl asymmetric deformations. These appear to be depolarised, although should contain polarised bands as well ($3a' + 3a''$). The contrast between the intensity of the symmetric NCO stretch which is strong in Raman but weak in the infra-red, while the asymmetric NCO stretch is weak in the Raman but strong in the infra-red was noted in $\text{CH}_3\text{SiH}_2\text{NCO}$ and SiH_3NCO .

The dimethyl silyl compounds would be expected to have two symmetric methyl deformations ($a' + a''$) and in the solid phase infra-red and Raman spectra these bands are discernible at 1258 and 1252 cm^{-1} . In monomethyl silyl compounds, the SiH_2 deformation bands are more intense than the methyl rocking modes in the region $1000\text{-}750\text{ cm}^{-1}$. However for dimethylsilyl compounds the methyl modes appear to be relatively more intense, and obviously there are fewer Si-H related vibrations. The bands at 917 and 901 cm^{-1} depolarised and polarised respectively, are assigned to the two methyl rocks ($a' + a''$) and the Si-H band (a') is assigned to the band at 845 cm^{-1} . A band at the same frequency was found in the spectrum of $\text{SiH}(\text{NCO})_3$ ¹⁴⁸ which has no methyl rocking modes to confuse the assignment. All these bands are relatively weak in the Raman spectrum. The asymmetric and symmetric Si-C stretches

are assigned to the bands at 780 and 750 cm^{-1} and show no significant shift on change of the phase.

The assignment of the bands between 720 and 600 cm^{-1} is not so straightforward. The vibrations with bands in this region are two methyl rocks ($a' + a''$), the out of plane Si-H bend (a'') and the bending modes of the NCO group ($a' + a''$). What is observed is a very strong Raman band at 690 cm^{-1} and three medium to weak bands at 710, 642 and 620. The infra-red solid phase spectrum also has an extra band at 600 cm^{-1} . The strong Raman band at 682 cm^{-1} can be assigned to the in plane methyl rock (a') by comparison with spectra of dimethylsilyl halides¹⁴⁹ in which the methyl rock is strong in the Raman but weaker in the infra-red. The second methyl rocking mode (a'') is then assigned to the weaker band at 706 cm^{-1} , and the Si-H bend, normally weaker than the methyl rock, is assigned to the band at 640 cm^{-1} in the Raman solid, and 625 cm^{-1} in the gas phase. This leaves one remaining band at 610 cm^{-1} in the gas phase infra-red, which splits to give two equal intensity bands in the solid phase. The separation of these bands (9 cm^{-1}) is reasonable for the assignment as the two modes of the NCO bend ($a' + a''$), to be made. In the Raman spectrum the NCO bend is characteristically weak, and only observed in the solid phase. The polarisation data for the bands in the 600-700 cm^{-1} region are consistent with the assignments made.

Finally, the relatively strong band at 544 cm^{-1} would

be expected to be the Si-N stretching vibration and the polarisation data support this assignment. The shoulder at 551 cm^{-1} could be the overtone of the band at 274 cm^{-1} and has enhanced intensity by Fermi resonance with the Si-N stretching fundamental. The interaction will also cause a shift to higher frequency away from the Si-N band. Also the band at 510 cm^{-1} could be an overtone of the band at 256 cm^{-1} .

Below 300 cm^{-1} three bands are observed in the solid and liquid Raman spectra. One would expect three bands at silicon in this region, plus the methyl group torsion (a'') which is usually very weak. These deformations are the CSiC scissors: bend(a') and two CSiN bends ($a' + a''$); the two a' components would probably mix and be well separated so the middle band is likely to be the a'' mode. Hence the assignment is SiC₂ bend at 277 cm^{-1} , the a'' CSiN bend at 255 cm^{-1} and a' CSiN bend at 222 cm^{-1} . No bands were observed that could give any indication of the frequency of the SiNC bending fundamental, although since no band was found above 150 cm^{-1} , the fundamental must be less than 75 cm^{-1} . In $(\text{CH}_3)_3\text{SiNCO}^{100}$ this is observed at 37 cm^{-1} with an overtone at 84 cm^{-1} , and for $\text{SiH}_3\text{NCO}^{98}$ the fundamental is assigned to a band at 64 cm^{-1} which is only found in the gas phase spectrum.

8.5 Vibrational Spectra of monomethylsilyl isothiocyanate

The molecule has the same shape and atomic arrangement as $\text{CH}_3\text{SiH}_2\text{NCO}$ and hence will have the same number of fundamentals. The spectra obtained are shown in Figures 8.14 to 8.17 and the band positions and assignments are given in Table 8.4.

The C-H stretching modes assigned to bands at 2988 and 2928 cm^{-1} are particularly weak in the infra-red spectra partly because the pressure achievable in the gas cell is low because of the compound's low vapour pressure. Also weak C-H bands seem to be inherent in isothiocyanate derivatives as $(\text{CH}_3)_3\text{SiNCS}^{100}$ and $(\text{CH}_3)_2\text{Si}(\text{NCS})_2^{148}$ are reported to have weak bands. The band at 2583 cm^{-1} is characteristic of silyl isothiocyanates and assigned as a combination band of the Si-N stretch and the NCS asymmetric stretch.

In the solid and liquid phase Raman spectra, the Si-H stretching band at 2200 cm^{-1} is broad and very strong, while in the solid phase infra-red, the band is sharp and weaker, splitting by 12 cm^{-1} on annealing. This split must be the symmetric and asymmetric Si-H stretching bands ($a' + a''$). A single broad band at 2080 cm^{-1} in the solid and liquid phase is assigned to what is commonly termed the asymmetric NCS stretch, although it is mainly the N=C vibration. In the gas phase this band appears as a doublet at 2090 and 2036 cm^{-1} . This band shape must be because of the overlap of the NCS asymmetric stretch fundamental and the

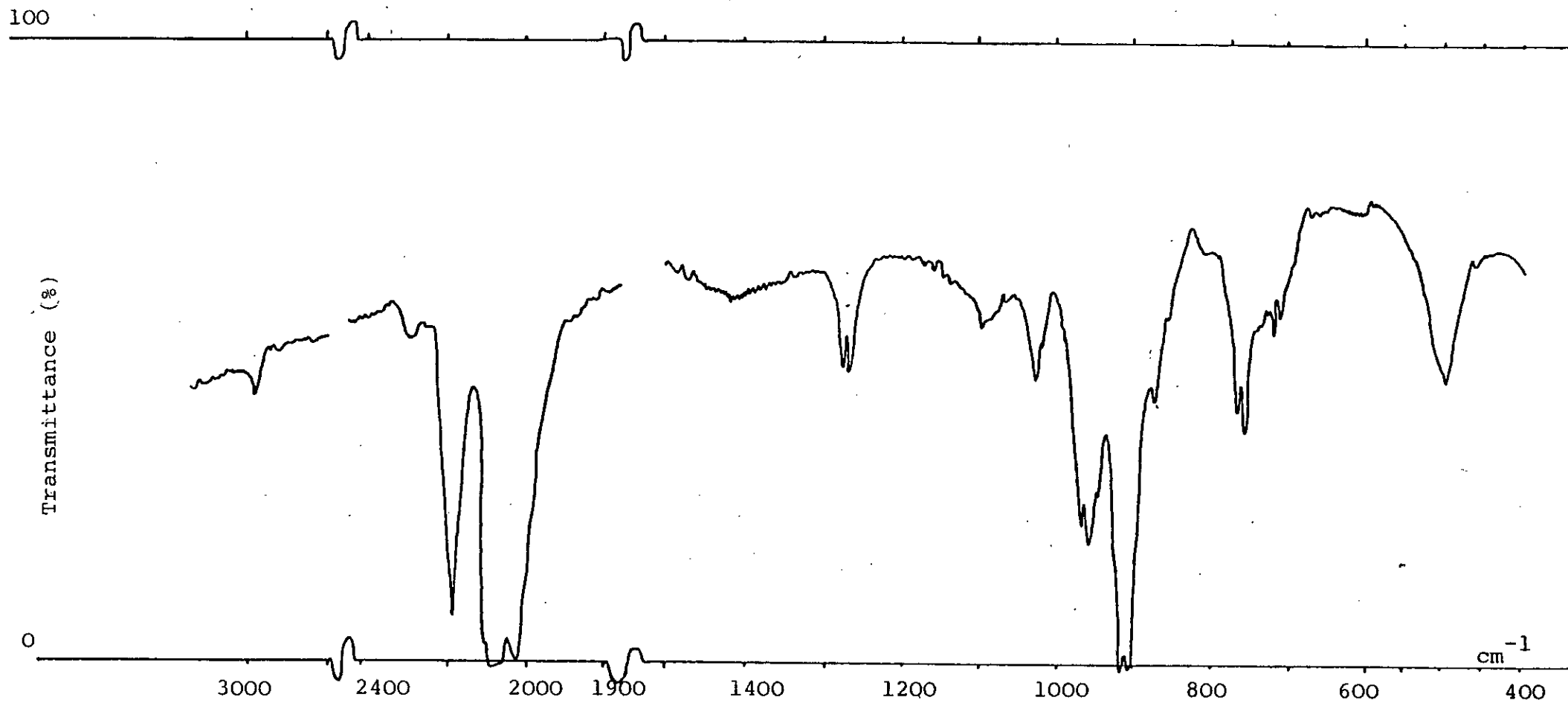


Figure 8.14: Infra-red spectrum of $\text{CH}_3\text{SiH}_2\text{NCS}$ in the gas phase (15 mmHg pressure)

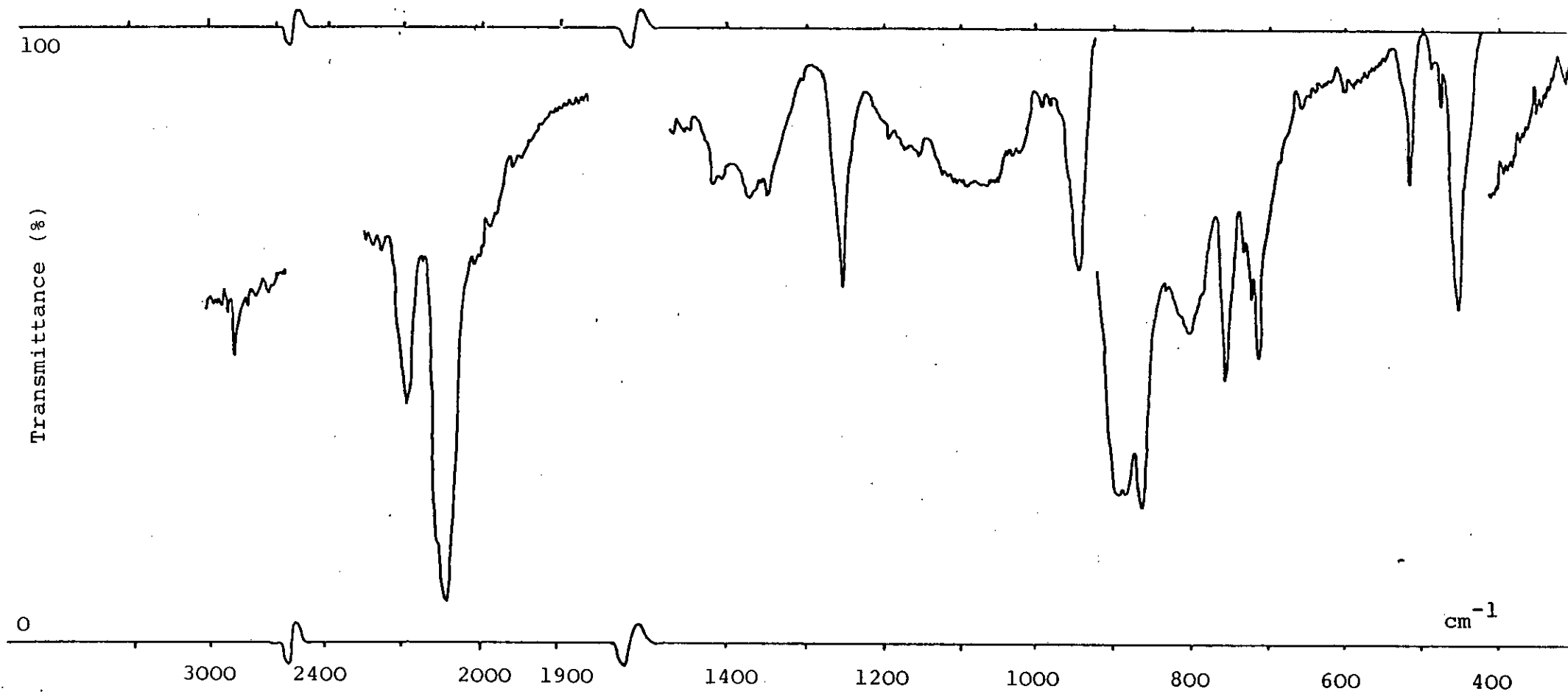


Figure 8.15: Infra-red spectrum of $\text{CH}_3\text{SiH}_2\text{NCS}$ in the solid phase

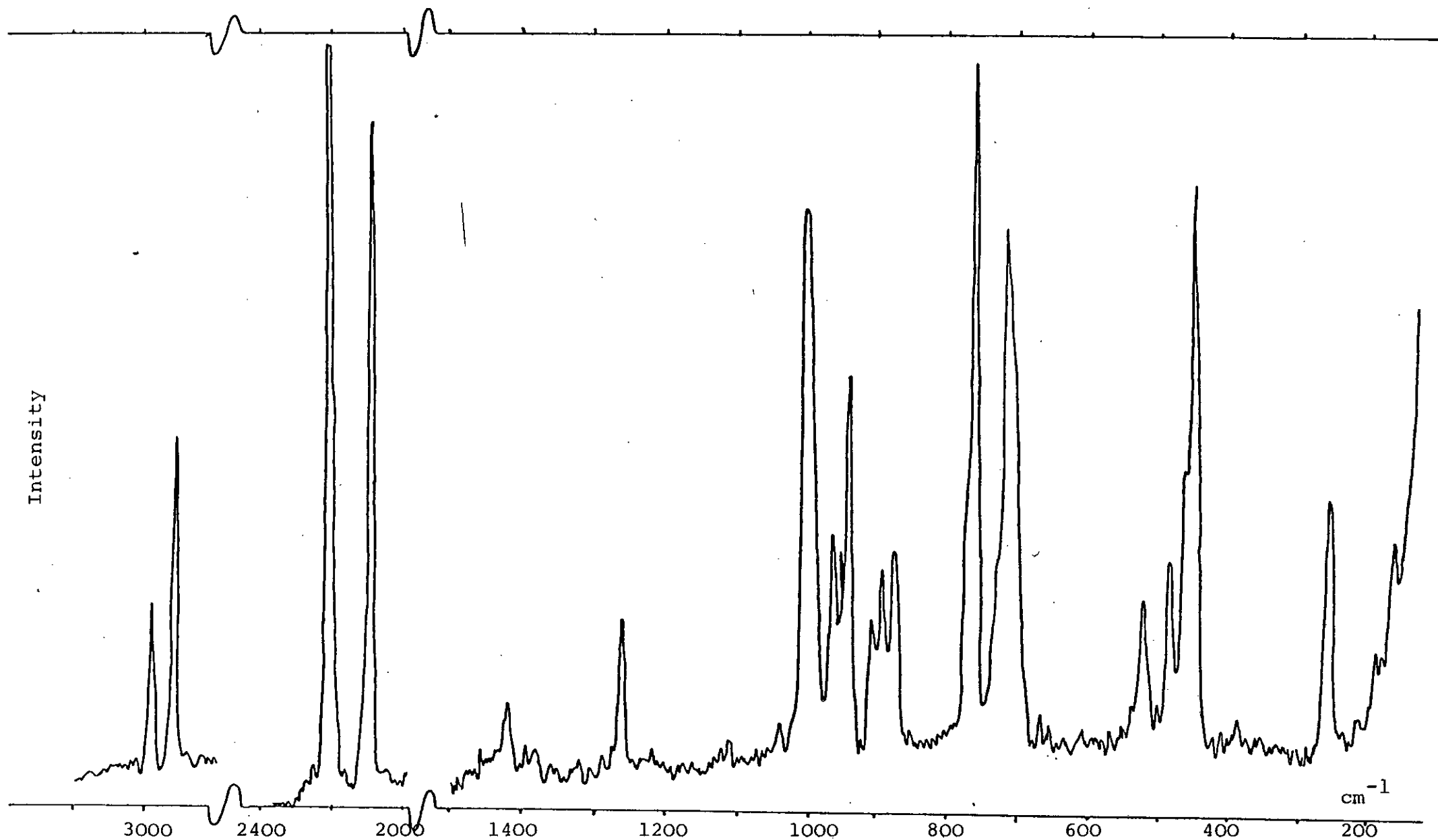


Figure 8.16: Raman spectrum of $\text{CH}_3\text{SiH}_2\text{NCS}$ in the solid phase

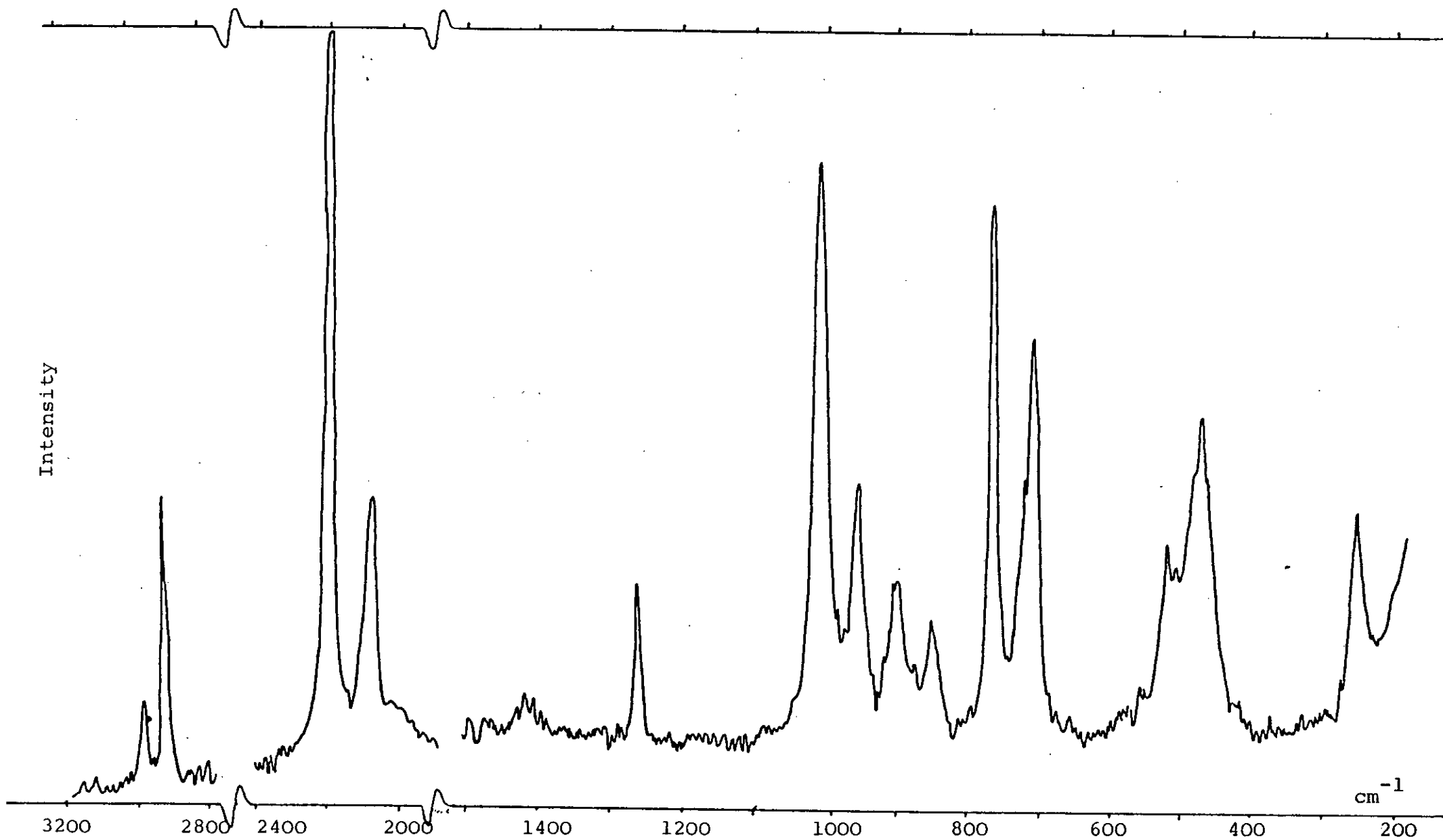


Figure 8.17: Raman spectrum of $\text{CH}_3\text{SiH}_2\text{NCS}$ in the liquid Raman

Table 8.4: Observed frequencies (cm^{-1}) and assignments for spectra of monomethylsilyl isothiocyanate

<u>Raman</u>		<u>Infra-red</u>		<u>Assignment</u>
<u>Liquid</u>	<u>Solid</u>	<u>Solid</u>	<u>Gas</u>	
2980 w,dp	2970 m	2967 vw	2988 w	a" C-H stretch(asym)
2910 m,p	2910 s		2928 w	a' C-H stretch(sym)
		2530 w	2583 w	$\nu(\text{Si-N}) + \nu(\text{NCS})$ asym=2543
			2299 w	
		2204 w		
2200 vvs,p	2200 vvs	2192 s	2194 s	a'a" Si-H stretch
2080 m	2080 vs	2093 vs	2090vvs	a' NCS stretch (asym)
		1990 w	2036vvs	$2\nu(\text{NCS})$ asym
1415 w	1405 w	1410 w		a'a" CH ₃ def asym
		1370 w		+ sym
		1344 w		
1260 m,p	1251 m	1254 m	1271 m	a' CH ₃ def (sym)
1010 vs,p	998 vs		1030 m	a' NCS stretch (sym)
955 m,dp	958 m	959 m	960 s	a' SiH ₂ bend
	945 w	948 s		
	933 s			
895 m,dp	901 w	895 vs	910 vs	a" SiH ₂ wag
	884 m			
850 w,p	868 m	865 vs	875 m	a' CH ₃ rock
765 vs,p	753 vs	759 s	763 m	a' Si-C stretch
		735 m		a" CH ₃ rock
		725 w		
710 s,dp	711 s	714 m	721 m	a" SiH ₂ twist
518 m,dp	514 m	519 m		a' SiH ₂ rock
(505 m)				
	476 m	477 w		(a' or a" NCS bend
	456 m,sh		499m,br	(a' Si-N stretch
470 s,p	441 s	453 s		
250 m,dp	251 m			a' CSiN bend
	156 vw			2 x SiNC bend

Abbreviations:

s strong, v very, m medium, w weak, br broad, p polarised, dp depolarised, asym asymmetric, sym symmetric, sh shoulder.

overtone of the NCS symmetric stretch. The enhanced intensity of the overtone must be due to Fermi resonance, which also causes a separation of the bands. The interaction giving enhanced intensity is greatest when the fundamental and overtone are close in frequency. Hence in the solid phase, when the NCS symmetric stretch decreases by 32 cm^{-1} to 998 cm^{-1} the separation between the overtone and asymmetric stretch will be increased and the Fermi-resonance effect decreases, giving rise to a single band at 2093 cm^{-1} , and a weak (unenhanced) band at 1990 cm^{-1} .

The symmetrical (a') and asymmetric (a'') methyl deformations are assigned to the bands at 1254 and 1410 cm^{-1} respectively, and this is supported by the polarisation data.

In the gas phase the "symmetric" stretch which is mainly a C=S stretch of the NCS group is assigned to the band at 1030 cm^{-1} , which is of medium intensity in the infra-red but very strong in the liquid Raman spectra, while in the solid phase no band is observed in the infra-red but in the Raman the band is strong and shifts to 998 cm^{-1} . These positions and relative intensities agree well with the data published for SiH_3NCS ¹¹⁵ and for $(\text{CH}_3)_3\text{SiNCS}$ ¹⁰⁰, but the infra-red data for $(\text{CH}_3)_3\text{SiNCS}$ from reference 148 do not agree with those from reference 100, in that the NCS asymmetric stretch is listed as very weak and the symmetric stretch as very strong, which is opposite to reference 100 and the observed spectra of $\text{CH}_3\text{SiH}_2\text{NCS}$.

The bands between $800\text{--}1000\text{ cm}^{-1}$ are easily assigned to the SiH_2 bend (a') at 960 cm^{-1} , the SiH_2 wag (a'') at 910 cm^{-1} and a methyl rock (a'') at 875 cm^{-1} , although the 960 cm^{-1} band is not strongly polarised. The Si-C stretching vibration (a') is assigned to the strong polarised band at 760 cm^{-1} and the SiH_2 twist to the broader depolarised band at 721 cm^{-1} in the gas phase and 710 cm^{-1} in the solid phase; the shift in frequency with phase is as found for $\text{CH}_3\text{SiH}_2\text{CN}$ and $\text{CH}_3\text{SiH}_2\text{NCO}$. A second methyl rocking motion is assigned to the medium intensity band at 735 cm^{-1} only observed in the solid phase Raman spectrum.

Below 700 cm^{-1} bands for the SiH_2 rock, the Si-N stretch, and possibly two NCS bending motions are expected. The gas phase spectrum has one single broad band centred at 499 cm^{-1} which splits to three bands in the solid and liquid phases. The assignment is complicated by the disagreement that exists over the position of the Si-N stretch and NCS bend in SiH_3NCS and $(\text{CH}_3)_3\text{SiNCS}$. Durig et al.¹⁰⁰ assigned Si-N in $(\text{CH}_3)_3\text{SiNCS}$ to 481 cm^{-1} and NCS bend to 430 cm^{-1} , while more recent work¹⁴⁸ has reversed the assignments with the stronger infra-red band at 438 cm^{-1} assigned to Si-N, and 483 cm^{-1} assigned to the bend. There is similar disagreement over SiH_3NCS , with one assignment¹¹⁵ of a weak band at 425 cm^{-1} (gas) to the NCS bend and the medium intensity band at 502 cm^{-1} to the Si-N stretch, and another group¹²² after comparison with matrix isolated labelled samples, disagreed and reversed the assignment.

The assignments made for $\text{CH}_3\text{SiH}_2\text{NCS}$ in the light of the frequencies in SiH_3NCS and $(\text{CH}_3)_3\text{SiNCS}$ are (in the solid phase) the SiH_2 rock to 514 cm^{-1} , NCS bend to 476 cm^{-1} and Si-N stretch to 441 cm^{-1} . The Si-N stretch is in most cases stronger than the NCS bend in infra-red and Raman, and usually shows a significant shift from gas to liquid to solid phase. Also the Si-N stretch should be polarised. The strongest band in this region is at 499 cm^{-1} in the gas, 470 cm^{-1} in liquid, and $441\text{--}453\text{ cm}^{-1}$ in the solid, and is polarised. Hence the assignment seems reasonable. The NCS bend is then assigned to the weaker band at 476 cm^{-1} and the remaining band at 514 cm^{-1} assigned to the SiH_2 rock. It is possible that the shoulder at 456 cm^{-1} only found in the solid phase Raman spectrum could be the second NCS bending mode.

Finally, a likely assignment of the 250 cm^{-1} band found only in the Raman spectrum, is to the CSiN bend (a') and the lowest frequency band at 156 cm^{-1} could be an overtone of the low frequency bend of SiNC giving an estimate of the fundamental of 78 cm^{-1} . This would compare well with Durig's observation for SiH_3NCS ¹¹⁵ of a weak band at 157 cm^{-1} in the Raman and the fundamental at 67 cm^{-1} .

8.6 Vibrational Spectra of dimethylsilyl isothiocyanate

This molecule should have the same point group and number of modes of vibration as dimethylsilyl isocyanate.

The infra-red and Raman spectra are shown in Figures 8.18 to 8.21. The gas phase spectrum is relatively weak because the compound has a very low vapour pressure, and it was impossible to introduce more material into the gas cell. To achieve more intense bands it would be necessary to run the spectrum with a longer path gas cell. The complete vibrational assignment is presented in Table 8.5.

Only one C-H band is observed that could be assigned to the asymmetric stretches ($2a' + 2a''$) at 2980 cm^{-1} and the symmetric stretches ($a' + a''$) are assigned to the band at 2920 cm^{-1} . The medium intensity band at the next highest frequency (2170 cm^{-1}) is easily assigned to the Si-H stretch (a'), and the broad band at 2060 cm^{-1} is assigned to the asymmetric NCS stretch. It is surprising that the same band in $(\text{CH}_3)_3\text{SiNCS}$ is reported in reference 148 to be very weak but in reference 100 to be very strong. The Si-H stretch is clearly polarised as expected, but the data for the NCS stretch are not clear. The additional band just below 2000 cm^{-1} is best assigned to the overtone of the NCS symmetric stretch.

The asymmetric methyl deformations are assigned to the infra-red bands at 1434, 1409, 1399 and 1372 cm^{-1} , and the symmetric methyl deformations to the sharp band at 1254 cm^{-1} , which showed no sign of splitting to its $a' + a''$ components. A characteristic shift of 10 cm^{-1} is found for this deformation vibration from the gas to solid phase

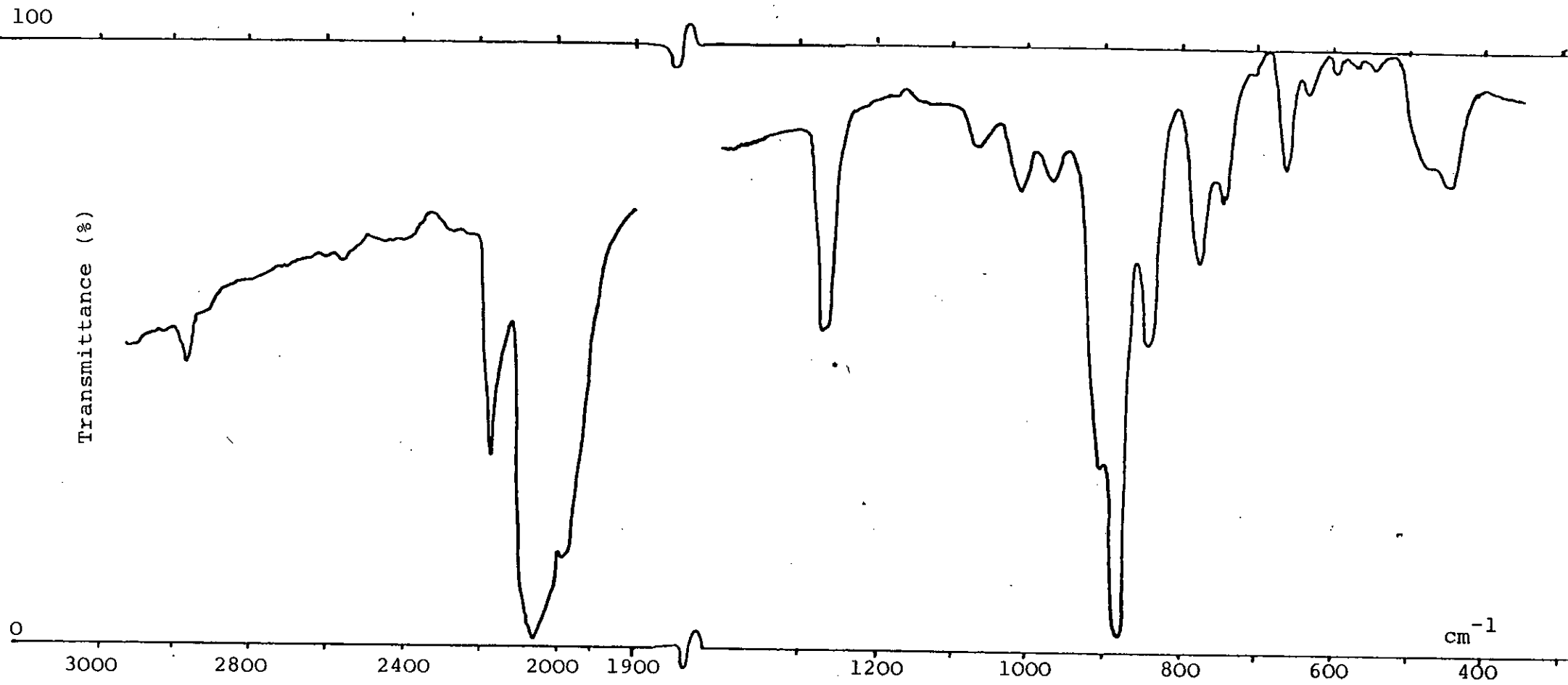


Figure 8.18: Infra-red spectrum of $(\text{CH}_3)_2\text{SiHNCS}$ in the gas phase (10 mmHg pressure)

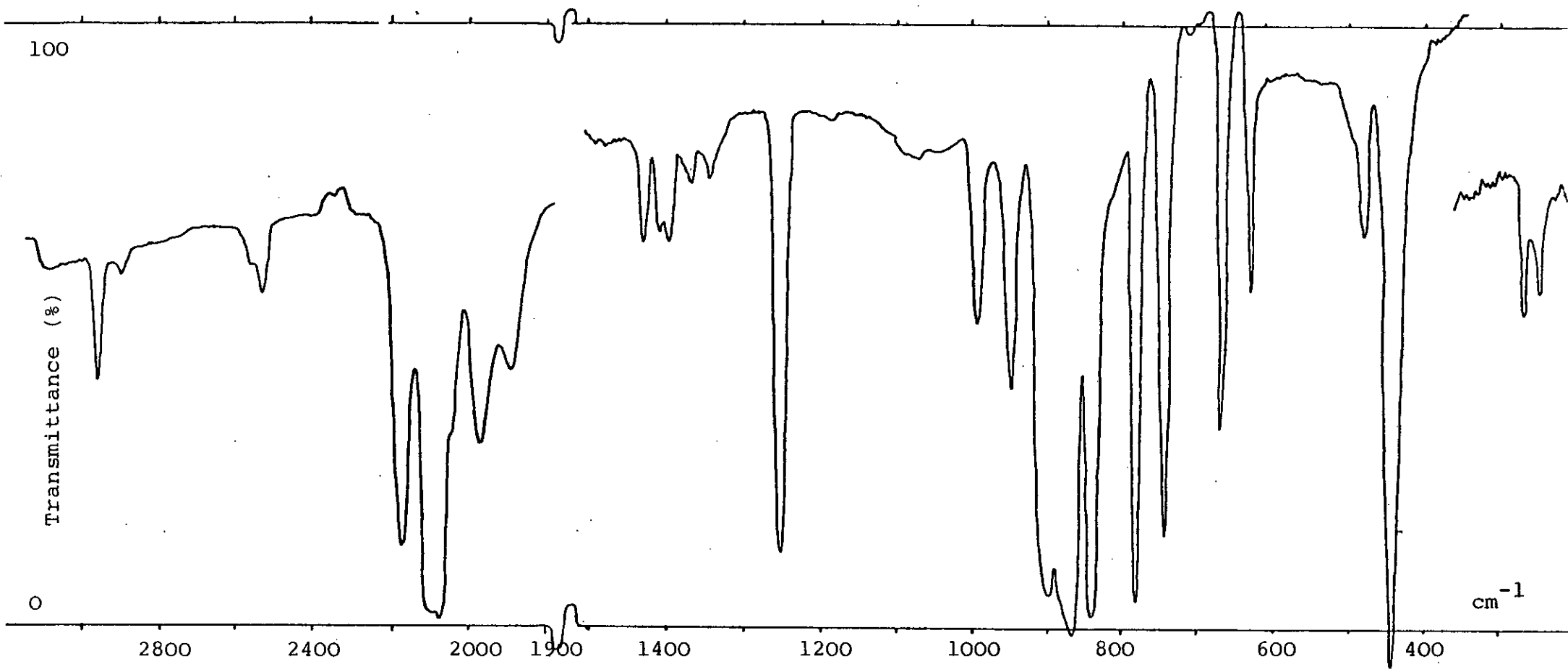


Figure 8.19: Infra-red spectrum of $(\text{CH}_3)_2\text{SiHNCS}$ in the solid phase

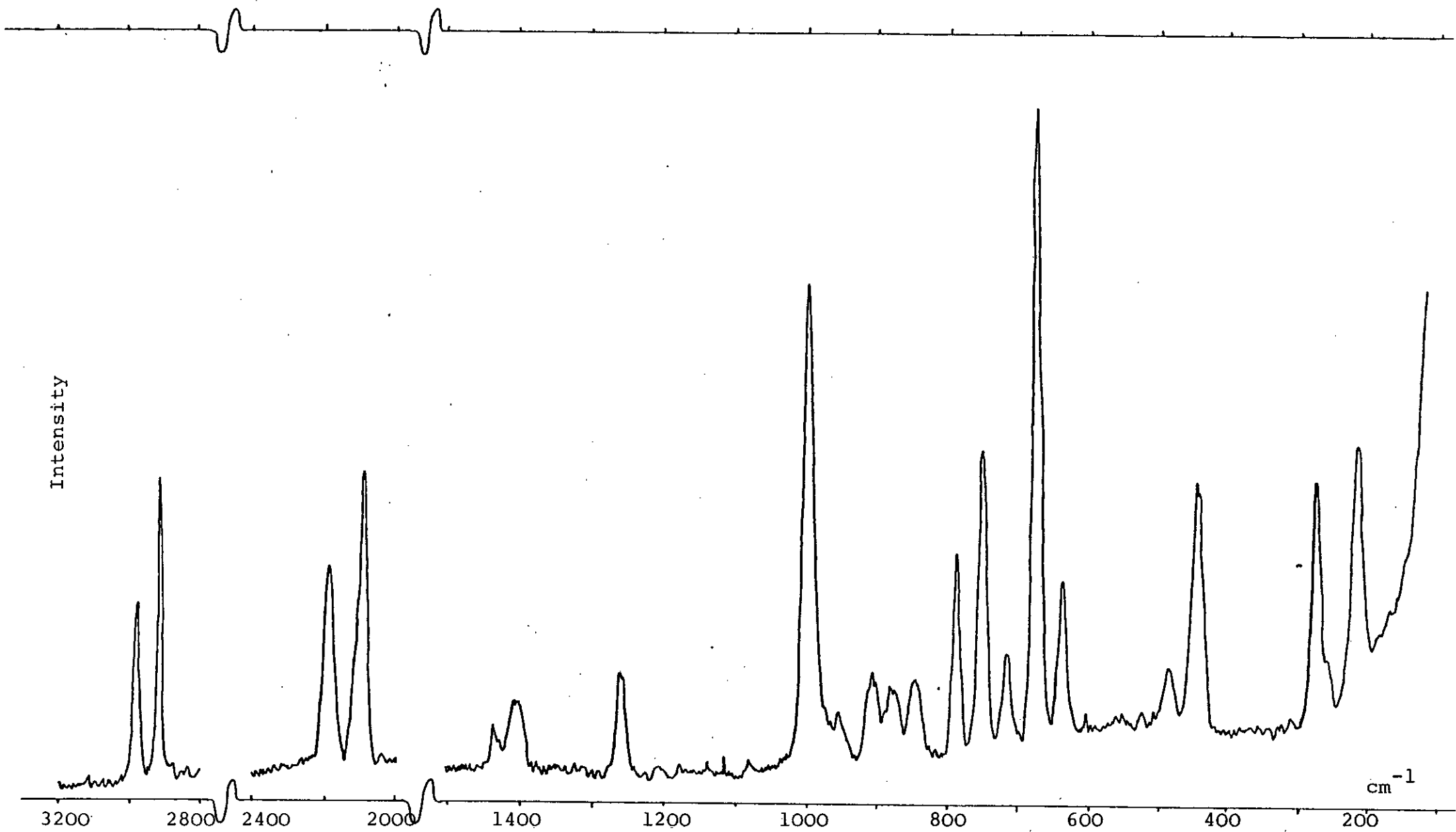


Figure 8.20: Raman spectrum of $(\text{CH}_3)_2\text{SiHNCS}$ in the solid phase

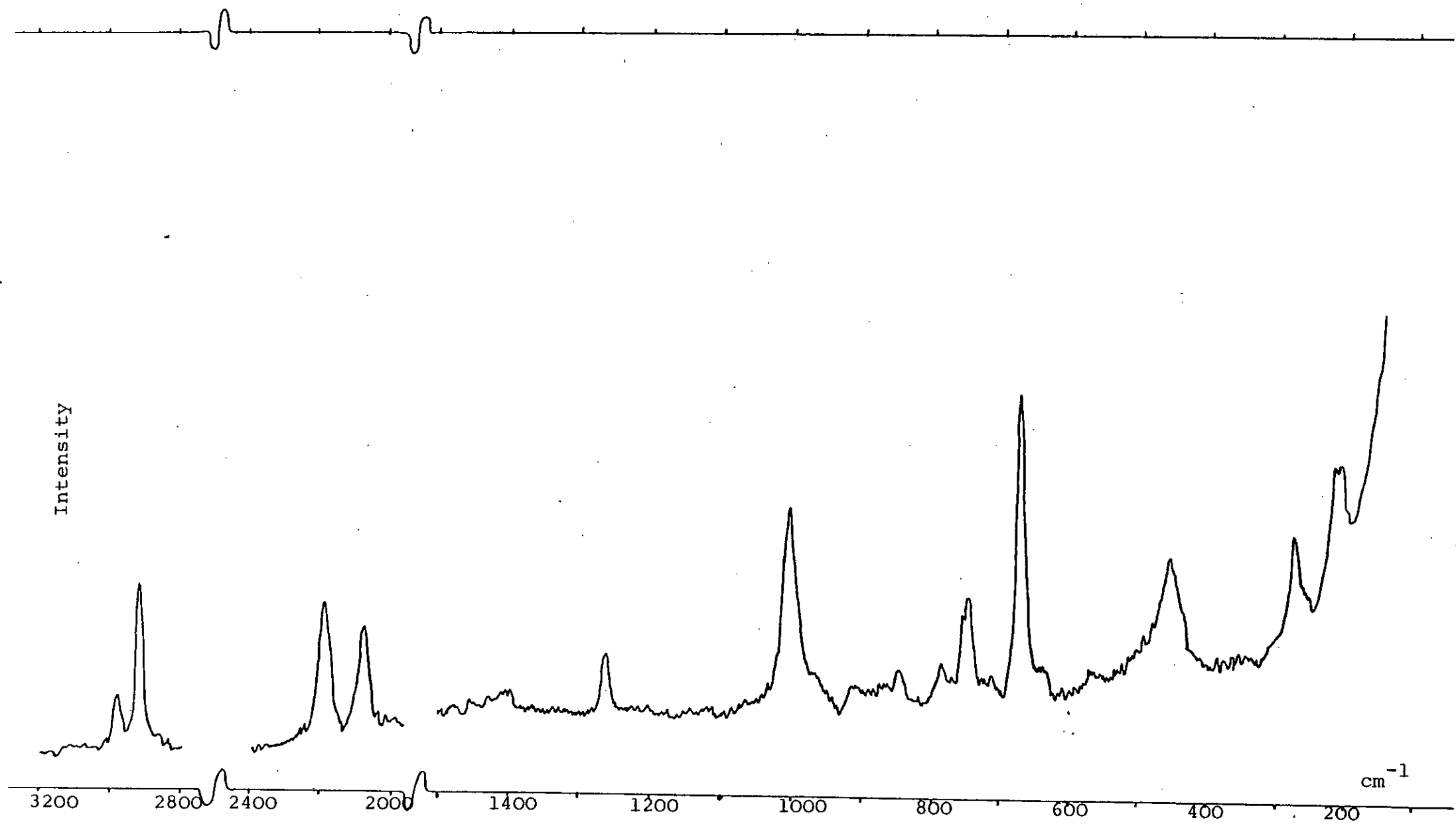


Figure 8.21: Raman spectrum of $(\text{CH}_3)_2\text{SiHNCS}$ in the liquid phase

Table 8.5: Observed frequencies (cm^{-1}) and assignments for dimethylsilyl isothiocyanate

<u>Raman</u>		<u>Infra-red</u>		<u>Assignment</u>
<u>Liquid</u>	<u>Solid</u>	<u>Solid</u>	<u>Gas</u>	
2980 w,dp	2980 m	2967 m	2980 w	a" C-H stretch (asym)
2920 s,p	2920 s	2906 vw 2530		a' C-H stretch (sym) Si-N + NCO Stretch(asym)
2185 m,p	2190 m	2180 s	2170 m	a' Si-H stretch
2080 m(p)	2090 s	2100 vs 1995 m 1949 m	2060 vvs 1995 s	a' NCS stretch (asym) 2 x NCS (sym)
	1432 w	1434 w	1430 vw	a"
1400 vw,dp	1400 w	1409 w 1399 w 1372 vw (1340 vw)		a' CH ₃ def (asym) a" a'
1265 w,p	1252 w	1254 s	1265	a',a" CH ₃ def (sym)
1000 s,p	994 s 952 w	996 m 951 m	1010 w 967 w	a' NCS stretch (sym) 2 x NCS bend
905 vw,dp	903 w	902 s	902 s	a" CH ₃ rock
875 vw,p	872 w	871 vs	880 vs	a' CH ₃ rock
845 w,dp	842 w	842 s	840 s	a' Si-H bend
785 w,dp	782 m	783 s	775 m	a" Si-C stretch (asym)
748 m,p	745 s	744 s	744 m	a' Si-C stretch (sym)
715 vw	710 m	711 vw	705 w	a" CH ₃ rock
670 vs,dp	670 vs	669 s	660 m	a' CH ₃ rock
640 w,dp	632 m 482 w	631 m 480 m	630 w 475 m	a" Si-H bend NCS bend
452 s,p,br	440	444 vs	445 m	Si-N stretch
275 m,dp	272 m	270 m 251 m		a' SiC ₂ scissors a" CSiN bend
212 m,dp	212 m			a' CSiN bend

which is believed to be a result of crystal packing and intermolecular interactions. The spectra show one band at 1010 cm^{-1} (996 cm^{-1} in solid) and one at 967 cm^{-1} (951 cm^{-1} in solid). Since the NCS stretch is usually weak in the infra-red and strong in the Raman, the higher frequency band is best assigned to the NCS fundamental, leaving the band at 967 cm^{-1} assigned as an overtone of the fundamental at 475 cm^{-1} . The two methyl rocks expected around 900 cm^{-1} are assigned to the bands at 902 cm^{-1} (a'') and 830 cm^{-1} (a'), and the less intense band at 840 cm^{-1} is assigned to the Si-H bend. Since it is polarised it must be the in-plane a' mode. The bands at 784 and 748 cm^{-1} are clearly assigned to the asymmetric and symmetric Si-C stretches in close agreement with $(\text{CH}_3)_2\text{SiHCN}^{72}$ and $(\text{CH}_3)_2\text{SiHNCO}$. The relative intensities of the two methyl rocking modes expected around 700 cm^{-1} are usually found to be very different, and this assignment attributes the strong polarised band at 670 cm^{-1} to the a' mode, and the weaker band at 710 cm^{-1} to the a'' mode. The third band in this cluster at 630 cm^{-1} and depolarised is the out of plane (a'') Si-H bend. The discussion over the reversal of Si-N stretch and NCS bend vibration frequencies in 8.5 also applies in this section. The position and intensities in the infra-red and Raman are the same as in $\text{CH}_3\text{SiH}_2\text{NCS}$, except in the gas phase the Si-N and NCS modes are distinguishable. Hence the assignment is of Si-N stretch to the band at 445 cm^{-1} and NCS bend to 475 cm^{-1} . Again the relative intensity of the Si-N stretch in the solid phase infra-red spectrum is greatly increased to become

the strongest band in the spectrum, and the enhanced intensity is attributed to strong Si...N and Si...O interactions in the solid phase. Future X-ray diffraction studies could confirm these predictions.

Below 300 cm^{-1} the assignments can only be tentative but the bands present are at similar frequencies to those found in the spectra of $(\text{CH}_3)_2\text{SiHNCO}$. Hence the assignments are 270 cm^{-1} to SiC_2 scissors (a'), 251 cm^{-1} to CSiN bend (a'') and 212 cm^{-1} to the second CSiN bend (a'). These assignments are made despite not agreeing with the polarisation data which are often unreliable for skeletal deformations.

There is no band at a low enough frequency to be the overtone of the SiNC bending mode.

8.7 Assignment of Infra-red and Raman Spectra

The assignments of the spectra and the justification of these assignments have been included in Sections 8.1 to 8.5 and in this section there is a discussion on the positions of the bands, noting certain trends that have been observed while some motions appear unchanged in the different compounds and in different phases. Included in the discussion are the data for $(\text{CH}_3)_2\text{SiHCN}$ taken from reference 64.

The C-H stretches are vibrations that do not show any significant change in the six methylsilyl compounds under

study. Similarly the methyl deformations between 1380-1420 cm^{-1} are constant. This is not surprising since these motions are almost entirely hydrogen movement and the silyl substituent will have little influence on the vibrational frequency. The only C-H vibration that does have a constant shift from solid to gas phase is the symmetric deformation of the methyl groups. Table 8.6 gives frequencies in the two phases of the three pseudohalides.

Table 8.6: Methyl symmetric deformation frequencies^a (cm^{-1})

	CN	NCO	NCS
CH_3SiH_2	1271-1258	1269-1250	1271-1251
$(\text{CH}_3)_2\text{SiH}$	1264-1263 1248	1269-1260 1254	1265-1252
$(\text{CH}_3)_3\text{Si}$		1262-1259	1262-1257

^agas phase position given first

As can be seen from the table, the shift varies from about 20 cm^{-1} to 15 cm^{-1} to 5 cm^{-1} for mono-, di- and trimethylsilyl derivatives respectively. The shift is attributed to the constraint of the molecule by intermolecular interactions which are likely to be most significant in the monomethyl derivatives and hence give the largest shift in vibrational frequency.

The frequencies of the SiH_2 bend (scissors) vibration show only a small shift for the isocyanate and isothiocyanate but is quite large for the cyanide (35 cm^{-1}). This may again be an artifact of the arrangement of the molecules in the unit cell of the crystal, and suggest that the SiH_2 is more influenced by adjacent molecules in $\text{CH}_3\text{SiH}_2\text{CN}$ than $\text{CH}_3\text{SiH}_2\text{NCO}$ or $\text{CH}_3\text{SiH}_2\text{NCS}$. Comparison with the crystal structures of SiH_3CN and SiH_3NCO indicates that the cyanide is linear chains of SiCN linked Si to N, while the SiNCO chains are arranged in a zig-zag pattern. And so assuming the crystal structure of the methyl derivatives is similar to the silyl compounds, the SiH_2 group will be constricted more by the linear chains of SiCN than SiNCO chains. There is however a change in frequency with phase of the SiH_2 wag (a'') in all three derivatives, suggesting that this motion is influenced by adjacent molecules in the crystal structure.

In contrast, the Si-H bends ($a' + a''$) in the dimethyl silyl derivatives are the same in all the pseudohalides and do not change with phase. Perhaps it is a little surprising that the Si-C stretching vibration is unaffected by phase, although since the bond is unlikely to be aligned with intermolecular interactions (unlike Si-N bond) the solid phase need not affect the Si-C vibration.

The bands assigned to the NCO and NCS bends were carefully studied to see if there was a splitting between the a' in plane, and a'' out of plane modes. A study of the

infra-red spectra of SiH_3NCO ⁹⁹ in different matrices showed two bands of 640 and 612 cm^{-1} , and in GeH_3NCO ¹⁴² bands at 642 and 611 cm^{-1} were observed. Since two bands were observed for these two isocyanates they were assumed to be bent in the solid phase, but for the methylsilyl compounds, group theory predicts two NCO bends because of the C_s symmetry, even if the SiNC angle is linear. However if the angle is large, the a' and a'' species may not be resolvable. For example the angle at nitrogen in $(\text{CH}_3)_3\text{CNCO}$ is known to be bent and the NCO bends are reported¹⁴⁸ at 621 and 592 cm^{-1} , while $(\text{CH}_3)_3\text{SiNCO}$ ⁹² which is thought to be linear at nitrogen has only one band at 624 cm^{-1} ¹⁰⁰. For the monomethyl and dimethyl silyl isocyanates, the only one to show any splitting of the NCO bend was $(\text{CH}_3)_2\text{SiHNCO}$, with bands at 600 and 609 cm^{-1} . The small splitting would tend to support the structural data that the angle at nitrogen is almost linear. No apparent trend in the change of the NCO or NCS bending frequency with addition of methyl groups to the silicon atom was found, although the symmetric silyl and trimethylsilyl derivatives of the isocyanates had bands at 620-622 cm^{-1} while the asymmetric monomethyl and dimethyl silyl isocyanates had bands at 606-610 cm^{-1} . Also there was no significant shift from gas to solid phase vibrational frequencies. The isothiocyanates however all have bending modes between 470-485 cm^{-1} , and no separation of the a' and a'' modes was observed, while $(\text{CH}_3)_3\text{CNCS}$ ¹⁴⁸, a bent molecule, does give two bands for the NCS bend at 522 and 492 cm^{-1} . The parent derivative, SiH_3NCS , has been studied in more

detail and the bands can all be assigned to be consistent with the molecule having C_{3v} symmetry in the solid and gas phase¹²², and from the spectra for mono- and dimethyl silyl isothiocyanates there is no evidence to suggest the SiNC angle is appreciably different.

The Si-N stretching frequency was found to be between 537-590 cm^{-1} for the isocyanates and slightly lower at 438-510 cm^{-1} for the isothiocyanates. This band was observed to shift with phase more than any other in the spectra. Table 8.7 gives a list of the fundamental's position in the gas and solid phase for the isocyanates and isothiocyanates

It is interesting to note that the shift in frequency is greatest for the monomethyl silyl derivatives, suggesting that these have the greatest intermolecular interactions which constrain the molecules in a crystal lattice. Also when the bond length and vibration frequencies of the Si-N are compared (see Table 8.7) as would be expected, the frequency decreases with a lengthening of the bond. This trend supports the reassignment of Si-N/NCS motions in $(\text{CH}_3)_3\text{SiNCS}$ for reference 100.

The largest shift for all the pseudohalides is for the Si-CN band in $\text{CH}_3\text{SiH}_2\text{CN}$. This shifts from 590 cm^{-1} in the gas phase to 522 cm^{-1} in the solid, and must be attributed to the SiCN chains aligning. There is also a great increase in intensity in the infra-red band, as is also found for the Si-N band on annealing. A similar shift

Table 8.7: Si-N frequencies in gas and solid phase (cm^{-1})

	<u>NCO</u>				<u>NCS</u>			
	<u>SiH₃</u>	<u>CH₃SiH₂</u>	<u>(CH₃)₂SiH</u>	<u>(CH₃)₃Si</u>	<u>SiH₃</u>	<u>CH₃SiH₂</u>	<u>(CH₃)₂SiH</u>	<u>(CH₃)₃Si</u>
Gas phase	590	571	563	537	[510] ^d	[499] ^d	452	442
Solid phase	571	540	540	516	487	453	445	430
Shift	19	31	23	21	23	46	7	12
Si-N bond length	170.3	171.8	172.1	176	170.4	171.0	172.1	178
Reference	a	a	a	b	122	a	a	b

^athis work

^busing the data from reference 100 but reassigning the bands for the NCS bend and Si-N stretch as discussed earlier

^cbond lengths in pm for the gas phase - references in Chapters 5 and 6.

^dthese frequencies are taken from the centre of the broad band that contains both the Si-N stretching and NCS bending vibration. Hence the true position of the vibration is not as accurately known as for dimethyl and trimethyl silyl isothiocyanates.

was found for $(\text{CH}_3)_2\text{SiHCN}$ ⁶⁴ from gas phase (562) to liquid phase (550) to solid phase (536 cm^{-1}).

From the spectra recorded, there is only tentative evidence for the position of the SiNC bending frequency, which is likely to be much lower in frequency than the CSiC deformation (in $(\text{CH}_3)_2\text{SiH}$ derivatives) and the CSiN bends, and further spectra in the region $0\text{-}200\text{ cm}^{-1}$ are really required.

Despite the large shift of the Si-N and Si-CN stretching bands in the solid phase, there is not a large shift for the NCO and NCS symmetric and asymmetric stretches or the $\text{C}\equiv\text{N}$ stretch. This suggests that intermolecular interactions do not have a significant effect on the vibration of multiple bonds, or that the NCO group is not involved in strong intermolecular interactions. In fact from the known crystal structure³³ there are Si...N and Si...O interactions which are about the same distance apart, suggesting that the multiple bond character of $\text{N}=\text{C}$ and $\text{C}=\text{O}$ has more effect on any shift of the vibrational frequency with phase than the intermolecular interactions.

8.8 Mass Spectra of methylsilyl pseudohalides

For the full characterisation of these compounds, the mass spectra were obtained for $\text{CH}_3\text{SiH}_2\text{CN}$, $\text{CH}_3\text{SiH}_2\text{NCO}$ and $(\text{CH}_3)_2\text{SiHNCO}$. It was found very difficult to obtain spectra of the isothiocyanates due to their involatility,

and all spectra suffered from the problems of the mass spectrometer never being thoroughly dry, resulting in hydrolysis products being prominent in the spectra. All the spectra were run using an ionising voltage of 70 eV.

Table 8.8: Mass spectrum of $\text{CH}_3\text{SiH}_2\text{NCO}$

m/e	Assigned species	Relative abundance
87	$[\text{CH}_3\text{SiH}_2\text{NCO}]^+$	12
86	$[\text{CH}_2\text{SiH}_2\text{NCO}]^+$	100
85	$[\text{CHSiH}_2\text{NCO}]^+$	22
72	$[\text{SiH}_2\text{NCO}]^+$	59
71	$[\text{SiHNC}]^+$ or $[\text{CH}_3\text{SiH}_2\text{NC}]^+$	10
70	$[\text{SiNCO}]^+$ or $[\text{CH}_2\text{SiH}_2\text{NC}]^+$	38
59	$[\text{CH}_3\text{SiH}_2\text{N}]^+$	6
45	$[\text{CH}_3\text{SiH}_2]^+$	6
44	$[\text{CH}_3\text{SiH}]^+$	7
43	$[\text{CH}_3\text{Si}]^+$	42
42	$[\text{CH}_2\text{Si}]^+$ or $[\text{NCO}]^+$	9
29	$[\text{SiH}]^+$	7
28	$[\text{Si}]^+$ or $[\text{CO}]$	9

Table 8.9: Mass spectrum of $(\text{CH}_3)_2\text{SiHNCO}$

m/e	Assigned species	Relative abundance
101	$[(\text{CH}_3)_2\text{SiHNCO}]^+$	9
100	$[(\text{CH}_3)_2\text{SiNCO}]^+$	56
88	$[(\text{CH}_3)_2\text{SiHNCO}]^+$	4
87	$[(\text{CH}_3)\text{HSiHNCO}]^+$	7
86	$[(\text{CH}_3)\text{SiHNCO}]^+$	74
73	$[\text{SiH}_3\text{NCO}]^+$	3
72	$[\text{SiH}_2\text{NCO}]^+$	8
71	$[\text{SiHNCO}]^+$	3
70	$[\text{SiNCO}]^+$	21
44	$[\text{CH}_3\text{SiH}]^+$	5
43	$[\text{CH}_3\text{Si}]^+$	24
42	$[\text{NCO}]^+$	7
32	$[\text{SiN}]^+$	30
28	$[\text{CO}]^+$	100

Table 8.10: Mass spectrum of $\text{CH}_3\text{SiH}_2\text{CN}$

m/e	Assigned species	Relative abundance
46	$[\text{CH}_3\text{SiH}_3]^+$	6
45	$[\text{CH}_3\text{SiH}_2]^+$	12
44	$[\text{CH}_3\text{SiH}]^+$	4
28	$[\text{Si}]^+$	6
27	$[\text{HCN}]^+$	100
26	$[\text{CN}]^+$	15

These mass spectra confirm the atomic arrangements deduced from the vibrational spectra and the molecular structures by electron diffraction. Interestingly, the isocyanates contain more fragments of silicon bound to the pseudohalide group than the cyanides, suggesting that the Si-NCO bond is stronger than the Si-CN bond, and less susceptible to cleavage.

8.9 Nuclear Magnetic Resonance Studies of Methylsilyl Pseudohalides

The following data were all collected for the samples with isotopes in natural abundance. Therefore for the carbon and silicon spectra one is relying on the 4.7% abundance of ^{29}Si (spin = $\frac{1}{2}$) and the 1.1% abundance of ^{13}C (spin = $\frac{1}{2}$). Greatly improved spectra could obviously have been obtained if the naturally occurring isotopes had been replaced by the nuclei with spin = $\frac{1}{2}$, as these would have had better signal to noise ratios. Also, naturally occurring ^{14}N (spin = 1) has a line broadening effect on the spectra, which could be removed by inserting ^{15}N (spin = $\frac{1}{2}$). The majority of spectra were run on a Bruker WH360 which is a Fourier transform instrument.

Chemical shifts are often dependent on solvent, concentration and temperature so these have, as far as possible, been kept constant for all the compounds. All chemical shifts were measured with respect to external TMS $\text{Si}(\text{CH}_3)_4$.

8.10 Results and Discussion

Firstly the size of the couplings and chemical shifts confirm the atomic arrangements proposed from the vibrational information, and the positions are consistent with silyl pseudohalides (see Table 8.11). There is no evidence to suggest fast exchange of atoms or groups of atoms in any of the samples studied.

The ^1H spectrum of $\text{CH}_3\text{SiH}_2\text{CN}$ was studied in detail to see if the 2-bond coupling of the low abundance isotopes of spin $\frac{1}{2}$ to hydrogen could be observed. For example, in the SiH_2 region the coupling to ^{13}C (abundance 1.1%) or in the CH_3 region the coupling of protons to ^{29}Si (abundance 4.7%). Unfortunately in all these cases the satellite peaks will be observed under the main multiplet and were not distinguishable. Also the pattern for the species $^{13}\text{CH}_3\text{-}^{29}\text{SiH}_2\text{CN}$ (abundance 0.052%) was not observed.

The spectra gave no indication that either monomethyl or dimethylsilyl cyanide contained any of the isocyanide isomer.

Most of the parameters in Table 8.11 are in good agreement with those observed for the silyl pseudohalides¹⁴², with obvious differences for the cyanides which have the pseudohalide group bonded through carbon to silicon. In the molecules $(\text{CH}_3)_n\text{SiH}_{3-n}\text{NCY}$ ($\text{Y} = \text{O}, \text{S}$), the Y atom has little influence on δH_C , δH_Si but does effect δC_N which increases in magnitude. However the chemical shifts are greatly influenced by the electron donating effect of the methyl

Table 8.11: Summary of nmr parameters of methylsilyl pseudohalides

	δ_{H_C}	$\delta_{\text{H}_{\text{Si}}}$	$\delta^{13}\text{C}_\text{H}^a$	$\delta^{13}\text{C}_\text{N}^a$	$\delta^{29}\text{Si}^a$	$^1J_{\text{Si-H}}$	$^2J_{\text{Si-CH}}$	$^1J_{\text{CH}}$	$^2J_{\text{CSiH}}$	$^3J_{\text{HH}}$
MeSiH ₂ CN	0.20	3.84	-9.7	n.o.	-59.9	227.5	7.9	124.9	5.6	4.3
Me ₂ SiHCN	0.42	4.22	-5.4	n.o.	-34.4	219.6	7.7	123.2	7.4	4
MeSiH ₂ NCO	0.20	4.33	-4.2	123.8	-34.6	223.6	8.4	122.4	8.5	4
Me ₂ SiHNCO	0.30	4.60	-	-	-14.0	217.2	10.6	121.2	-	3.2
MeSiH ₂ NCS	0.18	4.29	-5.2	n.o.	-35.4	235.9	-	123.2	8.2	4
Me ₂ SiHNCS	0.38	4.64	-1.9	142.5	-13.9	223	-	121	9.8	3.2
SiH ₃ CN	-	3.95	-	258.9	-87.4	238	-	-	-	-
SiH ₃ NCO	-	4.40	-	123.8	-58.1	234.9	-	-	-	-
SiH ₃ NCS	-	4.48	-	143.6	-59.7	240.2	-	-	-	-

δ in ppm

J in Hz

n.o. not observed

Figure 8.22: ^1H Nmr spectrum of $\text{CH}_3\text{SiH}_2\text{CN}$

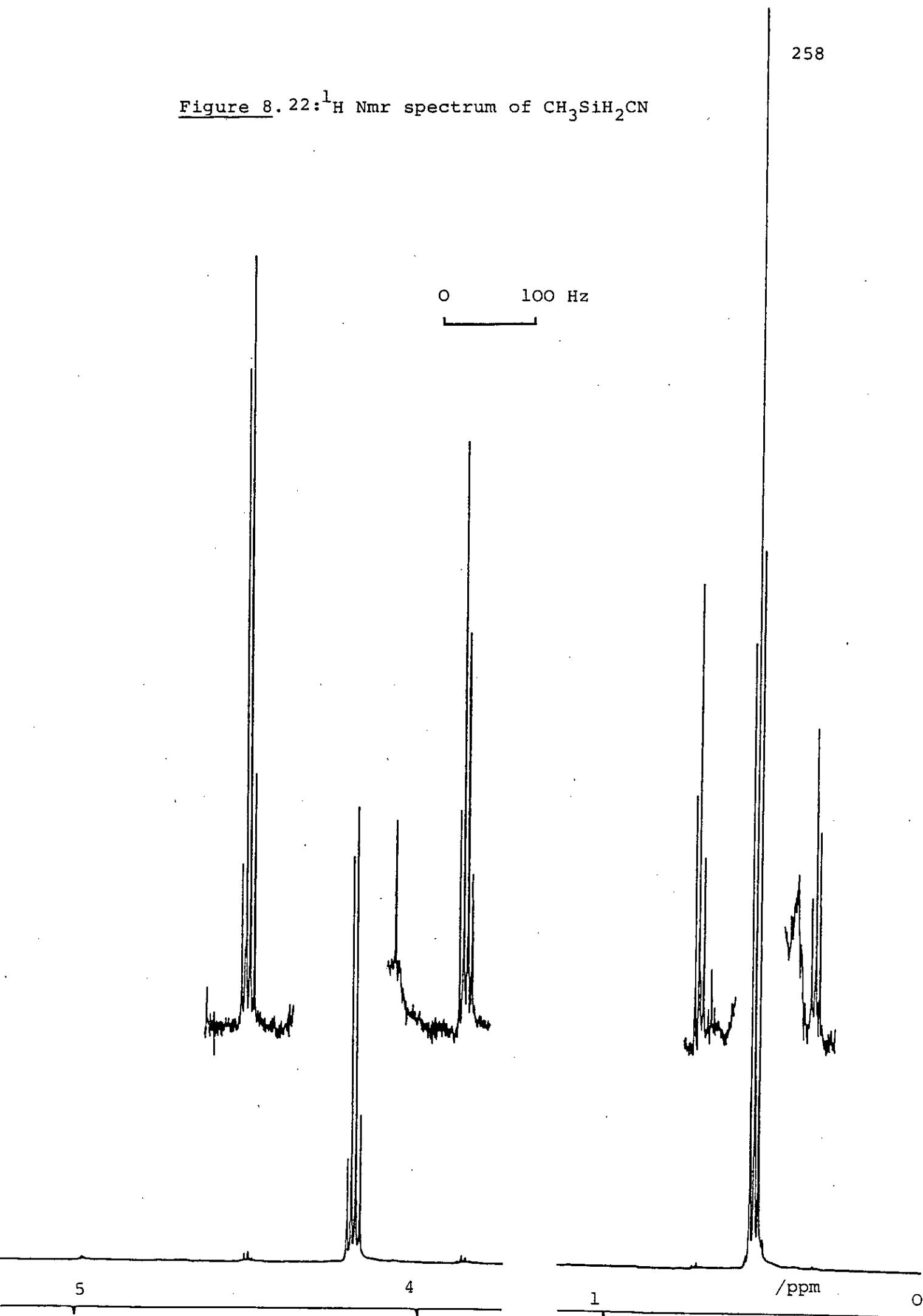


Figure 8.23: ^{13}C nmr spectrum of $\text{CH}_3\text{SiH}_2\text{CN}$ showing $-\text{CH}_3$ region

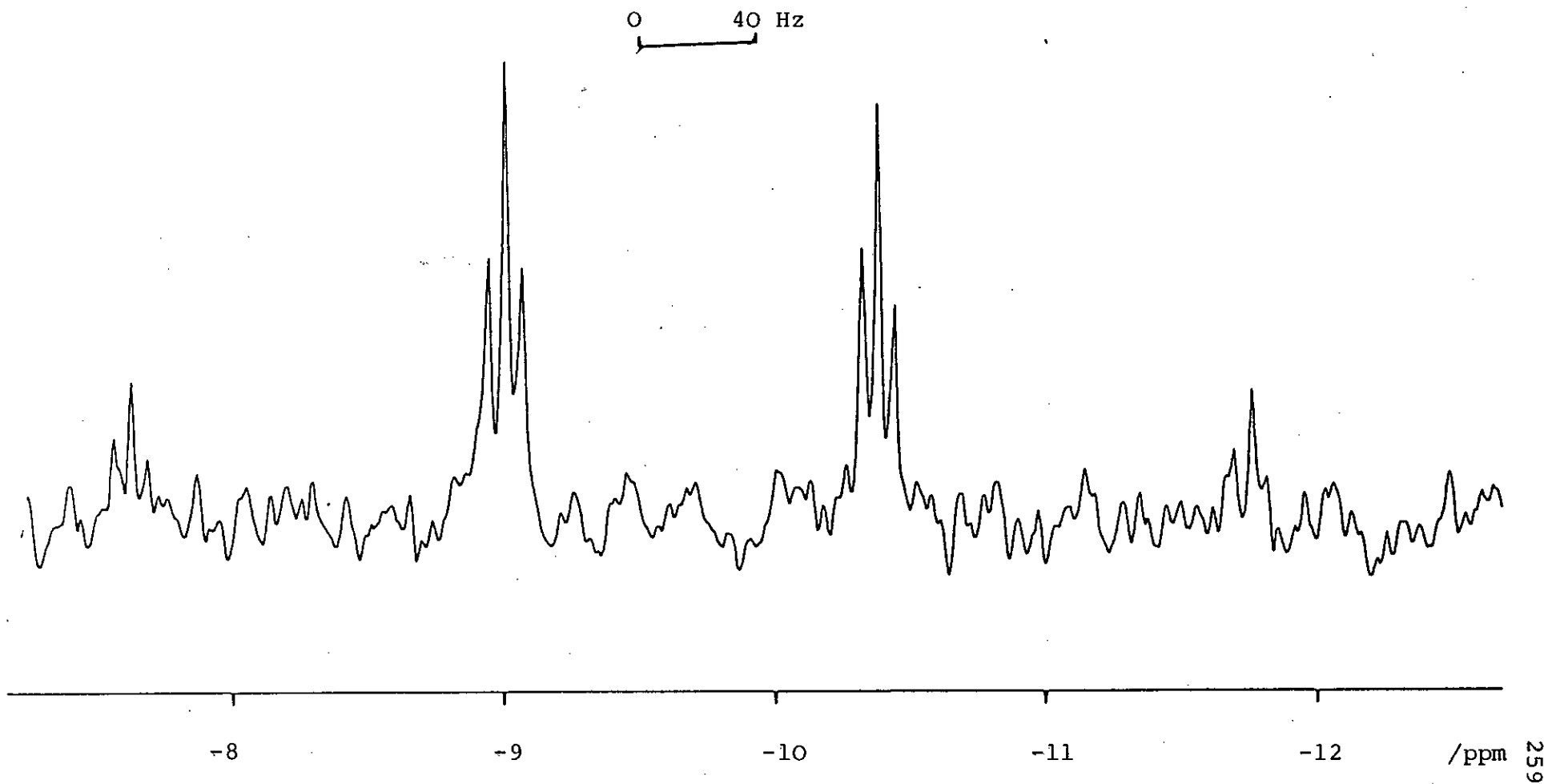
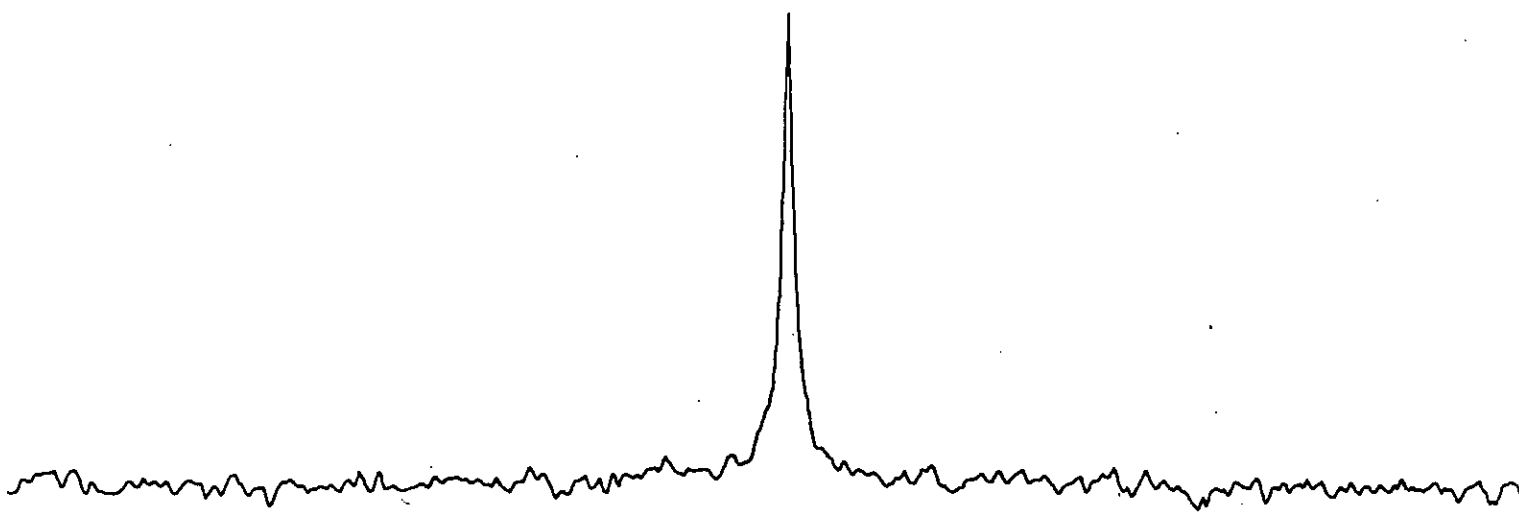


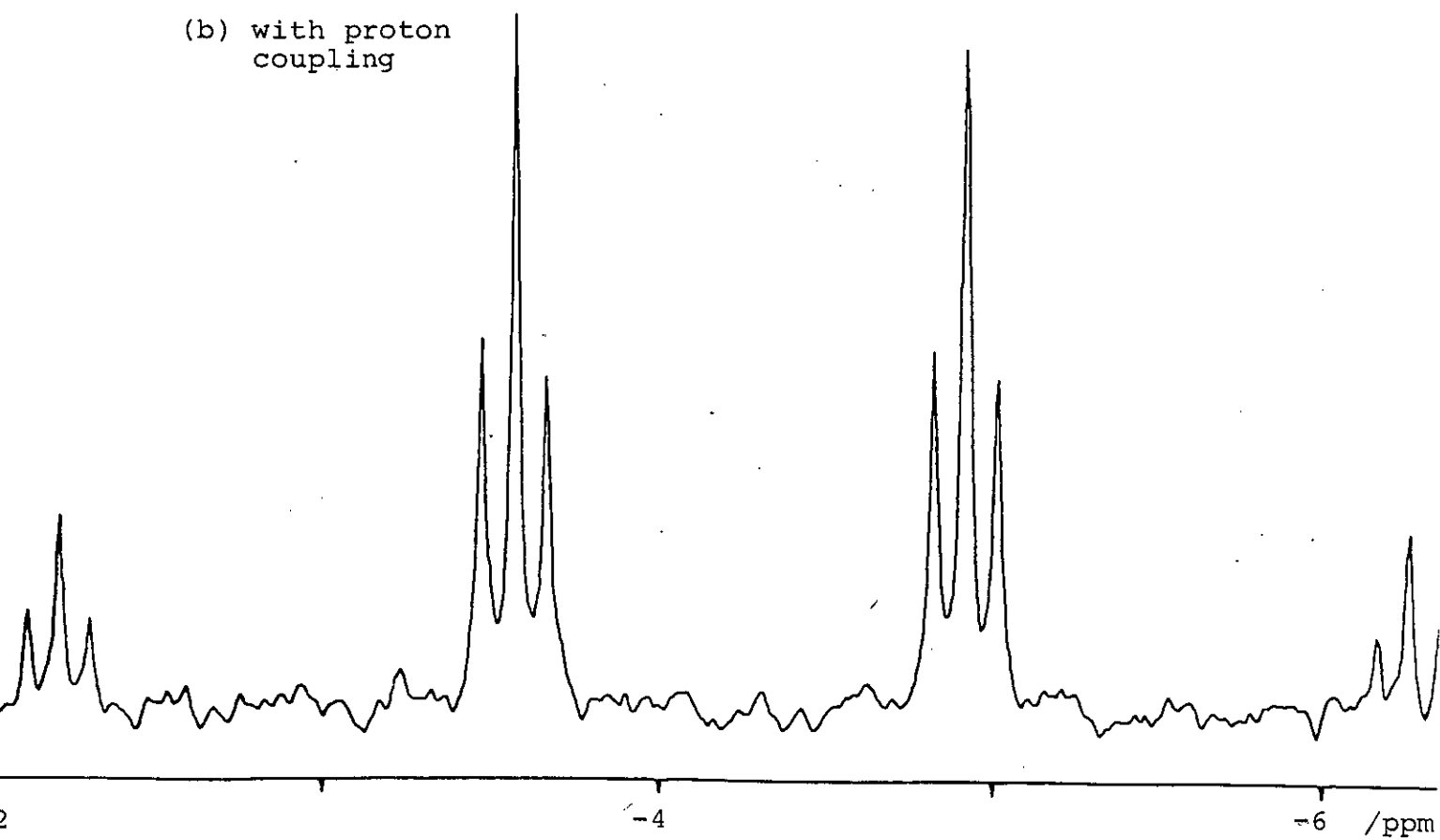
Figure 8.24: ^{13}C nmr spectrum of $\text{CH}_3\text{SiH}_2\text{NCO}$ showing $^{-13}\text{CH}_3$ region

(a) with proton decoupling



0 40 Hz

(b) with proton coupling



-6 /ppm

Figure 8.25: ^1H nmr spectrum of $(\text{CH}_3)_2\text{SiHCN}$

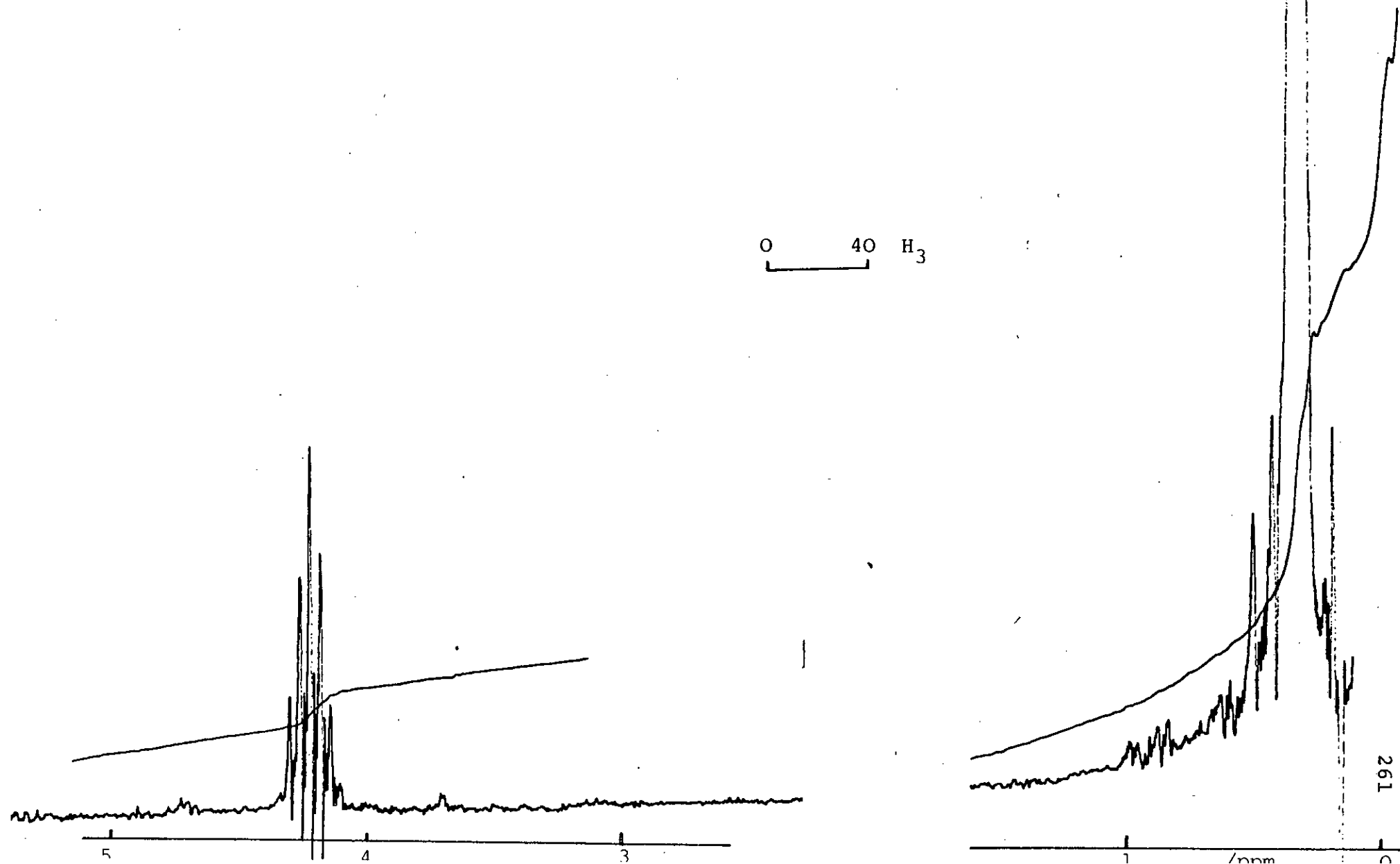


Figure 8.26: ^{13}C Nmr spectrum of $(\text{CH}_3)_2\text{SiHCN}$ showing $-\text{CH}_3$ region

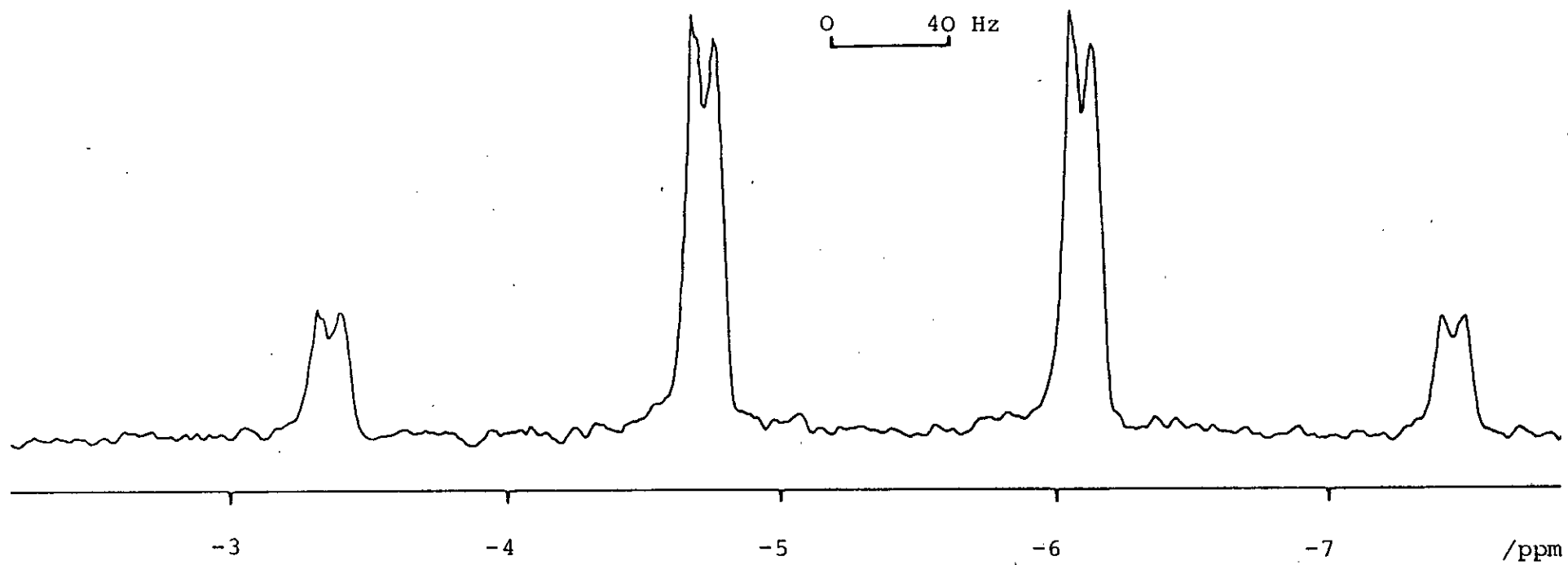
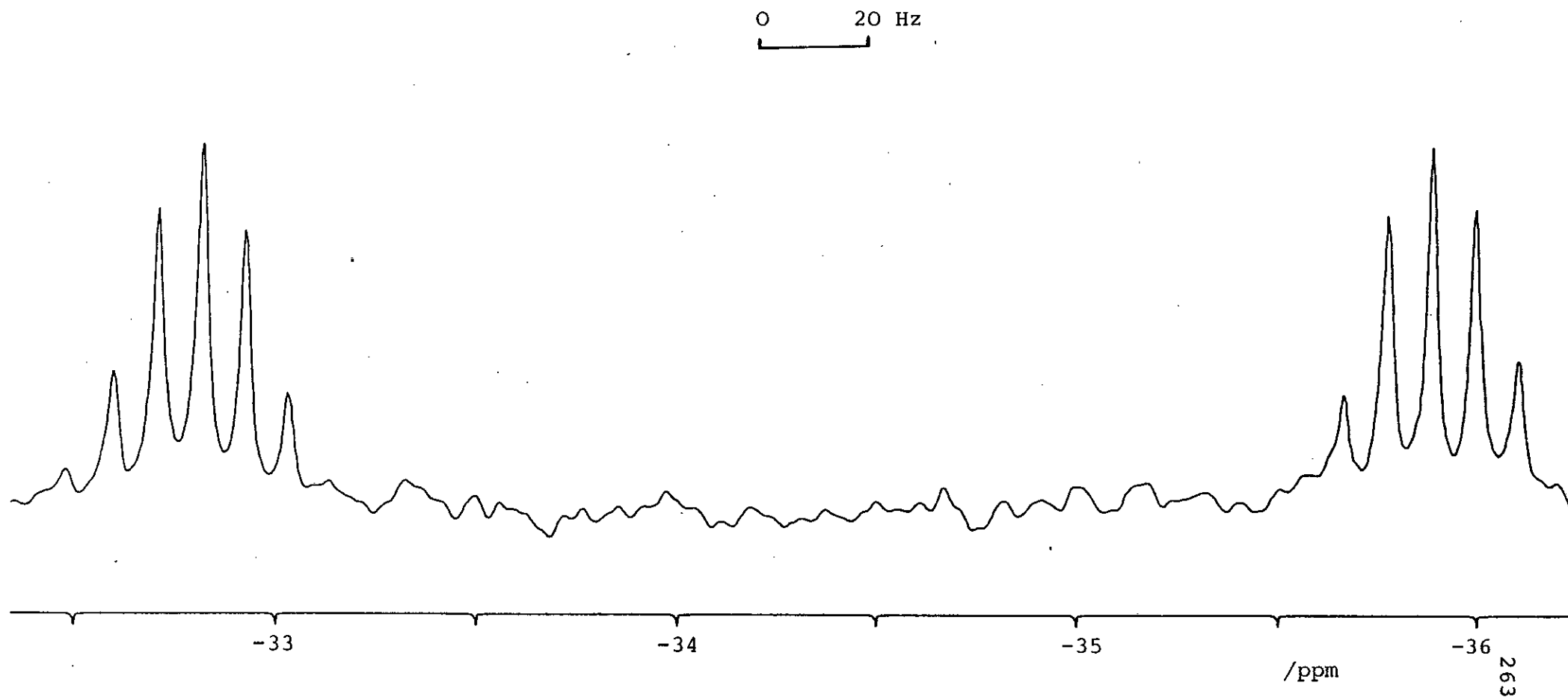


Figure 8.27: ^{29}Si Nmr spectrum of $(\text{CH}_3)_2\text{SiHCN}$



substituents on silicon, which cause an increase in magnitude, i.e. signal moves to higher field. It is also found that $^1J_{\text{SiH}}$ and $^3J_{\text{HH}}$ decrease in magnitude with substitution of methyl group but $^1J_{\text{CH}}$ stays almost constant.

Examples of the patterns obtained for the pseudohalides are given in Figures 8.22 - 8.27.

CHAPTER 9: FURTHER WORK

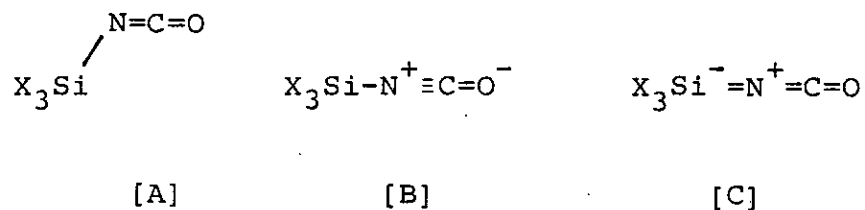
Following on from the work on the monothioacetates and monoselenoacetates, further attempts should be made to characterise $\text{CH}_3\text{C}(\text{OSe})\text{PF}_2$, which was found to be particularly unstable and hence difficult to purify. No reasonable infra-red spectra were obtainable due to the instability which may be catalysed by the decomposition products, but nmr work at low temperatures may be more feasible.

Also since it was found possible to synthesise both $\text{CH}_3\text{C}(\text{O})\text{SPF}_2$ and $\text{CH}_3\text{C}(\text{S})\text{OPF}_2$ isomers, according to the method of preparation, it would be interesting to attempt to grow crystals of the two isomers for an X-ray diffraction crystal structure determination, keeping the temperature below 240 K. A gas phase study of electron diffraction is not practicable since both isomers exist in appreciable quantities at room temperature.

The electron diffraction structural studies of $\text{CH}_3\text{COSGeH}_3$ and $\text{CH}_3\text{CSOSiH}_3$ were more straightforward because these only exist in one isomeric form. Now that a consistent pattern has begun to emerge for the bonding of Si-O and Ge-S and the angles COSi and CSGe , a further study of $\text{CH}_3\text{COOGeH}_3$ and $\text{CH}_3\text{CSSiH}_3$ would be interesting. Data for $\text{CH}_3\text{COOGeH}_3$ have now been collected and are now being refined (June 1983).

From the structures of monomethyl and dimethyl silyl isocyanates and isothiocyanates, the effect of the methyl groups appears to be a lengthening of the Si-N bond

attributable either to less (p-d) π bonding or the methyl groups are stabilising a valence bond structure with a single Si-N bond [B] and destabilising a structure with a double Si=N bond.



Further structural work on these pseudohalides should include a new determination of the structures of $(\text{CH}_3)_3\text{SiNCO}$ and $(\text{CH}_3)_3\text{SiNCS}$ which have only been studied⁹² some years ago and all the refined parameters have relatively large esds.

From the physical properties of the methylsilyl pseudohalides it appears that there are relatively strong intermolecular interactions present in the crystals. Hence a crystal structure should indicate the influence of the methyl groups on the molecular structure, and on the intermolecular interactions compared to SiH_3NCO , SiH_3NCS and SiH_3CN , which are all known to have strong Si...O and Si...N intermolecular contacts.

The apparent structures determined by electron diffraction for the isocyanates and isothiocyanates have bent configurations at nitrogen, but this may be attributed to the shrinkage effect caused by the high amplitude low-frequency bending motion of a linear SiNC chain. Further

elucidation of the bending motion could come from detailed far infra-red spectra ($0-200\text{ cm}^{-1}$) as was achieved for $\text{SiH}_3\text{NCO}^{142}$. However the spectra are likely to be complicated by the presence of methyl torsion bands (usually weak) and bands for torsions of the skeleton along the Si-N bond.

COURSES ATTENDED

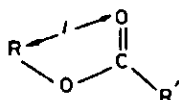
1. Fourier Transform Infra-red Spectroscopy -
Drs Cradock and Morrison
2. Mass Spectrometry - Prof J.H. Beynon
3. Biosynthesis - Prof A.I. Scott
4. Homogeneous Catalysis - Dr T.A. Stephenson
5. Computing - Dr Pounder
6. Chemical Physics 4 - course on determining structure
and vibrational analysis
7. German translation exam
8. Cambridge X-Ray Crystallographic Data-base.

The Molecular Structure of Silyl Monothioacetate in the Crystal at 130 K and in the Gas Phase

By Michael J. Barrow,* E. A. V. Ebsworth, Christopher M. Huntley, and David W. H. Rankin, Department of Chemistry, University of Edinburgh, West Mains Road, Edinburgh EH 9JJ

The structure of $\text{SiH}_3\text{OCSCH}_3$ has been determined in the solid by X-ray diffraction and in the gas by electron diffraction. At 130 K crystals are monoclinic, space group $P2_1/n$, with $a = 5.40$, $b = 8.77$, $c = 11.47$ Å, $\beta = 96.0^\circ$ (estimated standard deviations 0.3% assumed), and $Z = 4$. The final R value was 0.032 over 739 reflexions. The silyl group is bonded through oxygen: Si-O 1.699(5) Å (crystal) and 1.717(6) Å (gas). The Si-O and C=S bonds are eclipsed so that the intramolecular Si...S separations, 3.185(9) Å in the crystal and 3.143(9) Å in the gas, are appreciably less than the van der Waals distance. The heavy-atom skeleton deviates slightly, but significantly, from planarity in the crystal, where $\phi(\text{Si-O-C=S}) = -6.0(4)^\circ$. In the gas this torsion angle is ca. 10° . Interactions between neighbouring molecules in the crystal are consistent with weak secondary bonding between S and Si. The intermolecular C=S...Si-O systems have geometry: S...Si 3.382(10) Å, C=S...Si 100.8(4)°, and S...Si-O 166.3(3)°.

CRYSTALLINE carboxylic acids adopt a planar *cis* configuration for the acidic hydrogen with respect to the carbonyl oxygen (1a).



(1a; R = H)

(1b; R = CH_3)

(1c; R = SiH_3)

The same planar *cis* conformation is found in organic esters both in the solid, as in crystalline methyl acetate,¹ and in the gas, as in methyl formate² (1b). This conformation leads to intramolecular non-bonded distances, l , which are rather less than the sum of van der Waals radii. In crystalline methyl acetate the C...O separation is 2.61 Å; in gaseous methyl formate the separation is 2.68 Å, but the sum of the van der Waals radii for C and O atoms is 3.2 Å. Silyl esters also adopt the planar *cis* conformation, (1c), and the discrepancy between the Si...O(carbonyl) distance and the sum of the van der Waals radii becomes even more pronounced. Recent electron-diffraction analyses of gaseous silyl formate³ and gaseous silyl acetate¹ indicate some distortion of the Si-O-C=O torsion angle away from zero but only by ca. 15° . The resulting Si...O distances are 2.87 Å in the formate and 2.80 Å in the acetate, distances to be contrasted with a sum of van der Waals radii for Si and O atoms of 3.6 Å. In crystalline silyl acetate the heavy-atom skeleton is nearly planar but here the intramolecular Si...O(carbonyl) distance of 2.83 Å is overshadowed by an even shorter intermolecular O'...Si contact of 2.72 Å. The intermolecular O'...Si interaction is between the carbonyl oxygen atom of one molecule and the silicon atom of another and this O-Si...O' system is almost linear.

We have now completed structural studies of silyl monothioacetate, in both gas and crystalline phases. As compared with silyl acetate, the monothioester presents

additional structural possibilities. The substitution of one oxygen by sulphur introduces variations in atomic size and donor-acceptor character, the silyl group could be bonded through oxygen or through sulphur, and in the crystal there may be O...Si or S...Si interactions (we have recently shown that S...Si interactions occur in crystalline disilyl sulphide⁴).

EXPERIMENTAL

Samples of silyl monothioacetate were prepared by condensing silyl bromide into tributyltin monothioacetate.⁵ Purification was by fractional distillation *in vacuo* and purities were checked by i.r., n.m.r., and molecular-weight determinations.

X-Ray Diffraction.—**Crystal Data.** $\text{C}_2\text{H}_6\text{OSSi}$, $M = 106.2$, Monoclinic, $a = 5.40$, $b = 8.77$, $c = 11.47$ Å, $\beta = 96.0^\circ$ [estimated standard deviations (e.s.d.s) 0.3% assumed], $U = 540.2$ Å³, $Z = 4$, $D_c = 1.31$ g cm⁻³, Cu- K_α radiation (nickel filter), $\lambda = 1.5418$ Å, $\mu(\text{Cu-}K_\alpha) = 62.6$ cm⁻¹, space group $P2_1/n$ (C_{2h}^2 , no. 14) by systematic absences.

The compound melts at 210 K; cell parameters and intensities were measured at 130 K. The final least-squares weighting scheme was $w^{-1} = 1 + 0.0005 F_o^2$. The final value of the isotropic extinction parameter was $g = 1.07(8) \times 10^{-6}$ where $F_c' = F_c(1 - gF_c^2/\sin\theta)$. The final values of the discrepancy indices over 739 reflexions were $R = \Sigma|\Delta|/\Sigma|F_o| = 0.032$ and $R' = (\Sigma w\Delta^2/\Sigma wF_o^2)^{1/2} = 0.038$. A final difference-Fourier synthesis showed no peaks or troughs outside the range ± 0.2 e Å⁻³.

Procedure. Pure samples of the compound, which at room temperature is an air- and moisture-sensitive liquid, were sealed into thin-walled Pyrex capillaries (external diameter ca. 0.5 mm). The capillaries were mounted on goniometer heads using heat-insulating Tufnol inserts. Single crystals suitable for X-ray investigation were grown *in situ* on a Nonius Weissenberg goniometer. The goniometer was fitted with Nonius low-temperature nitrogen-gas-stream equipment with some locally devised modifications. Cell parameters and intensity data at 130 K were obtained from oscillation and Weissenberg photographs of two crystals, one aligned along [100], the other aligned along [110]. Intensity films were exposed for the Weissenberg levels hkl for $h = 0-4$ and $n + k, k, l$ for $n = 0-2$ using

Cu- K_{α} radiation and the equi-inclination multiple-film-pack method.

Integrated intensities were derived from microdensitometer measurements performed by the S.E.R.C. Microdensitometer Service at Daresbury Laboratory, Warrington.

The data from each crystal were corrected for absorption (numerical integration) and for Lorentz and polarisation effects after which the data levels were scaled together using common reflexions. In all, 1 831 intensities were measured in the hkl , hkl , hkl , hkl , hkl , and hkl regions of reciprocal space. After merging, there remained 739 unique observed reflections (merging R factor = 0.035).

TABLE 1

Weighting functions, correlation parameters, and scale factors for electron diffraction

Camera height/ mm	Δs	s_{\min}	sw_1 nm^{-1}	sw_2	s_{\max}	Correlation parameter	Scale factor
286.34	2.0	20	35	125	144	0.2939	0.651 (16)
128.40	4.0	52	70	220	280	0.0045	0.521 (21)

Structure solution and refinement. The space group imposes no restriction on molecular symmetry for $Z = 4$. The structure was solved by Patterson and Fourier methods and refined by weighted least-squares calculations to minimise the quantity $\sum w(|F_o| - |F_c|)^2$. All hydrogen atoms were located from a difference-Fourier synthesis and their positional and isotropic vibrational parameters were refined. Non-hydrogen atoms were refined with anisotropic vibrational parameters. During the later stages of refinement an empirical isotropic extinction correction was applied by means of a variable parameter in the least-squares calculations; an empirical least-squares weighting scheme was also introduced. Atomic scattering factors for H atoms were from ref. 6 and for other atoms from ref. 7. Allowance was made for the real and imaginary parts of the anomalous dispersion effect using $\Delta f'$ and $\Delta f''$ values from ref. 8. Calculations were performed using computers of the Edinburgh Regional Computing Centre and using programs written here and the program systems X-RAY 76,⁹ SHELX,¹⁰ and PLUTO.¹¹

Electron Diffraction.—Scattering intensities were recorded photographically on Kodak Electron Image plates using the Cornell-Edinburgh diffraction apparatus^{12,13} operating at 43 kV and with the sample and nozzle maintained at room temperature. Three plates were exposed at each of two nozzle-to-plate distances (128 and 286 mm), so providing data over the range 20–280 nm^{-1} in the scattering variable s . Separate diffraction experiments for benzene were used to calibrate the camera distances and electron wavelength [$\lambda = 0.05741(3)$ Å]. The photographic plates were traced by the S.E.R.C. Microdensitometer Service, using a Joyce-Loebl Microdensitometer 6.¹⁴

Calculations were performed using computers of the Edinburgh Regional Computing Centre and using established data-reduction^{13,14} and least-squares¹⁵ programs. Scattering factors were from ref. 16. Table 1 lists scale factors, correlation parameters, and the weighting points used to construct the weight matrix for least-squares refinements.

In the structural model used for refinements it was assumed that the central carbon atom is planar and that the OSiH_3 and CCH_3 groups have local C_{3v} symmetry. The molecular geometry is then defined by six bond lengths, five valence angles, and three torsion angles (see Table 2). The SiH_3 and CH_3 torsion angles were defined as zero when

one Si-H (or C-H) bond was staggered with respect to the C=S bond.

The refinement required care since there are several sets of overlapping peaks in the radial distribution curve (see Figure 1). The Si-H distance was fixed to permit refinement of the C-C distance. The three torsion angles were optimised by considering variations of the R factor as the angles were fixed at different values. Bonded distance amplitudes refined to sensible values although $u(\text{Si-H})$ was fixed and $u(\text{Si-O})$ and $u(\text{C-O})$ were constrained, in appropriate ratios, to $u(\text{C-S})$ and $u(\text{C-C})$ respectively. However this model still had a rather high R factor, $R_0 = 0.16$. A

dramatic improvement was possible when an allowance was included for contamination of the gaseous samples by disilyl sulphide which we know to be formed in a disproportionation reaction. The model was expanded to include (fixed) distances and amplitudes for Si-S, Si...Si, Si-H, Si...H,

TABLE 2

Gas-phase molecular parameters

(a) Independent parameters	Distance (Å) or angle (°)	Amplitude (Å)
$r_1(\text{C-H})$	1.048(10)	0.061(15)
$r_2(\text{C-C})$	1.484(14)	0.059(25)
$r_3(\text{C=S})$	1.615(8)	0.032(24)
$r_4(\text{C-O})$	1.345(7)	0.055 ^a
$r_5(\text{Si-O})$	1.717(6)	0.034 ^b
$r_6(\text{Si-H})$	1.480	0.088
	(fixed)	(fixed)
Angle 1 (C-C-O)	111.4(8)	
Angle 2 (O-C-S)	127(2)	
Angle 3 (Si-O-C)	118(2)	
Angle 4 (H-Si-O)	110 (fixed)	
Angle 5 (H-C-C)	110 (fixed)	
Torsion 1 (Si-O-C-S)	10°	
Torsion 2 (H-Si-O-C)	35°	
Torsion 3 (H-C-C-S)	70°	
(b) Dependent distances (Å) and amplitudes (Å)		
$d_7(\text{C}\cdots\text{S})$	2.075(15)	0.103(7)
$d_8(\text{C}\cdots\text{O})$	2.339(10)	0.060(18)
$d_9(\text{C}\cdots\text{H})$	2.088(18)	0.099(45)
$d_{10}(\text{C}\cdots\text{Si})$	2.632(22)	0.103 ^c
$d_{11}(\text{S}\cdots\text{O})$	2.652(20)	0.103 ^c
$d_{12}(\text{Si}\cdots\text{C})$	3.948(15)	0.092(15)
$d_{13}(\text{Si}\cdots\text{S})$	3.143(9)	0.138(9)

^a Proportional to u_1 , see text. ^b Proportional to u_2 , see text. ^c Torsion angles optimised by R -factor minimisation, see text. ^d Tied to $u_7(\text{C}\cdots\text{S})$.

and $\text{S}\cdots\text{H}$ with values taken from ref. 17. The proportion of $\text{S}(\text{SiH}_3)_2$ present was varied and a minimum R_0 value was obtained for 3.2% impurity (mole:mole basis) for the plates at the short camera distance and 11.5% impurity for the plates at the long distance. The final R factors were $R_0 = 0.102$ and $R_D = 0.078$.

RESULTS

Final values of atomic parameters for crystalline $\text{SiH}_3\text{-OCSC}_2\text{H}_5$ are given in Table 3 and details of the intramolecular

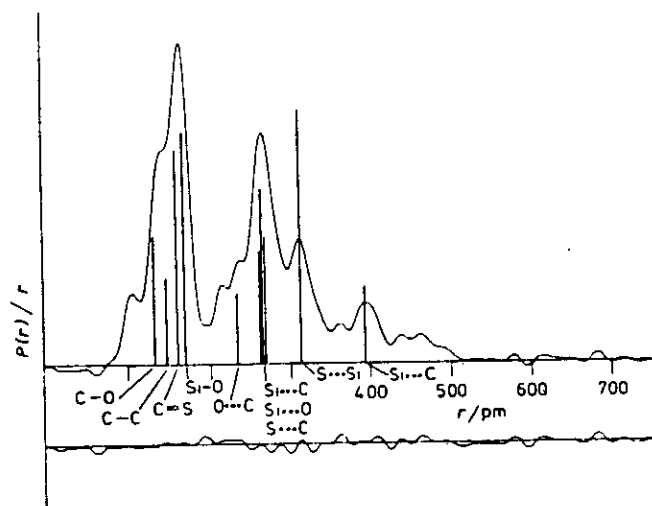


FIGURE 1 Gaseous silyl thioacetate: observed and final difference radial distribution curves, $P(r)/r$. Before Fourier inversion the data were multiplied by $s \cdot \exp[-0.000\ 015\ s^2 / (Z_{\text{H}} - f_{\text{H}})(Z_{\text{O}} - f_{\text{O}})]$

and intermolecular geometry in Tables 4 and 5. Figure 2 indicates the molecular geometry and atomic labelling scheme. Figure 3 shows the arrangement of molecules in the unit cell. Tables of observed and calculated structure factors and thermal vibration parameters are available as Supplementary Publication No. SUP 23254 (14 pp.).*

TABLE 3

Atomic parameters (with e.s.d.s in parentheses) for the crystal

Atom	X/a	Y/b	Z/c
Si(1)	0.251 66(17)	0.182 17(9)	0.070 02(7)
O(2)	0.475 6(4)	0.091 11(24)	0.159 18(18)
C(3)	0.498 6(6)	0.096 36(33)	0.274 69(24)
S(4)	0.327 99(16)	0.205 82(9)	0.348 55(6)
C(5)	0.698 4(7)	-0.006 58(40)	0.328 82(32)
H(11)	0.027(7)	0.134(4)	0.095(3)
H(12)	0.273(6)	0.332(3)	0.087(3)
H(13)	0.314(7)	0.140(5)	-0.034(3)
H(51)	0.704(7)	-0.022(4)	0.413(4)
H(52)	0.843(9)	0.027(5)	0.311(3)
H(53)	0.670(8)	-0.112(5)	0.288(3)

The cell parameters are subject to the usual errors associated with the Weissenberg film method; these errors are probably accentuated by the use of split-film cassettes for low-temperature work. Estimated standard deviations (e.s.d.s) given in Tables 3—5 do not include contributions from errors in the cell parameters but the e.s.d.s in the abstract and in Table 7 do include such contributions.

The final parameters for silyl thioacetate in the gas phase are listed in Table 2, and details of the least-squares correlation matrix are given in Table 6. The errors in Table 2 are e.s.d.s obtained from the least-squares analysis increased to allow for systematic errors. Observed and final difference molecular scattering curves are shown in Figure 4.

DISCUSSION

Gaseous silyl monothioacetate is difficult to study by electron diffraction (e.d.). The overlap of distances in

* For details see Notices to Authors No. 7, *J. Chem. Soc., Dalton Trans.*, 1981, Index issue.

the radial distribution function leads to high correlations between structural and vibrational parameters. The presence of small quantities of $\text{S}(\text{SiH}_3)_2$ in the gaseous samples adds a further complication. The e.d. results cannot therefore be of high precision. Nevertheless, they provide interesting parallels to and contrasts with the solid-phase results.

TABLE 4

Intramolecular geometry in the crystal

(a) Distances (Å) with e.s.d.s in parentheses

Si(1)—O(2)	1.699(2)	C(3)—C(5)	1.484(4)
Si(1)—H(11)	1.35(4)	C(5)—H(51)	0.99(4)
Si(1)—H(12)	1.33(3)	C(5)—H(52)	0.87(5)
Si(1)—H(13)	1.33(4)	C(5)—H(53)	1.03(4)
O(2)—C(3)	1.319(3)	Si(1) ... S(4)	3.185(1)
C(3)—S(4)	1.027(3)		

(b) Angles (°)

O(2)—Si(1)—H(11)	108.9(14)	S(4)—C(3)—C(5)	125.2(2)
O(2)—Si(1)—H(12)	109.4(13)	C(3)—C(5)—H(51)	115.4(22)
O(2)—Si(1)—H(13)	100.3(17)	C(3)—C(5)—H(52)	109.9(27)
Si(1)—O(2)—C(3)	125.1(2)	C(3)—C(5)—H(53)	107.4(23)
O(2)—C(3)—S(4)	123.0(2)	O(2)—Si(1) ... S(4)	54.4(1)
O(2)—C(3)—C(5)	111.8(3)	C(3)—S(4) ... Si(1)	57.4(1)

(c) Torsion angles (°)

Si(1)—O(2)—C(3)—S(4)	-6.0(4)
Si(1)—O(2)—C(3)—C(5)	174.8(3)
H(11)—Si(1)—O(2)—C(3)	-58.9(15)
H(12)—Si(1)—O(2)—C(3)	61.7(14)
H(13)—Si(1)—O(2)—C(3)	179.9(17)

(d) Distances (Å) of atoms from the least-squares best plane defined by Si(1), O(2), C(3), S(4), and C(5)

Si(1)	0.032(1)
O(2)	-0.049(2)
C(3)	-0.005(3)
S(4)	-0.006(1)
C(5)	0.027(4)
H(11)	1.19(3)
H(12)	-1.00(3)
H(13)	-0.06(4)
H(51)	0.23(4)
H(52)	-0.73(4)
H(53)	0.76(4)

The crystallographic study, like our previous X-ray studies of low-melting-point compounds of Si and Ge, was also faced with adverse factors. Low melting points, difficulties in crystallisation, ready decomposition, radiation damage, high X-ray absorption, and fluorescence all create problems. The nature of the low-temperature Weissenberg apparatus imposes some extra constraints particularly on the options available for measuring cell parameters and evaluating experimental layer scale factors. However this present analysis was one of the few where it proved possible to measure cell parameters and intensities from two different single crystals in different orientations and it is worth noting that there was very close agreement between the two sets of measurements.

Gas-phase and crystal structures confirm that the silyl group is bonded through oxygen, although the possibility of a very small amount of a sulphur-bonded species being present in the gas phase cannot be excluded. The Si—O bond lengths are 1.717(6) Å in the gas phase and 1.699(5) Å in the crystal and are equal within experi-

TABLE 5
Intermolecular geometry in the crystal *

(a) Shortest intermolecular contacts (Å)		
(i) Shortest H...H		
H(12) ... H(51 ^I)		2.60
H(12) ... H(52 ^{II})		2.85
H(11) ... H(53 ^{III})		2.86
H(12) ... H(51 ^{III})		2.88
(ii) Shortest C...H		
C(5) ... H(12 ^{IV})		3.16
C(3) ... H(53 ^{II})		3.25
(iii) Shortest O...H		
O(2) ... H(13 ^V)		2.79
O(2) ... H(11 ^{VI})		3.16
(iv) Shortest S...H		
S(4) ... H(52 ^{VII})		3.05
S(4) ... H(13 ^{VIII})		3.13
(v) Shortest Si...H		
Si(1) ... H(53 ^{III})		3.45
Si(1) ... H(51 ^I)		3.48
(vi) Shortest contacts between non-hydrogen atoms		
Si(1) ... S(4 ^I)		3.382(1)
O(2) ... S(4 ^{IV})		3.754(2)
S(4) ... C(5 ^{VII})		3.861(4)
Si(1) ... C(5 ^{III})		3.919(4)
(b) Important intermolecular angles (°)		
O(2)-Si(1) ... S(4 ^I)		166.3(1)
C(3)-S(4) ... Si(1 ^{VIII})		100.8(1)

* Roman numerals as superscripts refer to the following equivalent positions relative to the reference molecule at x, y, z : I $x - \frac{1}{2}, \frac{1}{2} - y, -\frac{1}{2} + z$; II $\frac{1}{2} - x, \frac{1}{2} + y, \frac{1}{2} - z$; III $\frac{1}{2} - x, \frac{1}{2} + y, \frac{1}{2} - z$; IV $\frac{1}{2} - x, y - \frac{1}{2}, \frac{1}{2} - z$; V $1 - x, -y, -z$; VI $1 + x, y, z$; VII $x - 1, y, z$; VIII $\frac{1}{2} + x, \frac{1}{2} - y, \frac{1}{2} + z$.

mental error. These distances, although rather long for Si-O bonds, are close to values reported for other silyl esters.^{1,3,18} The Si and S atoms are in the planar *cis* conformation in both phases. The apparent torsion angle of 10° found in the gas phase may be a shrinkage effect. The intramolecular Si...S contacts are 3.14 Å, gas, and 3.19 Å, solid. The sum of van der Waals radii for Si and S atoms is 3.9 Å so the intramolecular Si(1)...S(4) separation here is some 0.8 Å less than the van der Waals distance, the same as in silyl acetate.

In view of the fairly large uncertainties in some mole-

cular parameters in the gas phase, a detailed comparison between molecular geometries in gas and solid is not appropriate but attention should be drawn to the two parameters which show greatest divergence. First the O(2)-C(3) bond length is 1.345(7) Å in the gas but only 1.319(5) Å in the crystal, and secondly the angle Si(1)-O(2)-C(3) is much narrower [118(2)°] in the gas than in the crystal [125.1(4)°]. Similar changes to the O(2)-C(3) bond length and Si(1)-O(2)-C(3) bond angle were reported in the comparison between gaseous and crystalline silyl acetate.¹

Details of molecular geometries collected together in Table 7 point to a number of structural differences between crystalline methyl acetate, crystalline silyl

TABLE 6

Electron-diffraction analysis: portion of the least-squares correlation matrix showing all the off-diagonal elements greater than 50%

Angles								
r_1	1	2	3	u_1	u_2	u_7	r_1	
-83	-57	67	-64	86		54	r_2	
	-50				91		r_3	
		-59	59	53	-85		r_4	
			-96	-52			1) Angles	
						56	2) u_1	

TABLE 7

Comparison of crystal structures of methyl acetate, silyl acetate, and silyl monothioacetate (distances in Å, angles in degrees) ^a

	CH ₃ - OCOCH ₃ ^b	SiH ₃ - OCOCH ₃ ^b	SiH ₃ - OCSC ₂ H ₅ ^c
M(1)-O(2)	1.453(6)	1.696(6)	1.699(5)
O(2)-C(3)	1.337(6)	1.312(7)	1.319(5)
C(3)-Y(4)	1.200(6)	1.221(8)	1.627(6)
C(3)-C(5)	1.493(6)	1.476(8)	1.484(6)
M(1) ... Y(4)	2.611(9)	2.832(9)	3.185(9)
M(1)-O(2)-C(3)	114.9(5)	120.9(5)	125.1(4)
O(2)-C(3)-Y(4)	122.5(5)	120.6(6)	123.0(4)
ϕ [M(1)-O(2)-C(3)-Y(4)]	-1.2(5)	1.6(7)	-6.0(4)
ϕ [11(13)-M(1)-O(2)-C(3)]	179(3)	171(3)	180(2)
Y(4) ... M(1)		2.721(9)	3.382(10)
Y(4) ... M(1)-O(2)		173.1(4)	166.3(3)
C(3)-Y(4) ... M(1)		130.8(5)	100.8(4)

^a E.s.d.s given here include contributions from errors in cell parameters; M = C or Si. ^b Ref. 1, Y = O. ^c This work, Y = S.

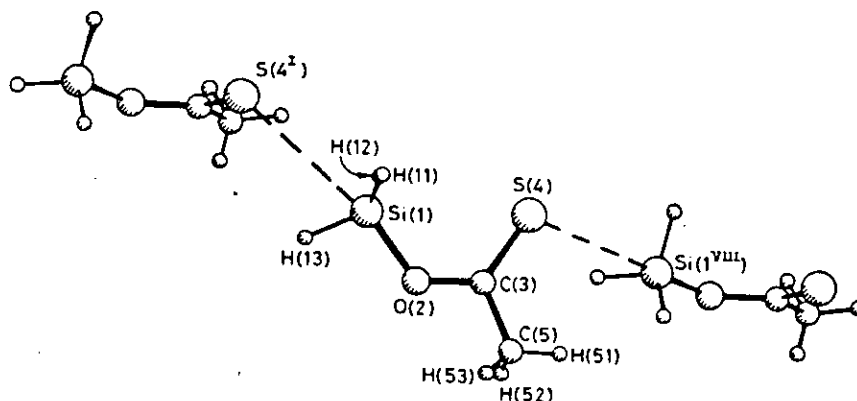


FIGURE 2 Crystalline silyl thioacetate: view of reference molecule and two neighbouring molecules showing labelling scheme and intermolecular Si...S contacts

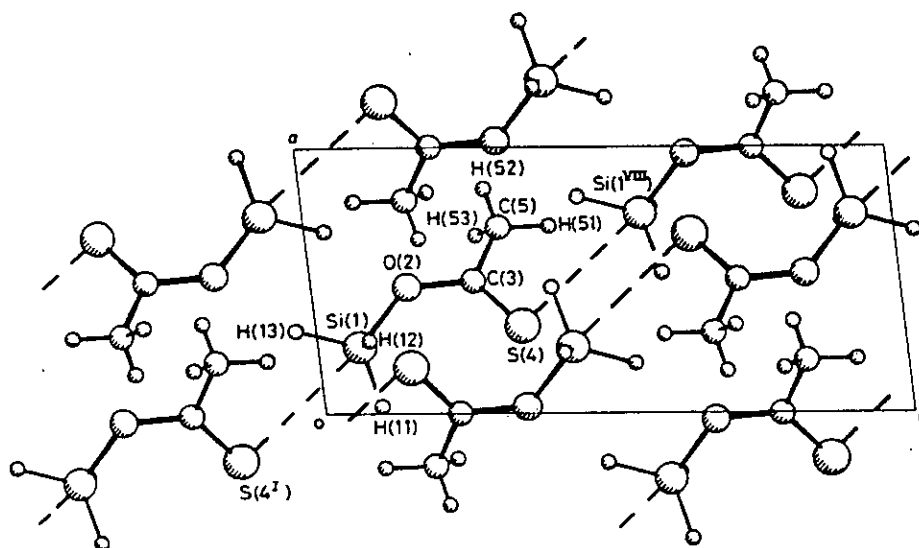


FIGURE 3 View of silyl thioacetate molecules in the crystal structure viewed down b . The $\text{Si} \cdots \text{S}'$ interactions are between molecules related by the n glide. Roman numeral superscripts are defined in Table 5

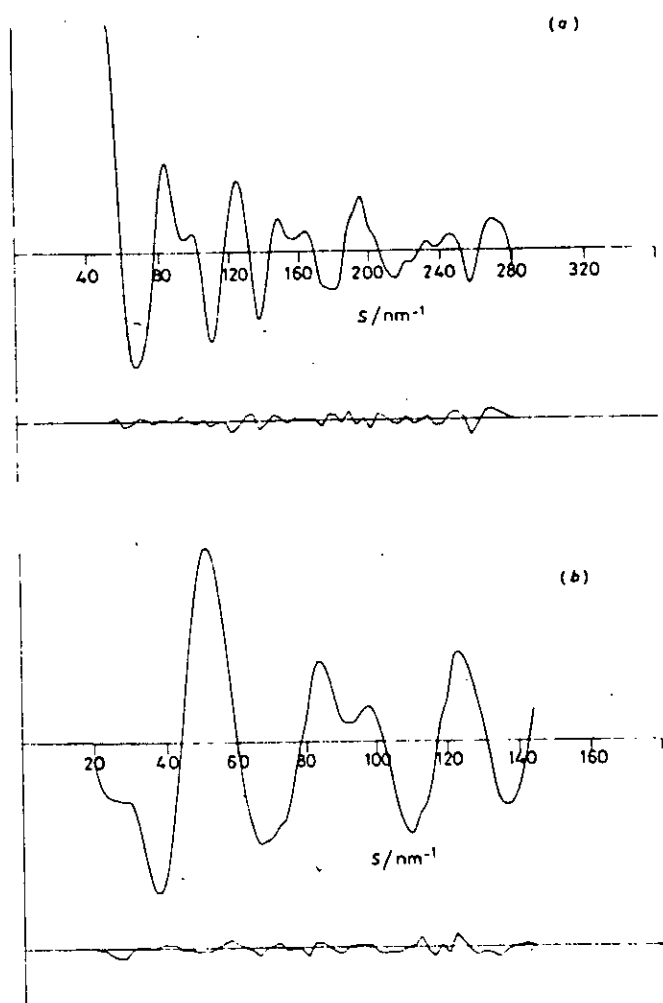


FIGURE 4 Gaseous silyl thioacetate: observed and final weighted difference molecular scattering intensities at camera distances of 128 (a) and 288 mm (b)

acetate, and crystalline silyl thioacetate. Going from methyl to silyl acetate results in a contraction of the $\text{O}(2)\text{-C}(3)$ bond length from 1.34 to 1.31 Å while the angle at $\text{O}(2)$ opens from 115 to 121°. [There are further, smaller, changes to bond lengths and angles at $\text{C}(3)$.] Substitution of the C=O group in silyl acetate by C=S , in the thioacetate, leaves the $\text{O}(2)\text{-C}(3)$ bond length essentially unchanged, now 1.32 Å, but the angle at $\text{O}(2)$ widens still further to 125°. There are concomitant deviations from molecular planarity. In methyl acetate the five heavy atoms are accurately coplanar, in silyl acetate the deviations from planarity are just about significant, but the thioacetate is non-planar: $\phi(\text{Si-O-C=S}) = -6.0(4)^\circ$ and $\phi(\text{Si-O-C-C}) = 174.8(3)^\circ$. These changes are obviously in accord with an increasing size effect for the $\text{M}(1)$ and $\text{Y}(4)$ ($\text{Y} = \text{S}$ or O) substituents although the nature of the intramolecular interaction between $\text{M}(1)$ and $\text{Y}(4)$ is unclear. In all three crystal structures the H_3M group is so orientated that $\text{H}(13)$ is planar *trans* with respect to $\text{Y}(4)$. In addition, although the hydrogen atoms are not very accurately located, the $\text{H-M}(1)\text{-O}(2)$ bond angles do imply that again in all three structures the C_3 axis of the H_3M group is not collinear with the $\text{M}(1)\text{-O}(2)$ bond but is shifted slightly to point more towards the $\text{Y}(4)$ substituent. These features were first reported, and well established, through two crystal-structure analyses of dimethyl(*t*-butyl)silyl esters of *aci*-nitroalkanes, when the intramolecular $\text{Si} \cdots \text{O}$ contacts were also much less than the van der Waals distance and were interpreted in terms of incipient intramolecular bond formation between O and Si .¹⁸

The dominating feature of the crystal structure of silyl thioacetate, as of silyl acetate, is the exceptionally short *intermolecular* contact between Si and $\text{S}(4')$, or $\text{O}(4')$ in silyl acetate. Not unexpectedly there are no comparable interactions in crystalline methyl acetate nor in the two dimethyl(*t*-butyl)silyl esters of *aci*-nitro-

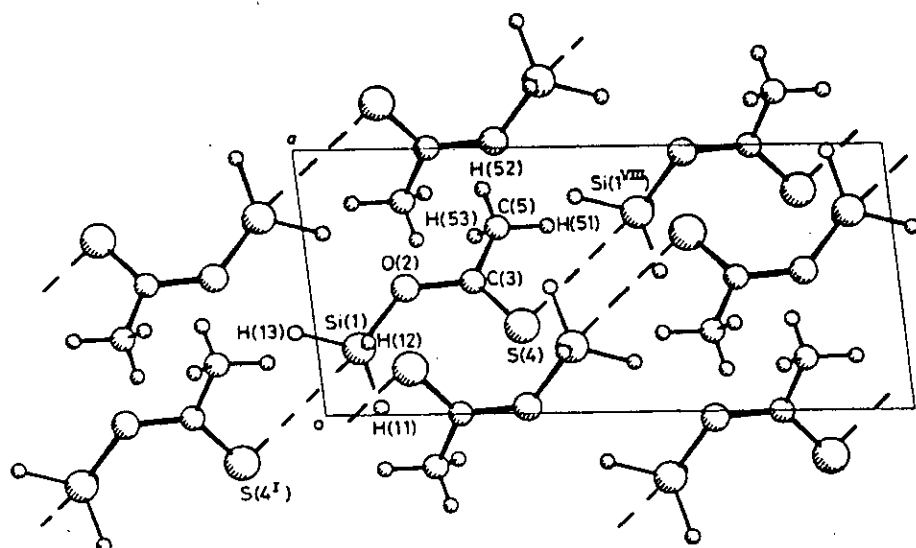


FIGURE 3 View of silyl thioacetate molecules in the crystal structure viewed down *b*. The Si...S' interactions are between molecules related by the *n* glide. Roman numeral superscripts are defined in Table 5

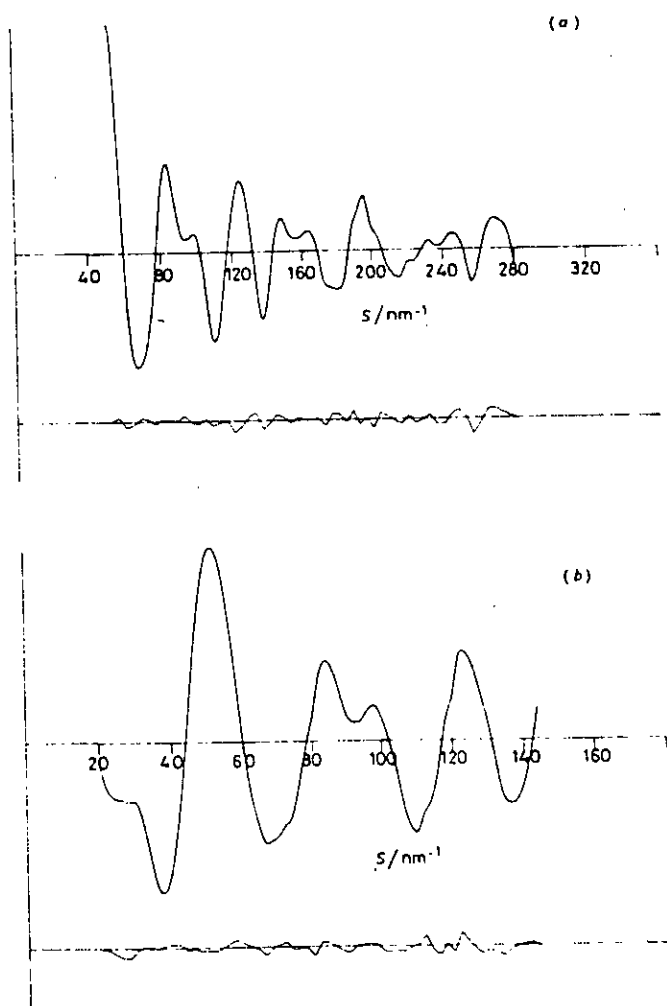


FIGURE 4 Gaseous silyl thioacetate: observed and final weighted difference molecular scattering intensities at camera distances of 128 (a) and 286 mm (b)

acetate, and crystalline silyl thioacetate. Going from methyl to silyl acetate results in a contraction of the O(2)-C(3) bond length from 1.34 to 1.31 Å while the angle at O(2) opens from 115 to 121°. [There are further, smaller, changes to bond lengths and angles at C(3).] Substitution of the C=O group in silyl acetate by C=S, in the thioacetate, leaves the O(2)-C(3) bond length essentially unchanged, now 1.32 Å, but the angle at O(2) widens still further to 125°. There are concomitant deviations from molecular planarity. In methyl acetate the five heavy atoms are accurately coplanar, in silyl acetate the deviations from planarity are just about significant, but the thioacetate is non-planar: $\phi(\text{Si-O-C=S}) = -6.0(4)^\circ$ and $\phi(\text{Si-O-C-C}) = 174.8(3)^\circ$. These changes are obviously in accord with an increasing size effect for the M(1) and Y(4) (Y = S or O) substituents although the nature of the intramolecular interaction between M(1) and Y(4) is unclear. In all three crystal structures the H₃M group is so orientated that H(13) is planar *trans* with respect to Y(4). In addition, although the hydrogen atoms are not very accurately located, the H-M(1)-O(2) bond angles do imply that again in all three structures the C₃ axis of the H₃M group is not collinear with the M(1)-O(2) bond but is shifted slightly to point more towards the Y(4) substituent. These features were first reported, and well established, through two crystal-structure analyses of dimethyl(*t*-butyl)silyl esters of *aci*-nitroalkanes, when the intramolecular Si...O contacts were also much less than the van der Waals distance and were interpreted in terms of incipient intramolecular bond formation between O and Si.¹⁸

The dominating feature of the crystal structure of silyl thioacetate, as of silyl acetate, is the exceptionally short *intermolecular* contact between Si and S(4'), or O(4') in silyl acetate. Not unexpectedly there are no comparable interactions in crystalline methyl acetate nor in the two dimethyl(*t*-butyl)silyl esters of *aci*-nitro-

The Molecular Structure of Germyl Monothioacetate in the Gas Phase, determined by Electron Diffraction

E. A. V. Ebsworth, Christopher M. Huntley, and David W. H. Rankin*

Department of Chemistry, University of Edinburgh, West Mains Road, Edinburgh EH9 3JJ

The molecular structure of gaseous germyl monothioacetate has been determined by electron diffraction. The only isomer present has the germyl group bonded to sulphur; the non-bonded $\text{Ge} \cdots \text{O}$ distance is substantially less than the sum of van der Waals radii for germanium and oxygen. Principal bond lengths and angles (r_s) are: $r(\text{Ge-S})$ 223.3(4), $r(\text{C-S})$ 176.5(7), $r(\text{C=O})$ 122.4(8), and $r(\text{C-C})$ 149.3(10) pm; GeSC 96.7(4), SCO 124.1(10), and CCO 116.4(13) $^\circ$. The heavy-atom skeleton is almost planar, with the Ge-S and C=O bonds arranged *cis* to one another.

The molecular structures of silyl formate¹ and silyl acetate² in the gas phase have recently been determined, and in each case the heavy-atom skeleton is planar, with the Si-O and C=O bonds mutually *cis*. This arrangement is associated with an unusually short intramolecular Si \cdots O distance of about 280 pm, which is considerably less than the van der Waals Si \cdots O distance (360 pm). In the solid phase, the structure of silyl acetate is little changed, although there is also an intermolecular Si \cdots O contact of 272 pm.

These observations have prompted us to consider the structures of other silyl and germyl esters. In silyl monothioacetate³ the silyl group is bonded to oxygen, and in the gas phase a planar heavy-atom structure is found, with a short contact between the silicon and the thiocarbonyl sulphur atoms. This structure is maintained in the solid phase, in which there is also a short intermolecular Si \cdots S contact. In contrast, the germyl group of germyl monothioacetate is bonded to sulphur.⁴ We have regrettably been unable to grow a single crystal of this compound. However, we are able to report the structure of the gas-phase form, which provides an interesting comparison with the gas-phase data for the silyl ester.

Experimental

A sample of germyl monothioacetate was prepared by reaction of monochlorogermane with tributyltin monothioacetate at room temperature, and was purified by fractional distillation and condensation *in vacuo*. Its purity was checked by i.r. spectroscopy and by molecular weight determination.

Electron-diffraction scattering intensities were recorded photographically on Kodak Electron Image plates using the Cornell/Edinburgh diffraction apparatus^{5,6} operating at ca. 43 kV. During exposures the nozzle and sample were maintained at room temperature. Three plates were obtained at each camera distance (128 and 286 mm), giving data over a range of 20–336 nm⁻¹ in the scattering variable, s . Intensity data were obtained in digital form using a computer-controlled Joyce-Loebl Microdensitometer 6⁷ at the S.E.R.C. Laboratory, Daresbury.

All calculations were carried out on an ICL 2972 computer at the Edinburgh Regional Computing Centre, using established data-reduction⁷ and least-squares refinement⁸ programs. Weighting points used in setting up the off-diagonal weight matrix used in refinements are given in Table 1, together with scale factors and correlation parameters. In all calculations the scattering factors of Schäfer *et al.*⁹ were used. The electron wavelength [5.610(3) pm] was determined by analysis of the diffraction pattern of gaseous benzene.

Structure Refinement.—During refinement of the structure of germyl monothioacetate it was assumed that SGeH₃ and

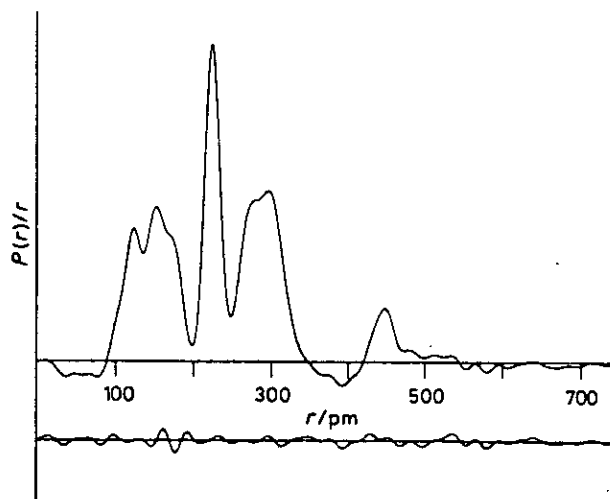


Figure 1. Observed and final difference radial distribution curves, $P(r)/r$. Before Fourier inversion the data were multiplied by $s \cdot \exp[-0.00002 s^2 / (Z_{\text{Ge}} - f_{\text{Ge}})(Z_{\text{S}} - f_{\text{S}})]$

CCH₃ groups each had local C_{3v} symmetry, and that the three bonds to the central carbon atom were coplanar. The geometry was then defined by six bond lengths, five valence angles, and three dihedral angles. The GeH₃ and CH₃ twist angles were defined to be zero when one Ge-H or C-H bond was staggered with respect to the C-S bond, while the angle describing the twist about the C-S bond was defined to be zero when the C=O and Ge-S bonds were *cis* with respect to each other.

Although the radial distribution curve (Figure 1) was dominated by the large Ge-S peak, there were three other peaks in the region associated with bonded distances, and it was possible to refine all bonded distances except Ge-H. In a series of refinements with this parameter fixed at various values, the lowest *R* factor was found when it was set at 152.5 pm, and this value was assumed in subsequent refinements. Similar methods were used to find optimum values of the three angles describing the conformation of the molecule. The three valence angles involving heavy atoms all refined normally, but the SGeH and CCH angles would not refine satisfactorily, and were therefore fixed at 110 $^\circ$.

Results and Discussion

The molecular parameters for germyl monothioacetate are given in Table 2: errors quoted (in parentheses) are estimated

Table 1. Weighting functions, scale factors, and correlation parameters

Camera height mm	Δs	$s_{min.}$	s_{w1} nm ⁻¹	s_{w2}	$s_{max.}$	Correlation parameter	Scale factor
128.29	4	76	84	220	296	0.328	0.883(30)
286.11	2	44	58	120	146	0.042	0.923(16)

Table 2. Molecular parameters

	Distance (pm)	Amplitude (pm)		Distance (pm)	Amplitude (pm)
(a) Independent distances					
r_1 (C-C)	149.3(10)	5.0 ^a	r_4 (C-S)	176.5(7)	4.8 ^a
r_2 (C-H)	108.7(12)	6.5 ^a	r_5 (Ge-S)	223.3(4)	5.7(4)
r_3 (C=O)	122.4(8)	3.9 ^a	r_6 (Ge-H)	152.5 ^b	8.8 ^a
(b) Dependent distances					
d_7 (C...O)	235.1(18)	8.0 ^a	d_{10} (Ge...C)	300.4(8)	10.9(13)
d_8 (S...C)	277.3(14)	7.3(14)	d_{11} (Ge...C)	445.6(10)	8.5(12)
d_9 (S...O)	265.3(12)		d_{12} (Ge...O)	297.2(14)	15.0 ^a
(c) Angles (°)					
1 (CCO)	116.4(13)		5 (CCH)	110.0 ^a	
2 (SCO)	124.1(10)		6 (twist GeH ₃)	5.0 ^b	
3 (GeSC)	96.7(4)		7 (twist CH ₃)	40.0 ^b	
4 (SGeH)	110.0 ^a		8 (dihedral GeSCO)	5.0 ^b	

^a Fixed. ^b See text.

Table 3. Portion of least-squares correlation matrix showing off-diagonal elements greater than 30%

r_2	r_3	Angle			u_8	k_1	r_1	r_4	r_5	} Angle
		1	2	3						
34	30	-62	48	-40						
		-43								
			-58	-73	-38	36				
				-70	-67					
					53	-32				
					-56					
						55				

standard deviations obtained in the least-squares analysis, increased to allow for systematic errors. Part of the least-squares correlation matrix is given in Table 3. The most significant correlations are between the three refined angles, and arise from the overlap of the associated non-bonded distances, most of which lie between 260 and 300 pm. The intensity data are illustrated in Figure 2, together with the difference curves for the final refinement, for which the R factor (R_G) was 0.11.

The refined data provide clear evidence that germyl monothioacetate exists essentially completely as the S-bonded isomer in the gas phase. No attempt was made to allow for small proportions of the O-bonded isomer in the refinements, as the radial-distribution difference curve (Figure 1) shows no significant features. This observation is supported by spectroscopic evidence.⁴

The geometrical parameters for germyl monothioacetate (Table 2) are much as would be expected, although there are some small differences between our results and those reported for related compounds that may be significant. The C-S distance [176.5(7) pm] is shorter than that in dimethyl sulphide¹⁰ [180.2(2) pm], but the difference is only about half as great as that between C-O distances in esters such as methyl acetate² and in dimethyl ether.¹¹ The Ge-S distance [223.3(4) pm] is greater than in digermyl sulphide¹² [220.9(4)

pm], and associated with this there is a narrowing of the angle at sulphur from 98.9(1) to 96.7(4)°. These changes are in the same direction as, but much smaller than, changes in Si-O distances and angles at oxygen in going from disilyl ether¹³ to silyl esters.¹⁻³ The origins of these structural changes are not yet apparent, but a fairly consistent pattern is emerging, and we intend to study esters with germanium bound to oxygen, and with silicon bound to sulphur, to gain greater understanding of the factors that influence structure.

As with all the esters we have studied,^{1-3,14} the heavy-atom skeleton is planar: the apparent small deviation from planarity is almost certainly a shrinkage effect. Thus the non-bonded Ge...O distance is very much shorter [297.2(14) pm] than the sum of van der Waals radii for germanium and oxygen (*ca.* 360 pm). This shortening is not as great as those we have observed for silyl esters (*ca.* 80 pm), but must nevertheless indicate that there is a strong interaction between germanium and oxygen. It is unfortunate that in this case we have been unable to determine the structure of this compound in the crystalline phase, and so study intermolecular Ge...O contacts, but it is hoped that the problems will be overcome with other germyl esters.

The Question of O-Bound Germyl Monothioacetate.—We studied the reaction between silyl monothioacetate and

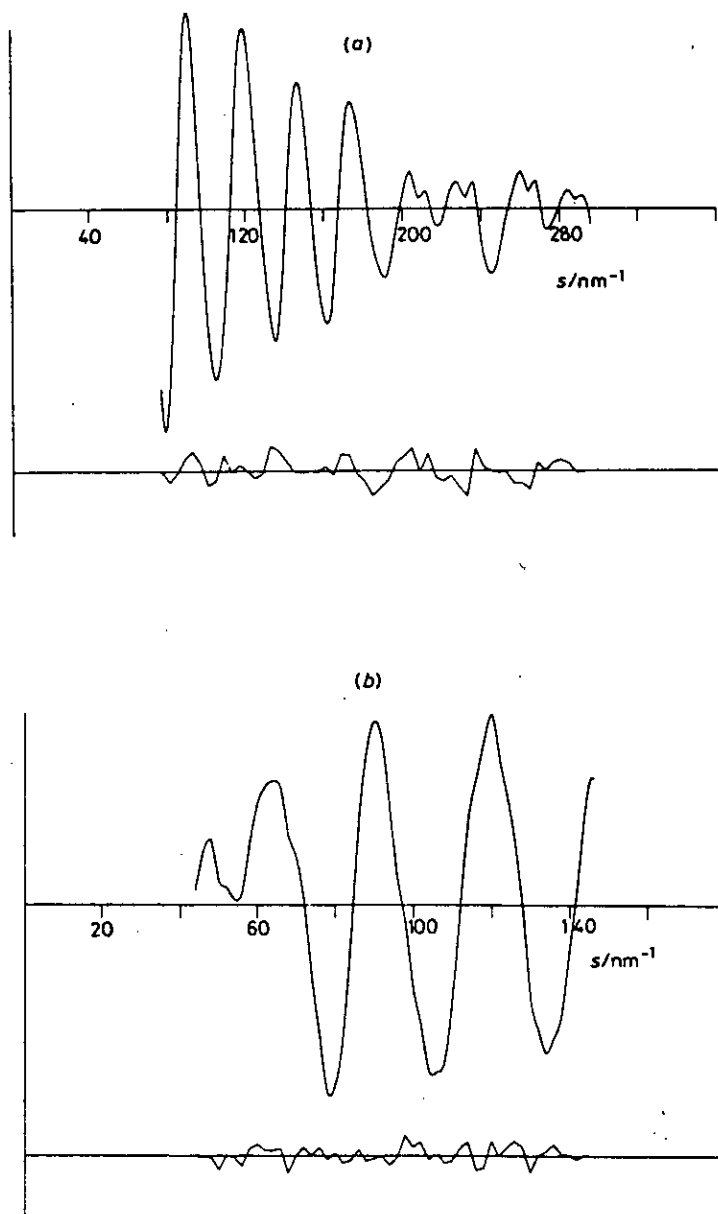


Figure 2. Observed and final weighted difference molecular scattering intensities at nozzle-to-plate distances of (a) 128 and (b) 286 mm

germyl fluoride by proton n.m.r. spectroscopy at low temperature to see if we could detect any of the O-bound isomer of germyl monothioacetate as an intermediate in the formation of the S-bound compound. From the proton resonance spectra of GeH_3 and SiH_3 compounds, we expected that the proton resonance of the GeH_3 group in the O-isomer would be near that observed for $(\text{GeH}_3)_2\text{O}$, whose chemical shift is about 5.30 p.p.m.¹⁵ The GeH_3 resonance of the S form is close to that of $(\text{GeH}_3)_2\text{S}$, at 4.60 p.p.m.¹⁵ The quality of the proton resonance spectra obtained at 180 K was poor, but sufficient to show that even at so low a temperature substantial reaction had occurred. Good quality spectra were obtained from 193 K upwards, and no peaks were observed that could plausibly be assigned to the O-bound isomer. At 193 K reaction appeared to be complete, and so if any of the O-bound isomer is formed it must rearrange to give the S-bound isomer too rapidly for us to detect. The proton chemical shifts for $\text{CH}_3\text{COSGeH}_3$ in toluene solution at 183 K are $\delta\text{H}(\text{C})$ 1.89 and $\delta\text{H}(\text{Ge})$ 4.32 p.p.m.

We also determined the i.r. spectrum of germyl monothioacetate in the gaseous and solid phases in order to see whether there were any substantial shifts in frequency with change in phase or whether new bands appeared in the spectrum of the solid. Our results are given in Table 4. In general there are shifts to lower frequency from the gas to the solid phase, but these are quite consistent with shifts observed in the spectra of other esters, including methyl acetate. Indeed, the shift in the CO-stretching mode is smaller for germyl thioacetate than for methyl acetate. There was no evidence from the i.r. spectrum for any change in structure from gas to solid or for unusually strong intermolecular interactions in the solid state. Furthermore, there is no splitting in the CO stretch such as would have been expected if the solid contained both *cis* and *trans* isomers.

We also recorded the mass spectrum. The principal fragments with their approximate relative intensities are given in Table 5. The fragmentation pattern is consistent with the structure we have given.

Table 4. Infrared spectra (cm^{-1}) of $\text{CH}_3\text{COSGeH}_3$

Gas	Solid	Assignment
2 130s	2 128s	$\nu_{\text{asym}}(\text{GeH})$
2 108s	2 102s	$\nu_{\text{sym}}(\text{GeH})$
1 709s	1 678vs	$\nu(\text{C=O})$
	1 415m	$\delta_{\text{asym}}(\text{CH})$
1 361m	1 354s	$\delta_{\text{sym}}(\text{CH})$
	1 261w	$\delta(\text{CH})$
1 132s	1 128s	$\rho(\text{CH}_3)$
1 088vw	1 095m	
1 018w	1 019w	$\rho(\text{CH}_3)$
955m	955s	$\nu(\text{C-C})$
	874m	$\delta(\text{GeH}_3)$
	862m	
	817vs	$\delta(\text{GeH}_3)$
	811vs	$\delta(\text{GeH}_3)$
	625s	$\nu(\text{C-S})$
	585w	$\rho(\text{GeH}_3)$
	466w	Deformation CCOS
	426w	
	291w	
		$\nu(\text{Ge-S})$

s = Strong, m = medium, w = weak, and v = very.

Spectra were recorded on a Perkin-Elmer 577 spectrophotometer. The solid phase was annealed until there was no further change in the spectrum.

Acknowledgements

We thank the S.E.R.C. for financial support: in particular, we thank Dr. M. Elder and his staff at the S.E.R.C. laboratory, Daresbury, for their helpfulness in providing the micro-densitometry service.

References

- 1 W. Bett, S. Cradock, and D. W. H. Rankin, *J. Mol. Struct.*, 1980, 66, 159.
- 2 M. J. Barrow, S. Cradock, E. A. V. Ebsworth, and D. W. H. Rankin, *J. Chem. Soc., Dalton Trans.*, 1981, 1988.
- 3 M. J. Barrow, E. A. V. Ebsworth, C. M. Huntley, and D. W. H. Rankin, *J. Chem. Soc., Dalton Trans.*, 1982, 1131.

Table 5. Mass spectrum of $\text{CH}_3\text{COSGeH}_3$ *

Ion ^b	m/e	Relative intensity
$[\text{GeH}_3\text{SOCCH}_3]^+$	152	20
$[\text{GeSC}]^+$	118	22
$[\text{GeS}]^+$	106	20
$[\text{Ge}]^+$	74	14
$[\text{COS}]^+$	60	2
$[\text{CS}]^+$	44	13
$[\text{CH}_3\text{CO}]^+$	43	100
$[\text{CCO}]^+$	40	11
$[\text{CO}]^+$	28	99
$[\text{CH}_3\text{C}]^+$	27	7
$[\text{GeO}]$	90	2

* Recorded on an MS902 spectrometer, with ionising voltage of 70 eV (ca. 1.12×10^{-17} J). Exact mass measurements of parent ion gave 151.935 73 (error 4 p.p.m.). ^b Fragments containing Ge all show a pattern reflecting the relative abundance of the Ge isotopes.

- 4 J. E. Drake, R. T. Hemmings, and H. E. Henderson, *Inorg. Nucl. Chem. Lett.*, 1976, 12, 563.
- 5 S. H. Bauer and K. Kimura, *J. Phys. Soc. Jpn.*, 1962, 17, 300.
- 6 C. M. Huntley, G. S. Laurensen, and D. W. H. Rankin, *J. Chem. Soc., Dalton Trans.*, 1980, 954.
- 7 S. Cradock, J. Koprowski, and D. W. H. Rankin, *J. Mol. Struct.*, 1981, 77, 113.
- 8 A. S. F. Boyd, G. S. Laurensen, and D. W. H. Rankin, *J. Mol. Struct.*, 1981, 71, 217.
- 9 L. Schäfer, A. C. Yates, and R. A. Bonham, *J. Chem. Phys.*, 1971, 55, 3055.
- 10 L. Pierce and M. Hayashi, *J. Chem. Phys.*, 1961, 35, 479.
- 11 K. Kimura and M. Kubo, *J. Chem. Phys.*, 1959, 30, 151.
- 12 C. Gliedewell, D. W. H. Rankin, A. G. Robiette, G. M. Sheldrick, B. Beagley, and S. Cradock, *J. Chem. Soc. A*, 1970, 315.
- 13 A. Almendinger, O. Bastiansen, V. Ewing, K. Hedberg, and M. Traetteberg, *Acta Chem. Scand.*, 1963, 17, 2455.
- 14 S. Cradock and D. W. H. Rankin, *J. Mol. Struct.*, 1980, 69, 145.
- 15 D. E. J. Arnold, J. S. Dryburgh, E. A. V. Ebsworth, and D. W. H. Rankin, *J. Chem. Soc., Dalton Trans.*, 1972, 2518.

Received 6th October 1982; Paper 2/1725

REFERENCES

1. H. Mark, R. Wierl, Naturwissenschaften, 18, (1930), 205.
2. E. Rutherford, Phil.Mag., 21, 669.
3. P. Debye, Ann.Physik, 46, (1915), 809.
4. P. Debye, Phyz.Z., 31, (1930), 419.
5. C. Davisson, L.H. Germer, Phys.Rev., 30, (1927), 705.
6. G.P. Thomson, Proc.Roy.Soc., A117, (1928), 600.
7. G.P. Thomson, Proc.Roy.Soc., A119, (1928), 651.
8. L. De Broglie, Phil.Mag., 47, (1924), 446.
9. M. Davis, 'Electron Diffraction in Gases', Marcel Dekker (1971)
10. Molecular Structure by Diffraction Methods, Vol. 1.
The Chemical Society Specialist Periodical Reports,
7-57.
11. K. Hedberg, "Critical Evaluation of Structural
Information from Gaseous Electron Diffraction", National
Academy of Sciences, Wahington D.C., 1974.
12. P.D. Blair, Personal Communication.
13. Y. Murato, Y. Morino, Acta.Cryst., 20, (1966), 605.
14. Y. Morino, K. Kuchitsu, Y. Murato, Acta.Cryst., 18,
(1965), 549.
15. I. Hargittai, University of Budapest
16. R.E. Hilderbrandt, Ph.D. Thesis, Cornell University 1969
17. H. Fetzner, Ph.D. Dissertation, The University of
Texas at Austin, (1966).
18. D.A. Swick and J. Kasle, Abstract American
Crystallographic Association Annual Conference, (1964).
19. D.M. Bridges, G.C. Holywell, D.W.H. Rankin and
J.M. Freeman, J.Organomet.Chem., 32, (1971), 87.

20. G.C. Holywell, D.W.H. Rankin, B. Beagley and J.M. Freeman, J.Chem.Soc.(A), (1971), 785.
21. L. Schafer, A.C. Yates, R.A. Bonham, J.Chem.Phys., 55, (1971), 3055.
22. B. Beagley and A.R. Conrad, Trans.Faraday Soc., 66, (1970), 2740.
23. B. Beagley and T.G. Hewitt, Trans.Faraday Soc., 64, (1968), 2561.
24. D.W.H. Rankin, J.Chem.Soc.(A), (1969), 1926.
25. C. Glidewell, D.W.H. Rankin and A.G. Robiette, J.Chem.Soc., (1970), 2935.
26. A. Almennigen, O. Bastiansen, V. Ewing, K. Hedberg and M. Traetteberg, Acta.Chem.Scand., 17, (1963), 2455.
27. C. Glidewell, D.W.H. Rankin, A.G. Robiette and G.M. Sheldrick, Inorg.Nucl.Chem.Letts., 5, (1969), 417.
28. C. Glidewell, A.G. Robiette, and G.M. Sheldrick, Chem.Phys.Letts., 16, (1972), 526.
29. A.A. Fraser and D.W.H. Rankin, personal communication.
30. J.A. Duckett, A.G. Robiette and I.M. Mills, J.Mol.Spect., 62, (1976), 34.
31. S. Cradock and D.C.J. Skea, J.Chem.Soc.(Faraday Trans.), 78, (1982), 787.
32. J.R. Durig, K.S. Kalasinsky and V.F. Kalasinsky, J.Chem.Phys., 62, (1978), 918.
33. M.J. Barrow, E.A.V. Ebsworth and M.M. Harding, J.C.S. Dalton, (1980), 1838.
34. H. Oberhammer and J.E. Boggs, J.A.C.S., 102, (1980), 7241.
35. L.N. Lewis and K.G. Caulton, Inorg.Chem., 19, (1980), 1840.
36. C. Glidewell and H.D. Holden, J.Mol.Struc.(Theo.Chem.), 89, (1982), 325.

37. L.S. Bartell, J.Chem.Phys., 32, (1960), 827.
38. C. Glidewell and A.G. Robiette, Chem.Phys.Letts., 28, (1974), 290.
39. B. Beagley, A.G. Robiette and G.M. Sheldrick, J.Chem.Soc.(A), (1968), 3002.
40. A. Almenningen, K. Hedberg and R. Seip, Acta.Chem.Scand., 17, (1963), 2264.
41. L. Pierce, M. Hayashi, J.Chem.Phys., 35, (1961), 479.
42. L.S. Bartell and H.K. Higginbottom, J.Chem.Phys., 42, (1965), 851.
43. R.W. Kilb and L. Pierce, J.Chem.Phys., 27, (1957), 108.
44. M.J. Barrow, S. Cradock, E.A.V. Ebsworth and D.W.H. Rankin, J.C.S. Dalton, (1981), 1988.
45. J.G. Morse, K. Cohn, R.W. Rudolph and R.W. Parry, Inorg.Synth., 10, (1967), 147.
46. J.E. Drake, R.T. Hemmings and H.E. Henderson, Inorg.Nucl.Chem.Letts., 12, (1976), 563.
47. T.M. Srivastava and M. Onyszchuk, Can.J.Chem., 41, (1963), 1244.
48. G. Fritz and D. Kummer, Z.Anorg.Chem., 308, (1961), 105.
49. G.M. Sheldrick, Ph.D. Thesis, Cambridge, (1966).
50. A. Stock and K. Somieski, Ber., 54 (1921), 740.
51. G. Brauer, Handbook of Inorganic Chemistry, Volume 1.
NEW YORK 1962
52. S. Cradock, E.A.V. Ebsworth and H.F. Jessop, J.C.S. Dalton, (1972), 359.
53. S. Cradock, E.A.V. Ebsworth, D.W.H. Rankin, W.J. Savage, J.C.S. Dalton, (1976), 1661.
54. W.L. Jolly, J.A.C.S., 83, (1961), 335.
55. N.S. Hosmane, Ph.D. Thesis, Edinburgh (1974).

56. T.N. Srivastava, J.E. Griffiths and M. Onyszchuk, Can.J.Chem., 40, (1962), 739.
57. G. Davidson, L.A. Woodward, K.M. MacKay and P. Robinson, Spect.Acta., 23A, (1967), 2386.
58. E.A.V. Ebsworth and M.J. Mays, J.Chem.Soc., (1962), 4844.
59. G. Brauer, Handbook of Preparative Inorganic Chemistry, Volume 1. NEW YORK 1967
60. S. Cradock, E.A.V. Ebsworth and N. Hosmane, J.Chem.Soc. Dalton, (1975), 1624.
61. E.A.V. Ebsworth and H.J. Emeleus, J.Chem.Soc., (1958), 2150.
62. H. Emeleus, M. Onyszchuk and W. Kuchen, Z.Anorg.Chem., 283, (1956), 74.
63. H. Kriegsman and G. Engelhardt, Z.Anorg.Chem., 310, (1961), 100.
64. J.R. Durig, P.J. Cooper and Y.S. Li, Inorg.Chem., 14, (1975), 2845.
65. W. Bett, S. Cradock and D.W.H. Rankin, J.Mol.Struct., 66, (1980), 159.
66. E.A.V. Ebsworth, D.W.H. Rankin, W. Skeger and J.G. Wright, J.Chem.Soc. Dalton, (1980), 1768.
67. R.W. Rudolph, ^{RC}Taylor, ^{RW}Parry, J.A.C.S., (1966), 3729.
68. M.J. Barrow, E.A.V. Ebsworth, C.M. Huntley, and D.W.H. Rankin, J.Chem.Soc. Dalton, (1982), 1131.
69. D.E.J. Arnold, and D.W.H. Rankin, J.Chem.Soc. Dalton, (1977), 1999.
70. D.E.J. Arnold, J.S. Dryburgh, E.A.V. Ebsworth and D.W.H. Rankin, J.Chem.Soc. Dalton, (1972), 2518.
71. Personal observation.

72. L.F. Johnson and W.C. Jankowski: C^{13} NMR Spectra.
73. J.F. Nixon and R. Schmutzler, Spectrochim.Acta., 20, (1964), 1835.
74. W. Bett and S. Cradock, Monat.Für.Chem., 111, (1980), 193.
75. W. Bett, personal communication.
77. D.E.J. Arnold, J.S. Dryburgh, E.A.V. Ebsworth and D.W.H. Rankin, J.C.S. Dalton, (1972), 2518.
78. J.R. Chipperfield and R.H. Prince, J.Chem.Soc., (1963), 3567.
79. I.B. Rabinovich, E.G. Kiparisova and Yu A. Aleksandrov, Dokl.Akad.Nauk. SSSR, 200, (1971), 1116.
80. D.E.C. Corbridge, Phosphoras - An Outline of its Chemistry, Biochemistry and Technology, (Elsevier). 1980
81. L. Pauling, Nature of the Chemical Bond, Cornell University Press, (1960).
82. S. Cradock and D.W.H. Rankin, J.Mol.Struct., 69, (1980), 145.
83. E.W. Colvin, A.K. Beck, B. Bastini, D. Seebach, Y. Kai and J.D. Dunitz, Helv.Chim.Acta., 63, (1980), 697.
84. C. Glidewell, D.W.H. Rankin, A.G. Robiette, G.M. Sheldrick and J.M. Freeman, J.Mol.Struct., 5, (1970), 417.
85. C. Glidewell, D.W.H. Rankin, A.G. Robiette and G.M. Sheldrick, J.Mol.Struct., 6, (1970), 231.
86. K. Kimura and M. Kubo, J.Chem.Phys., 30, (1959), 151.
87. M. Barrow's contribution to paper: J.C.S. Dalton, (1982), 1131.
88. M.J. Barrow, E.A.V. Ebsworth and M.M. Harding, J.C.S. Dalton, (1980), 1838.

89. C. Glidewell, D.W.H. Rankin, A.G. Robiette, G.M. Sheldrick, B. Beagley and S. Cradock, J.Chem.Soc. (A), (1970), 315.
90. V.W. Laurie, J.Chem.Phys., 30, (1959), 1210.
91. C. Glidewell and D.C. Liles, J. Organomet.Chem., 243, (1983), 291.
92. K. Kimura, K. Katada, S.H. Bauer, J.A.C.S., 88, (1966), 416.
93. R.L. Hilderbrand and S.H. Bauer, J.Mol.Struct., 3, (1969), 325.
94. W.C. Airey, C. Glidewell, A.G. Robiette and G.M. Sheldrick, J.Mol.Struct., 8, (1971), 435.
95. M.C.L. Gerry, J.C. Thompson and T.M. Sugden, Nature, 211, (1966), 846.
96. J.A. Duckett, A.G. Robiette and M.C.L. Gerry, J.Mol.Struct., 96, (1981), 374.
97. J.A. Duckett, A.G. Robiette and I.M. Mills, J.Mol.Spect., 62, (1976), 34.
98. S. Cradock and D.C.J. Skea, J.C.S. Faraday II, (1980), 860.
99. S. Cradock and D.C.J. Skea, J.C.S. Faraday II, (1982), 787.
100. J.R. Durig, J.F. Sullivan, A.W. Cox and B.J. Streusand, Spectrochimica Acta., 34A, (1978), 719.
101. P. Baybutt, M.F. Guest and I.H. Hillier, Proc.Roy.Soc. London A, 333, (1973), 225.
102. B. Beagley, J.J. Monahan and T.G. Hewitt, J.Mol.Struct., 8, (1971), 401.
103. A. Almenningen, H.M. Seip and R. Seip, Acta.Chem.Scand., 24, (1970), 1697.

104. W. Zeil, J. Hasse and M. Kakkouri, Discuss. Faraday Soc., 47, (1969), 149.
105. V. Shomaker^c and D.P. Stevenson, J.A.C.S., 63, (1941), 37.
106. S.J. Cyvin, Molecular Vibrations and Mean Square Amplitudes, (Elsevier). 1968
107. G. Gundersen and D.W.H. Rankin, to be published.
108. K. Hedberg, J.A.C.S., 77, (1955), 6491.
109. D.W.H. Rankin, A.G. Robiette, G.M. Sheldrick, W.S. Sheldrick, B.J. Aylett, I.A. Ellis and J.J. Monahan^g, J.Chem.Soc. (A), (1969), 1224.
110. C. Glidewell, D.W.H. Rankin, A.G. Robiette and G.M. Sheldrick, J.Mol.Struct., 6, (1970), 231.
111. A.G. Robiette, G.M. Sheldrick, W.S. Sheldrick, B. Beagley, D.W.J. Cruickshank, J.J. Monahan, B.J. Aylett and I.A. Ellis, Chem.Comm., (1968), 909.
- 111(a) S.J. Cyvin, J. Brunvoll and A.G. Robiette, Chem.Phys.Letts., 11, (1971), 263.
112. C. Glidewell, J.Organomet.Chem., 159, (1978), 23.
113. E.A.V. Ebsworth, R. Mould, R. Taylor, G.R. Wilkinson and L.A. Woodward, Trans.Faraday Soc., 58, (1962), 1062.
114. D.R. Jenkins, R. Kewley and T.M. Sugden, Trans. Faraday Soc. 58, (1962), 1284.
115. J.R. Durig, K.S. Kalasinsky and V.F. Kalasinsky, J.Phys.Chem., 82, (1978), 438.
116. J. Goubeau, E. Heuback, D. Paulin and I. Widmaier, Z.Anorg.Allgem.Chem., 300, (1959), 194.
117. G.L. Carlson, Spectrochim.Acta., 18, (1962), 1529.
118. T.J. Veszpremi, J. Nagy, I.A. Barta and G. Zsombok, J.Organometallic Chem., 185, (1980), 323.

119. D.W.W. Anderson, D.W.H. Rankin and A. Robertson, J.Mol.Struct., 14, (1972), 385.
120. C. Glidewell, Inorg.Chim.Acta., 29, (1978), 283.
121. S.G.D. Henderson, personal communication.
122. S. Cradock, J.C.S. Faraday Trans. II, 76, (1980), 496.
123. R. Kewley, K.V.L.N. Sastry and M. Winnewisser, J.Mol.Spectros., 10, (1963), 418.
124. C.M. Huntley, unpublished work.
125. J.D. Murdoch and D.W.H. Rankin, J.Mol.Struct., 31, (1976), 291.
126. K. Hedberg, J.A.C.S., 77, (1955), 6491.
127. J. Sheridan and A.C. Turner, Proc.Chem.Soc., (1960), 21.
128. M.C.L. Gerry and T.M. Sugden, Trans.Faraday Soc., 61, (1965), 2091.
129. J.R. Durig, W.O. George, Y.S. Li and R.O. Carter, J.Mol.Struct., 16, (1973), 47.
130. D.E.J. Arnold, S. Cradock, E.A.V. Ebsworth, J.D. Murdoch, D.W.H. Rankin, R.K. Harris and B.J. Kimber, J.C.S. Dalton, (1981), 1349.
131. K. Georgiou and A.C. Legon, J.Mol.Struct., 78, (1982), 257.
132. P. Blair, Honours Project, Edinburgh University, (1980).
133. G.R. Somayajula, J.Chem.Phys., 31, (1959), 919.
134. J.R. Durig and Y.S. Li, J.Mol.Struct., 21, (1974), 289.
135. D.R. Lide, J.Chem.Phys., 33, (1960), 1514.
136. J.M. O'Reilly and L. Pierce, J.Chem.Phys., 34, (1961), 1176
137. S. Cradock, A. Fraser and D.W.H. Rankin, J.Mol.Struct., 71, (1981), 209.
138. S. Cradock, J. Koprowski and D.W.H. Rankin, J.Mol.Struct., 77, (1981), 113.

139. M. Dakkouri and H. Oberhammer, Z.Naturforsch. Teil A.,
29, (1974), 513.
140. H.R. Linton and ^{ER} Nixon, Spectrochim.Acta., 10, (1958), 299.
141. H. Burger and G. Schirawski, Spectrochim.Acta.,
27, (1969), 159.
142. D.C.J. Skea, Ph.D. Thesis, University of Edinburgh, 1980.
143. E.A.V. Ebsworth, M. Onyszchuk and N. Sheppard,
J.Chem.Soc., (1958), 1453.
144. E.A.V. Ebsworth and S.G. Frankiss, J.Chem.Soc.,
(1963), 661.
145. Personal observation.
146. J.R. Durig, K.S. Kalasinsky and V.F. Kalasinsky,
J.Chem.Phys., 69, (1978), 918.
147. C.V. Stephenson, W.C. Coburn and W.S. Wilcox,
Spectrochim.Acta., 17, (1961), 933.
148. T.J. Veszpremi, J. Nagy, I.A. Barta and G. Zsomhok,
J.Organomet.Chem., 185, (1980), 323.
149. J.R. Durig and C.W. Hawley, J.Chem.Phys., 58, (1973), ~~273~~.
37